USGS
science for a changing world

Field-Trip Guide to Mount Hood, Oregon, Highlighting Eruptive History and Hazards

Scientific Investigations Report 2017–5022–G

U.S. Department of the Interior
U.S. Geological Survey

FRONT COVER
South flank of Mount Hood from Trillium Lake. USGS photo by D.E. Wieprecht, 1993.

Field-Trip Guide to Mount Hood, Oregon, Highlighting Eruptive History and Hazards

By William E. Scott and Cynthia A. Gardner

With sections on

A Summary of Recent Petrological and Geochemical Studies of Mount Hood, Oregon

By Adam J.R. Kent and Alison Koleszar

The Mount Hood Fault Zone—Late Quaternary and Holocene Fault Features Newly Mapped with High-resolution Lidar Imagery

By Ian P. Madin, Ashley R. Streig, William J. Burns, and Lina Ma

Seismicity At and Around Mount Hood, Oregon

By Weston Thelen and Seth C. Moran

Scientific Investigations Report 2017–5022–G

U.S. Department of the Interior
U.S. Geological Survey

U.S. Department of the Interior
RYAN K. ZINKE, Secretary

U.S. Geological Survey
William H. Werkheiser, Acting Director

U.S. Geological Survey, Reston, Virginia: 2017

Suggested citation:
Scott, W.E., and Gardner, C.A., 2017, Field-trip guide to Mount Hood, Oregon, highlighting eruptive history and hazards: U.S. Geological Survey Scientific Investigations Report 2017–5022–G, 115 p., https://doi.org/10.3133/sir20175022g.

2328-0328 (online)

Preface

The North American Cordillera is home to a greater diversity of volcanic provinces than any comparably sized region in the world. The interplay between changing plate-margin interactions, tectonic complexity, intra-crustal magma differentiation, and mantle melting have resulted in a wealth of volcanic landscapes. Field trips in this series visit many of these landscapes, including (1) active subduction-related arc volcanoes in the Cascade Range; (2) flood basalts of the Columbia Plateau; (3) bimodal volcanism of the Snake River Plain-Yellowstone volcanic system; (4) some of the world's largest known ignimbrites from southern Utah, central Colorado, and northern Nevada; (5) extension-related volcanism in the Rio Grande Rift and Basin and Range Province; and (6) the spectacular eastern Sierra Nevada featuring Long Valley Caldera and the iconic Bishop Tuff. Some of the field trips focus on volcanic eruptive and emplacement processes, calling attention to the fact that the western United States provides opportunities to examine a wide range of volcanological phenomena at many scales.

The 2017 Scientific Assembly of the International Association of Volcanology and Chemistry of the Earth's Interior (IAVCEI) in Portland, Oregon, marks the first time that the U.S. volcanological community has hosted this quadrennial meeting since 1989, when it was held in Santa Fe, New Mexico. The 1989 field-trip guides are still widely used by students and professionals alike. This new set of field guides is similarly a legacy collection that summarizes decades of advances in our understanding of magmatic and tectonic processes of volcanic western North America.

The field of volcanology has flourished since the 1989 IAVCEI meeting, and it has profited from detailed field investigations coupled with emerging new analytical methods. Mapping has been enhanced by plentiful major- and trace-element whole-rock and mineral data, technical advances in radiometric dating and collection of isotopic data, GPS (Global Positioning System) advances, and the availability of lidar (light detection and ranging) imagery. Spectacularly effective microbeam instruments, geodetic and geophysical data collection and processing, paleomagnetic determinations, and modeling capabilities have combined with mapping to provide new information and insights over the past 30 years. The collective works of the international community have made it possible to prepare wholly new guides to areas across the western United States. These comprehensive field guides are available, in large part, because of enormous contributions from many experienced geologists who have devoted entire careers to their field areas. Early career scientists are carrying forward and refining their foundational work with impressive results.

Our hope is that future generations of scientists as well as the general public will use these field guides as introductions to these fascinating areas and will be enticed toward further exploration and field-based research.

Michael Dungan, University of Oregon
Judy Fierstein, U.S. Geological Survey
Cynthia Gardner, U.S. Geological Survey
Dennis Geist, National Science Foundation
Anita Grunder, Oregon State University
John Wolff, Washington State University
Field-trip committee, IAVCEI 2017

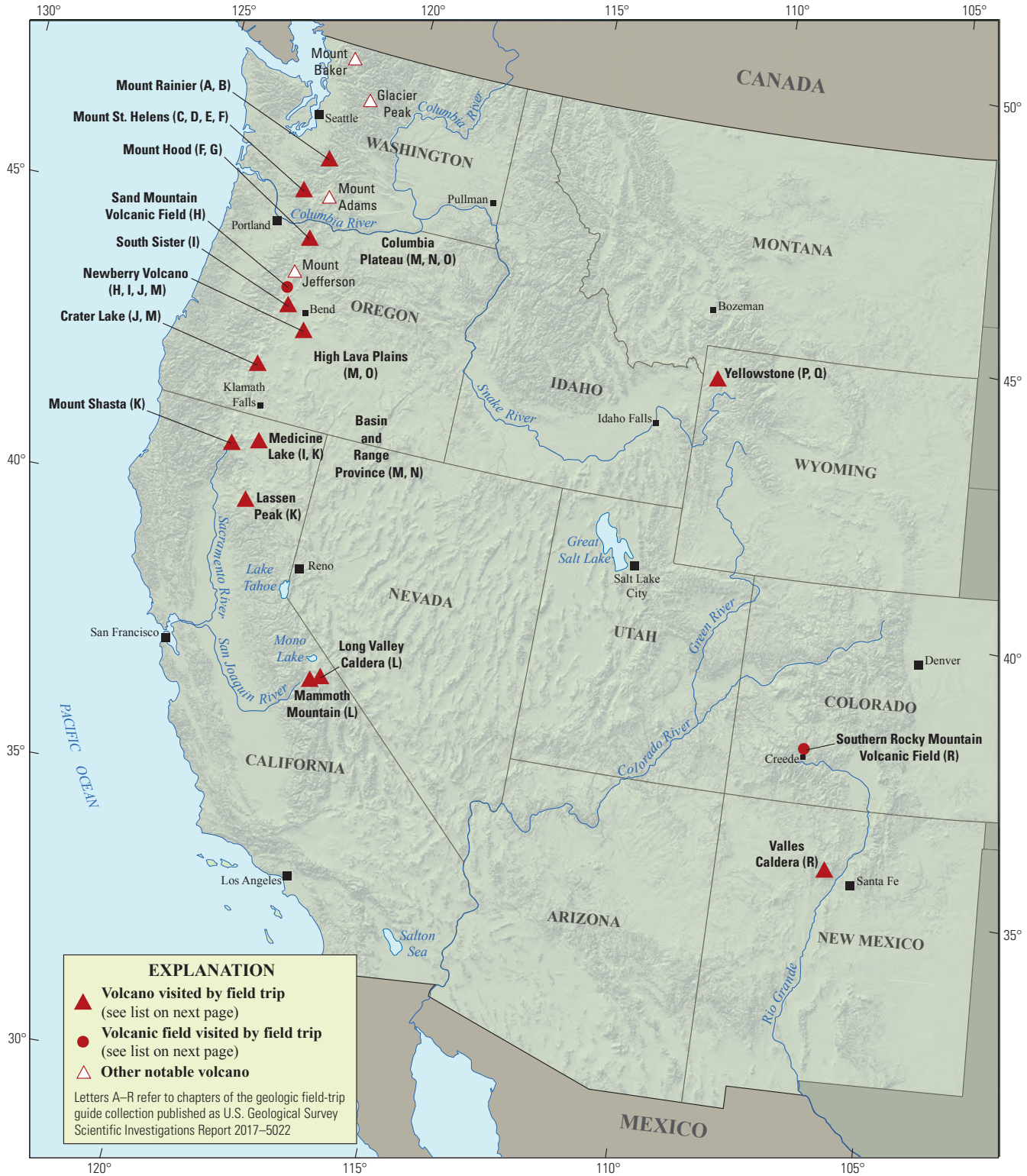

Map of the western United States showing volcanoes and volcanic fields visited by geologic field trips scheduled in conjunction with the 2017 meeting of the International Association of Volcanology and Chemistry of the Earth's Interior (IAVCEI) in Portland, Oregon, and available as chapters in U.S. Geological Survey Scientific Investigations Report 2017–5022. Shaded-relief base from U.S. Geological Survey National Elevation Dataset 30-meter digital elevation model data.

Chapter letter	Title
A	Field-Trip Guide to Volcanism and Its Interaction with Snow and Ice at Mount Rainier, Washington
B	Field-Trip Guide to Subaqueous Volcaniclastic Facies in the Ancestral Cascades Arc in Southern Washington State—The Ohanapecosh Formation and Wildcat Creek Beds
C	Field-Trip Guide for Exploring Pyroclastic Density Current Deposits from the May 18, 1980, Eruption of Mount St. Helens, Washington
D	Field-Trip Guide to Mount St. Helens, Washington—An overview of the Eruptive History and Petrology, Tephra Deposits, 1980 Pyroclastic Density Current Deposits, and the Crater
E	Field-Trip Guide to Mount St. Helens, Washington—Recent and Ancient Volcaniclastic Processes and Deposits
F	Geologic Field-Trip Guide of Volcaniclastic Sediments from Snow- and Ice-Capped Volcanoes—Mount St. Helens, Washington, and Mount Hood, Oregon
G	Field-Trip Guide to Mount Hood, Oregon, Highlighting Eruptive History and Hazards
H	Field-Trip Guide to Mafic Volcanism of the Cascade Range in Central Oregon—A Volcanic, Tectonic, Hydrologic, and Geomorphic Journey
I	Field-Trip Guide to Holocene Silicic Lava Flows and Domes at Newberry Volcano, Oregon, South Sister Volcano, Oregon, and Medicine Lake Volcano, California
J	Geologic Field-Trip Guide to Mount Mazama, Crater Lake Caldera, and Newberry Volcano, Oregon
K	Geologic Field-Trip Guide to Volcanoes of the Cascades Arc in Northern California
L	Geologic Field-Trip Guide to Long Valley Caldera, California
M	Field-Trip Guide to a Volcanic Transect of the Pacific Northwest
N	Field-Trip Guide to the Vents, Dikes, Stratigraphy, and Structure of the Columbia River Basalt Group, Eastern Oregon and Southeastern Washington
O	Field-Trip Guide to Flood Basalts, Associated Rhyolites, and Diverse Post-Plume Volcanism in Eastern Oregon
P	Field-Trip Guide to the Volcanic and Hydrothermal Landscape of Yellowstone Plateau, Montana and Wyoming
Q	Field-Trip Guide to the Petrology of Quaternary Volcanism on the Yellowstone Plateau, Idaho and Wyoming
R	Field-Trip Guide to Continental Arc to Rift Volcanism of the Southern Rocky Mountains—Southern Rocky Mountain, Taos Plateau, and Jemez Volcanic Fields of Southern Colorado and Northern New Mexico

Contributing Authors

Boise State University
Brittany D. Brand
Nicholas Pollock

Colgate University
Karen Harpp
Alison Koleszar

Durham University
Richard J. Brown

Eastern Oregon University
Mark L. Ferns

ETH Zurich
Olivier Bachmann

Georgia Institute of Technology
Josef Dufek

GNS Science, New Zealand
Natalia I. Deligne

Hamilton College
Richard M. Conrey

Massachusetts Institute of Technology
Timothy Grove

National Science Foundation
Dennis Geist (also with Colgate University and University of Idaho)

New Mexico Bureau of Geology and Mineral Resources
Paul W. Bauer
William C. McIntosh
Matthew J. Zimmerer

New Mexico State University
Emily R. Johnson

Northeastern University
Martin E. Ross

Oregon Department of Geology and Mineral Industries
William J. Burns
Lina Ma
Ian P. Madin
Jason D. McClaughry

Oregon State University
Adam J.R. Kent
Benjamin J. Drenth
William C. Evans
Judy Fierstein
Cynthia A. Gardner
V.J.S. Grauch
Christopher J. Harpel
Wes Hildreth
Richard P. Hoblitt
Peter W. Lipman
Jacob B. Lowenstern
Jon J. Major
Seth C. Moran
Lisa A. Morgan
Leah E. Morgan
L.J. Patrick Muffler
James E. O'Connor
John S. Pallister
Thomas C. Pierson
Joel E. Robinson
Juliet Ryan-Davis
Kevin M. Scott
William E. Scott
Wayne (Pat) Shanks
David R. Sherrod
Thomas W. Sisson
Mark Evan Stelten
Weston Thelen
Ren A. Thompson
Kenzie J. Turner
James W. Vallance
Alexa R. Van Eaton
Jorge A. Vazquez
Richard B. Waitt
Heather M. Wright

Portland State University
Jonathan H. Fink (also with University of British Columbia)
Martin J. Streck
Ashley R. Streig

San Diego State University
Victor E. Camp

Smithsonian Institution
Lee Siebert

Universidad Nacional Autónoma de San Luis Potosi
Damiano Sarocchi

University of California, Davis
Kari M. Cooper

University of Liverpool
Peter B. Kokelaar

University of Northern Colorado
Steven W. Anderson

University of Oregon
Ilya N. Binderman
Michael A. Dungan
Daniele McKay (also with Oregon State University and Oregon State University, Cascades)

University of Portland
Kristin Sweeney

University of Tasmania
Martin Jutzeler
Jocelyn McPhie

University of Utah
Jamie Farrell

U.S. Army Corps of Engineers
Keith I. Kelson

U.S. Forest Service
Gordon E. Grant (also with Oregon State University
Robert A. Jensen

U.S. Geological Survey
Charles R. Bacon
Andrew T. Calvert
Christine F. Chan
Robert L. Christiansen
Michael A. Clynne
Michael A. Cosca
Julie M. Donnelly-Nolan

U.S. Nuclear Regulatory Commission
Stephen Self (also with University of California, Berkeley)

Washington State University
Joseph R. Boro
Owen K. Neill
Stephen P. Reidel
John A. Wolff

Acknowledgments
Juliet Ryan-Davis and Kate Sullivan created the overview map, and Vivian Nguyen created the cover design for this collection of field-trip guide books. The field trip committee is grateful for their contributions.

Contents

Introduction....1
Highlights of Quaternary Volcanism....2
Some Definitions—Mount Hood, Pre-Hood Composite Volcanoes, and Regional Volcanoes....2
Mount Hood Volcano....2
Brief Summary of the Geochemistry of Mount Hood, Pre-Hood, and Regional Lavas....2
Summary of Mount Hood Eruptive History....4
Note on K-Ar and $^{40}Ar/^{39}Ar$ Ages....4
500–200 ka....5
200–100 ka....5
100–30 ka....5
~30–15 ka....5
Apparent Dormant Interval Between ~15 and 1.5 ka on Mount Hood....9
Two Late Holocene Eruptive Periods Starting at 1.5 ka....9
Route From Portland to Hood River....9
Portland Basin....9
Columbia Gorge....12
Field-Trip Stops....13
Stop 1. Panorama Point Overlook of the Cascade Range, Mount Hood, and Hood River Valley....13
Travel....14
Stop 2. Hood River Lahar....14
Travel....16
Stop 3. Andesite of Parkdale....16
Travel....17
Stop 4. Quarry in Lower Pleistocene Basalt of Tilly Jane; View of North Flank of Mount Hood....18
Travel....18
Stop 5. Basaltic Andesite and Andesite of Cloud Cap and Basaltic Andesite of Dog River....18
Travel....21
Stop 6. Quarry in Lava Flow of Cloud Cap Volcano....21
Travel....21
Stop 7. View Up Eliot Branch From Inspiration Point....27
Travel....28
Stop 8. Cloud Cap Inn....28
Travel....29
Stop 9. Pre-Hood Andesite of Doe Creek....30
Travel....30
1980 Debris Flow and Flood on Polallie Creek....30
Stop 10. Late Pleistocene Andesite Lava Flow of Tamanawas Falls, Part of Langille Crags-Texas Eruptive Episode of High-strontium Lava....31
Mafic Enclaves in Mount Hood Andesite....34
Travel....36
Stop 11. Pocket Creek—LGM End Moraines Rich in Dome Lava and View of Southeast Flank of Mount Hood....36

Travel....38
Stop 12. Bennett Pass Till Exposure....39
Travel....39
Stop 13. Main Parking Lot at Mount Hood Meadows Ski Resort....40
Travel....40
Stop 14. White River Pyroclastic-Flow and Lahar Deposits of Old Maid Age....44
Travel....46
Stop 15. Frog Lake Fault Scarps....46
Travel....46
Stop 16. U.S. Highway 26 Roadcuts in Andesite of South Flank....46
Travel....48
Stop 17. Three Stops Along Timberline Road....48
Stop 17A. Recessional Till Rich in Dome Lava....48
Stop 17B. Andesite of South Flank....48
Stop 17C. Deposits of Polallie Eruptive Period....50
Travel....50
Timberline Lodge Area....51
Stop 18. Hike East from Timberline Lodge on Timberline Trail to Rim of White River Canyon and Additional Sites....52
Stop 18A. Thin Deposit of Pyroclastic Density Current of Old Maid Age....52
Travel....55
Stop 18B. Andesite of South Flank Underlying Deposits of Pyroclastic Flows and Lahars of Latest Pleistocene and Late Holocene Age....55
Travel....57
Stop 18C. View from Rim of White River Canyon....57
Travel....59
Stop 18D. Ash-Cloud Deposits of Timberline Eruptive Period....59
Stop 19. Hike Timberline Trail West from Timberline Lodge to Little Zigzag and Zigzag Canyons .59
Stop 19A. Diamicts of Timberline Eruptive Period Exposed in Little Zigzag Canyon....59
Stop 19B. View Up Zigzag Canyon to Mississippi Head and Crater....62
Travel....63
Stop 20. Andesite of Yocum Falls....64
Travel....64
Stop 21. Quarry in Basaltic Andesite and Andesite of Little Zigzag River; Timberline Deposits and Contact Between Timberline and Polallie Deposits....64
Travel....64
Stop 22. Andesite of Lower Zigzag Canyon and Andesite of Lady Creek....64
Travel....65
Stop 23. Late Holocene Lahar Deposits Along Upper Sandy River....66
Travel....67
Stop 24. West Flank of Mount Hood and Sandy Glacier Volcano....67
Travel....68
Stop 25. Basalt of Bald Mountain, and View of West Flank of Mount Hood and Sandy Glacier Volcano....68
Travel....68
Stop 26. Jonsrud Viewpoint Park....70
Travel....71

Stop 27. Lahar and Lahar-Runout Deposits of Timberline Age on West Bank of Sandy River 71
Mount Hood Volcano Hazards.....71
References Cited.....73

Sections

A Summary of Recent Petrological and Geochemical Studies of Mount Hood, Oregon
By Adam J.R. Kent and Alison Koleszar.....77
The Mount Hood Fault Zone—Late Quaternary and Holocene Fault Features Newly Mapped with High-resolution Lidar Imagery
By Ian P. Madin, Ashley R. Streig, William J. Burns, and Lina Ma 99
Seismicity At and Around Mount Hood, Oregon
By Weston Thelen and Seth C. Moran 111

Figures

1. Map of field-trip route showing applicable roads, major waterways, and stops 1
2. Map of Quaternary volcanic vents in the Rainier-to-Mount Hood segment of the Cascade Arc 3
3. K_2O versus silica plot for lavas of Mount Hood 4
4. Shaded-relief lidar image of Mount Hood volcano showing lava flows between 500 and ~200 ka 6
5. Shaded-relief lidar image of Mount Hood volcano showing lava flows between ~200 and ~100 ka 7
6. Shaded-relief lidar image of Mount Hood volcano showing lava flows between 100 and ~30 ka 8
7. Shaded-relief lidar image of Mount Hood volcano showing eruptive products and glacial deposits younger than ~30 ka 10
8. Map of Boring Volcanic Field in Portland Basin showing vents and lava flows 11
9. Photograph of view to west of Sandy River delta.....11
10. Photograph of 58-ka Beacon Rock.....12
11. Panorama Point overlook of Cascade Range, Mount Hood, and Hood River Valley 13
12. Physiographic map of Hood River and Upper Hood River Valleys showing mapped fault lineaments and thrust faults 15
13. Photographs of Hood River lahar at Stop 2.....16
14. Andesite of Parkdale.....17
15. Shaded-relief lidar image of northeast flank of Mount Hood and surroundings showing field-trip stops, key geologic units, and other features.....19
16. Photomicrograph of basalt of Tilly Jane showing phenocrysts of plagioclase and olivine with a groundmass of primarily plagioclase and iron-titanium oxides.....20
17. Photograph of Mount Hood from quarry in basalt of Tilly Jane at Stop 4.....20
18. Shaded-relief lidar image showing lavas of regional Quaternary volcanoes in the Mount Hood area.....22
19. Plot of K_2O versus silica for regional lavas of Quaternary age surrounding Mount Hood.....23
20. Photographs of exposure at Stop 5 along O.R. 35 showing basaltic andesite lava flows of the 424-ka basaltic andesite and andesite of Cloud Cap overlying basaltic andesite of Dog River.....24

21. Upper-hemisphere plot of paleomagnetic directions for 424-ka basaltic andesite and andesite of Cloud Cap, ~475-ka andesite of Tilly Jane, and ~931-ka pre-Hood andesite of Doe Creek 25
22. Plot of K_2O versus silica for samples of basaltic andesite and andesite of Cloud Cap 25
23. Photomicrographs of samples representing higher- and lower-silica groups of basaltic andesite and andesite of Cloud Cap 26
24. Photograph of Stop 6 at small quarry along Cloud Cap Road in andesite lava flow of Cloud Cap volcano 26
25. Photograph of view to south looking up narrow, U-shaped glacial valley of Eliot Branch toward Mount Hood from Inspiration Point 27
26. Merged-photographic panorama of view to Mount Hood from Cloud Cap Inn 28
27. Merged-photographic panorama of Mount Hood from late-19th-century right-lateral moraine of Eliot Glacier 29
28. Graph showing cumulative change in length of Mount Hood's north-flank glaciers since beginning of photographic record in 1901 30
29. Photomicrograph of 931-ka pre-Hood andesite of Doe Creek showing porphyritic two-pyroxene lava with trace phenocrysts and microphenocrysts of amphibole 30
30. Plot of K_2O versus silica for lava flows and diamicts of pre-Hood composite volcanoes....31
31. Lidar shaded-relief map of Mount Hood region showing outcrop areas of lava flows of pre-Hood composite volcanoes....32
32. Lidar shaded-relief image of lava flow of Tamanawas Falls....33
33. Exposure of andesite lava flow of Tamanawas Falls near junction of Tamanawas Falls Trail with Tie Trail....35
34. Photomicrograph of andesite of Tamanawas Falls showing two-pyroxene clot and isolated plagioclase phenocrysts in a groundmass of plagioclase and iron-titanium oxides....35
35. Photograph of Tamanawas Falls, which is formed by Cold Spring Creek plunging over a head cut in an andesite lava flow 35
36. Photomicrographs of typical Mount Hood andesite lava and mafic enclave from flow on northwest flank that is part of andesite of Dollar Lake 36
37. Shaded-relief lidar image of Pocket Creek area....37
38. Photograph of southeast flank of Mount Hood from Stop 11 at top of roadcut on southeast side of Forest Road 3540....38
39. K_2O versus silica for samples of incipiently prismatically jointed blocks collected from till of last major glaciation rich in dome lava on south, southeast, and northeast flanks of Mount Hood 39
40. Merged photographs of till exposure on northwest side of O.R. 35 just south of overpass at Bennett Pass 40
41. Shaded-relief lidar image of Mount Hood Meadows Ski Resort and surrounding area showing partial extent of 70–60-ka andesite of Mount Hood Meadows and other units 41
42. View of southeast flank of Mount Hood from parking lot at main base of Mount Hood Meadows Ski Resort 42
43. Plot of K_2O versus silica for lava flows of andesite of Mount Hood Meadows....42
44. Upper-hemisphere plot of paleomagnetic directions with corresponding site dispersion cones for lava flows in the Mount Hood Meadows area....43
45. Shaded-relief lidar image of area surrounding Oregon Route 35 crossing of White River near East and West Sno-Parks....43
46. Photographs of exposure of pyroclastic-flow deposit of Old Maid age on west side of White River north of White River West Sno-Park 44
47. Photomicrograph of clast from pyroclastic-flow deposit of Old Maid age in White River....45
48. Plot of K_2O versus silica for products of Old Maid eruptive period....45

49. Merged photograph of U.S. Highway 26 roadcut that exposes ~130-ka andesite of south flank at Stop 16 46
50. Shaded-relief lidar image of south flank between U.S. Highway 26 and Timberline Lodge showing key units and field trip stops along Timberline Road 47
51. Upper-hemisphere plot of paleomagnetic directions with corresponding site dispersion cones for four Mount Hood lava flows of the ~130-ka andesite of south flank 48
52. Photograph of recessional morainal deposits along Timberline Road about 1.1. mi from U.S. Highway 26 49
53. Photograph of ~130-ka andesite of south flank (h4sf) with thick basal breccia exposed 2.7 mi from U.S. Highway 26 49
54. Photograph of deposits of Polallie eruptive period overlying andesite of south flank in cuts along Timberline Road about 4.6 mi from U.S. 26 and just north of Alpine Campground 50
55. Plot of K_2O versus silica for clasts from deposits of Polallie eruptive period, Steel Cliff lava dome, and prismatically jointed clasts from recessional till rich in Polallie dome lava, all from south flank localities 51
56. View from north edge of the main Timberline Lodge parking lot 52
57. Shaded-relief lidar image of area from Timberline Lodge to summit showing key features and location of hiking Stops 18 and 19, as well as Stop 17C 53
58. Photograph of dug pit east of Timberline Lodge in ~30-cm-thick, gray, friable deposit of pyroclastic density current of Old Maid age 54
59. Plot of K_2O versus silica for samples of blocks from deposits of Old Maid and Timberline eruptive periods showing ~0.1 percent higher K_2O in Timberline lava 55
60. Upper-hemisphere plot of paleomagnetic directions for pyroclastic-flow deposits from Old Maid, Timberline, and Polallie eruptive periods and the Crater Rock lava dome 56
61. Photograph of Stop 18B along Salmon River above Timberline Trail crossing 56
62. Plot of K_2O versus silica for samples of andesite of south flank arranged by geographic distribution 57
63. View of upper White River canyon from Stop 18C showing relations between lava flows and younger diamict units 58
64. View looking downstream from Stop 18C to confluence of three forks of upper White River 58
65. Ash-cloud deposits of late Holocene age 60
66. Deposits of Timberline eruptive period exposed along Little Zigzag Canyon at Stop 19A 61
67. View up 250-m-deep Zigzag Canyon from near Timberline Trail on southeast rim at Stop 19B 62
68. Shaded-relief lidar image of the area around the confluence of Little Zigzag and Zigzag Rivers, showing key units and field trip stops 63
69. Plot of K_2O versus silica content of units exposed around confluence of Little Zigzag and Zigzag Rivers 65
70. Photograph of exposure along north bank of upper Sandy River at Stop 23 that shows typical sequence of diamicts of late Holocene age 66
71. Photograph of west flank of Mount Hood, upper Sandy River valley, and Sandy Glacier volcano from East Lolo Pass Road 67
72. Photograph of west side of Mount Hood and products of 1.2-Ma Sandy Glacier volcano from Timberline Trail on south side of Bald Mountain 68
73. Shaded-relief lidar image of Sandy River near its confluence with Zigzag and Salmon Rivers 69
74. View east from Jonsrud Viewpoint Park of Sandy River as it turns northward toward Columbia River 70
75. Simplified volcano-hazard map of Mount Hood 72

Conversion Factors

Inch/Pound to SI

Multiply	By	To obtain
	Length	
inch (in.)	2.54	centimeter (cm)
inch (in.)	25.4	millimeter (mm)
foot (ft)	0.3048	meter (m)
mile (mi)	1.609	kilometer (km)
	Area	
square mile (mi^2)	2.590	square kilometer (km^2)
	Volume	
cubic mile (mi^3)	4.168	cubic kilometer (km^3)

Vertical coordinate information is referenced to the National Geodetic Vertical Datum of 1929. Horizontal coordinate information is referenced to the North American Datum of 1927 (NAD 27). Altitude, as used in this report, refers to distance above the vertical datum.

Field-Trip Guide to Mount Hood, Oregon, Highlighting Eruptive History and Hazards

By William E. Scott and Cynthia A. Gardner

Introduction

This guidebook describes stops of interest for a geological field trip around Mount Hood volcano. It was developed for the 2017 International Association of Volcanology and Chemistry of the Earth's Interior (IAVCEI) Scientific Assembly in Portland, Oregon. The intent of this guidebook and accompanying contributions is to provide an overview of Mount Hood, including its chief geologic processes, magmatic system, eruptive history, local tectonics, and hazards, by visiting a variety of readily accessible localities. We also describe coeval, largely monogenetic, volcanoes in the region. Accompanying the field-trip guidebook are separately authored contributions that discuss in detail the Mount Hood magmatic system and its products and behavior (Kent and Koleszar, this volume); Mount Hood earthquakes and their relation to regional tectonics and the volcanic system (Thelen and Moran, this volume); and young surface faults cutting the broader Mount Hood area whose extent has come to light after acquisition of regional light detection and ranging (lidar) coverage (Madin and others, this volume).

Our 2017 trip will visit a subset of the localities described herein; the others are included so that future visitors can tailor a trip to their interests. Most stops along roads have room to park a few vans, but few can accommodate a bus. Several stops require easy to moderate hikes on trails.

The trip makes an approximately 175-mile (mi) (280-kilometer [km]) clockwise loop around Mount Hood, starting and ending in Portland (fig 1). The route heads east on Interstate 84 (I-84) through the Columbia River Gorge National Scenic Area (http://www.fs.usda.gov/crgnsa). The guidebook points out only a few conspicuous features of note in the gorge, but many other guides to the gorge are available (for example, Tolan and Beeson, 1984a,b; O'Connor and Burns, 2009). The route continues south on the Mount Hood National Scenic Byway (http://traveloregon.com/trip-ideas/scenic-byways/mt-hood-scenic-byway) on Oregon Route 35 (O.R. 35) following Hood River, and returns to Portland on U.S. Highway 26 (U.S. 26) following Sandy River. The route traverses rocks as old as the early Miocene Eagle Creek Formation and overlying Columbia River Basalt Group (CRBG) of middle Miocene age, but chiefly lava flows and clastic products of arc volcanism of late Miocene to Holocene age. The three major forks of Hood River drain about two-thirds of the volcano; the Sandy River and three of its major tributaries drain much of the remainder. A small part of the south flank is drained by White River, which flows south and east to the Deschutes River.

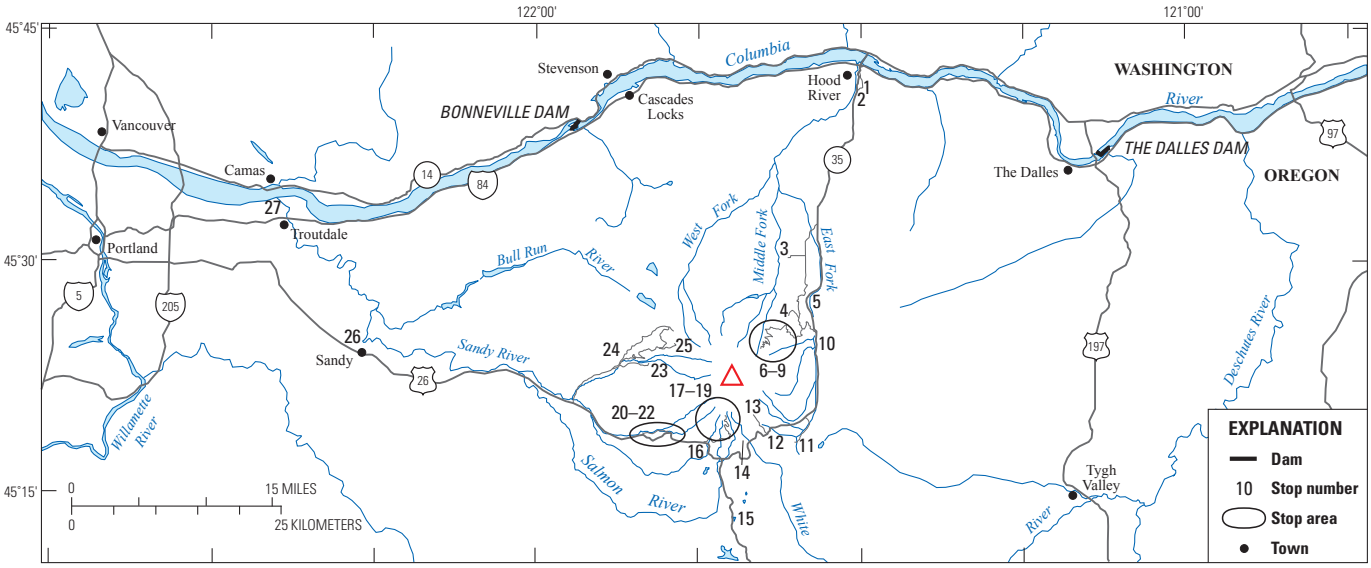

Figure 1. Map of field-trip route showing applicable roads, major waterways, and stops (numerals). Red triangle marks summit of Mount Hood.

Most trailhead parking requires a Northwest Forest Pass (Day ePass, $5, or Annual Pass, $30) or some other Interagency passes (http://www.fs.usda.gov/main/r6/passes-permits/recreation). Parking at Timberline Lodge does not require a pass.

Highlights of Quaternary Volcanism

In the Mount Hood region, Quaternary volcanism extends about 160 km west to east, from the forearc Boring Volcanic Field in the Portland Basin, through the Cascade Range, and eastward to the backarc Simcoe Mountains (fig. 2; Hildreth, 2007). More than 300 vents of Quaternary age lie within a band extending roughly 50 km north and south of the Columbia River, including the large composite volcanoes of Mount St. Helens, Mount Adams, and Mount Hood.

Some Definitions—Mount Hood, Pre-Hood Composite Volcanoes, and Regional Volcanoes

We consider Mount Hood and its eruptive products (lava flows and domes and fragmental deposits) to encompass the past 500,000 years of activity from vents located near the current summit. The area around Mount Hood has produced andesitic and dacitic lavas chemically and mineralogically similar to those of recent eruptions for millions of years, but we see no advantage in referring to all as "products of Mount Hood." The vent locations of what we categorize arbitrarily as pre-Hood Quaternary composite volcanoes are poorly constrained, but probably no more than several kilometers from the current vent. Pre-Hood products are found in small valley-bottom exposures or form ridges roughly radial to, but distant from, the current edifice. They range widely in age, from 1.5 Ma to about 600 ka.

We refer to the basaltic to andesitic vents of Quaternary age surrounding Mount Hood shown in figure 2 as regional volcanoes, most of which are probably monogenetic. Whether or not some of these regional volcanoes close to Mount Hood derive from or are influenced by Hood's magmatic system will be the focus of discussion at several stops and a topic for future research.

We follow volcanic-rock nomenclature typically used in studies of the Cascade Range—basalt, 47–52 weight percent SiO_2; basaltic andesite, 52–57 weight percent SiO_2; andesite, 57–63 weight percent SiO_2; and dacite 63–68 weight percent SiO_2. In the remainder of the text, we shorten mentions of weight percent (normalized volatile free) to simply "percent" except in labels of plot axes.

Many figures in this guidebook are derived from our in-preparation geologic map of Mount Hood volcano, which includes geochemical and geochronologic data. Map units are defined mainly by age, which is based on stratigraphic relations and dating by radiocarbon, K-Ar, and $^{40}Ar/^{39}Ar$ techniques; in some instances paleomagnetic data bolster correlations. Unit names are all informal, combining a rock composition and a geographic name, for example "andesite of Mount Hood Meadows." Map-unit labels, in this case h3hm, denote source (h, Mount Hood), age (3), and geographic name, Hood Meadows (hm). For non-Mount Hood sources, ph represents pre-Hood Quaternary composite volcano, and r represents a Quaternary regional vent. Age categories used for products of Hood, pre-Hood composite, and regional volcanoes are represented by a numeral: 1, <11.2 ka; 2, 11.2 to ~30 ka; 3, ~30 to100 ka; 4, ~100 to 500 ka; and 5, ~500 ka to 2.5 Ma.

Mount Hood Volcano

Mount Hood, elevation 3,427 meters (m) or 11,241 feet (ft), is a long-lived (since 500 ka) composite volcano that has erupted primarily andesite and rarely low-silica dacite (57.9–64.5 percent SiO_2; Wise, 1968, 1969; Crandell, 1980; White, 1980; Scott and others, 1997a; Cribb and Barton, 1997; Kent and others, 2010; Koleszar, 2011; Koleszar and others, 2012). Unlike Mount St. Helens, Mount Hood has not produced highly explosive eruptions that mantled broad areas of the Pacific Northwest with tephra fallout. Rather it has erupted lava chiefly as flows and domes. Lava flows of Pleistocene age compose most of the edifice; the farthest travelled lava flows reach about 12 km from the summit. Pyroclastic flows (block-and-ash flows) triggered by the collapse of growing lava domes have reached similar distances. Most tephra fallout around the volcano originated from ash clouds of pyroclastic flows; explosive eruptions produced only minor amounts. Lahars generated by pyroclastic flows that swiftly melted snow and ice, as well as lahars generated by large landslides, have surged tens of kilometers farther down valleys (Crandell, 1980; Cameron and Pringle, 1986, 1987; Scott and others, 1997a,b; Pierson and others, 2011). Owing to their erodibility, unconsolidated fragmental deposits older than the last major ice age are nearly absent on the edifice's surface and preserved only below lava flows that shielded them from erosion. In contrast, broad fans of fragmental deposits of latest-Pleistocene and late Holocene ages are widely preserved, and contribute markedly to the cone's morphology. Native Americans know the volcano as Wy'east (or Yi-east).

Brief Summary of the Geochemistry of Mount Hood, Pre-Hood, and Regional Lavas

The accompanying paper by Kent and Koleszar details their recent research on the workings of the Mount Hood magmatic system—here we summarize a few key points related to geochemistry that guide our geologic mapping and historical understanding of Mount Hood. Products of Mount Hood and its earlier Quaternary predecessors are similar in mineralogy, texture, and chemical composition, although some older lavas extend the compositional field to slightly higher silica and K_2O (fig. 3). Hood lavas are mostly 58.5–64.5 percent SiO_2 and range through about 1 percent K_2O at a given SiO_2

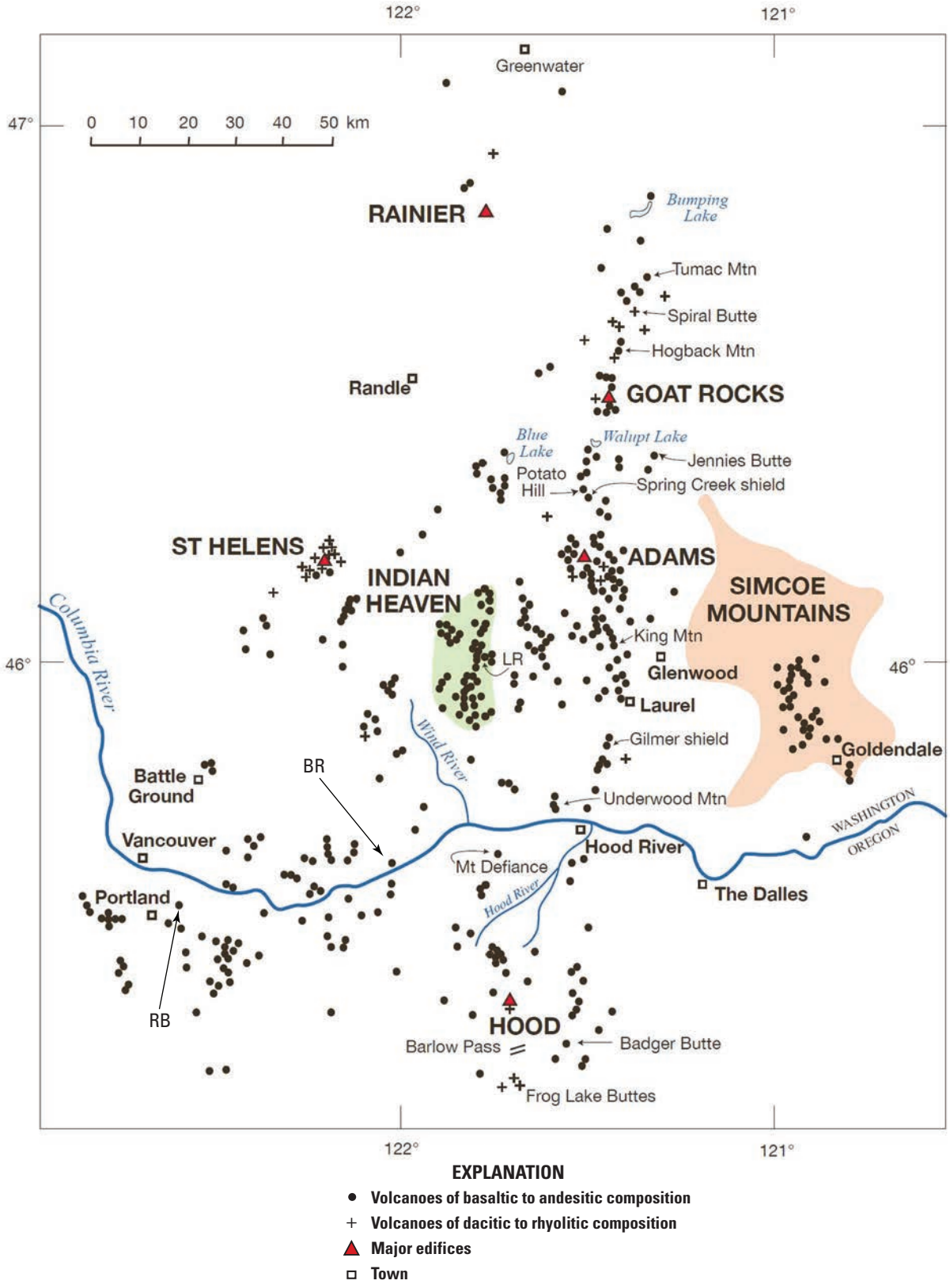

Figure 2. Map of Quaternary volcanic vents in the Rainier-to-Mount Hood segment of the Cascade Arc (modified from Hildreth, 2007, fig. 8). Only vents of Quaternary age are shown within broad orange outline of Simcoe Mountains Volcanic Field (4.5–0.6 Ma). Hildreth notes that the vents plotted are primarily younger than 1 Ma, rather than encompassing the entire Quaternary, which is defined as beginning at ~2.6 Ma. BR, Beacon Rock; LR, Lemei Rock shield; RB, Rocky Butte.

content. We have found that plots of K_2O versus SiO_2 provide a simple illustration of variations and similarities among map units; variation diagrams using other major elements are typically more scattered. Lavas are crystal-rich, with plagioclase dominating a variable mafic mineral content of orthopyroxene or orthopyroxene > clinopyroxene, iron-titanium oxides, and in some samples, amphibole. Olivine is rare and chiefly in the few lavas with 57–58 percent silica. Light-colored, rounded, mafic enclaves of mostly basaltic andesite composition consisting of plagioclase, pyroxene, and occasionally amphibole, but not olivine, are present in variable proportions in most units.

The array of lava compositions from regional volcanoes ranges from 50 to 60 percent silica, overlapping the field of Mount Hood mafic enclaves, and is co-linear with Mount Hood and pre-Hood lavas (fig. 3).

Several stops discuss aspects of geochemistry and petrology in more detail.

Summary of Mount Hood Eruptive History

We briefly summarize Mount Hood's eruptive history in several time slices, each of which is accompanied by a map that shows outcrop areas and inferred areas where units are not deeply buried. We use the term unit to refer to a mappable lava flow or sequence of lava flows and domes with their associated fragmental deposits. We define units primarily on the basis of field relations, chemical similarity, distribution and geomorphic form, K-Ar and argon geochronology, radiocarbon dating, paleomagnetic data, and soil and weathering features. We can constrain emplacement of some units to a few centuries or less, other units may span millennia. Individual units range in volume (dense-rock equivalent or DRE) from ~10^6 to 10^8 m^3.

Note on K-Ar and $^{40}Ar/^{39}Ar$ Ages

There is an ongoing effort to improve the dating of map units. We have about 80 K-Ar age determinations from the

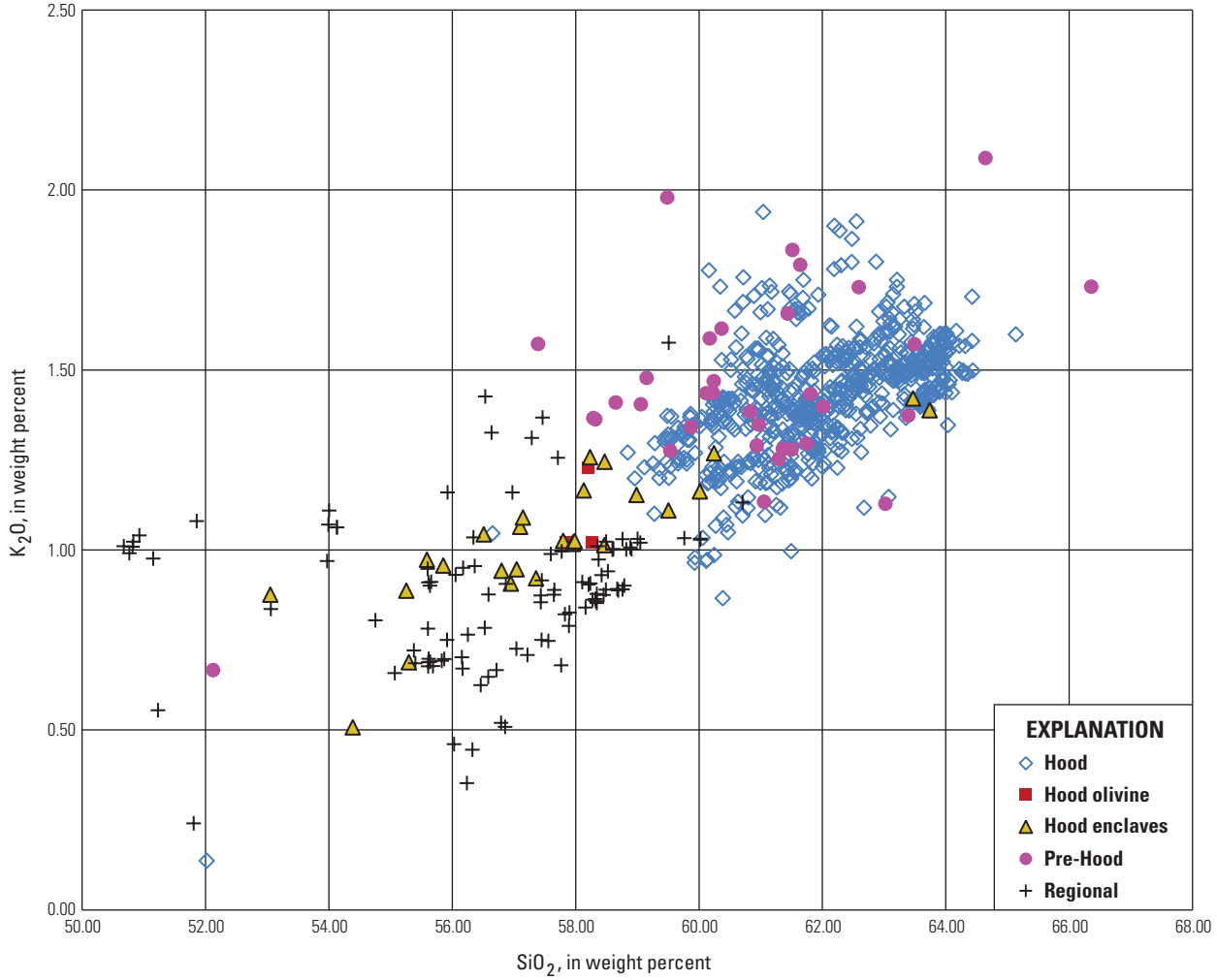

Figure 3. K_2O versus silica plot for lavas of Mount Hood, including separate categories for olivine-bearing lavas and mafic enclaves; Quaternary pre-Hood composite volcanoes; and Quaternary regional volcanoes. The majority of the plotted analyses are from our work (analyses performed at U.S. Geological Survey laboratories and at Peter Hooper GeoAnalytical Lab at Washington State University), supplemented with published analyses by White (1980), Bargar and others (1993), Darr (2006), Kent and others (2010), and Koleszar (2011). Analyses published in the pioneering work by Wise (1969) are not plotted.

U.S. Geological Survey (USGS) laboratory in Menlo Park, Calif., which were made by Marvin Lanphere (most were discussed in Scott and others [1997a]). For the past several years, Andy Calvert of the USGS has been determining $^{40}Ar/^{39}Ar$ ages for some rocks without previous K-Ar ages, but has redated about 15 of the K-Ar samples. This effort was aided by the resampling of several units by David Ferguson, Harvard University, in 2014. The $^{40}Ar/^{39}Ar$ ages are typically older than the K-Ar ages, in some cases by tens of thousands of years; they also have smaller uncertainties. We have permission (2016) from Andy and David to use their data and do not further attribute dates to them. Previous studies report several K-Ar ages (Keith and others, 1985) and K-Ar ages (Thouret, 2005) that are cited in this guidebook. On the basis of these K-Ar and $^{40}Ar/^{39}Ar$ ages, stratigraphic relations, and other age data, we have judged best-age estimates that we use in the text and figures. In some discussions we list ages and their uncertainties when pertinent to specific interpretations. The convention for ages of units given in text and figures is as follows: (1) Numerals preceded by a tilde are approximate averages of two or more ages (for a single technique) from a map unit. (2) For units with both K-Ar and $^{40}Ar/^{39}Ar$ ages, we use the $^{40}Ar/^{39}Ar$ age, which in all cases has a smaller uncertainty. (3) We use > and < for minimum and maximum limiting ages, respectively, and limiting age ranges in a few cases.

500–200 ka

Only two dated units of Mount Hood lava flows are known from the earliest part of this time period (fig. 4). They are close to 500 ka and exposed on the northeast flank below lava flows of the Cloud Cap regional volcano. The andesite of Wallalute Falls (about 62 percent SiO_2) is only known from a small exposure near Cloud Cap Inn (Stop 7). The andesite of Tilly Jane (h4tj) is relatively mafic (58.8–59.9 percent SiO_2; 1.2–1.4 percent K_2O) and forms a 5-km-long ridge between the East Fork Hood River and Tilly Jane Creek. It likely followed an ancestral canyon of the East Fork and displaced the river eastward. There are exposures of this unit along Cooper Spur Road not far from Cooper Spur Mountain Resort. A few undated units could be of similar age, but the record between 500 and 350 ka is sparse indicating that either the volcano was not very active or, more likely, most products of this age are largely buried or eroded. Three dated lava-flow units (346, ~320, and 279 ka) and perhaps a few undated ones represent the middle of this time period. The oldest one (h4bg) is exposed intermittently at the base of a canyon wall on the east flank; the younger two lie on the upper west flank over products of the pre-Hood Sandy Glacier volcano. One flow caps part of Yocum Ridge (h4ym) and one is exposed adjacent to Sandy Glacier at about 7,600 ft altitude (h4sg).

The andesite of Dollar Lake (h4dl) crops out over a broad area of the north and northwest flanks. Two K-Ar ages from the north flank are ~224 ka; a K-Ar age from the northwest flank is 241 ka but has been redated by Ar^{40}/Ar^{39} to 266 ka. Of similar age but unknown stratigraphic relation is olivine-phyric lava (h4oc) that crops outs in a small area along Compass Creek on the north flank. As discussed later, we question if this is more likely to be a product of a regional vent. Stop 22 visits the 210-ka andesite of lower Zigzag Canyon (h4zl). The middle and upper reaches of Zigzag Canyon expose lavas of similar age but varying chemistry.

200–100 ka

Broad areas are covered by lavas flows that compose about 11 map units dating from this time period (fig. 5), which spans the last major interglacial period and the preceding glaciation. One of the few middle Pleistocene sequences of lava-dome derived diamict lie within or below lava flows of this time period. Several lava-flow units show evidence of having been emplaced during a time of extensive glaciers. Lavas lie on south, west, and east sectors; the lack of lava flows of this age in the north sector may reflect removal of such material by the debris avalanche that spawned the Hood River lahar (Stop 2) at roughly 100 ka. Several mappable units of lava flows that vary little in chemistry, but span about 50,000 years, form prominent ridges on the east flank that abut an upland of volcanic rocks of Miocene and Pliocene age. Stops 11 and 13 have distant views of 200–100-ka lavas; Stops 16, 17, and 18 visit exposures in the ~130-ka andesite of south flank (h4sf).

100–30 ka

Ten to twelve lava-flow units date from this period (fig. 6), which includes the onset and build-up to the near maximum of late Pleistocene glaciation and chiefly follows the north-flank debris avalanche and Hood River lahar (Stop 2). Many of the units show evidence of interaction with expanded valley glaciers—units h3nl, h3tx, h3cm, h3bs, and h3ic. The north sector grew considerably as several major lava-flow sequences filled in the debris-avalanche scar. The southeast, west, and northwest sectors also have multiple units. We have spent considerable effort studying the andesite of Mount Hood Meadows (h3hm; Stop 13) to test our rationale for defining map units based on chemistry, paleomagnetic data, and geomorphic expression. Two units (h3lc, andesite of Langille Crags, and h3tx, andesite of Texas) compose high-strontium (700–1,200 parts per million [ppm]) lava flows, a rare occurrence on Mount Hood, in the northeast sector (Stops 7, 8, and 10) and a minor flow in the west sector. Such flows span a time period of at least 20,000 years and perhaps twice as long. Parts of the modern summit are known to date from this time interval.

~30–15 ka

This time period, which we call the Polallie eruptive period (Crandell, 1980), spans both the maximum extent and recession of glaciers during the last ice age, during which lava domes and stubby lava flows built much of the upper 600 m of the volcano (fig. 7). One lava flow reached about 7,200 ft on the west-southwest flank near the end of this time period

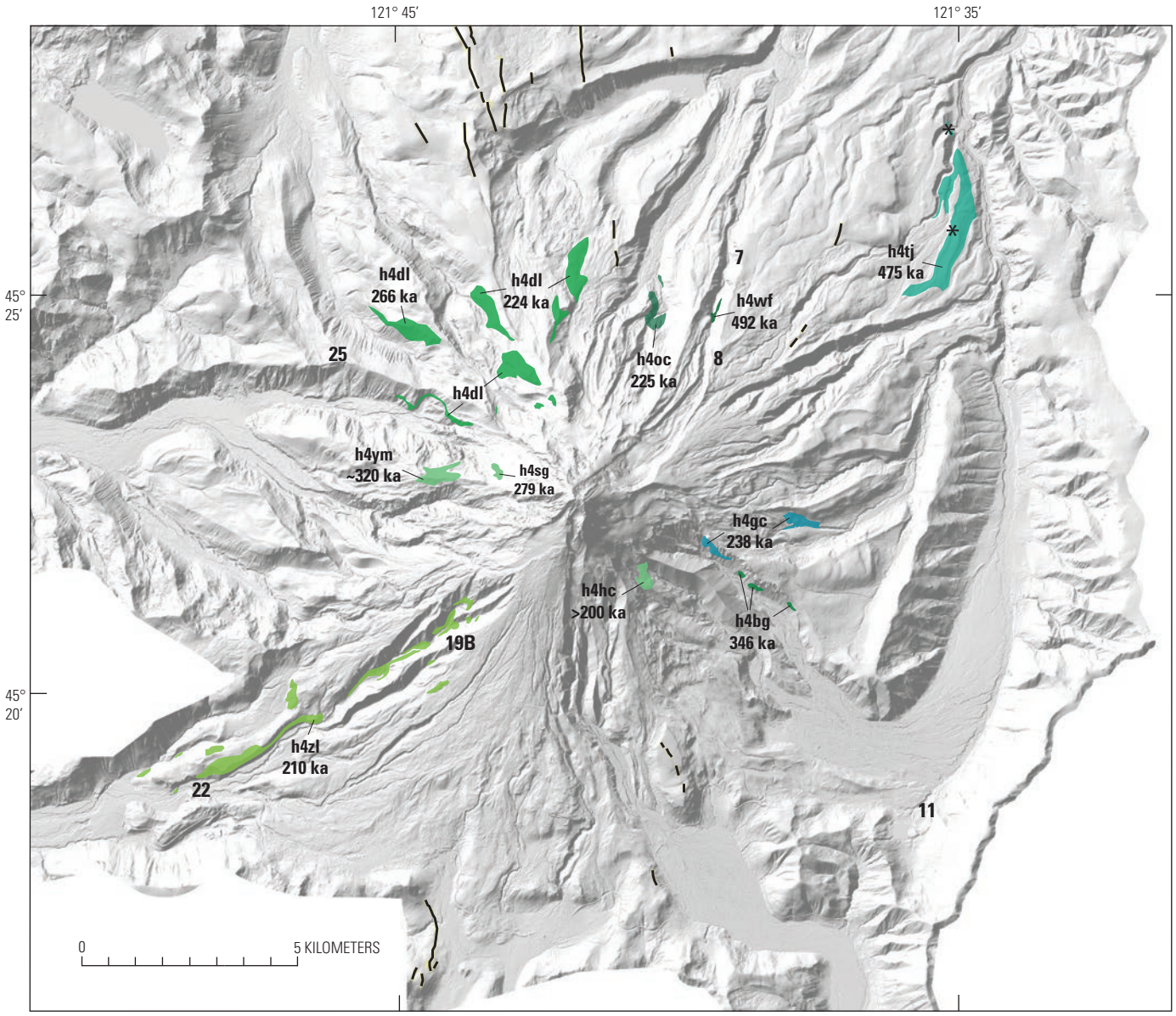

Base from 2010 Oregon Department of Geology and Mineral Industries, Oregon Lidar Consortium, Mount Hood lidar data quadrangle series, hillslope-shaded, bare-earth elevation model, 3 ft interval; Badger Lake, Bull Run Lake, Dog River, Government Camp, Mount Hood North, and Mount Hood South quadrangles

EXPLANATION

h4zl	Andesite of Zigzag Canyon	h4bg	Andesite of base of Gnarl Ridge
h4oc	Olivine Andesite of Compass Creek	h4tj	Andesite of Tilly Jane
h4dl	Andesite of Dollar Lake	h4wf	Andesite of Wallalute Falls
h4gc	Andesite of Gnarl-Cold Spring	——	Fault scarp
h4hc	Dacite of head of Clark Creek	*	Paleomagnetic data
h4sg	Andesite of Sandy Glacier	22	Field-trip stop
h4ym	Andesite of Yocum Ridge		

Figure 4. Shaded-relief lidar image of Mount Hood volcano showing lava flows between 500 and ~200 ka. In approximate order of increasing age: h4zl, andesite of Zigzag Canyon; h4oc, olivine andesite of Compass Creek; h4dl, andesite of Dollar Lake; h4gc, andesite of Gnarl-Cold Spring; h4hc, dacite of head of Clark Creek; h4sg, andesite of Sandy Glacier; h4ym, andesite of Yocum Ridge; h4bg, andesite of base of Gnarl Ridge; h4tj, andesite of Tilly Jane; and h4wf, andesite of Wallalute Falls. Ages of units represent our best estimate based on K-Ar and $^{40}Ar/^{39}Ar$ data as well as other evidence, see Note on K-Ar and $^{40}Ar/^{39}Ar$ ages, p. 5.

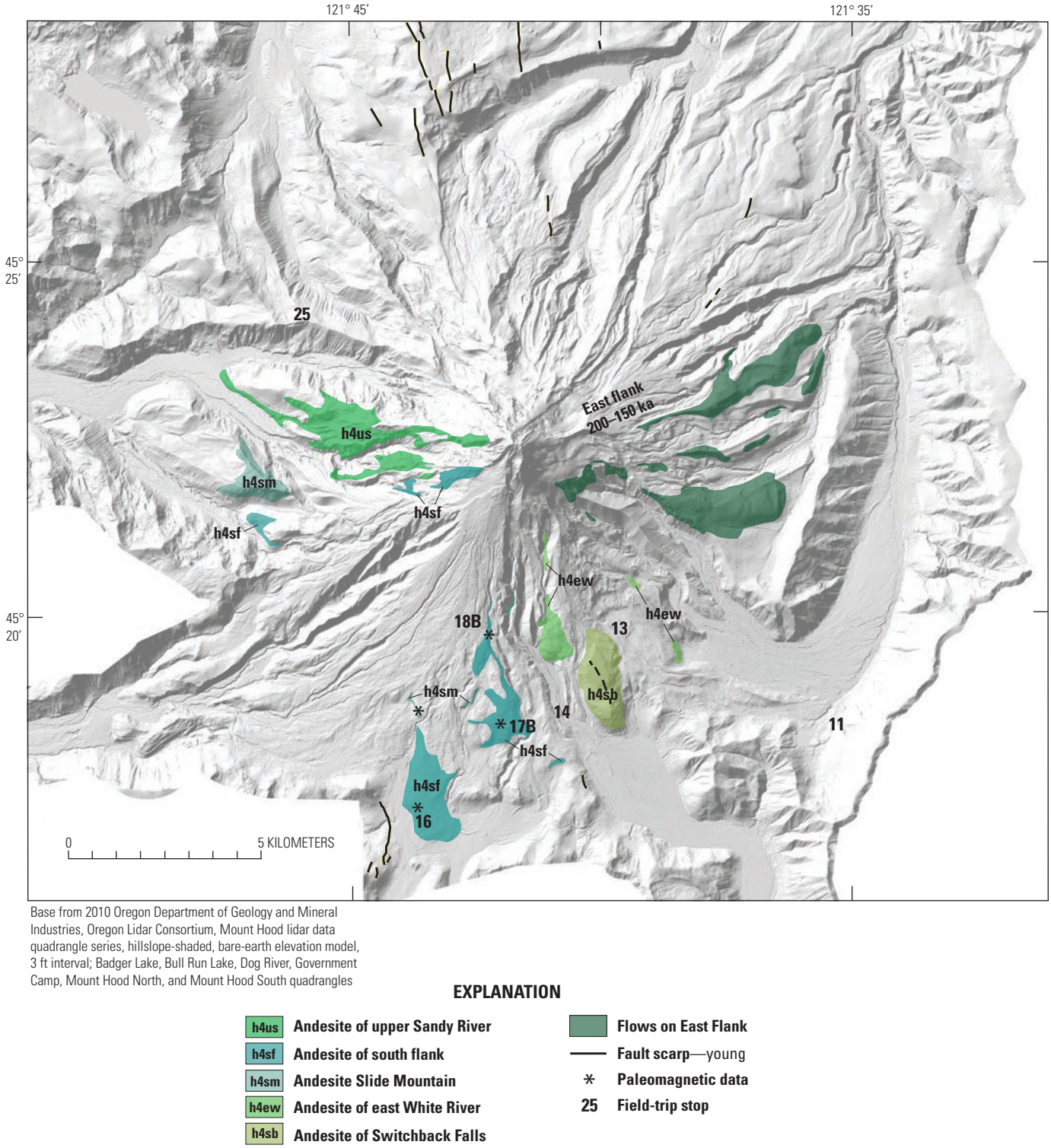

Figure 5. Shaded-relief lidar image of Mount Hood volcano showing lava flows between ~200 and ~100 ka. Several of the flows display evidence of emplacement at times of expanded glaciers—units h4sb, ~170-ka andesite of Switchback Falls; h4sm, ~200-ka andesite of Slide Mountain; parts of h4us, ~140-ka andesite of upper Sandy River; and several ridge-forming lava flows on east flank. Other units are h4sf, ~130-ka andesite of south flank, which also has a western extension; and h4ew, 140-ka andesite of east White River. Note absence of lava flows of this age in northern sector, where flows of this age may have been removed by debris avalanche that created ~100-ka Hood River lahar (fig. 13, Stop 2). Ages of units represent our best estimate based on K-Ar and $^{40}Ar/^{39}Ar$ data as well as other evidence, see Note on K-Ar and $^{40}Ar/^{39}Ar$ ages, p. 5.

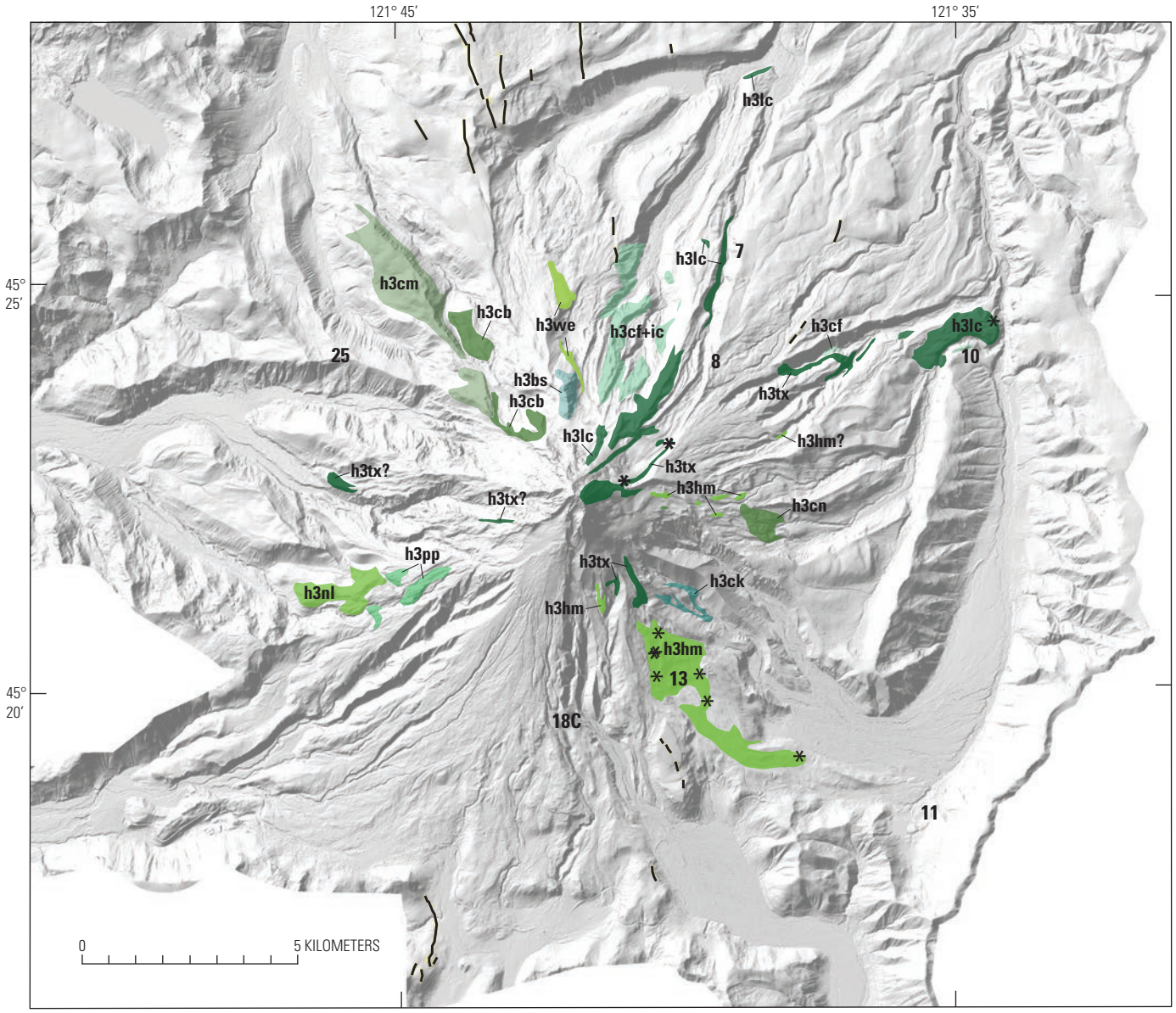

Base from 2010 Oregon Department of Geology and Mineral Industries, Oregon Lidar Consortium, Mount Hood lidar data quadrangle series, hillslope-shaded, bare-earth elevation model, 3 ft interval; Badger Lake, Bull Run Lake, Dog River, Government Camp, Mount Hood North, and Mount Hood South quadrangles

EXPLANATION

- h3bs — Andesite and dacite of Barrett Spur
- h3lc — Andesite of Langille Crags
- h3tx — Andesite of Texas
- h3pp — Andesite of Paradise Park
- h3hm — Andesite of Mount Hood Meadows
- h3cm — Andesite of Cathedral and McNeil Ridges
- h3ic — Ice-contact lava of Compass Creek
- h3ck — Andesite of Clark Creek
- h3we — Andesite of west Elk Cove
- h3cf — Andesite of Coe Falls
- h3nl — Andesite of north wall of Lost Creek
- h3cn — Andesite of North Fork Cold Spring Creek
- h3cb — Andesite of Cairn Basin
- Fault scarp
- * Paleomagnetic data
- 25 Field-trip stop

(Stop 19B), but activity primarily consisted of the collapse of near-summit domes and flows to produce extensive fragmental deposits (Stops 4, 7, 8, 17C, 18B,C). Some of this material was emplaced on ridge tops flanked by extensive glaciers or directly on glaciers and transported to end moraines or left as hummocky stagnant-ice deposits (Stops 11 and 17A). Coeval ash clouds of the flows deposited thick, fine-grained tephra on the flanks of Mount Hood (Stop 18D) and in the Upper Hood River Valley, where soils formed from the ash now support major agricultural production.

Apparent Dormant Interval Between ~15 and 1.5 ka on Mount Hood

One regional unit, the andesite of Parkdale (PK in fig. 7), erupted from a vent about 12 km north-northeast of Mount Hood's summit at about 7.7 ka (Stop 3), but we find no evidence of eruptive activity on Mount Hood during this time period.

Two Late Holocene Eruptive Periods Starting at 1.5 ka

Both late Holocene eruptive periods consisted of lava-dome growth in the breached summit crater created by debris avalanche(s) early in the first period. Repeated collapse of growing domes sent pyroclastic flows down south- and west-draining valleys that ultimately created large bouldery debris fans on the south, and to lesser extent, west flanks (fig. 7). Deposits of lahars along with minor interbedded tephra deposits are also present in fans. After Crandell (1980), we call the older and more voluminous of the eruptive periods, Timberline (Stops 18B,D, 19A, 21, 23, 27), and the younger, Old Maid (Stops 14, 18A,C, 22, and 23). The Timberline eruptive period lasted for a few decades about 1.5 ka, and produced an estimated bulk volume of 1.0–2.0 km^3 of lahar and pyroclastic-flow deposits and tephra. Isolation of the vent in the breached crater precluded pyroclastic flows from entering valleys draining about two-thirds of the volcano, chiefly in the Hood River watershed. The age of the Old Maid eruptive period is well constrained by dendrochronology from 1781 to the mid-1790s C.E. (Pierson and others, 2011). We estimate a bulk volume of the remnant lava dome (Crater Rock), flow deposits, and tephra of about 0.25–0.5 km^3.

Route From Portland to Hood River

Portland Basin

The trip begins in the Portland Basin, which lies in the Cascades forearc. The following description is summarized from Evarts and others (2009). The basin's geologic setting is rare in that it is traversed by the continental-scale Columbia River, which has maintained a course in this region through the active Cascade volcanic arc since at least middle Miocene time. The basin lies between uplifted Paleogene volcanic rocks of the Cascades, and the folded and faulted Portland Hills just west of the city (fig. 8). The basin has a complex tectonic origin of north-south margin-parallel compression, expressed by dextral shear on northwest-striking faults. A Miocene to Holocene sedimentary fill of primarily Columbia River origin reaches to at least 400 m below sea level. Tens of late Pleistocene megafloods generated by repeated outbursts from the 2,200 km^3, glacier-dammed Lake Missoula in western Montana and northern Idaho flooded the basin to depths of more than 100 m. Large gravel bars deposited by the floods lie in the eastern part of the basin near the mouth of the Columbia Gorge. Throughout late Pliocene and Pleistocene time, eruptions from at least 80 vents in the basin and its margins produced the Boring Volcanic Field of monogenetic scoria cones and shield volcanoes (Evarts and others, 2009; Fleck and others, 2014). We pass several Boring volcanoes on our route, including Rocky Butte (≤133 ka; near the I-84/I-205 intersection) and Beacon Rock (58±6 ka), the youngest volcano of the field (fig. 2).

Just east of Exit 17 (Troutdale), I-84 crosses the Sandy River, which drains about one-third of Mount Hood. A broad fan (Sandy River delta) composed chiefly of Hood volcaniclastic deposits interbedded with Columbia River sediments forces the Columbia channel northward (fig. 9). Future lahars and related sedimentation could severely affect highway, rail, and river transportation in this area. Sandy River is a shortened version of its original name, Quicksand River, which was given to it by the Lewis and Clark Corps of Discovery in 1805 and 1806. Their exploration occurred shortly after the Old Maid eruptive period of 1781 to the mid-1790s, when the river was choked with eruption-related sediment (Pierson and others, 2011).

Figure 6. Shaded-relief lidar image of Mount Hood volcano showing lava flows between 100 and ~30 ka. Several of the flows display evidence of emplacement at times of expanded glaciers—units h3bs, andesite and dacite of Barrett Spur; h3cm, ~60-ka andesite of Cathedral and McNeil Ridges; h3nl, 80-ka andesite of north wall of Lost Creek; h3we, 100–90-ka andesite of west Elk Cove; and parts of h3cf+h3ic, 90 to ~70-ka andesites of Coe Falls and ice-contact lava of Compass Creek. A sequence of high-strontium lava flows emplaced between 50 and 30 ka and perhaps as early as 70 ka are shown in darkest green—h3lc, andesite of Langille Crags and h3tx, andesite of Texas—parts of which were also emplaced during times of extensive glaciers. Other units in this age range apparently emplaced during times of less extensive glacier cover are h3pp, ~100-ka andesite of Paradise Park; h3cn, 88-ka andesite of North Fork Cold Spring Creek; h3cb, ~90-ka andesite of Cairn Basin; h3ck, ~70-ka andesite of Clark Creek; and h3hm, 70–60-ka andesite of Mount Hood Meadows. Ages of units represent our best estimate based on K-Ar and $^{40}Ar/^{39}Ar$ data as well as other evidence, see Note on K-Ar and $^{40}Ar/^{39}Ar$ ages, p. 5.

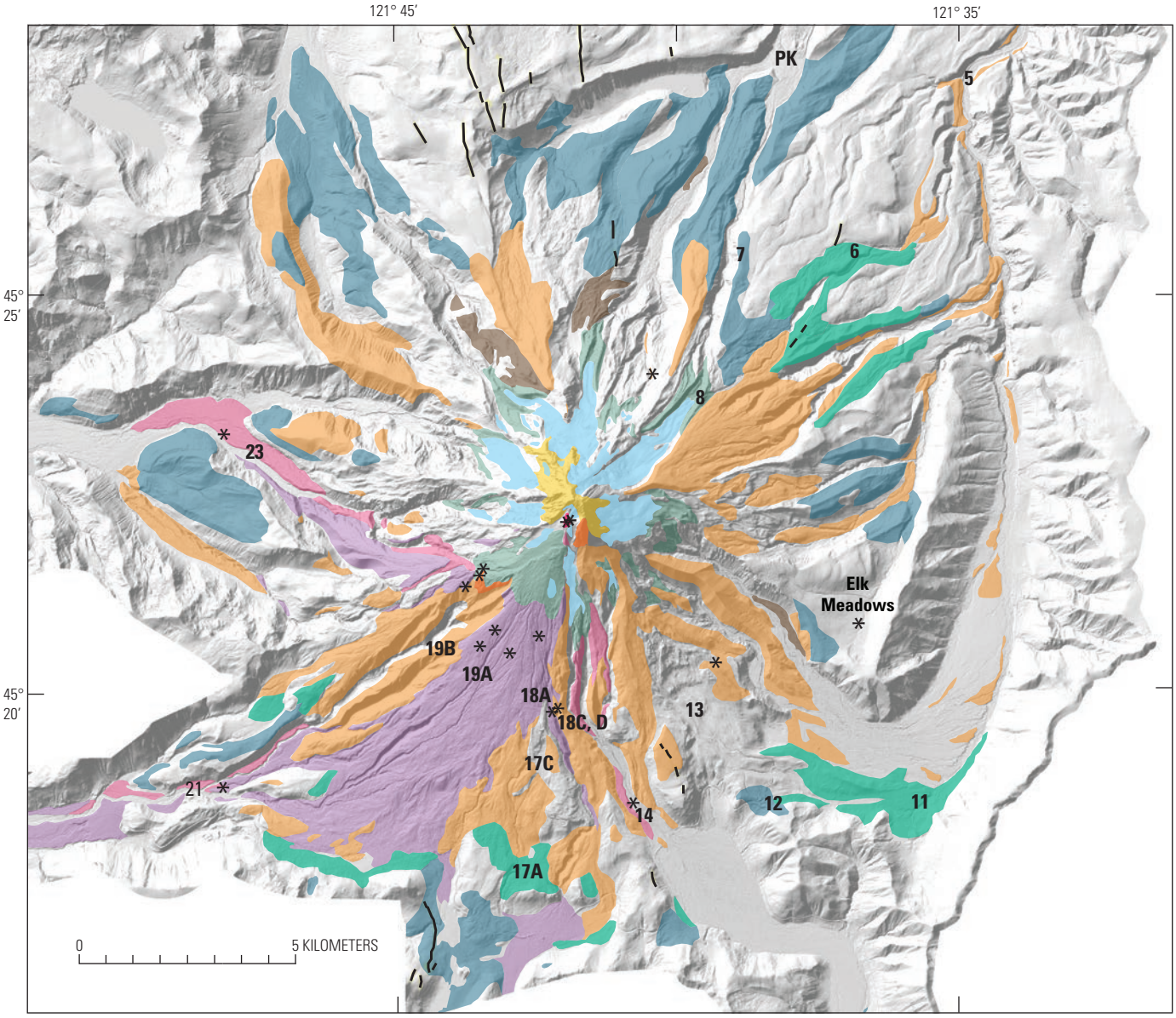

Base from 2010 Oregon Department of Geology and Mineral Industries, Oregon Lidar Consortium, Mount Hood lidar data quadrangle series, hillslope-shaded, bare-earth elevation model, 3 ft interval; Badger Lake, Bull Run Lake, Dog River, Government Camp, Mount Hood North, and Mount Hood South quadrangles

EXPLANATION

- **Fragmental deposits and lava dome (dark) of Old Maid age**
- **Fragmental deposits of Timberline age**
- **Debris avalanche and related lahar deposits of Timberline age**
- **Lava dome of Steel Cliff (dark) and fragmental deposits of Polallie age**
- **Lava domes/fragmental deposits of summit; Polallie and pre-Polallie age**
- **Glacial deposits**
  Till of moraine belts at and near last glacial maximum consists primarily of clasts of lava-flow lithologies
- Till on south and east flanks rich in andesite and dacite derived from summit lava domes
- Moraines of late Neoglacial age
- Present glaciers and perennial snowfields
- **Fault scarp**
- **Paleomagnetic data**
- **21 Field-trip stop**

Figure 7. Shaded-relief lidar image of Mount Hood volcano showing eruptive products and glacial deposits younger than ~30 ka. Summit units shown in gold color are poorly dated and some could pre-date 30 ka. PK marks vent for 7.7-ka Parkdale lava flow.

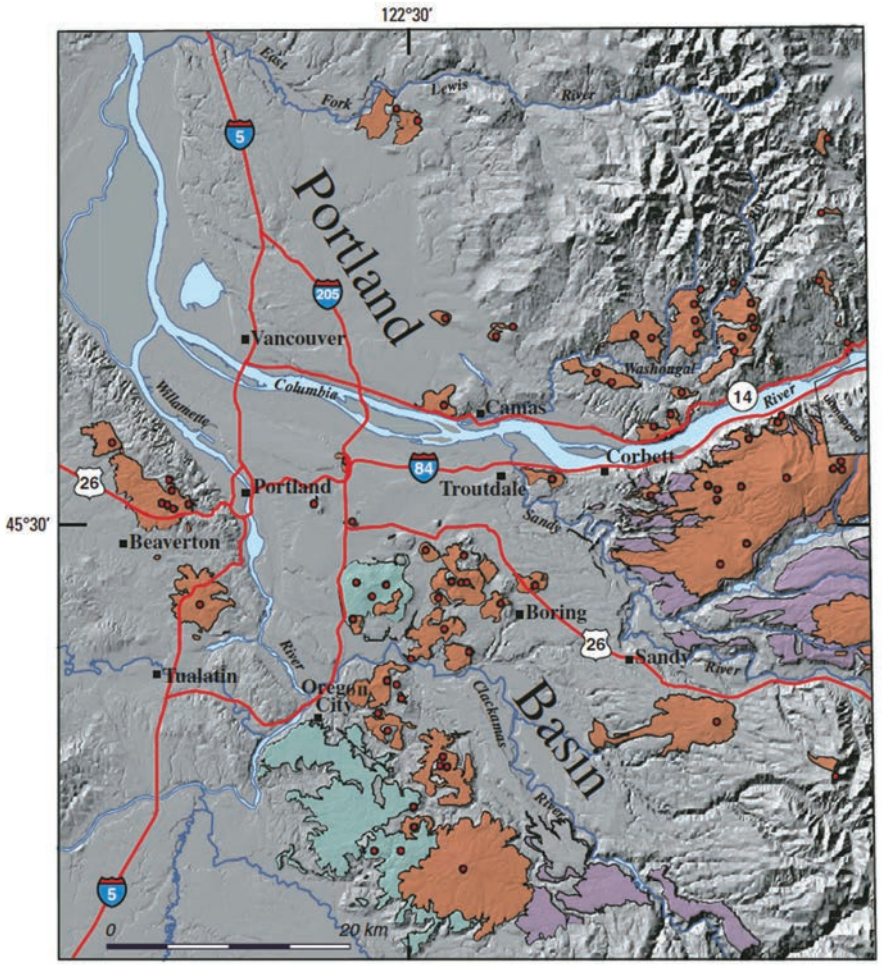

Figure 8. Map of Boring Volcanic Field in Portland Basin showing vents (red circles) and lava flows (low-K tholeiite in light blue and other basalt, basaltic andesite, and andesite in orange; low-K tholeiite from vents in High Cascades in purple). From Evarts and others (2009).

Figure 9. Photograph of view to west of Sandy River delta, which diverts the Columbia River northward towards the communities of Camas and Washougal, Washington; Interstate 84 to left of river. Star marks Stop 27. Higher western part of delta hosting Troutdale Airport (to right of yellow star) is composed chiefly of lahar and lahar-runout deposits and related alluvium of 1.5-ka Timberline eruptive period. The lower east part of the delta (below star) bears deposits of Old Maid eruptive period (late 18th century). Both parts of delta also contain Sandy River alluvium and flood deposits of Columbia River (Rapp, 2005).

Columbia Gorge

From Sandy River to Hood River, I-84 follows the Columbia Gorge, which in 1986 was designated a National Scenic Area wherein land use and development are regulated to preserve scenic qualities. Much of the following is summarized from previous field-trip guides (Tolan and Beeson, 1984a,b; Scott and others, 1997a; O'Connor and Burns, 2009). The gorge owes its existence to the mighty Columbia River having kept pace with volcanism and tectonism in the Cascade arc and Columbia basin. The river drains more than 660,000 km^2 in the northwestern U.S. and southwestern Canada. The gorge has witnessed both immense floods of basalt, originating from vents in the Washington-Oregon-Idaho border country during the middle Miocene (Columbia River Basalt Group), and immense floods of water, originating in western Montana as the late Pleistocene Cordilleran ice sheet dammed one of the Columbia's tributaries to create a huge lake that catastrophically drained numerous times (Missoula floods). In addition, generally south-dipping rock structures throughout the gorge set the stage for huge landslides on the Washington side, which have repeatedly dammed the river and diverted it to the south side of the gorge. The steeper Oregon side of the gorge is more prone to rockfalls and debris flows caused by intense rainstorms.

Just east of Exit 30, 183-m-high Multnomah Falls is one of the most visited tourist attractions in Oregon. The falls, which expose several flows of CRBG, is one of many on the south side of the gorge.

Between Exits 35 and 37, Beacon Rock is intermittently visible on the Washington shore (fig. 10). Beacon Rock is the youngest known volcano of the Boring Volcanic Field at 58±6 ka (Fleck and others, 2014). The massive rock is a volcanic plug of basaltic andesite; the remainder of the volcano, presumably a scoria cone, was removed by passage of tens of Missoula floods, the largest of which flowed more than 200-m deep through this reach. Beacon Rock is a Washington State Park. Visitors can climb to the 260-m summit on a trail with stairs and handrails.

Exits 41 and 42 pass the Bonneville Navigation Lock and Dam, which was completed in 1938, a second powerhouse began operation in 1982, and a new larger lock was opened in 1993. This was the first of 11 large hydroelectric projects built on the mainstem Columbia River in the United States. The river is affected by tides as far upstream (230 km) as the dam. The pool behind the dam is at an altitude of about 21 m above sea level and drowns the natural rapids known as the "Cascades of the Columbia," from which the Cascade Range takes its name. Roadcuts expose lahar deposits of the lower Miocene Eagle Creek Formation, which underlies the Columbia River Basalt Group. Great cliffs of CRBG and Eagle Creek Formation high on the north side of the valley mark the head of the huge Bonneville landslide, a complex landslide that covers about 35 km^2. The main failure plane is the south-dipping contact at the base of the relatively permeable Eagle Creek Formation, which lies on a thick impermeable clayey saprolite developed in the underlying Oligocene Ohanapecosh Formation. Movement about 500 years ago temporarily dammed the Columbia to an altitude of about 75 m, giving rise to the Native American legend of the "Bridge of the Gods."

Near Exit 51, conical Wind Mountain, located on the Washington side of the Columbia, is formed of an ~6-Ma

Figure 10. Photograph of 58-ka Beacon Rock, the youngest volcano of the Boring Volcanic Field (Evarts and others, 2009; Fleck and others, 2014). Beacon Rock, which lies on the north bank of the Columbia River, is a massive plug; the remainder of the volcano, presumably scoria and agglutinate, was swept away by latest Pleistocene Missoula floods. Photograph copyright Lyn Topinka, used with permission.

quartz diorite intrusion (Korosec, 1987). One of the great gorge landslides wraps around Wind Mountain and forms a narrow reach of the Columbia.

Near milepost 60, roadcuts expose pillow lavas of Pliocene age. These exposures are part of a pillow-palagonite sequence that ascends westward along the base of capping Pliocene lava flows in the Columbia Gorge. Such lava flows dammed the Columbia to create lakes into which pillow-lava deltas formed, that in turn, could be buried by advancing flows. A K-Ar age of 3.53±0.08 Ma (weighted mean of two ages) was obtained from the base of this sequence at Perham Creek, about 5.5 km to the southwest (Conrey and others, 1996).

Cross the Hood River, which drains the east and north flanks of Mount Hood. Note the broad beaches at the mouth of Hood River that have grown markedly in recent decades as storm-triggered debris flows on Mount Hood sent large sediment loads downstream. The beaches are the focus of local wind and water sports. Take Exit 64 to southbound O.R. 35. Continue straight through 4-way-stop at intersection of O.R. 35 and U.S. 30; roadcuts ahead on left are in CRBG; stay in left southbound lane.

About 0.3 mi farther south, turn left onto the scenic tour route (Eastside Road) and follow signs to Panorama Point, a total distance of 1.5 mi. Turn right into Panorama Point County Park and continue to parking lot at top of hill. Restrooms are available.

Field-Trip Stops

Stop 1. Panorama Point Overlook of the Cascade Range, Mount Hood, and Hood River Valley

Location: 45.6869° N., 121.4872° W.; we also provide locations based on the Universal Transverse Mercator grid (UTM), zone 10T, and distance in meters east and north of the zone's southwest corner, in this case UTM 10T 617800E and 5060150N; altitude 600 ft

A few major features of Mount Hood stand out from this view (fig. 11). Below and east of the summit lies Cooper Spur, a remnant of a broad fan of pyroclastic-flow and lahar deposits of the Polallie eruptive period that originated from near-summit lava domes. Ridges radiating outward from the lower flanks are underlain primarily by andesite lava flows. The steep, rugged north face contrasts markedly with the smooth fan-aproned south face that will be visible at later stops. This contrast results from Holocene eruptive activity, primarily lava-dome growth and collapse, having been restricted to the south flank.

The Hood River Valley is a complex structural depression extending north into Washington and southward toward Mount

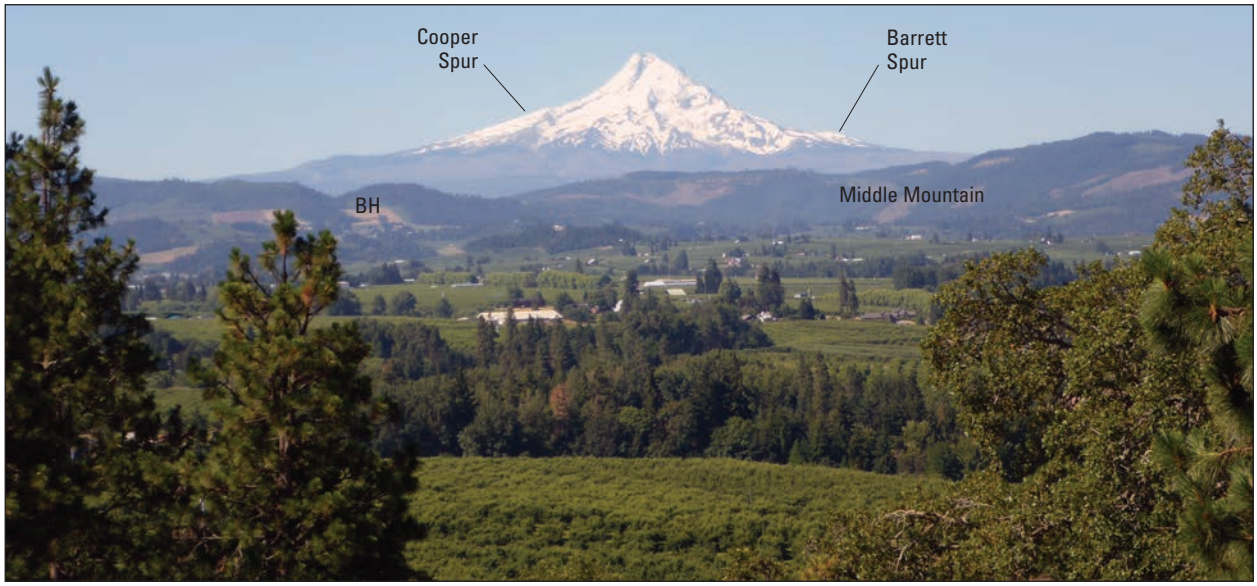

Figure 11. Panorama Point overlook of Cascade Range, Mount Hood, and Hood River Valley. Mount Hood lies 40 km to south-southwest. Fault-controlled Middle Mountain blocks view of Upper Hood River Valley. Both valleys are major producers of fruit (pears, cherries, apples) and berries. Wine grapes are also a major crop in Hood River Valley. Cooper and Barrett Spurs are prominent mid-flank landmarks formed by a thick pyroclastic fan and glacial-age lava flow, respectively. BH, Quaternary Booth Hill volcano.

Hood (fig. 12); see recent summary in McClaughry and others (2012). During extrusion of the CRBG and continuing until about 3 Ma, the region was in a compressive regime as evidenced by folds and thrust faults. After 3 Ma, intra-arc extension has dominated, creating a half graben about 20–25 km wide with Hood River Valley at its eastern side. The valley's east margin is a series of steeply dipping normal faults that displace the CRBG by about 550 m in the area of Panorama Point. The valley extends north into Washington but is filled by an early Pleistocene (0.85±0.02 Ma, Hammond and Korosec, 1983) shield volcano, Underwood Mountain. The west side of the valley slopes gently upward toward the Cascade Range crest. Pliocene and Pleistocene lava flows blanket the CRBG on most of the visible upland surfaces. A series of parallel north-northwest-striking extensional faults, recently named the Mount Hood Fault Zone (Madin and Ma, 2012; Madin and others, this volume) may define the western extent of the half-graben. Lidar surveys and trenching show some of these faults cut glacial deposits of latest Pleistocene age.

The floor of Hood River Valley is mantled by middle Pleistocene alluvial deposits of the Hood River and at least one voluminous lahar deposit derived from Mount Hood (Stop 2). Missoula flood deposits form a late Pleistocene capping of sand and silt as thick as 30 m in some parts of the valley. The largest floods inundated the valley to an altitude of about 300 m (Benito and O'Connor, 2003); large erratic boulders of Northern Rocky Mountain provenance were ice-rafted into the valley and stranded.

Mount Hood lies 40 km south-southwest of Panorama Point. Much closer (14 km) and nearly in line with it is Middle Mountain, which is underlain by CRBG. The field trip route passes through the gap east of Middle Mountain whereas Hood River wraps around its west side. Cinder cones and lava flows of latest Pliocene and Pleistocene age dot the valley. Lava flows from Booth Hill (fig. 12), which are crossed by O.R. 35 east of Middle Mountain, have K-Ar ages of 2.07±0.60 Ma and 167±88 ka (Conrey and others, 1996; McClaughry and others, 2012). Upper Hood River Valley lies south of Middle Mountain, out of view from Panorama Point. The geomorphic and structural setting of the two valleys is similar.

Travel

Leave Panorama Point heading south (right) and drive about 0.5 mi to intersection with Whiskey Creek Drive. Turn right and proceed 0.5 mi to O.R. 35. Turn left onto O.R. 35, cross under Mount Hood Railroad overpass, and pull into wide gravel-covered area immediately on right. There is little room for people and trains (passenger, freight, and maintenance), so check with the railroad (https://www.mthoodrr.com/rides/) before visiting this site. Exposures lie a short distance south along track as it descends into an inner gorge of Hood River. Beware of poison oak, which grows on the slopes above and below the tracks along with friendly oaks.

Stop 2. Hood River Lahar

Location: 45.6812° N., 121.5072° W.; UTM 10T 616260E, 5059490N; altitude 400 ft

Cuts along the Mount Hood Railroad below O.R. 35 expose deposits (fig. 13) of a lahar from Mount Hood that swept through this inner gorge of Hood River, crossed the Columbia River valley, and flowed at least 4 km up the White Salmon River valley on the Washington side (Vallance, 1999). The White Salmon River drains Mount Adams volcano, but the presence of amphibole-phyric andesite clasts indicates that Mount Hood, rather than Mount Adams, is the lahar's source. The lahar reached an altitude at Stop 2 of at least 400 ft (adjacent river channel is at 200 ft). At the mouth of the White Salmon valley, the deposits reach an altitude of 350 ft, which suggests the lahar filled the Columbia River valley, at least temporarily, more than 330 ft (100 m) deep. The massive lahar deposit is locally tens of meters thick and contains wood fragments that have radiocarbon ages >38 ka. Along this cut, the lahar deposit has a thickness of about 20 m (no more than half is exposed in any single place) and lies on bouldery alluvium. The lahar deposit is overlain by poorly exposed sandy Missoula-flood deposits of latest Pleistocene age.

The Hood River lahar contains clasts of volcanic rocks, many of which are from sources other than Mount Hood. By the time it had reached this site 45 km downstream from Mount Hood, the lahar had incorporated material from deposits along the valley, including large rounded boulders (fig. 13*C*). A substantial fraction of fresh, subangular to subrounded, dense to vesicular, porphyritic andesite clasts in the deposit are thought to originate from Mount Hood on the basis of mineralogy, fresh appearance, and chemistry. Fragile intraclasts (fig. 13*C*) as large as several meters in diameter are composed of volcanic diamict. From paleomagnetic evidence, Vallance (1999) showed that some of these intraclasts are composed of pyroclastic-flow deposits. Clasts collected from the Hood River lahar deposit at two localities (not Stop 2) yielded K-Ar ages of 61±21 ka and a more precise 109±9 ka; a sandy lahar deposit immediately below the Hood River lahar at the latter locality yielded an age of 120±11 ka. These ages coupled with weathering and soil evidence suggest an age of roughly 100 ka.

The lahar-deposit matrix contains 7–9 percent clay-size fraction of plagioclase, smectite, and, locally, kaolinite (Vallance, 1999); hydrothermally altered and stained andesite clasts are common. Such lahars originate as debris avalanches of weakened, altered, water-rich masses from the upper flanks of volcanoes. At later stops we will discuss a likely source area.

Deposits of the Hood River lahar are found near present river level and reached a modest altitude (<20 m?) above exposures at Stop 2. If the lahar flowed down a valley of similar size to the current one, the minimum cross-sectional area of the flow would have been about 23,000 m^2. The empirical relationship developed by Iverson and others (1998) linking lahar cross-sectional area and volume suggests the Hood River lahar was on order of 10^8 m^3 (23,000 m^2=$0.05V^{2/3}$; yielding 0.3 km^3).

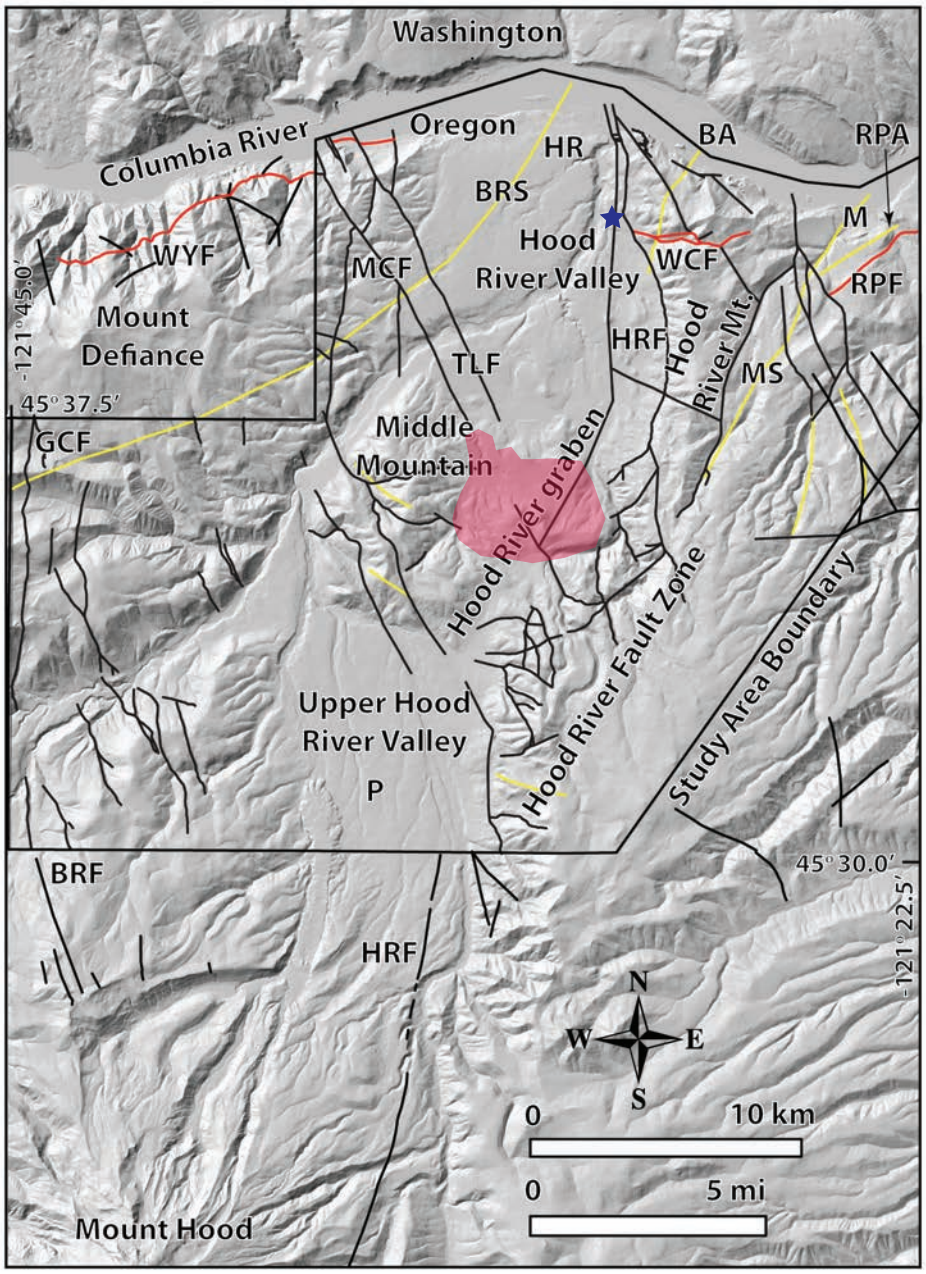

EXPLANATION

Lava flows of Booth Hill volcano
Thrust fault
Fault lineament
Yakima Fold Belt —axes of major folds
Panorama Point (Stop 1)

Other features

BA	Bingen anticline
BRF	Blue Ridge Fault
BRS	Bull Run syncline
GCF	Gate Creek Fault
HR	City of Hood River
HRF	Hood River Fault
M	Mosier
MCF	Mitchell Creek Fault
MS	Mosier syncline
P	Parkdale
RPF	Rocky Prairie Fault
TLF	Tunnel Lake Fault
WCF	Whiskey Creek Fault
WYF	Wygant Fault

Figure 12. Physiographic map of Hood River and Upper Hood River Valleys showing mapped fault lineaments and thrust faults. Figure modified from McClaughry and others (2012, fig. 3).

Figure 13. Photographs of Hood River lahar at Stop 2. *A*, View of north end of railroad cut. *B*, Photograph of diamict showing fines-rich matrix with yellowish cast imparted by content of hydrothermal minerals. *C*, Photograph showing well-rounded boulder incorporated from Hood River alluvium and fragile intraclast (light-gray mass below left of round boulder) of Mount Hood pyroclastic-flow deposits.

Travel

Continue south on O.R. 35 to the community of Mount Hood, and turn right on O.R. 281 toward Parkdale, cross East Fork Hood River, and ascend through a series of poorly exposed lahar deposits (including the Hood River lahar) to a broad upland surface covered with orchards. At intersection bear right on Base Line Road (continuation of O.R. 281) toward Parkdale. Parkdale has the last food store and gas station along the route until Government Camp. Turn left on Clear Creek Road at west end of Parkdale, just after crossing railroad tracks. Drive one mile south of Parkdale and turn right (west) on Culbertson Road, which ends at Lava Nursery, (541) 352-7307. Check at office regarding access to Parkdale lava flow. Best route to lava flow is due west of office complex.

Stop 3. Andesite of Parkdale

Location: 45.5029° N., 121.6143° W.; UTM 10T 608260E, 5039533N; altitude 1,880 ft

The Parkdale lava flow, dated at 7.7 ka (Harris, 1973), is the youngest eruption of a Cascade regional volcano between Mount Adams and Mount Jefferson. The flow erupted from a linear vent flanked by agglutinate and scoria and moved down

the ancestral Middle Fork Hood River valley about 7 km (fig. 14*A*). The vent lies about 12 km from the summit of Mount Hood. The blocky flow (fig. 14*B*) has a volume of 200–300 $\times 10^6$ m^3, with an average thickness of about 45 m. Eleven analyses of Parkdale lava reveal a limited compositional range of 58.3–58.8 percent SiO_2; 1.1–1.2 percent K_2O. Although the compositional range of the andesite of Parkdale is narrow, the petrography shows two assemblages. All samples contain plagioclase and orthopyroxene phenocrysts in a groundmass as well as a microphenocryst assemblage of plagioclase, orthopyroxene, clinopyroxene (<1 percent), and either heavily resorbed amphibole (1–2 percent) or subhedral olivine (1–2 percent), but seemingly not both.

The age of the Parkdale lava flow (~7.7 ka) is roughly coeval with the eruption of Mount Mazama that created Crater Lake caldera. On Mount Hood, original fall thickness of Mazama tephra is about 5 cm, but the stratigraphic relation of the tephra to the Parkdale lava flow is uncertain. Mazama tephra has not been found on the surface of the Parkdale lava flow, but preservation is unlikely on the coarse blocky top, nor is it present in the single site that exposes the flow's base.

Travel

Return east on Culbertson Road, cross Clear Creek Road and continue 0.5 mi; turn right (south) on Cooper Spur Road. At 4.3 miles south of Culbertson Road, pass a small outcrop of basaltic andesite (55.7 percent SiO_2; 0.69 percent K_2O) of the regional Cloud Cap volcano (424 ka). About 1.6 mi farther south, turn right on gravel-surfaced Forest Road 3511 (F.R. 3511); at the top of the grade there are views to north of Mount Adams. Stop 4 is in an idle rock quarry about 1.2 mi from Cooper Spur Road.

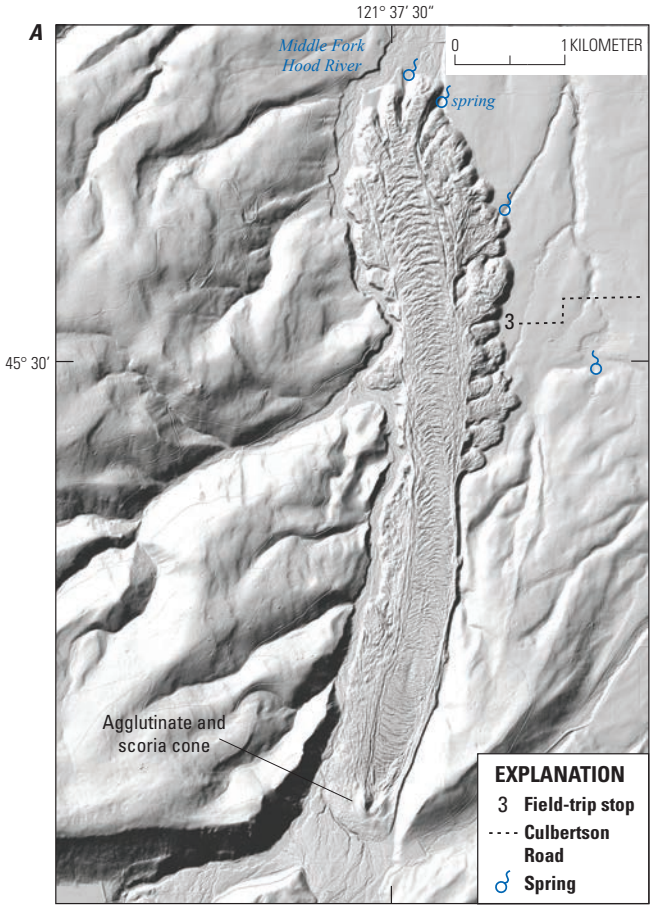

Base from 2010 Oregon Department of Geology and Mineral Industries, Oregon Lidar Consortium, Mount Hood lidar data quadrangle series, hillslope-shaded, bare-earth elevation model, 3 ft interval; Dee, Dog River, Mount Hood North, and Parkdale quadrangles

Figure 14. Andesite of Parkdale (Stop 3). *A*, Shaded-relief lidar image of flow showing lobes, levees, and flow ridges. Average thickness of flow is about 45 m. The number 3 marks field-trip stop at Lava Nursery. Middle Fork Hood River follows west (left) margin of flow. Note small pre-flow terrace remnant at east side of snout and springs emerging from margin of flow. *B*, Photograph showing typical fresh blocky surface of lava flow.

Stop 4. Quarry in Lower Pleistocene Basalt of Tilly Jane; View of North Flank of Mount Hood

Location: 45.4411° N., 121.6099° W.; UTM 10T 608719E, 5032675N; altitude 3,680 ft

The basalt of Tilly Jane (r5tj) comprises at least three separate, and not necessarily coeval or genetically related, bodies of basalt and minor basaltic andesite. The quarry flow forms a broad, gently north-sloping surface that has locally steep and embayed eroded east and west margins (fig. 15). The surface is likely part of a shield volcano whose vent is obscured. Well-weathered, poorly exposed diamicts (probably glacial and volcanic) bury much of southwestern part of this surface. A sample from the east margin south of the quarry has a K-Ar age of 2.5 Ma and reversed magnetic polarity (D=163°, I = -63.0°). Four analyses of the flow show little variation, 50.7–50.9 percent SiO_2 and about 1.0 percent K_2O, among the most mafic Pleistocene lavas in the region. Samples contain phenocrysts of plagioclase (10 percent) and olivine (2 percent) in a groundmass of chiefly plagioclase and iron-titanium oxides (fig. 16).

The top of the northeast quarry wall has a good view of Mount Hood (fig. 17) about 10 km to the southwest. Except for minor tephra fallout and modest rock avalanches and lahars from steep upper slopes, this flank was not affected directly by late Holocene eruptions from the breached crater south of the summit ridge. The Hood River lahar that was discussed at Stop 2 originated from a debris avalanche on Mount Hood's upper north flank at roughly 100 ka. Much of the upper part of the volcano is younger than that, so morphological evidence of any avalanche scar is now obscured. Barrett Spur is a thick, fin-shaped sequence of lava flows that was likely emplaced in a canyon melted into a thick glacier.

The basalt of Tilly Jane is the product of what we call a regional volcano (fig. 18), which we distinguish from a major composite volcano such as Mount Hood. Regional volcanoes are probably monogenetic, relatively short-lived volcanoes that erupt primarily basaltic andesite, but locally basalt and andesite (typically <60 percent SiO_2). From here we see two other regional volcanoes, Cloud Cap (424 ka), whose vent (unexposed) was likely about 5 km northeast of the Mount Hood summit, and The Pinnacle (151 ka), about 7.5 km west-southwest of the quarry and 6 km north of the Mount Hood summit. On a K_2O versus silica plot, the lavas of many regional volcanoes shown on figure 18 form tight compositional arrays (fig. 19; units r1pk, r3lc, r4tp, r4lz, r4cc, and r5tj). More scatter appears in the remaining units, which probably combine lava flows from different sources. The 'others' category includes lavas from numerous sources distributed through the area that are not assigned to individual map units. Most regional lavas are collinear with the Mount Hood trend (figs. 3 and 19), but a few whose vents are more distant from Mount Hood have higher K_2O, including the basalt of Tilly Jane.

The relation between Mount Hood and regional lavas is unclear. The density of regional lava vents ≤500 ka appears greater in the Hood area than elsewhere within about 50 km of the volcano's summit. Is this apparent density real or a function of more detailed mapping? If real, is it because Mount Hood focuses activity in the area or do the regional volcanoes rise largely oblivious to the presence of the Mount Hood magmatic system? Are the regional lavas part of the same mixing trend that forms the andesites and dacites of Mount Hood (Kent and Koleszar, this volume)? If so, then what is the origin for chemically similar regional lavas that are not derived from the Mount Hood magmatic system? Answers to these questions await further assessment.

Whereas several regional units appear to be geographically related to the Mount Hood Fault Zone north of Mount Hood (fig. 18), to the south there are few units located near faults (which continue south of figure 18) with the exception of the ~1.4-Ma dacite of Frog Lake (Stop 15; figs. 1, 2).

Travel

Return to Cooper Spur Road, turn right (south) and drive about 3.5 mi to O.R. 35. Turn left (north) on O.R. 35 and drive about 3.5 mi to a large exposure of lava flows just before the bridge across East Fork Hood River. Parking is available on the wide shoulder of the southbound lane.

Stop 5. Basaltic Andesite and Andesite of Cloud Cap and Basaltic Andesite of Dog River

Location: 45.4641° N., 121.5749° W.; UTM 10T 611409E, 5032675N; altitude 2,240 ft. **Caution: Watch out for rockfalls.**

Cliffs and roadcuts expose two sequences of intracanyon lava flows and a clastic unit plastered against them (fig. 20). The upper sequence (two or more flows here; 55.4–55.6 percent SiO_2; 0.89–0.90 percent K_2O) forms part of the normal-polarity, plagioclase-, orthopyroxene-, and olivine-bearing basaltic andesite to andesite lava flows of Cloud Cap volcano (r4cc). The lower sequence (one flow here) is from vents high on the east rim of the canyon (basaltic andesite of Dog River; r4dr; 55.9 percent SiO_2; 1.16 percent K_2O) (figs. 18, 19). The clastic unit is composed of lahar deposits of Polallie age and outwash deposits of the last ice age that are plastered against the cliff. An extensive terrace of this sediment lies to the south, locally cut through by O.R. 35. Northward along the exposure's base, Tertiary andesite crops out below the lava of Cloud Cap near river level. The primitive road along the exposure lies over a water conduit that transports water from

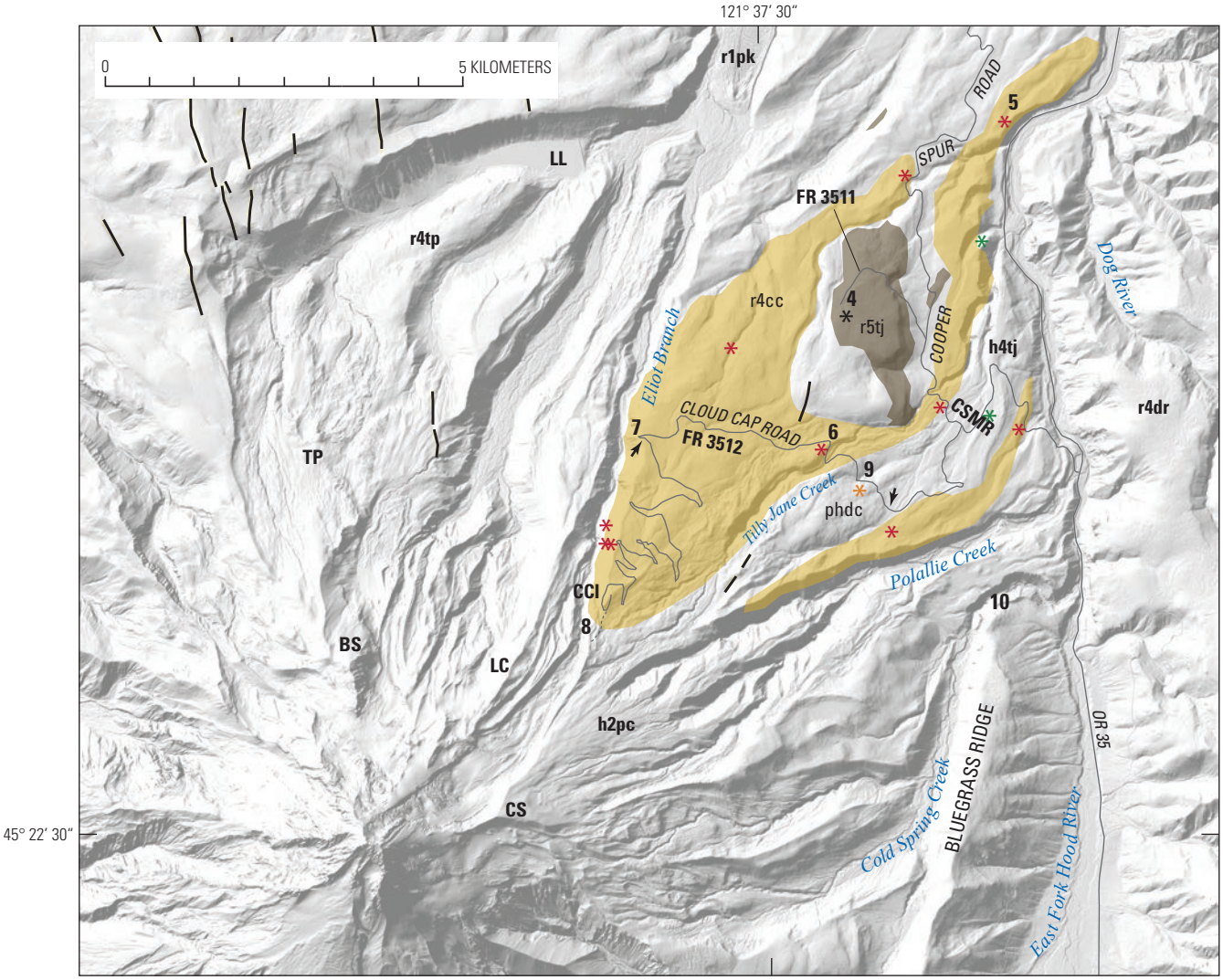

Base from 2010 Oregon Department of Geology and Mineral Industries, Oregon Lidar Consortium, Mount Hood lidar data quadrangle series, hillslope-shaded, bare-earth elevation model, 3 ft interval; Badger Lake, Dog River, Government Camp, Mount Hood North, and Mount Hood South quadrangles

EXPLANATION

- r5tj **Basalt of Tilly Jane**—2.5-Ma
- r4cc **Basaltic andesite and andesite of Cloud Cap**—424-ka

Other Features

- BS Barrett Spur
- CCI Cloud Cap Inn
- CS Cooper Spur
- CSMR Cooper Spur Mountain Resort
- LC Langille Crags
- LL Laurance Lake
- TP The Pinnacle vent
- Gate
- Fault scarp
- Paleomagnetic data
- 10 Field-trip stop
- Road
- Trail

Figure 15. Shaded-relief lidar image of northeast flank of Mount Hood and surroundings showing field-trip stops, key geologic units, and other features. Units include r5tj, 2.5-Ma basalt of Tilly Jane; phdc, 931-ka pre-Hood andesite of Doe Creek; r4dr, lower Pleistocene basaltic andesite of Dog River; h4tj, 475-ka andesite of Tilly Jane; r4cc, 424-ka basaltic andesite and andesite of Cloud Cap; r4tp, 151-ka basaltic andesite of The Pinnacle (TP marks vent); h2pc, deposits of Polallie eruptive period; r1pk, vent and south end of andesite of Parkdale. Sites of paleomagnetic data marked by colored asterisks (red, r4cc; green, h4tj; and orange, phdc); data plotted in figure 21. Ages of units represent our best estimate based on K-Ar and $^{40}Ar/^{39}Ar$ data as well as other evidence, see Note on K-Ar and $^{40}Ar/^{39}Ar$ ages, p. 5. Arrows mark gates on Cloud Cap Road that close in autumn and open in late spring to early summer depending on snow conditions.

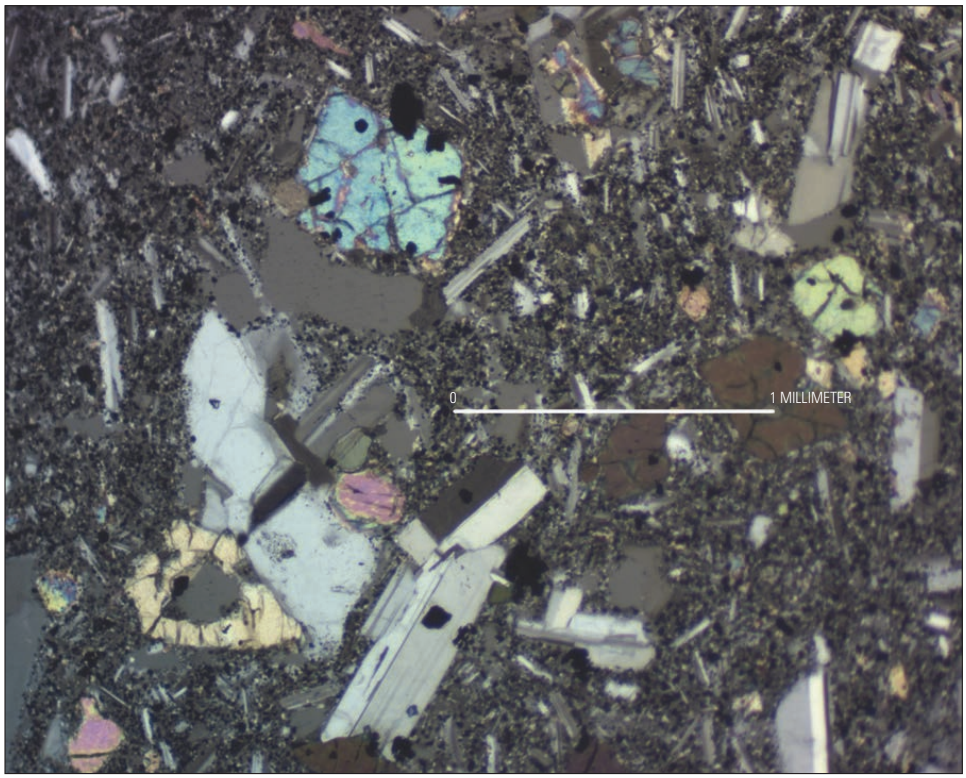

Figure 16. Photomicrograph of basalt of Tilly Jane (r5tj; sample 940616-1) showing phenocrysts of plagioclase (hues of gray) and olivine (brighter colors) with a groundmass of primarily plagioclase and iron-titanium oxides. Taken using a binocular microscope under cross-polarized light.

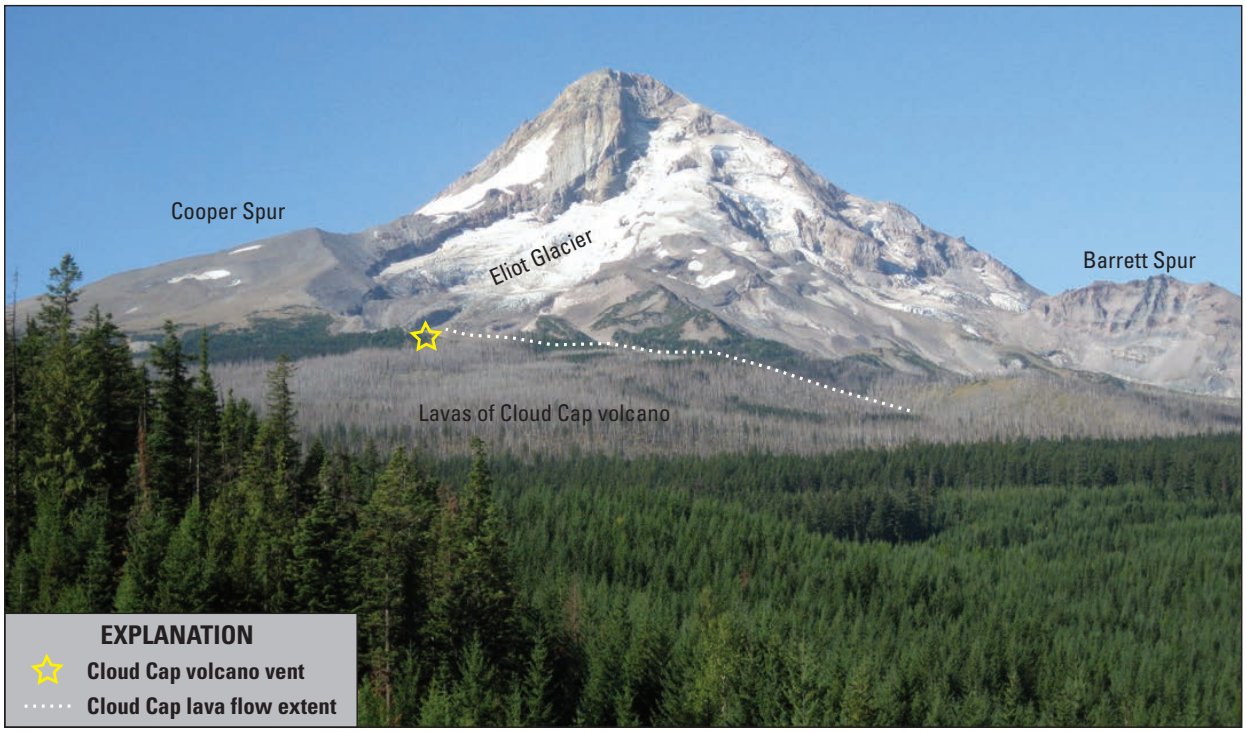

Figure 17. Photograph of Mount Hood from quarry in basalt of Tilly Jane at Stop 4. Lavas of Cloud Cap volcano (r4cc; 224 ka) were erupted from a vent probably located near present-day Cloud Cap Inn (out of view behind yellow star). Barrett Spur is formed of a thick sequence of silicic andesite to low-silica dacite lava flows (h3bs) that were probably erupted during a time of extensive glacier cover and emplaced in a narrow ice canyon. Cooper Spur is a remnant of a fan of lithic pyroclastic-flow deposits of the Polallie eruptive period, emplaced at the end of the last ice age (Crandell, 1980; Thouret, 2005). The summit is formed of a cluster of andesite and dacite lava domes and stubby lava flows of late Pleistocene age. The broad area of low ridges to the right of Eliot Glacier and west of the Cloud Cap contact is formed by lava flows of the 50–30 ka andesite of Langille Crags, which is notable for its high strontium content (640–927 ppm). Dead forest is the result of recent forest fires.

Crystal Springs, which emerge at the base of the Cloud Cap lavas a short distance up the tributary canyon at the south end of the cliff.

Parts of both lava-flow sequences show evidence of emplacement against paleovalley walls in the form of fanned arrays of small columns and locally quenched glassy lava. Flowing from the southwest and entering the paleovalley occupied by the basaltic andesite of Dog River, the Cloud Cap lavas displaced the East Fork Hood River eastward to its present position. Subsequent incision cut a canyon close to present stream level by the onset of late Pleistocene glaciation. Bouldery outwash gravel of the last glaciation forms the lower part of the clastic unit that is plastered against the cliff here; the upper part consists of lahar deposits of Polallie age. Both aggraded the East Fork as much as 50 m above the present channel.

Lava flows of the Cloud Cap volcano are temporally and spatially related to the main andesitic cone-building lavas that form Mount Hood. Numerous (>10) lava flows of Cloud Cap exposed in the east canyon wall of Eliot Branch have a combined thickness exceeding 100 m (Stop 7). A sample from near the middle of the Cloud Cap sequence has an age of 424±19 ka.

Paleomagnetic directions for both basaltic andesite and andesite parts of Cloud Cap lavas are similar (figs. 21, 22). More than 10 sites were sampled at distances of 1–11 km from the presumed source area, although some sites yielded dispersions too great to be meaningful (σ_{95}>6°). The similarity in directions suggests that the entire sequence was probably emplaced within several centuries. A previous K-Ar age of 590±30 ka was obtained from a flow near the top of the Cloud Cap sequence (Keith and others, 1985), but we favor the younger age of 424 ka because Cloud Cap lavas overlie Mount Hood andesites dated at 475±14 ka and 492±15 ka.

The lower-silica group of Cloud Cap lava (fig. 22) is typically porphyritic plagioclase-olivine basaltic andesite with numerous microphenocrysts of olivine with reaction rims (fig. 23*A*). Some olivines are completely oxidized. Groundmass is plagioclase and olivine, ± orthopyroxene, ± clinopyroxene?, and iron-titanium oxides. Plagioclase phenocryts are mostly clean with sieve textures apparent only in the largest crystals. The higher-silica, andesite group is characterized by phenocrysts of plagioclase and orthopyroxene > clinopyroxene with only a trace of olivine, typically as microphenocrysts or in groundmass (fig. 23*B*).

Travel

Drive south on O.R. 35 and turn right on Cooper Spur Road. Roadcuts expose lahar deposits of the latest Pleistocene Polallie eruptive period, outwash of the last glaciation, and older diamicts. At 0.8 mi from intersection, platy andesite (58.4 percent SiO_2; 0.9 percent K_2O) of the Cloud Cap sequence is exposed in cuts (fig. 15). About 1 mi farther a small roadcut on the left exposes relatively low-silica Mount Hood andesite of Tilly Jane (h4tj; 59.7 percent SiO_2; 1.29 percent K_2O; 475±14 ka; figs. 4, 15). Continue 0.4 mi and turn left onto Cloud Cap Road across from Cooper Spur Mountain Resort (where IAVCEI field trip will spend its first night). Cloud Cap Inn, 10.3 mi ahead, does not provide any services. A Forest Service campground (fee area) near the inn has pit toilets and water. The road is paved for about 1 mi and open year round to the Cooper Spur Ski Area. The remainder is gated and opened seasonally, typically in stages (see gates, fig. 15), June through October, depending on snow conditions. Owing to seasonal travel restrictions on successively higher sections of the road, the stops beyond the gates offer partly repetitive material. Continue about 1 mi on Cloud Cap Road past gate, pass aspen-filled quarry of Stop 9, cross right-lateral moraines of the glacier of last ice age that flowed down Tilly Jane Creek valley, cross Tilly Jane Creek, and stop at small quarry at top of grade in a lava flow of the Cloud Cap volcano.

Stop 6. Quarry in Lava Flow of Cloud Cap Volcano

Location: 45.4230° N., 121.6133° W.; UTM 10T 608489E, 5030656N; altitude 4,040 ft

This small quarry provides a good exposure (fig. 24) of an andesite lava flow (58.6 percent SiO_2; 1.00 percent K_2O) of the 424-ka basaltic andesite and andesite of Cloud Cap. A lower platy-jointed zone is probably not far above the unexposed flow base. A massive upper zone has been stripped of surface breccia by glacial erosion. This lava flow is among the more silicic lava flows of Cloud Cap. In the more mafic (<56.5 percent SiO_2) Cloud Cap lavas, mafic phenocrysts and microphenocrysts are exclusively olivine; here the mafic phenocryst and microphenocryst assemblage is orthopyroxene > clinopyroxene with only trace amounts of olivine.

The paleomagnetic direction for this site, D=346.5°, I=66.4° (σ_{95}=2.3°), is very close to the mean of site means (~345°, 65°) for all of the sampled Cloud Cap lava flows (fig. 21).

Travel

Continue on Cloud Cap Road. Hummocky terrain for the next ~0.5 mi is the left-lateral moraine belt of the ice-age glacier in Tilly Jane Creek valley. Large forest fires burned through this area in 2008 and 2011. About 2 mi from Stop 6, the road makes a hairpin turn at Inspiration Point. Park in barren area on the inside of the turn. Walk a short distance west of the guardrail to points with a clear view up the valley.

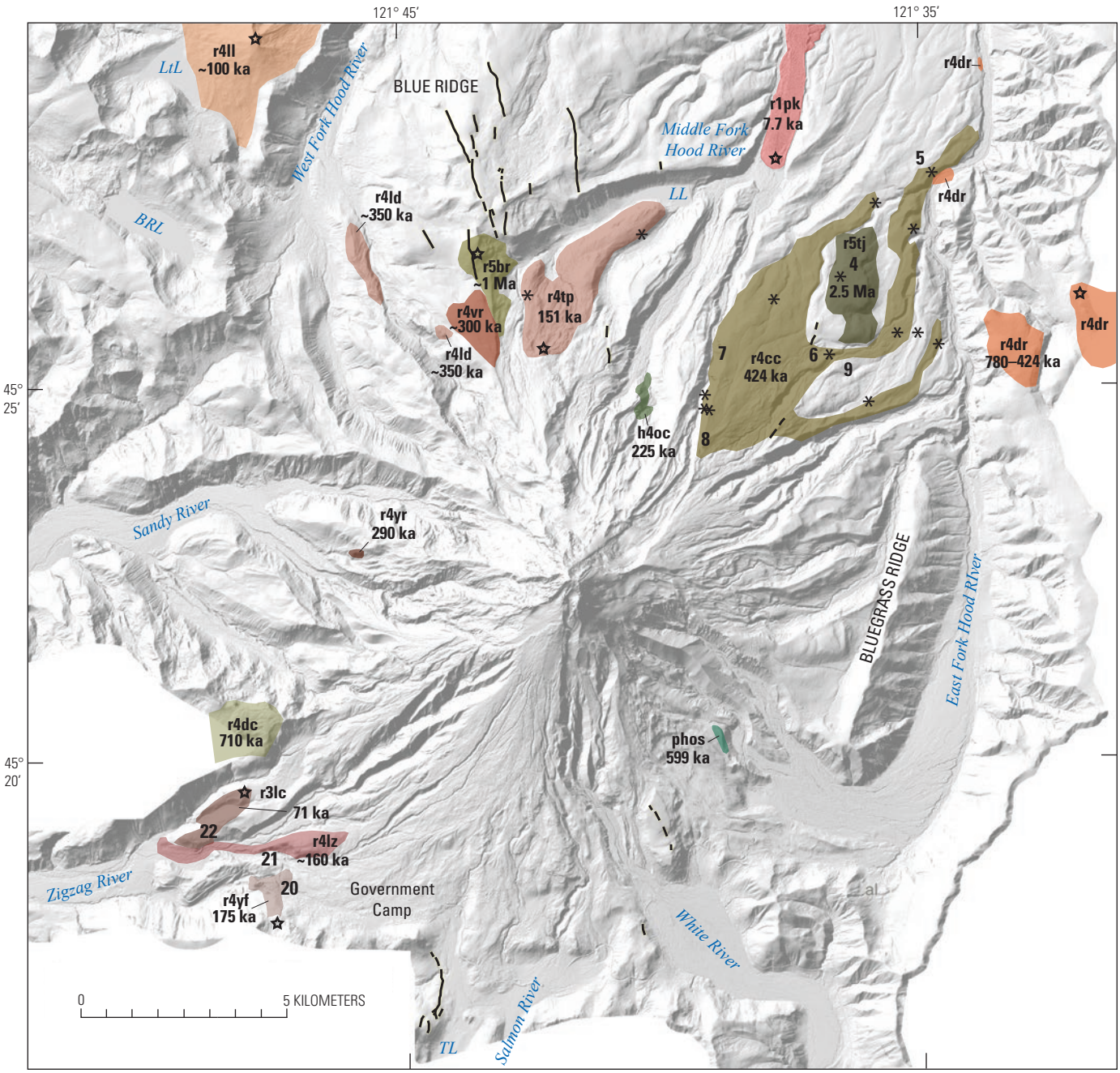

Base from 2010 Oregon Department of Geology and Mineral Industries, Oregon Lidar Consortium, Mount Hood lidar data quadrangle series, hillslope-shaded, bare-earth elevation model, 3 ft interval; Badger Lake, Bull Run Lake, Dog River, Government Camp, Mount Hood North, and Mount Hood South quadrangles

EXPLANATION

- r1pk — Andesite of Parkdale
- r3lc — Andesite of Lady Creek
- r4ll — Basaltic andesite of Lost Lake Butte
- r4tp — Basaltic andesite and andesite of The Pinnacle
- r4lz — Basaltic andesite and andesite of Little Zigzag River
- r4yf — Andesite of Yocum Falls
- r4yr — Andesite of Yocum Ridge
- r4vr — Basaltic andesite and andesite of Vista Ridge
- r4ld — Basaltic andesite of Ladd Creek
- r4cc — Basaltic andesite and andesite of Cloud Cap
- r4dr — Basaltic andesite of Dog River
- r4dc — Basaltic andesite of Devils Canyon
- r5br — Basalt and basaltic andesite of Blue Ridge
- r5tj — Basalt of Tilly Jane
- h4oc — Olivine basaltic andesite and andesite of Compass Creek
- phos — Olivine basaltic andesite of Shooting Star
- Fault scarp—Quaternary
- Paleomagnetic data
- Known or suspected vents
- 10 — Field-trip stop

Figure 18. Shaded-relief lidar image showing lavas of regional Quaternary volcanoes in the Mount Hood area, as well as known or suspected vent locations. Ages of units represent our best estimate based on K-Ar and $^{40}Ar/^{39}Ar$ data as well as other evidence, see Note on K-Ar and $^{40}Ar/^{39}Ar$ ages, p. 5. In approximate order of increasing age: r1pk, andesite of Parkdale; r3lc, andesite of Lady Creek; r4ll, basaltic andesite of Lost Lake Butte; r4tp, basaltic andesite and andesite of The Pinnacle; r4lz, basaltic andesite and andesite of Little Zigzag River; r4yf, andesite of Yocum Falls; r4yr, andesite of Yocum Ridge; r4vr, basaltic andesite and andesite of Vista Ridge; r4ld, basaltic andesite of Ladd Creek; r4cc, basaltic andesite and andesite of Cloud Cap; r4dr, basaltic andesite of Dog River; r4dc, basaltic andesite of Devils Canyon (Sherrod and Scott, 1995); r5br, basalt and basaltic andesite of Blue Ridge (only vent north of Vista Ridge shown; other vents to north are as young as middle Pleistocene); r5tj, basalt of Tilly Jane. Also shown are two bodies of olivine-bearing lava assigned to Mount Hood and pre-Hood volcano that may instead be from regional vents on flanks; h4oc, olivine basaltic andesite and andesite of Compass Creek; phos, olivine basaltic andesite of Shooting Star. LtL, Lost Lake; LL, Laurance Lake; BRL, Bull Run Lake.

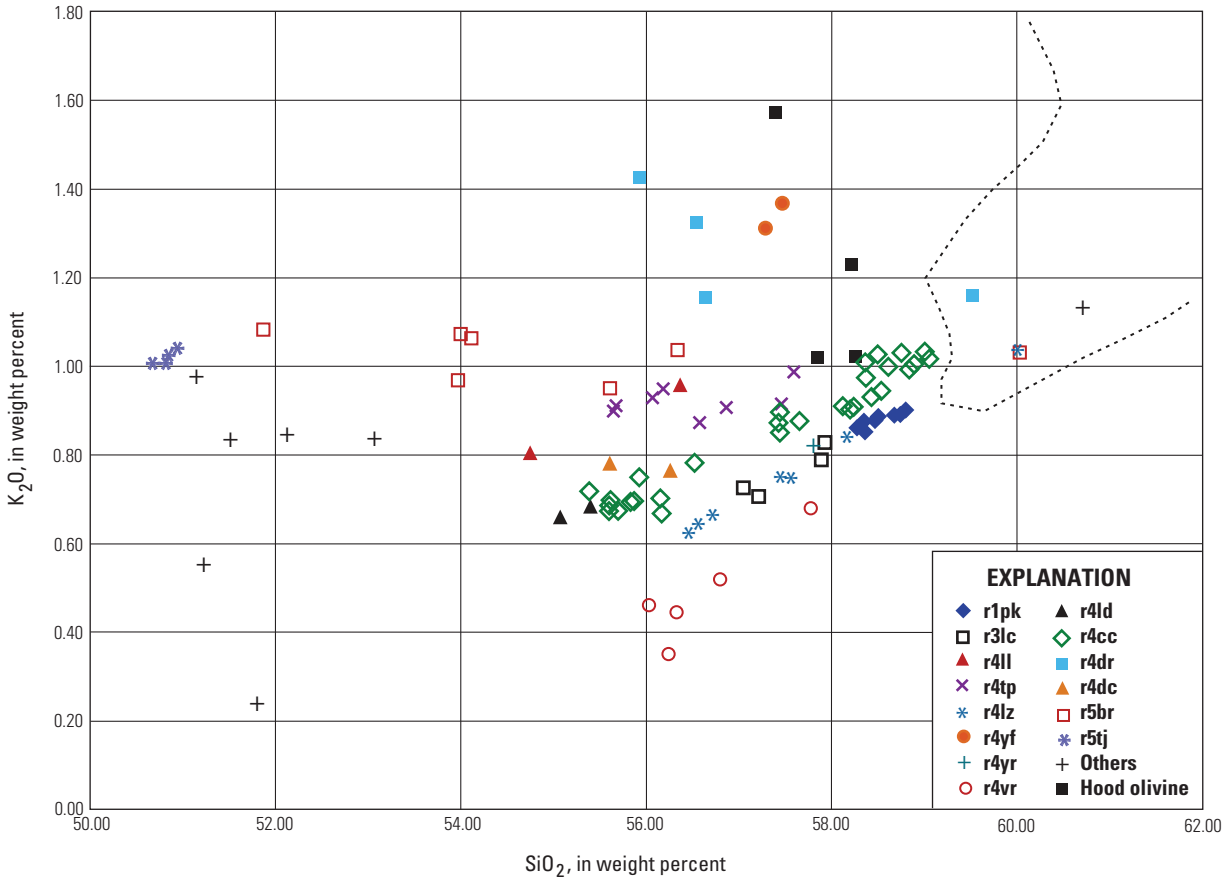

Figure 19. Plot of K_2O versus silica (volatile free) for regional lavas of Quaternary age surrounding Mount Hood. Others category includes samples of several units scattered through area. Dashed black line encloses bulk of analyzed samples of Mount Hood lava less than 62 weight percent SiO_2; a few scatter outside of the line, such as the olivine bearing lavas of Compass Creek and Shooting Star (Hood olivine). Known vents of regional volcanoes are primarily within 12 km of Mount Hood's summit; about half of unknown vents lie within 6 km. Data from Bargar and others (1993) and this study. r1pk, andesite of Parkdale; r3lc, andesite of Lady Creek; r4ll, basaltic andesite of Lost Lake Butte; r4tp, basaltic andesite and andesite of The Pinnacle; r4lz, basaltic andesite and andesite of Little Zigzag River; r4yf, andesite of Yocum Falls; r4yr, andesite of Yocum Ridge; r4vr, basaltic andesite and andesite of Vista Ridge; r4ld, basaltic andesite of Ladd Creek; r4cc, basaltic andesite and andesite of Cloud Cap; r4dr, basaltic andesite of Dog River; r4dc, basaltic andesite of Devils Canyon (Sherrod and Scott, 1995); r5br, basalt and basaltic andesite of Blue Ridge; r5tj, basalt of Tilly Jane.

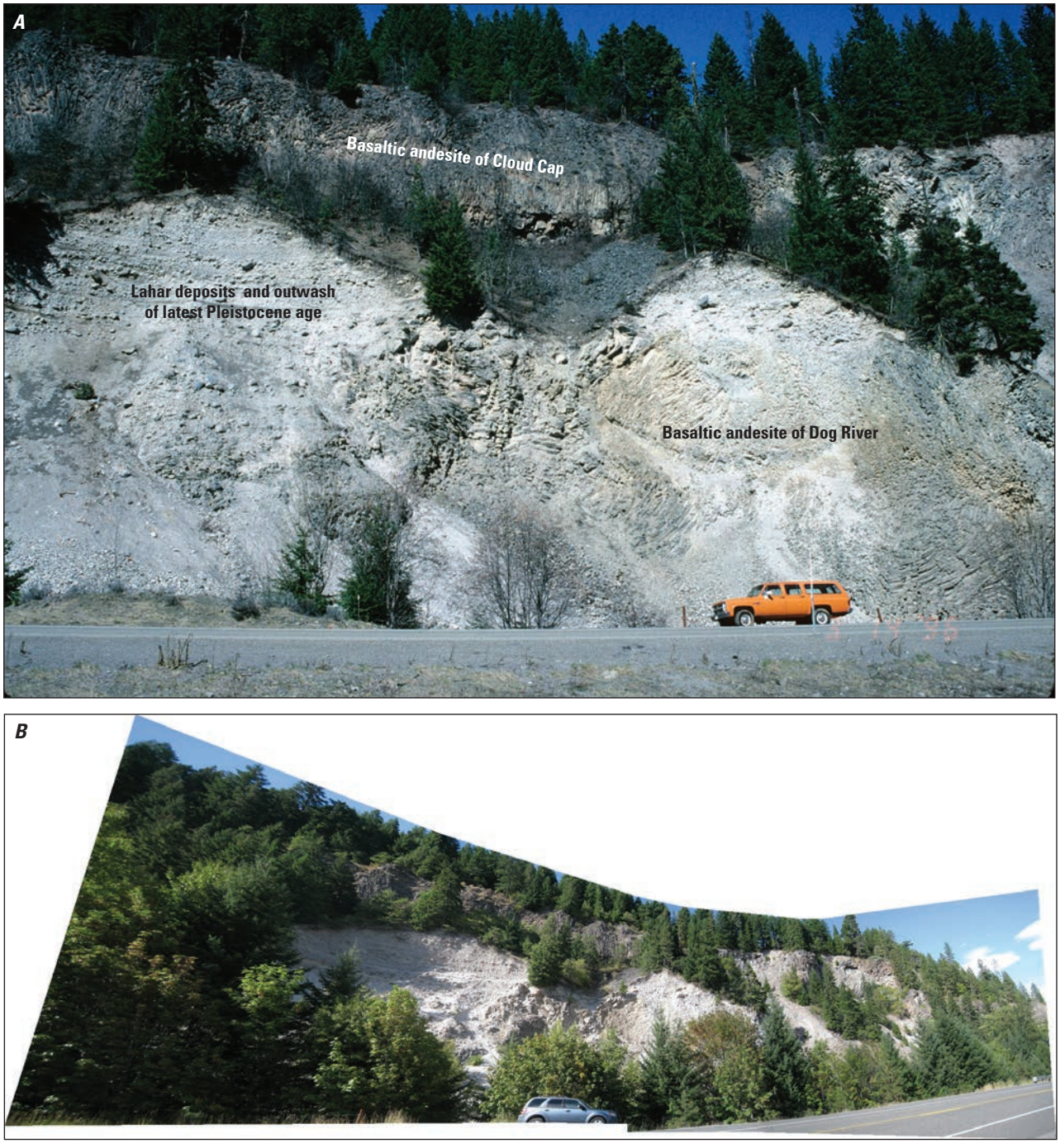

Figure 20. Photographs of exposure at Stop 5 along O.R. 35 showing basaltic andesite lava flows of the 424-ka basaltic andesite and andesite of Cloud Cap overlying basaltic andesite of Dog River. Lahar deposits and outwash are remnant of sediment fill in valley during last ice age plastered against cliff. *A*, View of outcrop in May 1994 prior to regrowth of roadside trees. *B*, Panorama of broader view from 2014 (vehicles are parked in approximately same place). Basaltic andesite of Cloud Cap thickens at north end of exposure where it directly overlies andesite of Tertiary age. Both units have fanned columnar joints indicative of cooling against paleovalley walls.

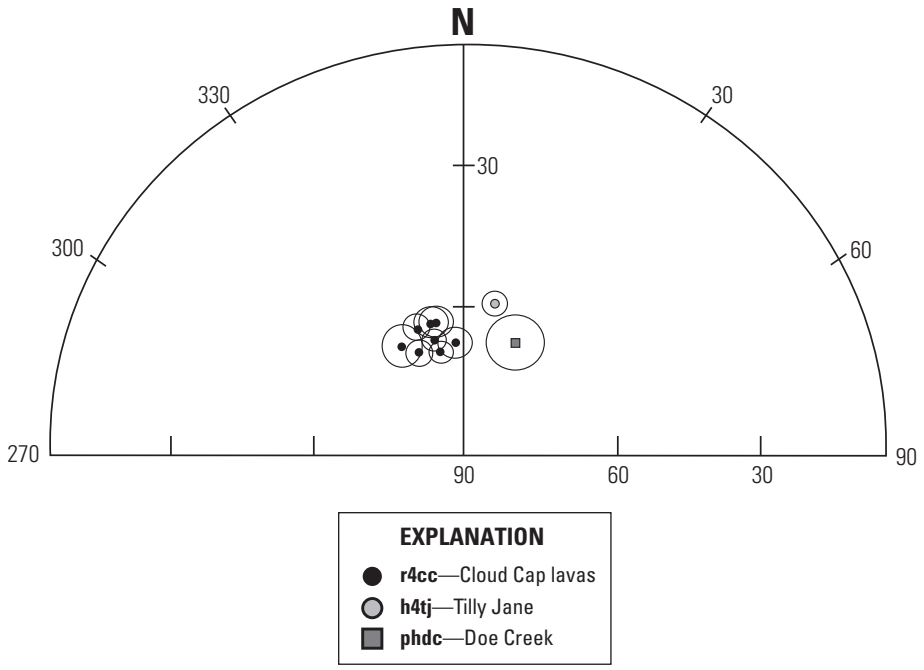

Figure 21. Upper-hemisphere plot of paleomagnetic directions for 424-ka basaltic andesite and andesite of Cloud Cap (r4cc; mean of site means is about D=345°, I=65°), ~475-ka andesite of Tilly Jane (h4tj; D=11°; I=59°), and ~931-ka pre-Hood andesite of Doe Creek (phdc; D=23.6°, I=64.5°). Note that pre-Hood andesite of Doe Creek has normal polarity, even though its age lies within the reverse-polarity Matuyama Chron. The similarity of directions for Cloud Cap lavas suggests that the entire sequence was probably emplaced within several centuries.

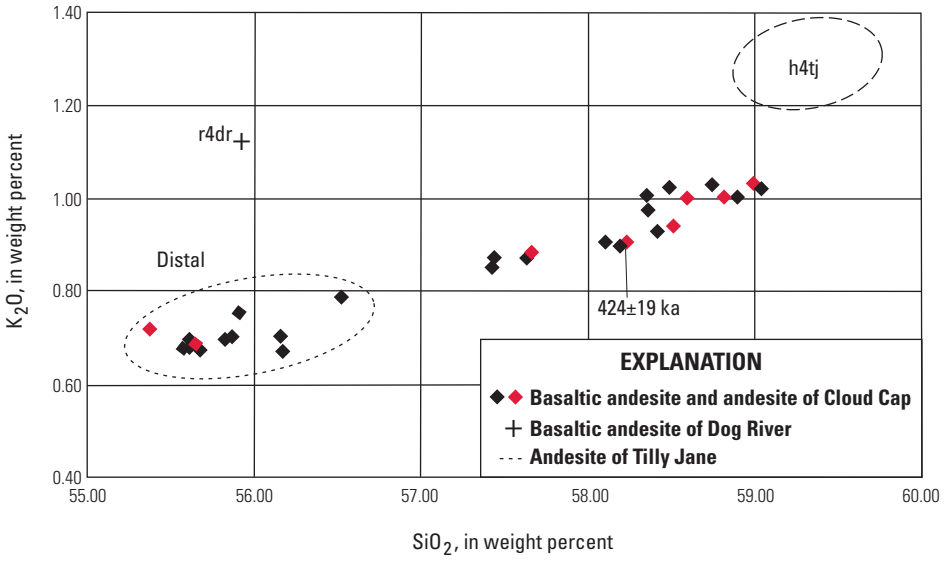

Figure 22. Plot of K_2O versus silica for samples of basaltic andesite and andesite of Cloud Cap; red symbols mark samples collected at or near sites with paleomagnetic data. Distal group consists primarily of samples collected 8–11 km from inferred vent, a few are from closer in, but at base of section along Eliot Branch. Also shown is sample of basaltic andesite of Dog River (r4dr) from Stop 5 and line that encloses field of analyses of 475-ka andesite of Tilly Jane (h4tj).

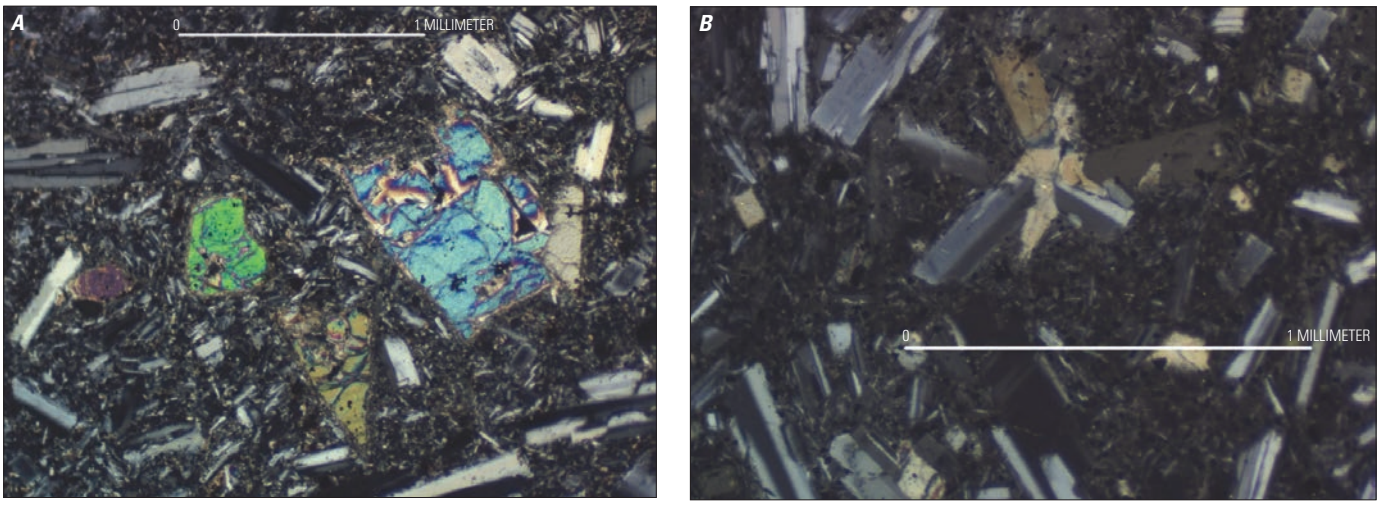

Figure 23. Photomicrographs of samples representing higher- and lower-silica groups of basaltic andesite and andesite of Cloud Cap (fig. 22). *A*, Sample of basaltic andesite (r4cc; 55.6 percent SiO_2; sample 940609-2) displays mafic phenocrysts and microphenocrysts that are exclusively olivine. Viewed with a binocular microscope under cross-polarized light. *B*, Sample of andesite (r4cc; 58.5 percent SiO_2; sample 940818-1) showing orthopyroxene as the dominant mafic phenocryst. In the more silicic Cloud Cap lavas the mafic phenocryst and microphenocryst assemblage is orthopyroxene > clinopyroxene with only trace amounts of olivine, mostly as microphenocrysts or in the groundmass. Viewed with a binocular microscope under cross-polarized light.

Figure 24. Photograph of Stop 6 at small quarry along Cloud Cap Road in andesite lava flow of Cloud Cap volcano, showing characteristic lower platy jointing and more massive upper part. Any surface breccia that was originally present has been removed by glacial erosion. Sample from here has 58.6 percent SiO_2 and is representative of proximal lavas. Paleomagnetic data was also obtained from this site, see text.

Stop 7. View Up Eliot Branch From Inspiration Point

Location: 45.4244° N., 121.6474° W.; UTM 10T 605820E, 5030773N; 4,580 ft altitude

Inspiration Point is on the east rim of the narrow canyon of Eliot Branch with a good view to Mount Hood (fig. 25). A lateral moraine of the last glacial maximum drapes the rim, overlying about 160 m of lava flows of Cloud Cap volcano (r4cc). We have analyzed 11 lava flows in 2 sections of the east canyon wall. Five flows from a section 700 m up canyon from Stop 7 show an up-section increase in silica (56.5–58.8 percent) and a consistent increase in K_2O (0.78–1.03 percent). Six flows from a section 1.5 km up canyon near Cloud Cap Inn have a smaller compositional range, with silica increasing crudely up section (57.4–59.0 percent) and K_2O increasing up section consistently (0.87–1.03 percent). Paleomagnetic data on flows through the section have essentially the same secular-variation direction (fig. 21) implying relatively rapid emplacement (less than a few centuries).

Across the canyon, at least two lava flows of high-strontium (744–867 ppm) Mount Hood andesite of Langille Crags (61.5–62.6 percent SiO_2; 1.67–1.91 percent K_2O) crop out locally below till. Flows of this unit can be traced as high as Snowdome, where ages are as young as ~30 ka. A sample of the upper lava flow from about 800 m down canyon yielded a K-Ar age of 42±7 ka and a $^{40}Ar/^{39}Ar$ age of 48.6±2.7 ka. Rim to rim, the canyon is about 400-m wide, 165-m deep, straight, and U-shaped—a narrow glacial valley eroded along the contact between Langille Crags and Cloud Cap lava flows. The ~50 to ~30-ka age of the andesite of Langille Crags suggests that this part of the canyon was occupied by a glacier only during the last major glaciation. Andesite of Wallalute Falls, 492±15 ka, is the oldest unit we assign to Mount Hood volcano. The sequence of diamicts exposed recently by high

Figure 25. Photograph of view to south looking up narrow, U-shaped glacial valley of Eliot Branch toward Mount Hood from Inspiration Point (Stop 7). Valley is eroded along contact between ~424-ka basaltic andesite and andesite of Cloud Cap on east and 50–30-ka andesite of Langille Crags on west. Both overlie the 492-ka andesite of Wallalute Falls.

flows in Eliot Branch has not been studied and its stratigraphic position is uncertain. It may all be remnants of a thick valley fill of deposits of Polallie age that followed the last glaciation. Alternately some may pre-date one or more of the lava flows.

Travel

Continue on Cloud Cap Road. The deep gully heading up slope that the road crosses several times was the old wagon and automobile road to Cloud Cap Inn. Roadcuts expose diamicts and in a few places, lava of Cloud Cap volcano. At T-intersection after about 5 mi and 9 switchbacks, turn right. Cloud Cap Inn, campground, and parking areas lie about 0.7 mi ahead.

Stop 8. Cloud Cap Inn

Location: 45.4048° N., 121.6529° W.; UTM 10T 605426E, 5028584N; 5,920 ft altitude

Construction of Cloud Cap Inn began in March 1889 and the first guests registered on August 6 of that year (Grauer, 1975). The inn was operated by Sarah Langille, "Lady of the Mountain," and her two sons. The younger, Will, reportedly took only 10 hours to circle the volcano in 1893, crossing all 9 named glaciers. The inn was evidently a rocky business venture and never terribly successful. Attempts were made in the 1920s to build a more grandiose four-story inn, a cable railway from Cloud Cap Inn to Cooper Spur, and an aerial tramway from Cooper Spur to the summit. Environmentalists of the day opposed the idea, but it took the Great Depression to quash the proposed development. The inn languished until the 1950s when the Forest Service gave the Hood River Crag Rats, a local mountaineering and search-and-rescue organization, use of the building under a special-use permit. The Crag Rats saved the building from further decay and in 1974 the inn was put on the National Register of Historic Places. The Crag Rats continue to repair and refurbish the inn.

With good visibility three other major Cascade volcanoes are visible to the north: Mount St. Helens (100 km north-northwest), Mount Rainier (165 km north), and Mount Adams (90 km north-northeast).

Several late Pleistocene units dominate the view of the volcano from Cloud Cap Inn (fig. 26). Block-and-ash-flow deposits of Polallie age that form Cooper Spur overlie a lava flow along the east margin of Eliot Glacier. The lava flow and the massive face above the glacier are composed of 35–30-ka high-strontium lava, as are masses poking out of the glacier's debris mantle, the treed ridges of Langille Crags leading to Snowdome, and the lava flow exposed along the west side of Eliot Branch. Strontium contents of these flows range from 763–1,100 ppm. The Polallie deposits are chemically distinct from the lava flows and must have been derived from a different source in the summit area. These block-and-ash flows and related lahar deposits extend to the East Fork Hood River along Polallie Creek (figs. 7, 15). Barrett Spur is a short, narrow ridge that is disconnected from the main cone and formed of a >250-m-thick lava-flow sequence of andesite and low-silica dacite. An imprecise K-Ar date (25±12 ka) suggests it is of late Pleistocene age. We infer it was emplaced in a thick glacier, perhaps during the last major glaciation. Any evidence of ice contact (quenched glassy margins, hyaloclastite, and so on) has been removed by subsequent glacial erosion and mass wasting.

The sequence of high-strontium lava flows are traceable for about 10.5 km, extending from the head of Eliot Glacier and the Snowdome past Inspiration Point (Stop 7) and along the relatively narrow divide between Eliot and Coe Branches

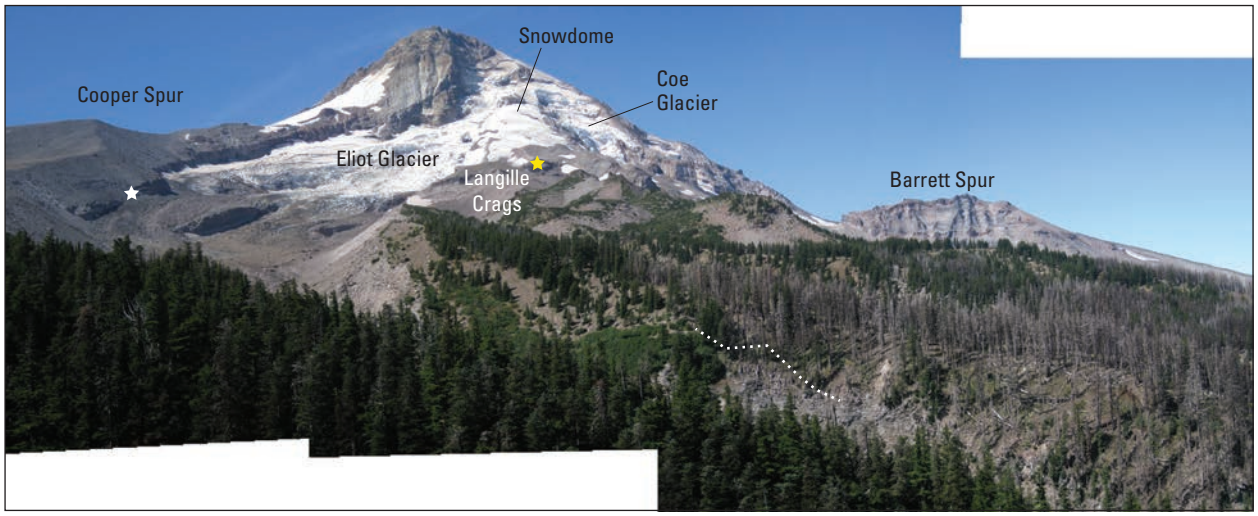

Figure 26. Merged-photographic panorama of view to Mount Hood from Cloud Cap Inn. Massive headwall of Eliot Glacier, cliff along south side of glacier, Langille Crags, Snowdome, and canyon wall in lower right are all high-strontium lava flows of andesite of Langille Crags and andesite of Texas. White star, approximate location of sample dated at 34±2 ka (K-Ar; Thouret, 2005); yellow star, location of sample with ages of 42±9 ka (K-Ar) and 31.4±3.3 ka ($^{40}Ar/^{39}Ar$); dotted white line, approximate margin of Eliot Glacier in 1901 (Reid, 1905).

to Laurance Lake Road (fig. 6). The K-Ar and $^{40}Ar/^{39}Ar$ ages suggest that the high-strontium lavas span a time period of about 10,000–20,000 years. Stop 10 is a short hike to distal outcrops of a northeasterly extension of this sequence with ages of 29±11 ka (K-Ar) and 46.1±2.2 ($^{40}Ar/^{39}Ar$) and Stop 13 has a view of a southeastern extension of the unit with ages of 25±13 ka (K-Ar) and 44.5±2.3 ka ($^{40}Ar/^{39}Ar$) (fig. 6).

Lava flows of the Cloud Cap volcano can be traced south from the inn for only a few hundred meters before they are buried beneath thick glacial deposits, but the thinness of flows and presence of agglutinate suggest the vent was not far from Cloud Cap Inn, which is about 5 km from Mount Hood's summit.

The Timberline Trail, which passes by Cloud Cap Saddle Campground, and various climbers' trails provide access to Eliot Glacier and beyond. Northwest Forest Pass is required to park May 15 to October 1. The Mount Hood Wilderness Area boundary lies just south of the campground. Hiking parties are restricted to 12 or fewer individuals and they must fill out a permit and carry it with them. Head south and east on Timberline Trail for about 150 m to a junction with a primitive climbers' trail. Bear right on the trail, which heads up steeply through forested moraines of late-glacial age. Numerous anastomosing trails exist, but head generally south-southwest until reaching the base of a steep unforested right-lateral moraine. Continue up to the moraine crest for a view up valley (location: 45.3988° N., 121.6568° W.; UTM 10T 605135E, 5027915N; 6,200 ft altitude).

Steep, barren lateral moraines mark the late-19th to early-20th century extent of Eliot Glacier during its late neoglacial (also called the Little Ice Age) advance (fig. 27). Much of the till is derived from rockfalls and rock avalanches from the steep headwall, as well as by passage of the glacier below steep slopes of unconsolidated diamicts of Polallie age below Cooper Spur. Torrential rain in early November 2006 caused Eliot Branch to deeply incise this reach above Wallalute Falls, which generated debris flows that traveled about 15 km downstream causing substantial damage. The record of retreat of Eliot and other glaciers on Mount Hood (fig. 28) is similar to that of most glaciers in the Pacific Northwest.

Numerous sections of deposits of the Polallie eruptive period are accessible from the Cloud Cap area by way of the Timberline Trail (to Cooper Spur) and Tilly Jane Trail to exposures at the head of Polallie Creek (for trail information see https://www.fs.usda.gov/Internet/FSE_DOCUMENTS/stelprdb5401659.pdf). The latter exposures are as much as 100 m high, steep, and subject to rockfall. Several figures in Thouret (2005) describe sections of Polallie deposits in the this area and over much of the east flank of the volcano.

Travel

Return down Cloud Cap Road. About 0.7 mi past the small quarry of Stop 6, park in pullout on right in old quarry overgrown with aspen trees.

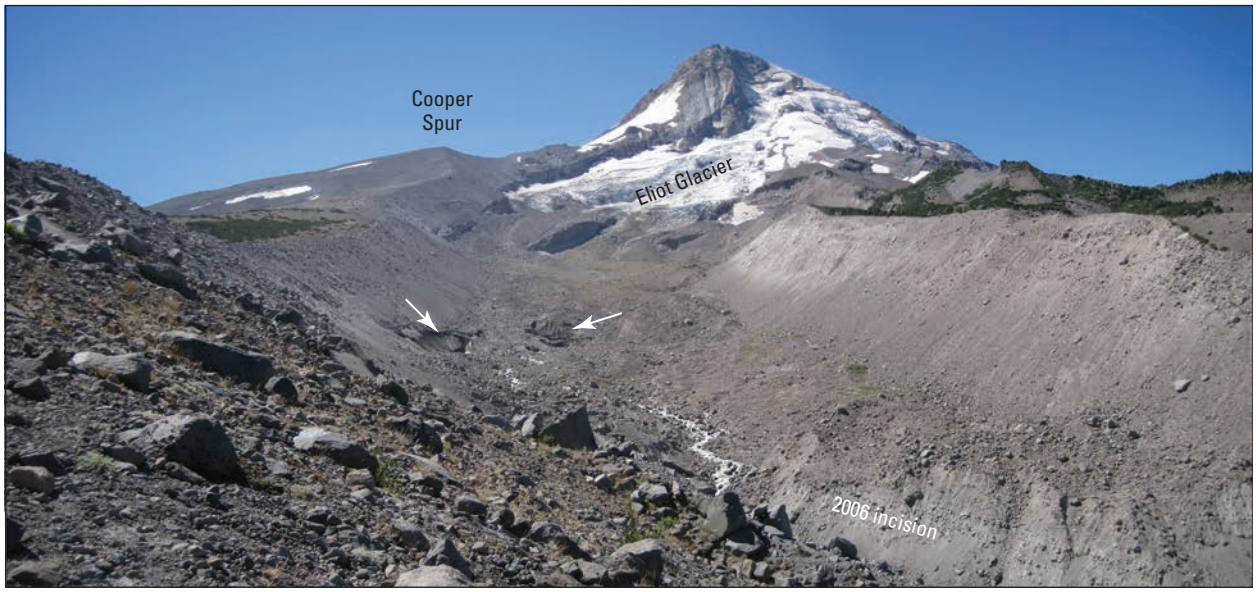

Figure 27. Merged-photographic panorama of Mount Hood from late-19th-century right-lateral moraine of Eliot Glacier. In 1901, when the earliest known photographs were taken, the snout of the glacier lay about 225 m down valley from viewpoint (fig. 26; Reid, 1905; Lilliquist and Walker, 2006). Eliot Branch emerges from tunnels (white arrows) at debris-covered snout about 800 m up valley from 1901 terminus. The continuous debris cover on more than one-half of the ablation area reduces the melting rate (Lundstrom and others, 1993), thereby permitting the glacier to maintain a greater area than under debris-free conditions. The floor of Eliot Branch was incised by as much as 30 m during storm-induced debris flows of November 2006.

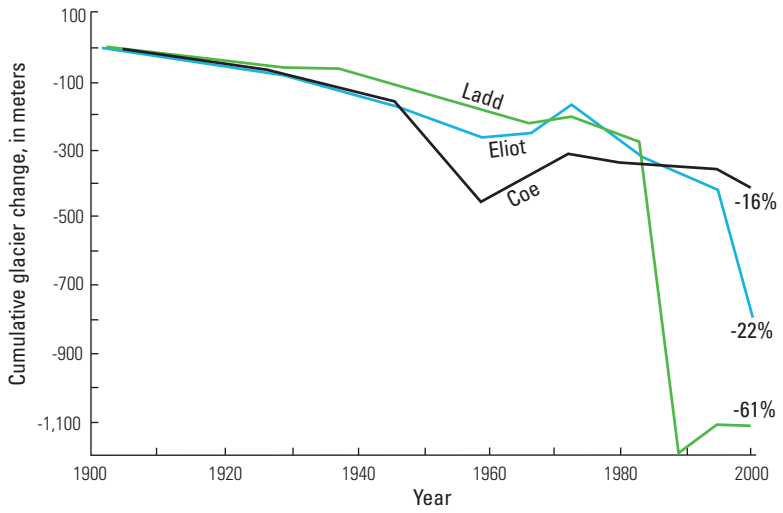

Figure 28. Graph showing cumulative change in length of Mount Hood's north-flank glaciers since beginning of photographic record in 1901 (modified from Lilliquist and Walker, 2006). Percentages are relative change in length for each glacier.

Stop 9. Pre-Hood Andesite of Doe Creek

Location: 45.4183° N., 121.6077° W.; UTM 10T 608935E, 5030148N; 3,900 ft altitude

The pre-Hood andesite of Doe Creek is a coarsely porphyritic (45 percent crystals), two-pyroxene andesite with a fine-grained groundmass (fig. 29). Plagioclase phenocrysts are mostly clear; phenocrysts to groundmass consist of plagioclase (6 percent), orthopyroxene (2 percent), clinopyroxene (1 percent), iron-titanium oxides (1 percent), largely replaced amphibole (<0.5 percent), and trace olivine (<0.2 percent).

Eruptions of pre-Hood composite volcanoes were similar in style and products to those of Mount Hood during the past 500,000 years (figs. 3, 30). Pre-Hood lava flows are found scattered on west, north, and east flanks (fig. 31). We group pre-Hood lavas into seven units that range in age from 1.5 Ma to 600 ka. Vent areas are unknown but probably lay within a couple kilometers of Mount Hood's summit. Andesite of Doe Creek has a K-Ar age of 931±15 ka and exhibits normal polarity within the reversed-polarity Matuyama Chron. Lanphere and others (1997) suggested that this and similarly dated lava flows with normal polarity from the Mount Baker area may be part of the Kamikatsura event (900.3±4.7 ka; Coe and others, 2004) or a new polarity event.

Travel

Retrace route to Cooper Spur Road, turn right on Cooper Spur Road and right (south) on O.R. 35 toward Government Camp. Cross Polallie Creek, which originates on the broad fan of pyroclastic-flow and lahar deposits of Polallie age that forms Cooper Spur on the northeast flank of Mount Hood (figs. 7, 15). Last glacial maximum (LGM) glaciers in Polallie Creek valley terminated about 1 km upstream from O.R. 35 (fig. 32).

1980 Debris Flow and Flood on Polallie Creek

Intense rainfall on Christmas Day 1980 triggered a landslide in deposits of Polallie age (h2pc) that form a steeply sloping valley head (located just north of label h2pc on fig. 15). The landslide transformed into a debris flow as it entrained material from the valley walls and channel, and entered East Fork Hood River, carrying a volume about 20 times greater than the initial landslide (Gallino and Pierson, 1985). One person was killed when the debris flow burst from Polallie Creek canyon and overran the truck in which he was sleeping at the former Polallie Creek Campground. The debris

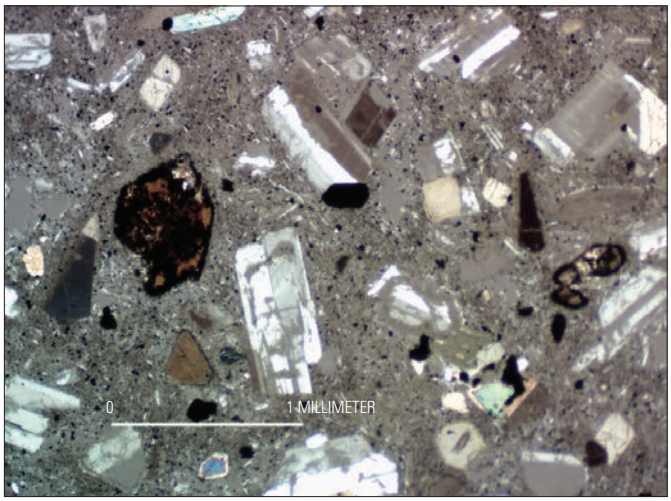

Figure 29. Photomicrograph of 931-ka pre-Hood andesite (60.8 percent SiO_2) of Doe Creek (phdc; sample 940609-1) showing porphyritic two-pyroxene lava with trace phenocrysts and microphenocrysts of amphibole (<1 percent). This image is atypical of unit owing to the high concentration of amphibole. Viewed with a binocular microscope.

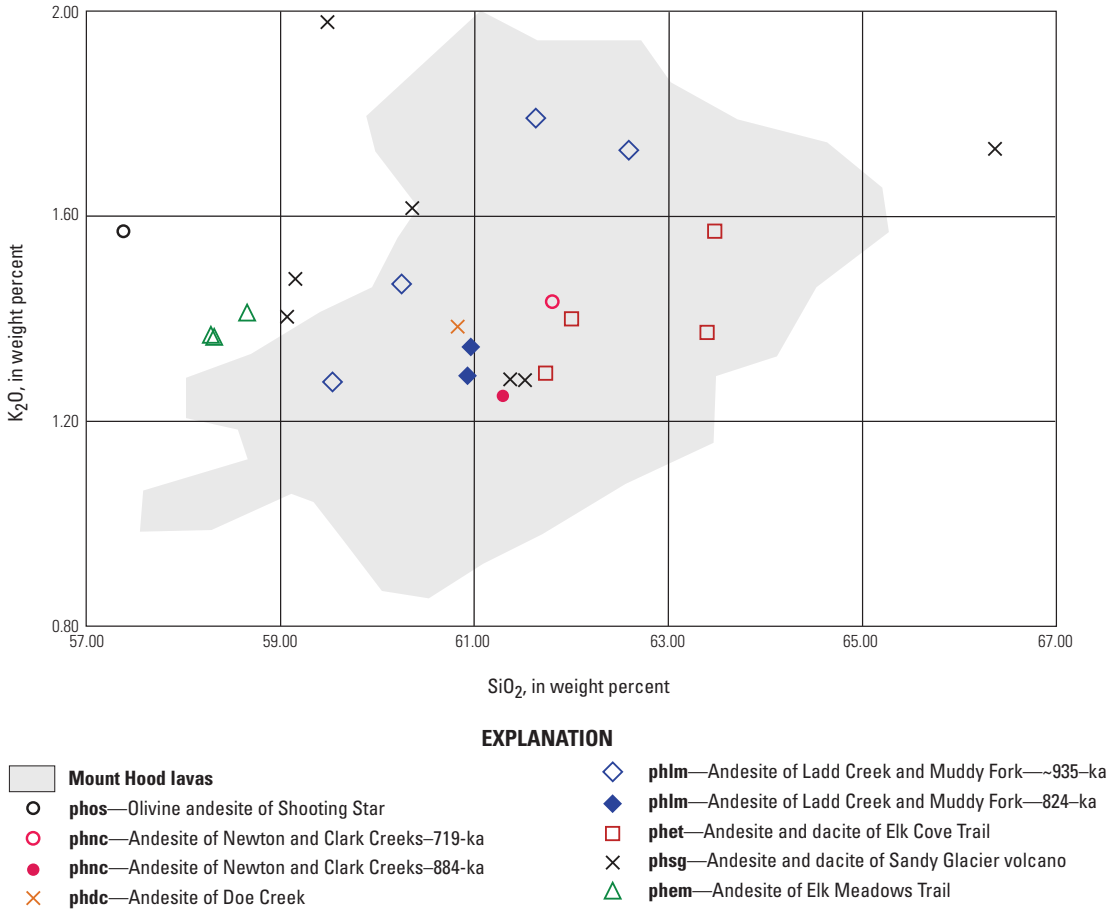

Figure 30. Plot of K_2O versus silica for lava flows and diamicts of pre-Hood composite volcanoes. Most pre-Hood analyses fall within field for Mount Hood lavas. Two units, phnc and phld, each combine rocks from two separate outcrop areas that yield different K-Ar ages.

flow came to rest at the mouth of Polallie Creek and temporarily dammed the East Fork. About 12 minutes later the dam failed and a flood surged down the East Fork, destroying about 5 mi of highway (old O.R. 35 lay close to the river) and causing a total of $13 million in damage.

For the next 1.4 mi, O.R. 35 follows a narrow canyon of East Fork Hood River whose origin is the subject of the next stop. Park in the wide turnout at the Tamanawas Falls Trailhead. Northwest Forest Pass is required to park May 15 to October 1.

Stop 10. Late Pleistocene Andesite Lava Flow of Tamanawas Falls, Part of Langille Crags-Texas Eruptive Episode of High-strontium Lava

Location of trailhead along O.R. 35: 45.3974° N., 121.5704° W.; UTM 10T 611894E, 5027869N; 3,040 ft altitude

The episode of ~20,000 year duration that ended about 30 ka, produced a series of high-strontium lava flows and fragmental deposits on the north, northeast, and southeast flanks of Mount Hood (fig. 6). Strontium contents range from about 700 to 1,100 ppm, compared to typical concentrations of 500–700 ppm for most Mount Hood lavas. The high-strontium lavas also contain some of the highest K_2O for their silica contents. We map these lavas as andesite of Langille Crags (h3lc; 60.9–62.9 percent SiO_2; 1.7–1.9 percent K_2O) and andesite of Texas (h3tx; 60.2–61.8 percent SiO_2; 1.5–1.8 percent K_2O). A small lava flow of high-strontium lava in the upper Sandy River valley on the west flank has a K-Ar age of 46±10 and a $^{40}Ar/^{39}Ar$ age of 71.3±2.5. We have no other analyses of high-strontium lava of the older age elsewhere on Mount Hood; we are undecided if it should be considered part of the same episode.

The andesite lava flow that creates Tamanawas Falls is similar in age (29±11 ka, K-Ar; 46.1±2.2 ka, $^{40}Ar/^{39}Ar$) and chemistry to the andesite of Langille Crags in lower Eliot Branch (Stop 7, fig. 25). The flow of Tamanawas Falls filled the ancestral valley of East Fork Hood River to a depth of 50–80 m and blocked the river (fig. 32). The lava flow

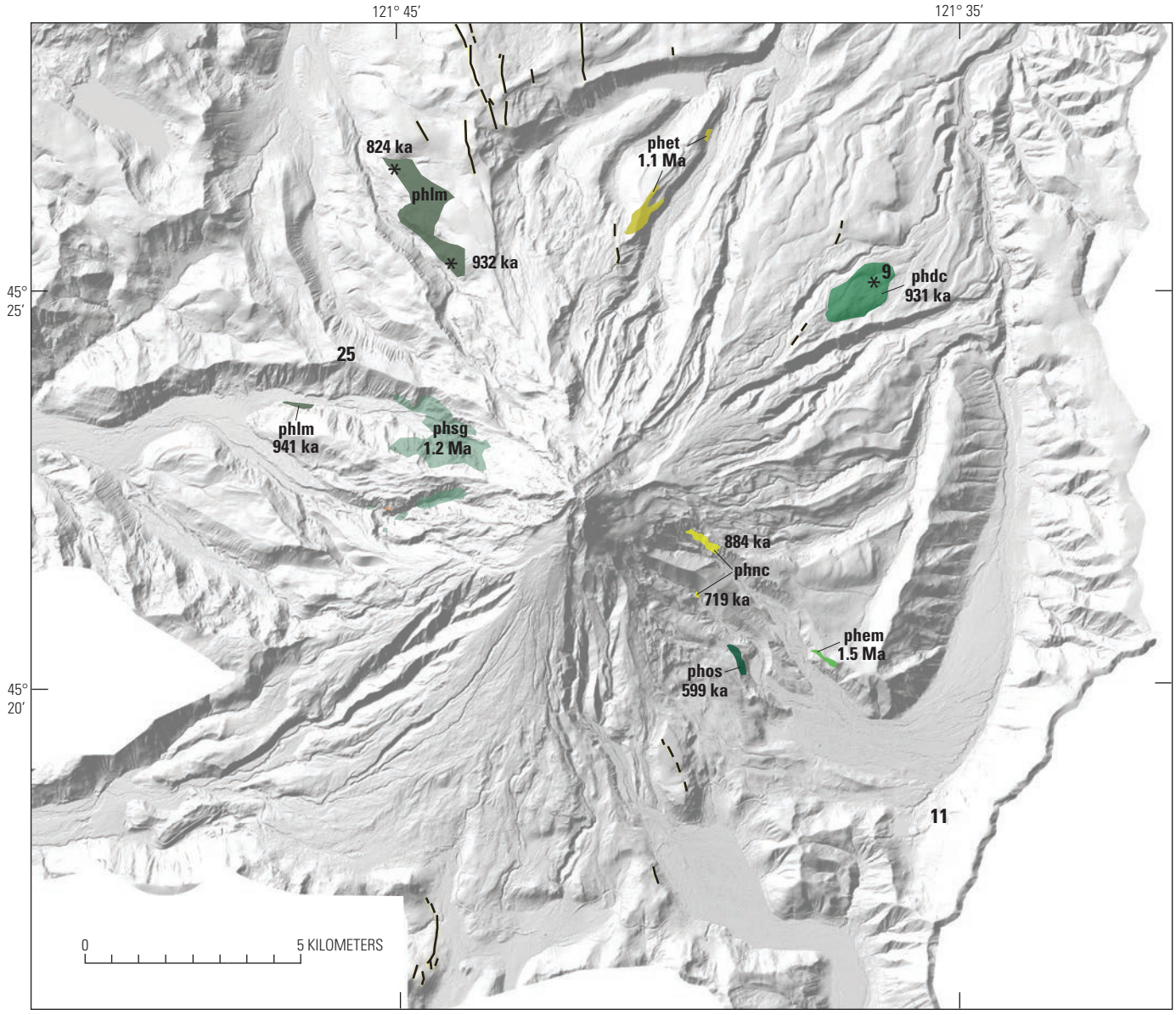

Base from 2010 Oregon Department of Geology and Mineral Industries, Oregon Lidar Consortium, Mount Hood lidar data quadrangle series, hillslope-shaded, bare-earth elevation model, 3 ft interval; Badger Lake, Bull Run Lake, Dog River, Government Camp, Mount Hood North, and Mount Hood South quadrangles

EXPLANATION

- phos — Olivine andesite of Shooting Star
- phnc — Andesite of Newton and Clark Creeks
- phlm — Andesite of Ladd Creek and Muddy Fork
- phdc — Andesite of Doe Creek
- phet — Andesite and dacite of Elk Cove Trail
- phsg — Andesite and dacite of Sandy Glacier volcano
- phem — Andesite of Elk Meadows Trail
- Fault scarp
- Paleomagnetic data
- 11 — Field-trip stop

Figure 31. Lidar shaded-relief map of Mount Hood region showing outcrop areas of lava flows of pre-Hood (>500 ka) composite volcanoes. Vents for the flows are not known, but assumed to be within a few kilometers of the current Mount Hood vent area. Ages of units represent our best estimate based on K-Ar data as well as other evidence, see Note on K-Ar and $^{40}Ar/^{39}Ar$ Ages, p. 5.

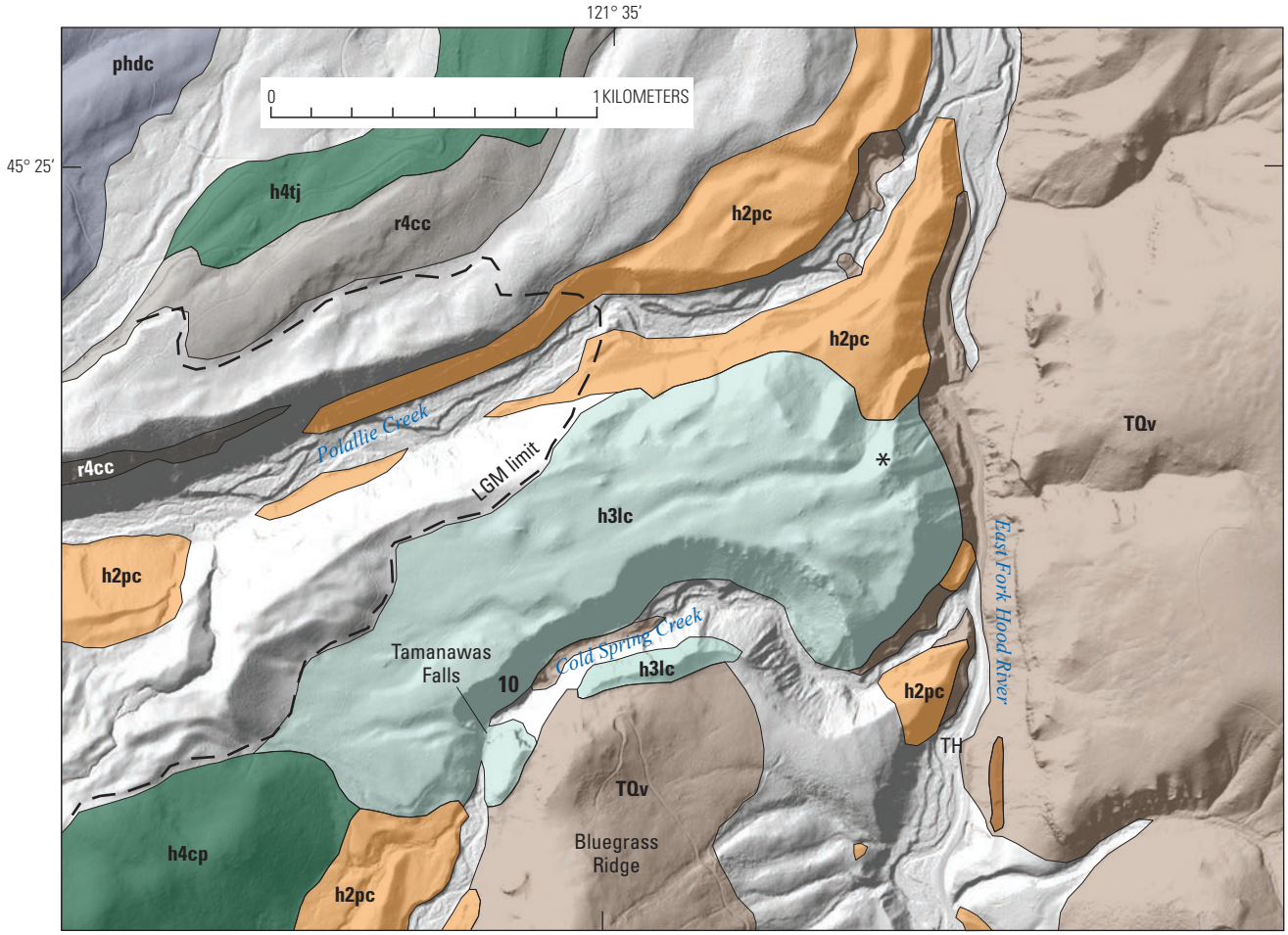

Base from 2010 Oregon Department of Geology and Mineral Industries, Oregon Lidar Consortium, Mount Hood lidar data quadrangle series, hillslope-shaded, bare-earth elevation model, 3 ft interval; Dog River quadrangle

EXPLANATION

h2pc	Deposits of Pollalie eruptive period	phdc	Andesite of Doe Creek
h3lc	Andesite of Langille Crags	TQv	Volcanic units
h4cp	Andesite of Cold Springs-Polallie divide	— —	LGM limit
r4cc	Basaltic andesite and andesite of Cloud Cap	*	Paleomagnetic data
h4tj	Andesite of Tilly Jane	10	Field-trip stop

Figure 32. Lidar shaded-relief image of lava flow of Tamanawas Falls, part of andesite of Langille Crags (h3lc). The lava flow descended the paleovalley of Polallie Creek bounded by the andesite of Tilly Jane (h4tj) and basaltic andesite and andesite of Cloud Cap (r4cc) on the north and andesite of Cold Springs-Polallie divide (h4cp) on the south and blocked East Fork Hood River. Subsequent incision created narrow canyons of East Fork and lower Cold Spring Creek; Tamanawas Falls marks the upstream extent of incision. Volcanic units of late Tertiary to perhaps early Quaternary age (TQv) form Bluegrass Ridge and high terrain east of East Fork. Valley-bottom exposures of old rocks along Polallie and Cold Springs creeks attest to eastward migration of East Fork valley as Mount Hood lava flows and those of regional volcanoes such as Cloud Cap displaced river intermittently eastward. Dashed line encloses last glacial maximum terminal moraine of Polallie Creek glacier that buries northwestern margin of lava flow of Tamanawas Falls. Deposits of Polallie eruptive period (h2pc) formed fills, now dissected, within the moraine loop during waning phase of last ice age. TH, Tamanawas Falls Trailhead.

terminated against the ancestral east valley wall and subsequent incision by the river at the flow's snout cut a narrow canyon through Miocene volcanic rocks and diamicts at the base of the eastern escarpment. Polallie Creek follows the northern flow margin, and Cold Spring Creek incised a narrow canyon along the southern margin. Tamanawas Falls marks a retreating head scarp in the lava flow along Cold Spring Creek. Roadcuts along O.R. 35 south of the lava flow expose lacustrine, alluvial, outwash, and lahar sediments deposited during a period when the lava-flow blockage impeded river flow. This event was one of a series of lava-flow and sediment blockages and drainage rearrangements as Mount Hood products repeatedly impinged on the East Fork valley over hundreds of thousands of years. Lava flows from regional volcanoes, such as Cloud Cap (Stop 5), also contributed.

We cannot trace the lava flow of Tamanawas Falls much farther westward toward the volcano than the margin of figure 32. We infer that it was emplaced during a time of extensive glacier cover prior to the LGM (MIS 3–4); perhaps it was fed through a narrow ice-bound channel. Cutting of the canyon along Cold Spring Creek was likely accomplished during the last ice age as outwash streams from glaciers on the east side of Mount Hood fed the creek. Today the creek originates chiefly at springs in upper tributaries; no contribution comes directly from streams draining modern glaciers. The trail to the falls has ample evidence of high flows generated by major rainstorms, but present-day flows are significantly smaller than those of the ice-age stream.

Hike the East Fork Trail and Tamanawas Falls Trail (#650A) from the trailhead located along O.R. 35 at the south edge of figure 32. The map and trail description are available at http://www.fs.usda.gov/recarea/mthood/recreation/hiking/recarea/?recid=53300&actid=50. The route crosses the East Fork Hood River on a foot bridge and follows the west bank of the East Fork, then traverses terraces and follows the north bank of Cold Spring Creek to the falls; the total distance to the falls is about 1.5 mi (2.5 km). On route, the trail crosses a few small outcrops of Tertiary lava characterized by alteration and tectonic jointing.

The first outcrops of in-place lava flow of Tamanawas Falls appear near the junction of the Tamanawas Falls Trail and the Tamanawas Tie Trail (figs. 32, 33; Stop 10; 45.4034° N., 121.5859° W.; UTM 10T 610670E, 5028517N; altitude 3,400 ft). Basal flow breccia is exposed locally; massive and platy jointing dominate. For Mount Hood, the lava is sparsely porphyritic (29 percent crystals), two-pyroxene andesite (orthopyroxene > clinopyroxene) with microphenocrysts of amphibole, which are all almost completely replaced by iron-titanium oxides (fig. 34). Microphenocryts consist of plagioclase (6 percent), orthopyroxene (2.9 percent), clinopyroxene, (2.6 percent), replaced amphibole (3 percent), and iron-titanium oxides (1.4 percent) in a groundmass of plagioclase, oxides ± olivine or ± clinopyroxene. Plagioclase phenocrysts (11 percent) are sparse for Mount Hood lavas although still greater than mafic phenocryts (orthopyroxene, 2 percent; clinopyroxene, 1 percent) and are generally large, euhedral, and show little evidence of disequilibrium. Rounded, light-colored, fine-grained mafic enclaves are locally common in Mount Hood lava flows, but are uncharacteristically rare in this part of the lava flow of Tamanawas Falls. Six samples of the lava flow of Tamanawas Falls range from 60.4–61.7 percent SiO_2; 1.71–1.76 percent K_2O, and 829–957 ppm strontium. Tamanawas Falls is about 0.2 mi farther ahead, where trail ends (fig. 35).

Mafic Enclaves in Mount Hood Andesite

Mafic enclaves are common in many Mount Hood lavas, but rarely exceed more than a few volume percent of a given body. Mafic enclaves and porphyritic inclusions are rounded with smooth-to-crenulated contacts suggesting magma-to-magma interaction, although rare, angular enclaves with sharp, linear contacts (rock to magma) also occur. Rounded enclaves are more vesicular and have fewer percent phenocrysts than their host lavas, but usually mirror the host rocks in terms of phenocryst assemblage (Scott and others, 1997a; Woods, 2004); in rare cases, however, host lavas devoid of hornblende phenocrysts have coarse enclaves with what appear to have been hornblende phenocrysts that have been totally replaced by iron-titanium oxides. Although enclaves have fewer phenocrysts overall, they are more crystalline than their host due to abundant groundmass crystallization (fig. 36).

Most enclaves lie compositionally within the field of regional and low-silica Mount Hood lavas (fig. 3). Coarse-grained enclaves tend to be more silicic than finer-grained enclaves; the most silicic enclave sampled is found in clasts of Old Maid age, reach 62 percent SiO_2, and vary from their host rock primarily in having lower vesicularity (Koleszar, 2011). The more mafic enclaves (54–56 percent SiO_2) lack olivine phenocrysts or microphenocrysts, which are present in regional lavas of similar silica content.

Woods (2004) showed that there is little difference in plagioclase, orthopyroxene, or amphibole phenocryst composition between host rocks and enclaves, but that host-rock phenocrysts often showed a more complex crystallization history than those in enclaves. In many cases host rock and enclave phenocrysts show less evolved compositions at rims (in other words, higher An content or Mg#) for all phenocryst types, suggesting late-stage interaction with more mafic magma.

Both Woods (2004) and Koleszar (2011) conclude that the mafic enclaves and host rocks are all products of magma mixing. Koleszar (2011) demonstrates that possible end members for the host lavas (and by inference the enclaves) are calc-alkaline basalt and silicic melt likely formed by partial melting of mafic amphibolite in the lower to middle crust; neither end member is found as an eruptive product at Mount Hood.

Figure 33. Exposure of andesite lava flow of Tamanawas Falls near junction of Tamanawas Falls Trail with Tie Trail (10 on fig. 32). Thick basal breccia exposed locally. Total flow thickness exposed is about 70 m; rocks of Tertiary age are exposed in canyon bottom, but contact with lava flow not visible. Outcrops characterized by alternating zones of massive and platy jointing.

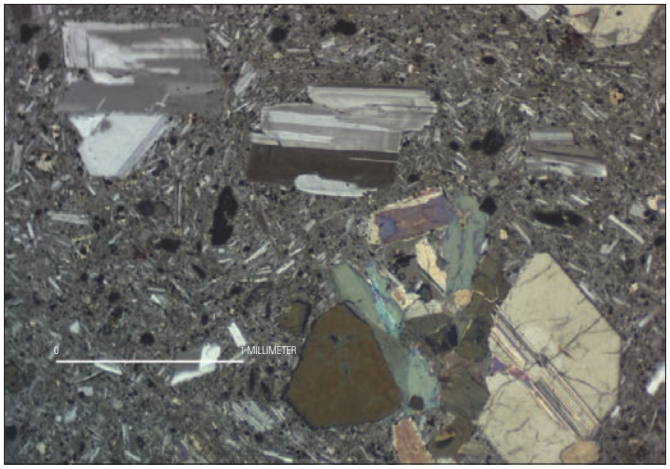

Figure 34. Photomicrograph of andesite of Tamanawas Falls (h3lc; sample 920820-1) showing two-pyroxene clot and isolated plagioclase phenocrysts in a groundmass of plagioclase and iron-titanium oxides. A little left of center is an amphibole microphenocryst that has been totally replaced by iron-titanium oxides. Viewed with a binocular microscope under partial cross-polarized light.

Figure 35. Photograph of Tamanawas Falls, which is formed by Cold Spring Creek plunging over a head cut in an andesite lava flow. Intensely fractured section and breccia at base of falls undermines falls and facilitates collapse and headward retreat.

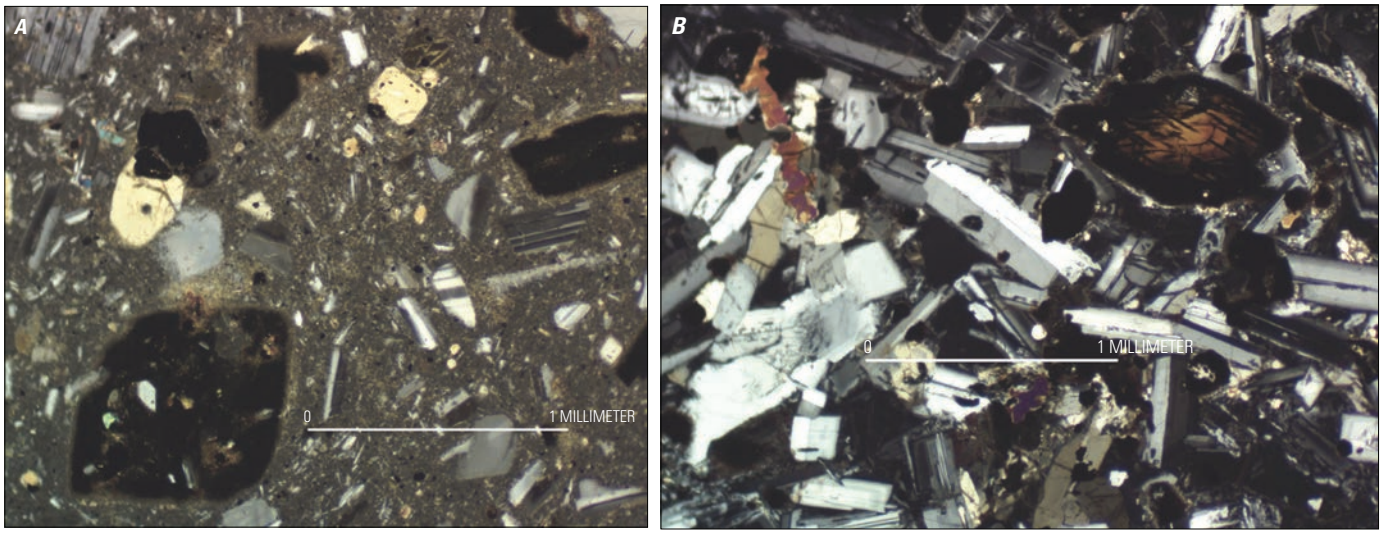

Figure 36. Photomicrographs of (*A*) typical Mount Hood andesite lava (sample 960930-1) and (*B*) mafic enclave (sample 960930-2) from flow on northwest flank that is part of andesite of Dollar Lake (h4dl; 266 ka; fig. 4). *A*, Host andesite flow (61.2 percent SiO_2) has crystal assemblage of plagioclase > orthopyroxene ≥ amphibole. Amphibole is largely to completely replaced by iron-titanium oxides. *B*, Enclave (53.0 percent SiO_2) has crystal assemblage of plagioclase > orthopyroxene ≥ amphibole and, like host lava, amphibole is largely replaced by iron-titanium oxides. Most enclaves in Mount Hood lavas have lower silica content than their hosts and are of basaltic andesite composition. However, unlike regional basaltic andesite lavas at this silica content, enclaves do not contain olivine. Viewed with a binocular microscope under cross-polarized light.

Travel

Continue south on O.R. 35 through the broad valley of East Fork Hood River. For the first 0.5 mi, roadcuts expose sediments deposited behind blockages caused by the lava flow of Tamanawas Falls and perhaps by sediment fans at the mouth of Polallie Creek. Farther south, roadcuts expose gravelly debris-flow and alluvial deposits of fans at the base of the eastern valley wall. Geologic mapping shows that there is no significant fault offset of rock units across the East Fork valley. If, as inferred, the Hood River Fault Zone continues southward, it must lie on the west side of Bluegrass Ridge, which forms the western valley wall. Mount Hood lava flows and glacial deposits have accumulated along the western side of Bluegrass Ridge and bury the fault zone (figs. 5,15; Sherrod and Scott, 1995).

At about 4 mi south of the parking area for Stop 10, O.R. 35 leaves the debris fans at the base of the eastern valley wall, crosses East Fork Hood River, and heads up the center of a broad valley fill of Mount Hood lahar, glacial, and alluvial deposits of latest Pleistocene to late Holocene age. Debris flows generated by landslides and intense rainstorms originate in deposits of the Polallie eruptive period on the east flank, especially in late autumn and early winter. Some flows have affected O.R. 35, most recently in November 2006. A major construction project ensued that raised the road bed, armored ditches, and installed numerous large box culverts to carry future flows.

About 1 mi southwest of the East Fork bridge, turn left (southeast) on F.R. 3540, which lies at the northeast end of the Pocket Creek Sno-Park; the road is paved and mostly one lane with turnouts (fig. 37). The first ~0.5 mi traverses debris-flow and alluvial deposits of late Holocene age and then descends to the East Fork Hood River through lahar and alluvial deposits of Polallie age, which are exposed locally in roadcuts. At 0.6 mi, cross the river and head southwest in outwash and till of the last glaciation, breached locally by fan deposits of the eastern valley wall. Southeast-flank glaciers flowed down the East Fork, Clark, and Newton valleys and spread out in the broad lowland where the East Fork turns north, blocking the head of Pocket Creek valley and extending about 2 km to north. The northern part of the terminal area is now buried beneath late-glacial and Holocene deposits. The terrain ahead becomes more hummocky and ridged in a widening moraine belt. At about 2.1 mi from O.R. 35 there are several pullouts for parking on the right. Hike up the roadcut for a view of the southeast flank of Mount Hood. This area was logged in late 20th century and regrowth is encroaching on views.

Stop 11. Pocket Creek—LGM End Moraines Rich in Dome Lava and View of Southeast Flank of Mount Hood

Location: 45.3064° N., 121.5937° W.; UTM 10T 610249E, 5017727N; altitude 3,840 ft

This wide view accentuates the contrast between the steep area of near-summit lava domes and the broad, more gently sloping flank areas of lava flows and fragmental fans (fig. 38). Most of the area below Newton Clark Glacier and

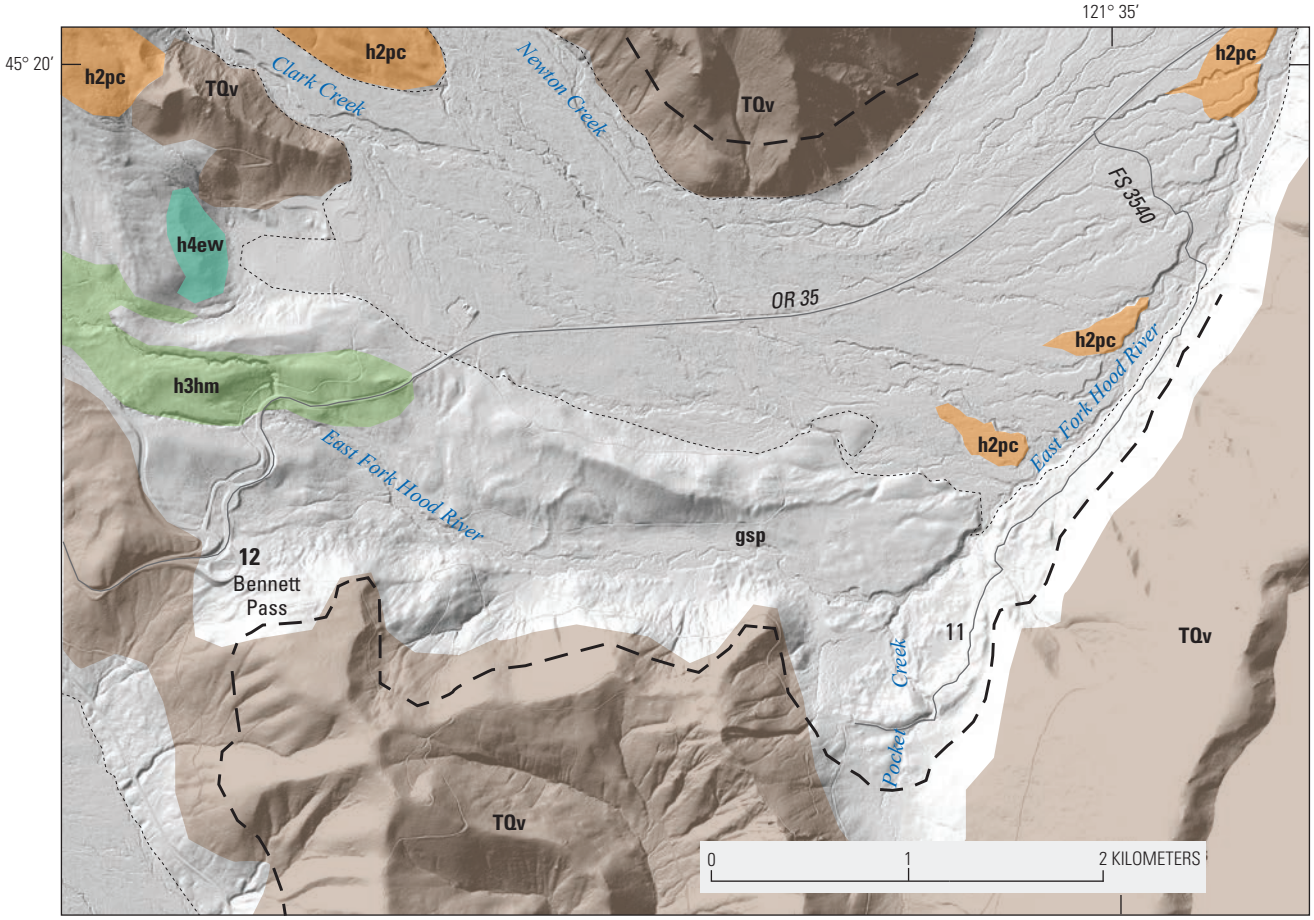

Base from 2010 Oregon Department of Geology and Mineral Industries, Oregon Lidar Consortium, Mount Hood lidar data quadrangle series, hillslope-shaded, bare-earth elevation model, 3 ft interval; Badger Lake and Mount Hood South quadrangles

EXPLANATION

- h2pc — **Pyroclastic deposits of Polallie eruptive period**
- gsp — **Till rich in dome debris of Polallie age**
- h3hm — **Distal lava flows of andesite of Mount Hood Meadows**
- h4ew — **Andesite of east fork White River**
- TQv — **Volcanic rocks**
- **Outer limit of last glacial maximum**
- **Holocene debris-flow and alluvial deposits**—derived from erosion of major pyroclastic fill of Polallie age
- **Road**
- 12 — **Field-trip stop**

Figure 37. Shaded-relief lidar image of Pocket Creek area. Till of the last glaciation forms moraines and hummocky terrain well displayed by lidar; much of the till is rich in dome debris of Polallie age (gsp). Distal lava flows of andesite of Mount Hood Meadows (h3hm) and an older unit, andesite of east fork White River (h4ew), are locally exposed where till is thin. TQv, volcanic rocks of late Tertiary and perhaps early Quaternary age.

continuing down Gnarl Ridge is formed by a sequence of lava flows about 346–180 ka (figs. 4, 5); valley bottoms expose some older lava flows of pre-Hood composite volcanoes (fig. 18). Lava flows, mainly 200–150 ka, continue north of Gnarl Ridge where ridges and intervening valleys form the headwaters of Cold Spring Creek, which flows north along the west side of Bluegrass Ridge, a ridge of Miocene and Pliocene lavas east of the southward extension of the Hood River fault system. In contrast, East Fork Hood River has maintained a topographic low through Tertiary terrane and the Hood River fault system, which has allowed Mount Hood lava flows and fragmental deposits to extend southeastward. The Newton Clark medial ridge and ridges above and below Mount Hood Meadows consist of pyroclastic-flow, lahar, and debris-avalanche deposits of Polallie age that date from last-glacial and early postglacial time (Thouret, 2005). The moraine belt in the Pocket Creek area represents glacially transported products of such glacial-age eruptions.

Roadcuts at Stop 11 and elsewhere along F.R. 3540 expose till with a significant component of dense to vesicular dome lava, much of which displays incipient prismatic jointing or are joint-bounded fragments. Samples of jointed blocks collected randomly in the southeastern sector have 62.5–63.9 percent SiO_2, straddling the boundary between andesite and dacite (fig. 39), quite similar to eruptive products of late Holocene age. Most southeastern samples form tight arrays along with samples from adjacent sectors, from which we infer a succession of summit-dome sources. The scatter on the plot and from samples elsewhere around the volcano is consistent with multiple sources throughout the last major glaciation. Lack of clasts with high strontium concentrations similar to those of the 50–30-ka units on the north and northeast flanks (Stops 7, 8, and 10) imply the source domes postdate the high-strontium episode. We infer that most of the debris originated from rockfalls and pyroclastic flows generated from growing summit lava domes, and were then transported as superglacial drift to end moraines. The sandy matrix of the till is also consistent with this origin.

Travel

F.R. 3540 follows the moraine belt for another 0.6 mi. The pavement ends in a wide area with room to turn around. Return to O.R. 35 along F.R. 3540 and turn left (southwest) on O.R. 35. At 2.5 mi from F.R. 3540, roadcuts expose a distal lava flow of the andesite of Mount Hood Meadows overlain by till. The snout of the flow is about 8.5 km from the likely vent area. About 0.4 mi past the lava-flow outcrop, cross East Fork Hood River, which plunges over Sahalie Falls on the south edge of the lava flow. Take the exit to Mount Hood Meadows in another 0.4 mi. After exiting, turn left, cross overpass, and turn left into Bennett Pass Sno-Park. Walk back across overpass and down to roadcuts on west side of O.R. 35. Be cautious of traffic as cuts are on inside of curve.

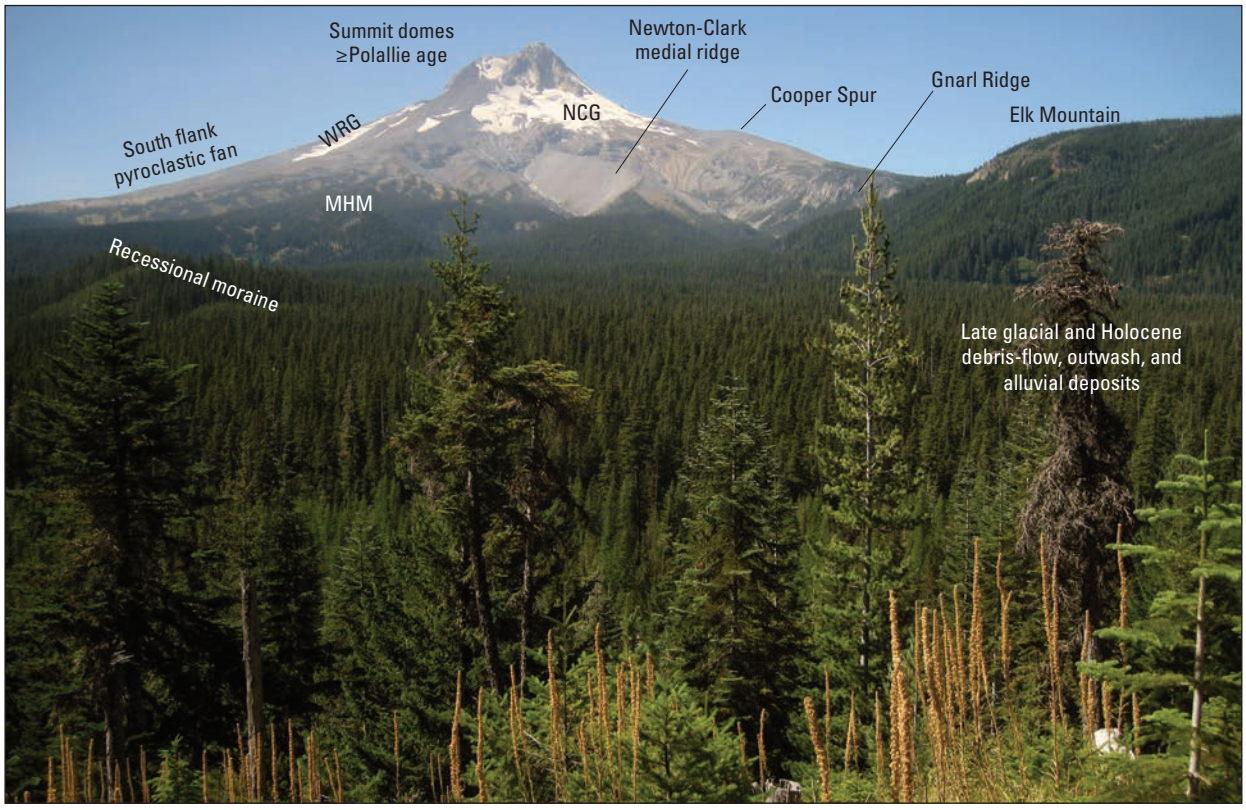

Figure 38. Photograph of southeast flank of Mount Hood from Stop 11 at top of roadcut on southeast side of Forest Road 3540. Elk Mountain is at south end of Bluegrass Ridge and consists of late Tertiary volcanic rocks. WRG, White River Glacier; NCG, Newton Clark Glacier; MHM, Mount Hood Meadows Ski Resort.

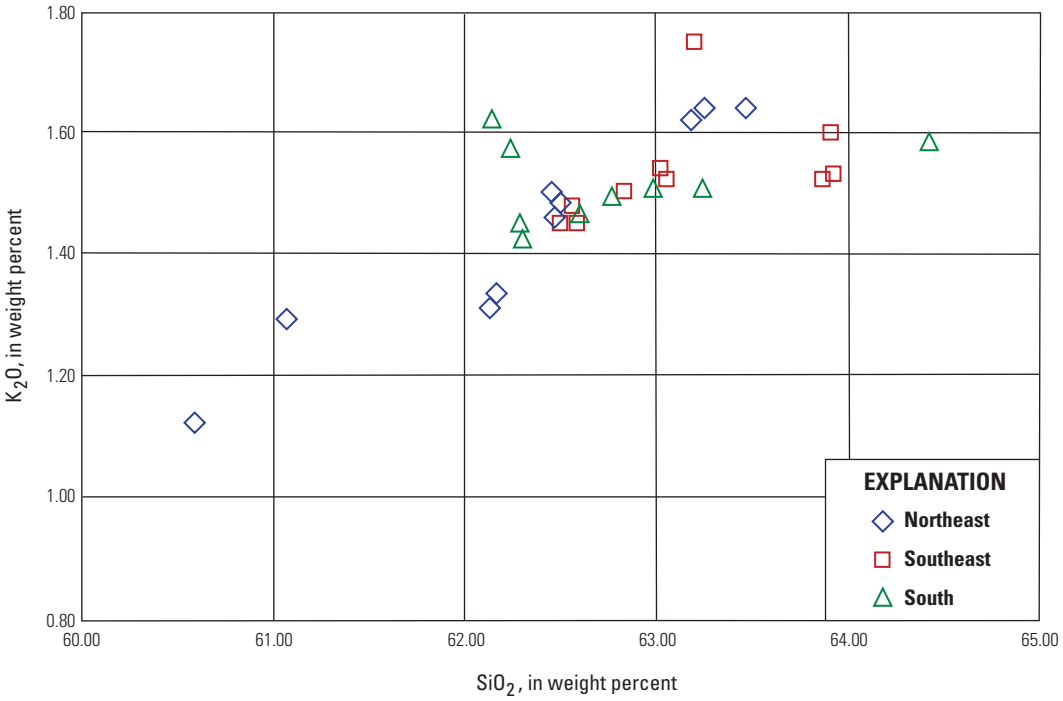

Figure 39. K_2O versus silica for samples of incipiently prismatically jointed blocks collected from till of last major glaciation rich in dome lava on south, southeast, and northeast flanks of Mount Hood. Stop 11 is on southeast flank. Till originated as rockfall and pyroclastic flows from growing lava domes that formed thick mantles of superglacial debris, which were transported to end moraines or deposited as ablation till as glaciers thinned and stagnated.

Stop 12. Bennett Pass Till Exposure

Bennett Pass Sno-Park: 45.3103° N., 121.6407° W.; UTM 10T 606558E, 5018104N; altitude 4,680 ft

Bennett Pass forms the drainage divide between the White and Hood Rivers. Roadcuts along O.R. 35 at the pass used to expose three diamicts that mantle a ridge cored by Miocene volcanic rocks. Crandell (1980) interpreted the diamicts as multiple tills separated by buried soils. The lowest till and buried soil are no longer exposed, but the approximate position of the soil is marked by the dotted line in figure 40. The diamicts display the characteristics that distinguish till from similar-looking diamicts formed by volcanic and colluvial processes. Striated and glacially shaped (soled and roughly pentagonal) clasts are common in the units, especially the lower two. The matrix contains more silt than do typical granular lahar and block-and-ash-flow deposits and is locally compact. Bedding is absent or crude, unlike typical sequences of volcanic diamicts. The middle unit has a few poorly bedded, slightly graded diamicts that may be flow till (essentially debris-flow emplacement of superglacial drift), as might be expected in a moraine.

About half of the clasts in the upper unit are highly porphyritic and vesicular, similar to clasts found in deposits of Polallie age derived from the collapse of growing lava domes. Moraines of the LGM along Pocket Creek (Stop 11) contain a high proportion of such clasts, many of them incipiently prismatically jointed, suggesting that dome growth and collapse was occurring during the glacial advance. The denser clasts are likely derived from glacial erosion of the andesite of Mount Hood Meadows and older units.

The soils that separate the units are quite different in degree of development. The lower, no-longer-exposed soil is as much as 1 m thick, although it has been beveled by erosion, and has an incipient argillic (textural) B horizon. Overall it displays a greater degree of development than does the surface soil formed since the LGM. The upper buried soil is thinner than the lower, is less intensely oxidized, and has no argillic horizon. The uppermost buried soil probably represents a limited time of soil formation and the two upper units may both date from the last glaciation. Small pumice lapilli, an example of the rare pumiceous products of Mount Hood, are scattered throughout the upper part of the uppermost buried soil.

The age of the unexposed lower till is unknown but is probably about 150 ka (MIS 6), considering the degree of development of the lower buried soil and our estimates of the timing of pre-LGM glaciations.

Travel

Head west across the O.R. 35 overpass toward Mount Hood Meadows Ski Resort. Roadcuts are chiefly in till, but exposures are poor. Cuts are typically mantled with a thick cover of red or gray road sand that snowplows throw onto the cuts. Most of the route after the first 0.5 mi is underlain by andesite of Mount Hood Meadows, which is rarely exposed below till. At about 1.7 mi from Bennett Pass, reach a gated parking lot. During non-ski season, gate is open during work hours, but locked at 5 p.m.

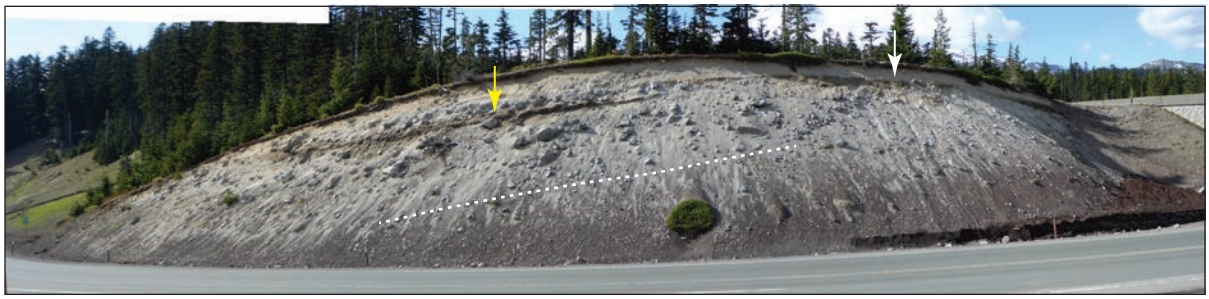

Figure 40. Merged photographs of till exposure on northwest side of O.R. 35 just south of overpass at Bennett Pass. White dotted line marks approximate position of buried soil formed in lowest till unit as seen in 1989, prior to deposition of colluvial apron and construction of overpass. Yellow arrow marks buried soil formed in middle till unit. White arrow marks area on face of roadcut with thin accumulation of oxidized fine-grained material eroded from surface soil; it is not a continuation of buried soil marked by yellow arrow. Apparently the youngest till forms much of right side of exposure and bevels the older sequence of tills and buried soils.

Stop 13. Main Parking Lot at Mount Hood Meadows Ski Resort

Location: 45.3287° N., 121.6614° W.; UTM 10T 604902E, 5020116N; altitude 5,320 ft

Mount Hood Meadows Ski Resort is an easily accessible area for viewing part of a ~0.2-km^3 sequence of andesite lava flows that were emplaced about 70–60 ka. Glacial erosion has largely stripped surface breccia from the flows, but they retain much of their original morphology of steep-margin lobes (figs. 41, 42). We have sampled the lava flows extensively to explore if a morphologically coherent and mappable sequence of flows has a geochemical character and secular-paleomagnetic direction that can serve as a basis for differentiation and correlation. Analyses form coherent arrays on variation diagrams, especially K_2O versus silica (fig. 43). Two parallel trends are separated by about 0.10 percent K_2O. A high flow on the northwestern margin of the flow field is relatively low in silica (and high in K_2O for its silica content) compared to the rest of the flows. Paleomagnetic data from six sites fall into two groups, both with steep (65–70°) inclinations, but sites on the high northwest flow, which may be stratigraphically younger, have declinations of about 20°, whereas sites on the main and distal flows have declinations of about 325° (fig. 44). The high, northwest flow has $^{40}Ar/^{39}Ar$ ages of 63.3±2.7 and 71.1±3 ka coupled with a K-Ar age of 55±14 ka; the main area has yielded K-Ar ages of 56±9 and 61±11 ka. The range of the ages allows sufficient time for movement of the magnetic field. We interpret the data as implying emplacement of much of the main sequence over the relatively brief time interval of a few centuries; the northwest flow could be younger or older by a millennium or more. The andesite of Texas (K-Ar age 25±13 ka; $^{40}Ar/^{39}Ar$ age 44.5±2.3 ka; 700–1,040 ppm strontium) is part of the high-strontium sequence of lava flows viewed at Stops 7, 8, and 10, and provides a minimum limiting age for the andesite of Mount Hood Meadows. Lava flows in the upper White River (K-Ar age of 77±8 ka) and at the head of forks of Cold Spring Creek (fig. 6) are included in the andesite of Mount Hood Meadows on the basis of chemical similarity (fig. 43). Additional $^{40}Ar/^{39}Ar$ ages may help to constrain the duration of the eruptive episode, which emplaced a broad apron of flows from the south to east-northeast sectors, but the most voluminous and farthest-traveled flows occupied the topographic low south of Bluegrass Ridge.

The coherent chemistry, paleomagnetic data, and morphologic relations of the andesite of Mount Hood Meadows provide us some degree of confidence in using this approach to define map units.

Steel Cliff lava dome (figs. 7, 42) and an apron of fragmental deposits of Polallie age lie above Mount Hood Meadows (figs. 41, 42). Crandell (1980) recognized that, although substantial Polallie deposits lie at the margins of Mount Hood Meadows, there are no Polallie deposits of consequence within the Meadows, indicating that a glacier must have occupied the area at least during the early part of the Polallie eruptive period. Steel Cliff has an imprecise K-Ar age of 16±8 ka. The faulted, planar wedge of Polallie deposits southwest of the main parking lot (fig. 41) probably approximates the glacier-surface altitude at the time of eruption when the Meadows area was under ice.

Travel

Return to O.R. 35 and head southwest toward Government Camp. Approaching the White River, the high, steep slope on right is the snout of ~170-ka andesite of Switchback Falls (h4sb); roadcuts expose mostly colluvium. Cross the White River and turn right into White River West Sno-Park (location: 45.3043° N., 121.6733° W.; UTM 10T 604010E, 5017388N; altitude 4,240 ft). The highway bridge is part of post-2006 O.R. 35 improvements aimed at increasing resilience to debris flows and sediment aggradation. The old bridge was shorter and lower, and frequently buried by or its approaches severed by debris flows spawned by intense rainstorms in the upper White River. Much of the surface disturbance here is result of regrading and re-channelizing the river after such events. Hopefully the new bridge will allow flows

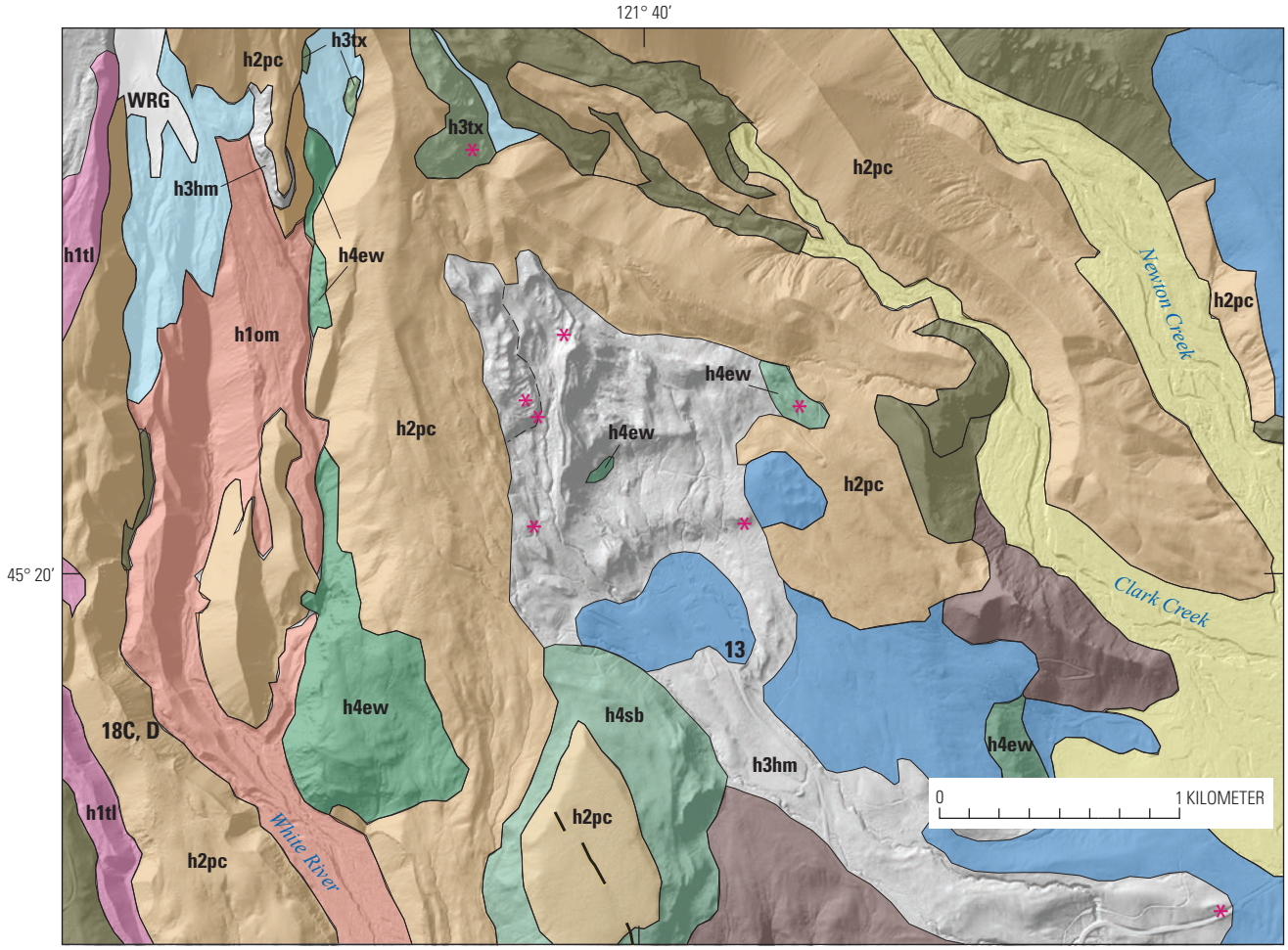

Base from 2010 Oregon Department of Geology and Mineral Industries, Oregon Lidar Consortium, Mount Hood lidar data quadrangle series, hillslope-shaded, bare-earth elevation model, 3 ft interval; Mount Hood South quadrangle

EXPLANATION

- h1om — **Deposits of Old Maid eruptive period**—also includes post-Old Maid alluvium of White River
- h1tl — **Deposits of Timberline eruptive period**
- h2pc — **Deposits of Polallie eruptive period**
- h3tx — **Andesite of Texas**
- h3hm — **Andesite of Mount Hood Meadows**
- h4ew — **Andesite of east White River**—140-ka
- h4sb — **Andesite of Switchback Falls**—~170-ka
- **Other Mount Hood lavas**
- **Alluvium and debris-flow deposits**—Late Pleistocene and Holocene
- **Till of late neoglacial age**
- **Till of last glaciation**
- **Volcanic rocks of late Tertiary age**
- **Contact**
- **Fault scarp**
- * **Paleomagnetic data**
- 10 **Field-trip stop**

Figure 41. Shaded-relief lidar image of Mount Hood Meadows Ski Resort and surrounding area showing partial extent of 70–60-ka andesite of Mount Hood Meadows (h3hm; distal tongue in lower right largely buried by till) and other units. WRG, White River Glacier.

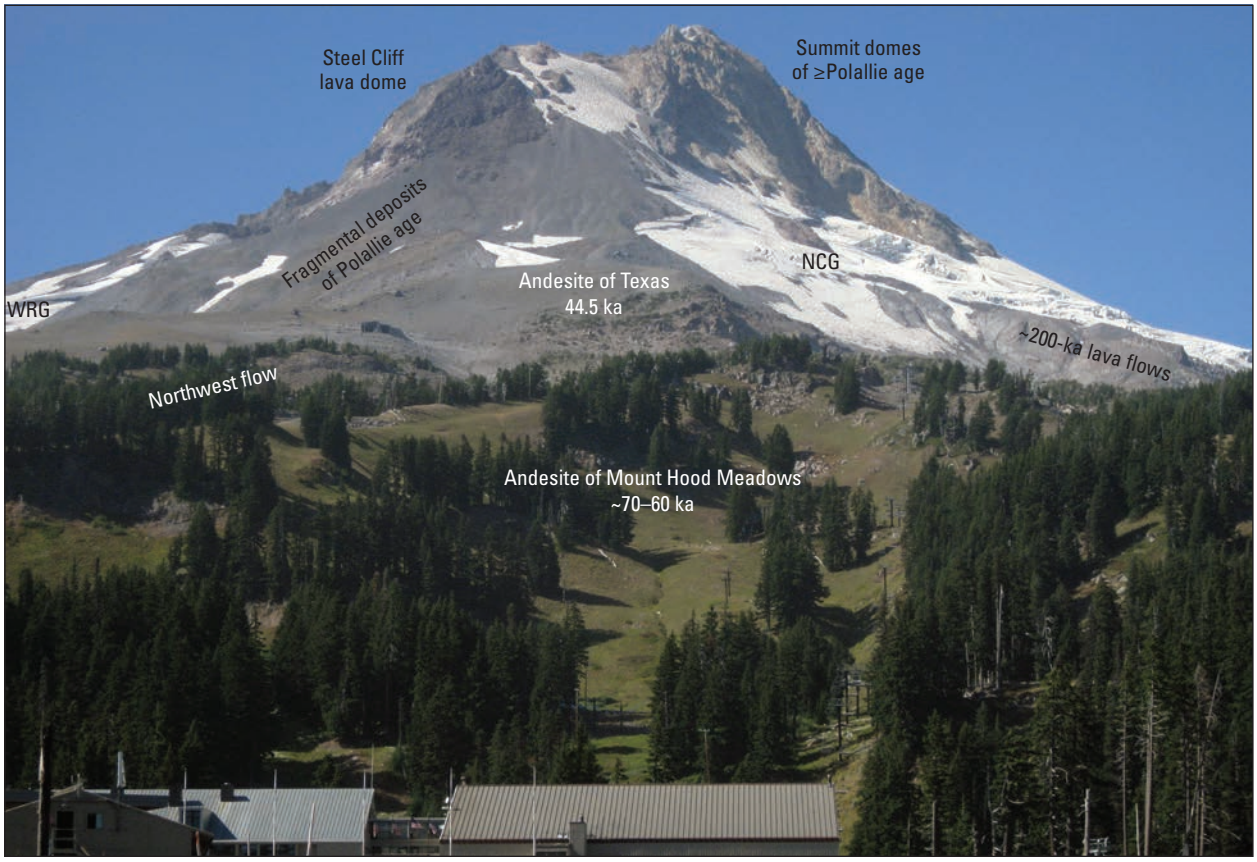

Figure 42. View of southeast flank of Mount Hood from parking lot at main base of Mount Hood Meadows Ski Resort. Northwest lava flow is part of andesite of Mount Hood Meadows, but has a different paleomagnetic direction than the rest, suggesting eruptions spanned a sufficient time interval to record significant secular change. NCG, Newton Clark Glacier; WRG, White River Glacier.

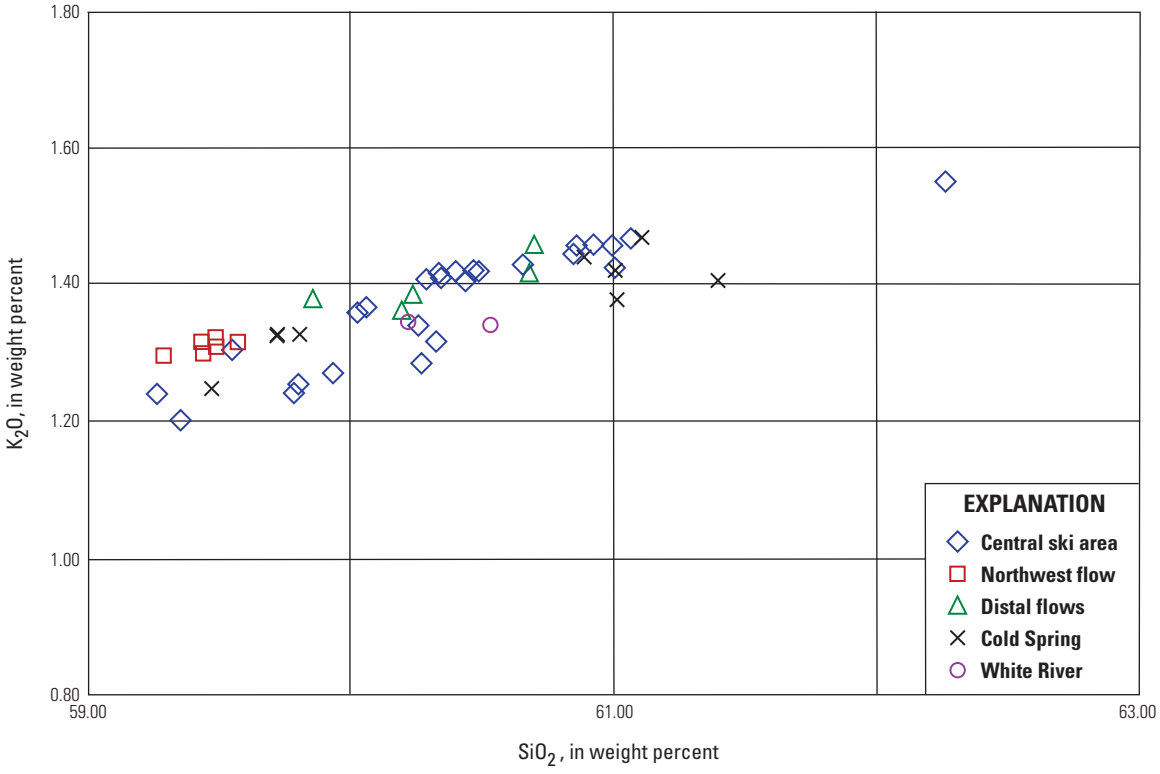

Figure 43. Plot of K_2O versus silica for lava flows of andesite of Mount Hood Meadows. Northwest flow is a topographically distinct flow that can be traced for about 1 km and has a paleomagnetic direction distinct from those of the central and distal flows (fig. 44). Distal flows extend from Meadows parking lot to Oregon Route 35. Cold Spring, lava in upper forks of Cold Spring Creek; White River, flow exposed in upper east fork White River.

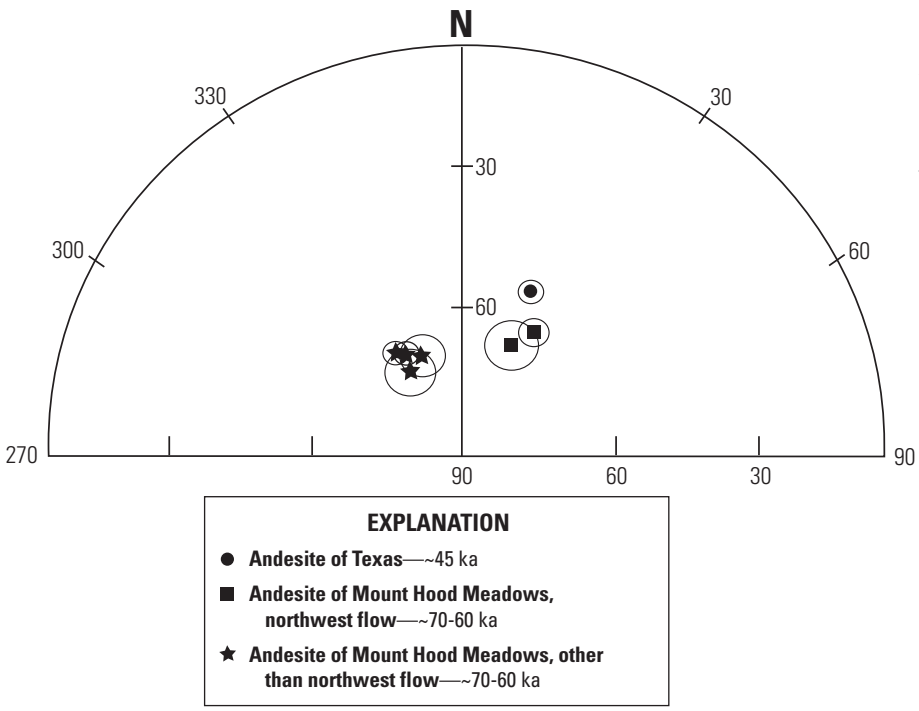

Figure 44. Upper-hemisphere plot of paleomagnetic directions with corresponding site dispersion cones (σ95) for lava flows in the Mount Hood Meadows area. Note that the paleomagnetic data clearly separates lava flows with similar K-Ar and $^{40}Ar/^{39}Ar$ ages and chemical composition (fig. 43).

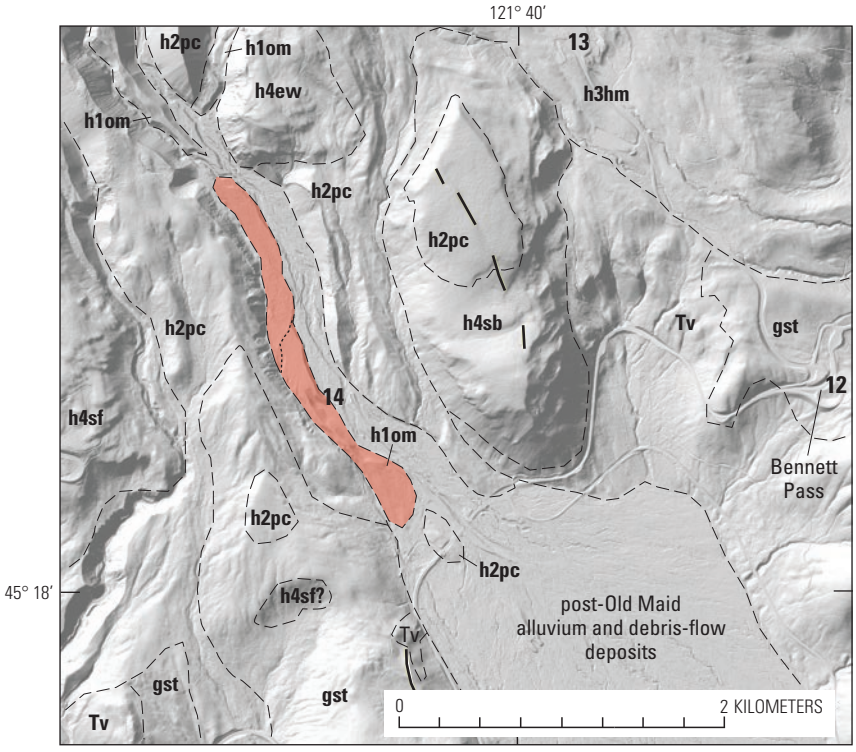

Base from 2010 Oregon Department of Geology and Mineral Industries, Oregon Lidar Consortium, Mount Hood lidar data quadrangle series, hillslope-shaded, bare-earth elevation model, 3 ft interval; Mount Hood South quadrangle

Figure 45. Shaded-relief lidar image of area surrounding Oregon Route 35 crossing of White River near East and West Sno-Parks. Numeral 14 marks site of outcrop in figure 46. Dotted line separates deposits of Old Maid eruptive period into a southern half with pyroclastic-flow deposit at or near surface, and a northern half in which a sequence of lahar deposits thickly bury the pyroclastic-flow deposit. Broad aggrading fan of post-Old Maid age originates from erosion of unconsolidated deposits in upper White River (Stop 17C). hlom, deposits of Old Maid eruptive period; h2pc; deposits of Polallie eruptive period; gst, till of last glaciation; h3hm, 70–60-ka andesite of Mount Hood Meadows; h4sf, ~130-ka andesite of south flank; h4ew, 140-ka andesite of east fork White River ; h4sb, ~170-ka andesite of Switchback Falls; Tv, undivided volcanic rocks of Tertiary age. Fault scarps of postglacial age (1) cut the mantle of Polallie deposits on andesite of Switchback Falls down to the east, and (2) cut till (gst) down to the west and forms a fault-parallel drainage that breaches the scarp just above left corner of the scale bar.

EXPLANATION

- h1om — Deposits of Old Maid eruptive period
- Contact
- Fault scarp of post glacial age
- 14 — Field-trip stop

to pass through this reach and take advantage of the broad depositional area downstream from the bridge.

Hike about 1 km northwest from the parking lot along an unimproved, gated road to large outcrops on the west side of White River (fig. 45).

Stop 14. White River Pyroclastic-Flow and Lahar Deposits of Old Maid Age

Location: 45.3107° N., 121.6819° W.; UTM 10T 603327E, 5018098N; altitude 4,560 ft

This stop focuses on a pyroclastic-flow deposit produced by the collapse of a growing lava dome at the site of present-day Crater Rock during the Old Maid eruptive period. The Old Maid is the youngest major eruptive period at Mount Hood (Crandell, 1980). On the basis of dendrochronology, it began in 1781 C.E. and lasted until the mid-1790s (see summary in Pierson and others, 2011). For decades the Oregon Department of Transportation mined and crushed the deposit for winter road sand; before mining, the deposit extended about 1 km farther down valley. Total travel distance of the pyroclastic flow from Crater Rock was about 8 km over a vertical drop of about 1,900 m, or H/L=0.24, a typical value for block-and-ash pyroclastic flows originating from lava-dome collapse.

Crandell (1980) studied this exposure soon after a 1964 flood greatly eroded the terrace scarp (fig. 46*A*). A lower lahar deposit (now buried in colluvium shed from the scarp) that

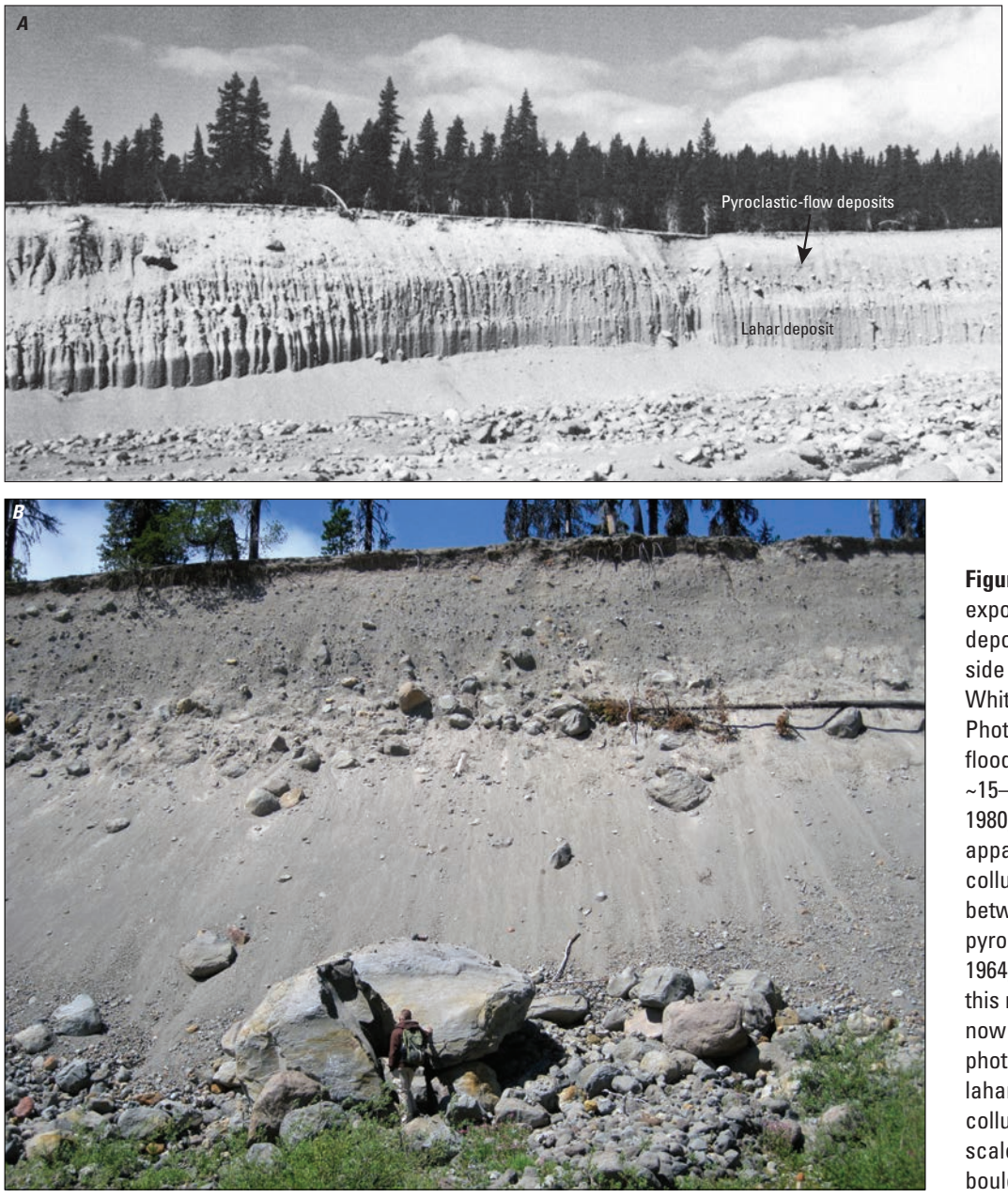

Figure 46. Photographs of exposure of pyroclastic-flow deposit of Old Maid age on west side of White River north of White River West Sno-Park. *A*, Photograph taken shortly after flood of 1964 eroded the scarp of ~15–20-m-high terrace (Crandell, 1980, fig. 13). The textural break apparent a few meters above colluvial apron marks the contact between lower lahar and upper pyroclastic-flow deposits. Since 1964, White River has aggraded this reach and active channel is now in center of valley. *B*, Recent photograph of exposure; lower lahar deposits now buried in colluvial apron. Note person for scale in front of large cracked boulder in lower center.

extended below river level is overlain by at least one, and perhaps several, pyroclastic-flow deposit(s). The pyroclastic-flow deposit contains clasts of dense to vesicular, highly porphyritic dacite in a gray to pinkish-gray, friable, granular sandy matrix (fig. 46*B*). Many clasts are prismatically jointed, indicative of rapid cooling of hot blocks after emplacement. Other evidence of hot emplacement includes abundant charcoal fragments, pinkish deposit top indicative of high-temperature oxidation, and vertical fluid-escape pipes. The deposit contains a conspicuous content of hydrothermally altered clasts, many are of dense pre-Old Maid lava that forms the walls and floor of the breached crater in which Crater Rock resides.

A few hundred meters upstream, several lahar deposits overlie the pyroclastic-flow deposit, which eventually disappears below river level (fig. 45). Stop 18C will include views of upper White River valley and downstream to this site.

Dacite of Old Maid age is crystal rich with a mineral assemblage of plagioclase > orthopyroxene > amphibole with most amphibole rimmed or totally replaced by iron-titanium oxides (fig. 47). Lava samples range from 63.1 to 64.4 percent SiO_2 and form a tight array in variation plots (fig. 48).

The andesite of Switchback Falls (h4sb; K-Ar age 163±14 ka; $^{40}Ar/^{39}Ar$ ages 162.6±2.7 and 177.4±4.1 ka; 61.0–62.0 percent SiO_2), which forms the east side of White River valley (fig. 45), has a morphology that suggests emplacement during a time of significant glacier cover. At the LGM, White River Glacier extended about 7 km downstream from the O.R. 35 bridge and some earlier glacial maxima probably reached farther, filling this reach of the valley to a depth of several hundred meters. The maximum exposed thickness of the flow is about 100 m and the flow is probably at least partly perched on a ridge formed by volcanic rocks of Tertiary age. The ages are broadly consistent with eruption during marine oxygen-isotope stage (MIS) 6, which in the Pacific Northwest is typically represented by more extensive glacial extent than that of the LGM (MIS 2). The northern part of the lava flow has a smooth, sediment-covered surface cut by a north-northwest-striking fault with as much as 2 m of normal slip (east

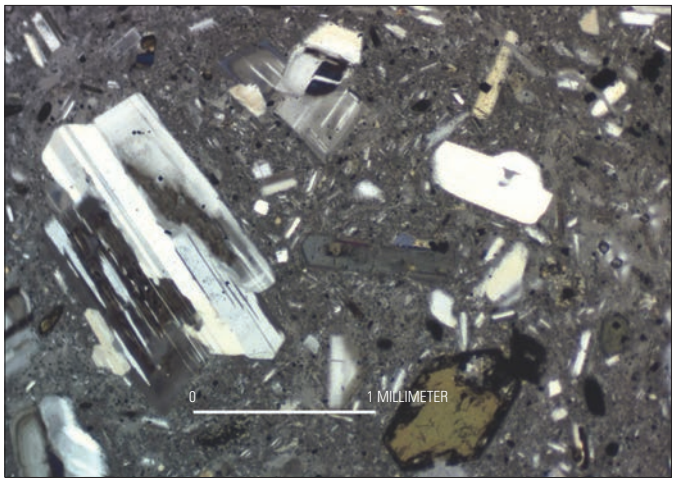

Figure 47. Photomicrograph of clast (sample G891004-3) from pyroclastic-flow deposit of Old Maid age in White River (Stop 14). Lava (63.1 percent SiO_2) has mineral assemblage of plagioclase > orthopyroxene ≥ amphibole. As in most Mount Hood lava, amphibole is heavily rimmed by, or completely replaced by, iron-titanium oxides. Viewed with a binocular microscope under partial cross-polarized light.

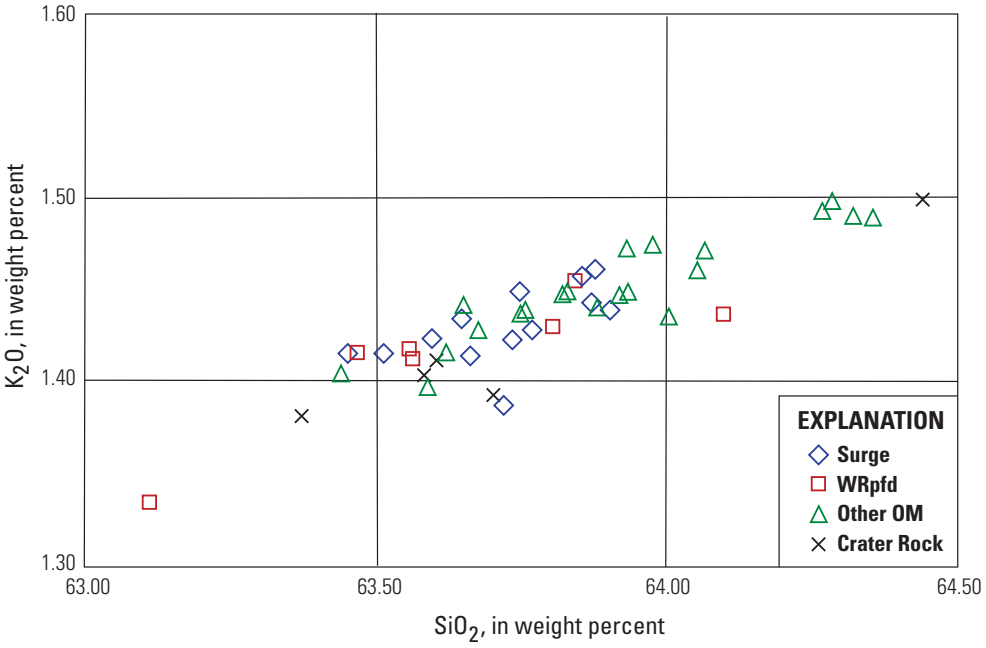

Figure 48. Plot of K_2O versus silica for products of Old Maid eruptive period. Surge, samples collected from deposit of low-density pyroclastic density current described at Stop 18A just east of Timberline Lodge; WRpfd, pyroclastic-flow deposit at Stop 14; Other OM, other Old Maid deposits collected from Sandy River drainage; Crater Rock, samples collected from south and east sides of lava dome.

side down). Although exposure is poor, we infer the surface is formed in deposits of Polallie age emplaced during MIS 2 that are now covered in thick tephra deposits of latest Pleistocene and late Holocene age.

Travel

Continue south on O.R. 35 over Barlow Pass, the divide between the White River and the Salmon River, the eastern-most tributary of Sandy River. Parts of the mid- to late-19th century Barlow Road are still visible around the pass. This toll road crossed the Cascades, carrying settlers on the Oregon Trail who preferred the rugged land route to a perilous and expensive raft trip through the Columbia Gorge. The route took advantage of several key geologic features. Lahars of Old Maid age and posteruption aggradation of the late 18th and early 19th centuries provided open areas through the thick forest for movement of wagons along the White River valley. A conspicuous lateral moraine west of Barlow Pass provided a gently descending grade along the steep southeastern valley wall of Salmon River valley. Regardless, the trip must have been treacherous and difficult owing to thick forests of huge trees, swamps, and terrifyingly steep sections such as the infamous Laurel Hill grade west of Government Camp. About 4 mi from White River West Sno-Park, turn east toward Bend on U.S. 26 if you want to go to Stop 15 at Frog Lake. If you are heading to Stop 16 and Timberline Lodge, head west toward Portland. The highway junction is built on a Salmon River fan of lahar (and perhaps pyroclastic-flow) deposits of Timberline age. Stop 15 is about 4.7 mi ahead on eastbound U.S. 26; turn into Frog Lake Sno-Park and head toward the campground and lake. Stop 16 is 1.3 mi ahead on the right side of westbound U.S. 26.

Stop 15. Frog Lake Fault Scarps

Please see the accompanying section by Madin and others. Frog Lake Buttes, which lie east of the lake, are located about 17 km south of Hood and shown in the dacite to rhyolite category in figure 2. They are lava domes of andesite to low-silica dacite (62–63.5 percent) of early Pleistocene age, perhaps 1.37±0.04 Ma (Sherrod and Scott, 1995).

Travel

Return on U.S. 26 to the junction with O.R. 35; continue west on U.S. 26 for 1.3 mi.

Stop 16. U.S. Highway 26 Roadcuts in Andesite of South Flank

Location: 45.2899° N., 121.7334° W.; UTM 10T 599328E, 5015718N; altitude 3,840 ft

Caution: U.S. 26 is a busy and noisy trans-Cascades highway that is three lanes wide. There are wide shoulders and pullouts. The following pages offer some lava-flow outcrops on less-busy roads that are more conducive to discussion.

Extensive roadcuts along U.S. 26 (fig. 49) expose a typical Mount Hood andesite flow (61.5–61.8 percent SiO_2; ~1.25 percent K_2O; 3 samples) that locally contains abundant mafic enclaves. The flow is part of the andesite of south flank and samples from here yielded a K/Ar age of 121±13 ka and a $^{40}Ar/^{39}Ar$ age of 128.6±2.9 ka. The mineral assemblage of this flow is dominated by plagioclase and orthopyroxene with minor clinopyroxene; total crystal content is 34 percent. Two types of enclaves are present: a common fine-grained type (57.4 and 59.5 percent SiO_2) with a mineral assemblage similar to the host rock (plagioclase >> orthopyroxene, minor clinopyroxene) and a coarser-grained type (56.5 percent SiO_2) that is dominated by plagioclase with lesser amounts of orthopyroxene and likely former phenocrysts of amphibole that have been completely replaced by iron-titanium oxides. Enclaves from Mount Hood lavas have lower silica contents than their hosts and are typically basaltic andesite in chemical composition. Nonetheless, mineralogically the enclaves are more similar to their andesitic hosts in that they lack olivine, a common mineral phase of basaltic andesites from regional volcanoes.

The lava flow along U.S. 26, locally overlain by till of the last ice age, is one of a sequence we call the andesite of south flank (h4sf), which can be traced from just south of U.S. 26 to a bit above Timberline Lodge, a total altitude range of about 800 m (fig. 50). The farthest travelled part of the flow sequence is about 10 km from the present vent. Paleomagnetic

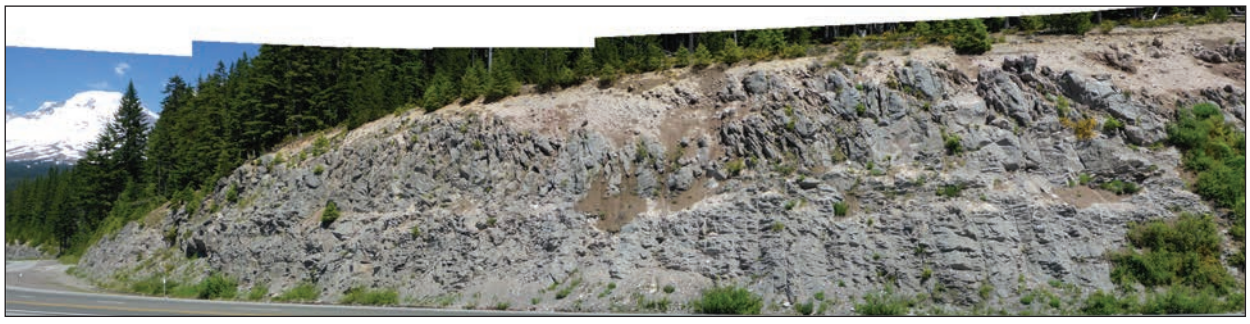

Figure 49. Merged photograph of U.S. Highway 26 roadcut that exposes ~130-ka andesite of south flank (h4sf) at Stop 16.

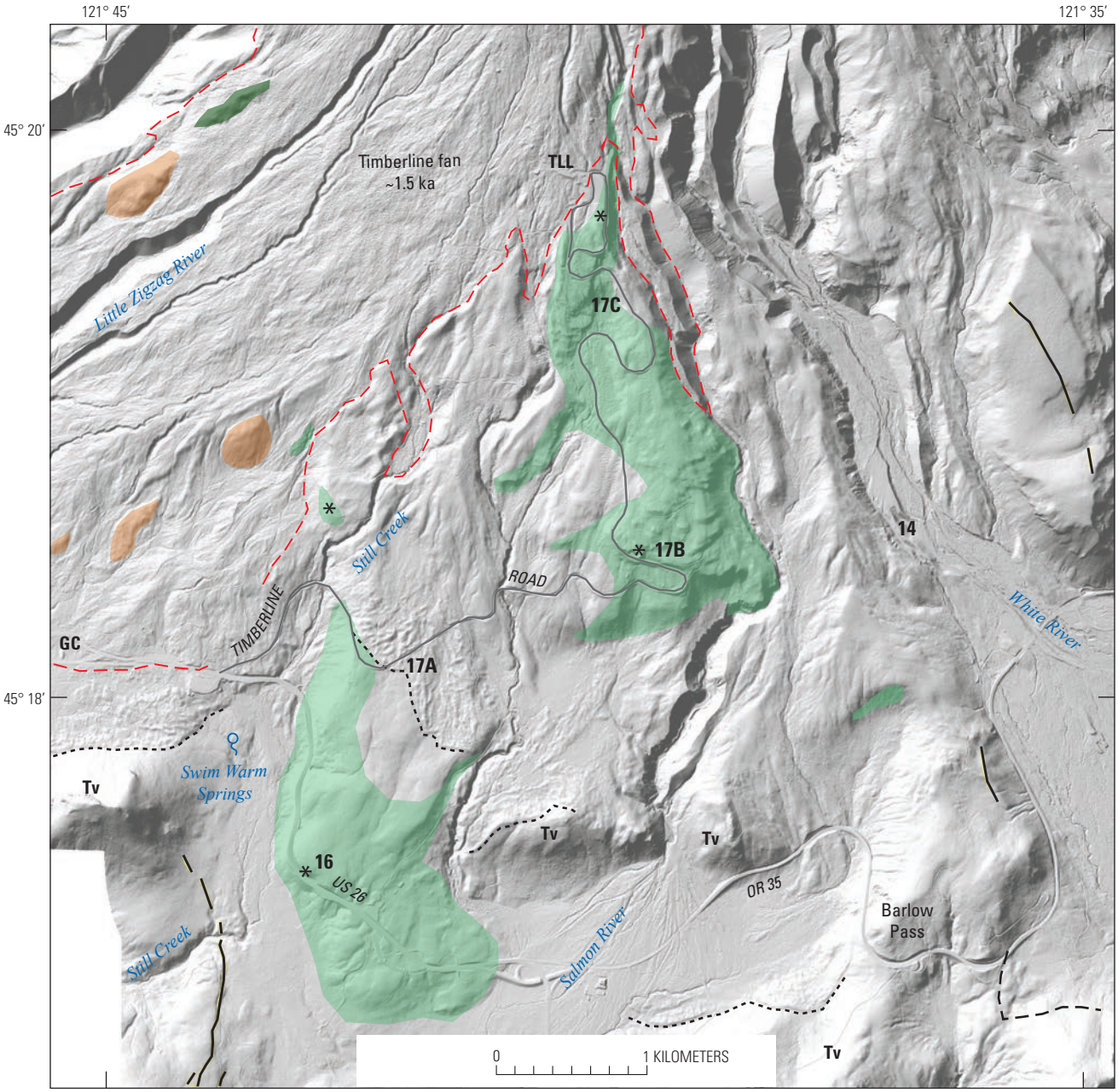

Base from 2010 Oregon Department of Geology and Mineral Industries, Oregon Lidar Consortium, Mount Hood lidar data quadrangle series, hillslope-shaded, bare-earth elevation model, 3 ft interval; Mount Hood South quadrangle

EXPLANATION

- h4sf — Andesite of south flank
- Andesite of Zigzag Canyon
- Deposits of Polallie eruptive period
- Faults—Quaternary
- Timberline fan (1.5 ka)
- Downslope limit of till rich in dome lava
- Road
- Limit of glaciers during last glacial maximum
- Paleomagnetic data
- 21 — Field-trip stop

Figure 50. Shaded-relief lidar image of south flank between U.S. Highway 26 and Timberline Lodge (TLL) showing key units and field trip stops along Timberline Road. Bright green areas in center of image are places where ~130-ka andesite of south flank (h4sf) is at or close to surface. Most of the area between the green polygons is likely underlain by the flow, but consists of thick cover of till or deposits of Polallie age. Short-dashed lines are downslope limit of till rich in dome lava; much of till is hummocky as at Stop 17A. Long-dashed black line is limit of glaciers during last glacial maximum, much of which lies south of figure. GC, Government Camp; Tv, volcanic rocks of late Tertiary age.

data suggest the flows were not erupted during a single time period, but rather in at least two pulses separated by a sufficiently long time period for the secular magnetic field to move (fig. 51). Lavas of similar age and composition are also found on the west flank from below Illumination Rock into lower Lost Creek, a distance of about 6.5 km (fig. 5).

Travel

Continue west on U.S. 26 for 1.25 mi to Timberline Road. Turn right for the 5.5-mi drive to Timberline Lodge.

Stop 17. Three Stops Along Timberline Road

The road from U.S. 26 to Timberline Lodge (fig. 50) offers numerous roadcut exposures and wide shoulders for parking. Three localities are described here (Stops 17A–C) illustrating three different eruptive and glacial units.

Stop 17A. Recessional Till Rich in Dome Lava

Location: 45.3024° N., 121.7245° W.; UTM 10T 600005E, 5017116N; altitude 4,320 ft

Timberline Road cuts through hummocky terrain, creating a series of degraded exposures in till consisting primarily of dome lava in a sandy matrix; typical faceted, soled, and striated till stones are rare (fig. 52). Note the distinctive surface texture of the terrain, wide distribution, and some puzzling linear boundaries on lidar imagery (fig. 50). Closed depressions abound, many 5–10-m deep. In contrast to dome-lava-rich till forming the maximum last-glacial advance as at Stop 11 in the southeastern sector (fig. 37), such till in the southern sector is in a recessional position, upslope from the LGM till that is largely devoid of dome lava. Apparently during the glacial maximum, the glacier flowing over this area was not depositing till with abundant dome lava, but during recession conditions changed and the till became rich in dome lava. We infer that extrusion of an appropriately located collapsing summit lava dome of Polallie age generated rockfalls and pyroclastic flows, thereby mantling the glacier with debris that was transported farther downslope. Thinning of the receding glacier mantled in debris led to stagnation and eventual melt out of residual ice and creation of this hummocky morainal terrain.

Stop 17B. Andesite of South Flank

Location: 45.3084° N., 121.7049° W.; UTM 10T 601525E, 5017805N; altitude 4,840 ft

A wide turnout on the south side of the road for parking and a small quarry on the north side make this a safe and quiet spot for studying the 128-ka andesite of south flank (h4sf). The switchback below the stop is needed as the road climbs the steep slope at the nose of a lava-flow lobe. Wise (1968) in his Mount Hood guidebook for the July 1968 Andesite Conference surmised that the thick basal breccia in this outcrop (fig. 53) was the result of explosive interaction between the lava flow and snow or ice. Much of the lava is oxidized to a reddish hue. Three lava samples along this cut and small

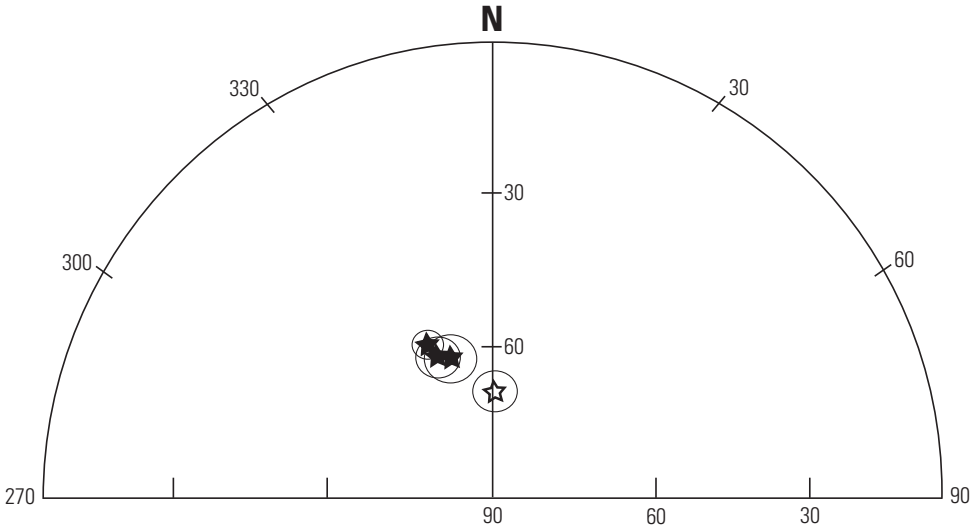

Figure 51. Upper-hemisphere plot of paleomagnetic directions with corresponding site dispersion cones (σ95) for four Mount Hood lava flows of the ~130-ka andesite of south flank (h4sf). Filled stars correspond to two sites along Timberline Road and a site along West Leg Road (symbol in small green polygon northwest of Still Creek label); the open star corresponds to the lava flow at Stop 16 along U.S. Highway 26 (U.S. 26; sites shown on fig. 50). K-Ar and $^{40}Ar/^{39}Ar$ ages for the flows overlap, but the paleomagnetic data show a separation in time between emplacement of the lava flow along U.S. 26 and the others, even though the U.S. 26 and West Leg Road lava flows have similar chemistry.

Figure 52. Photograph of recessional morainal deposits along Timberline Road about 1.1. mi from U.S. Highway 26 (Stop 17A). Succession of high and low roadcuts is a result of the road traversing ridges and depressions. A short walk into the forest reveals striking dead-ice topography. Till is largely derived from collapse of growing near-summit lava domes of Polallie age. Inset shows soled and striated clast from till.

Figure 53. Photograph of ~130-ka andesite of south flank (h4sf) with thick basal breccia exposed 2.7 mi from U.S. Highway 26 (Stop 17B). Outcrops here are also the site for paleomagnetic data. A small quarry to left of outcrop provides a good location to study flow.

quarry have 60.3–60.5 percent SiO_2 and ~1.22 percent K_2O; three mafic enclaves from the cut have 55.3–57.1 percent SiO_2 and 0.69–1.06 percent K_2O. One plutonic inclusion has 54.4 percent SiO_2 and 0.51 percent K_2O.

Stop 17C. Deposits of Polallie Eruptive Period

Location: 45.3235° N., 121.7052° W.; UTM 10T 601481E, 5019486N; altitude 5,520 ft

Wide turnouts on the west side of the road just north of the entrance to Alpine Campground and another at a curve across from the north end of the long roadcut on the east side of the road make this a good place to look at diamicts of the Polallie eruptive period where they overlie oxidized lava of the andesite of south flank (fig. 54). The diamicts are dome-lava rich, coarse grained, and crudely bedded. The matrix is granular and locally friable. The deposits form a surface that appears to be equivalent altitudinally to that defined by deposits we will see at Stop 18C on the rim of White River canyon. The vertical section there reveals tens of meters of meter-thick, laterally extensive diamicts of pyroclastic-flow and lahar origin. We infer the sequence at Stop 17C is similar, but thinner and more accessible. The sequence is younger than the recessional till at Stop 17A and, in the absence of glaciers, formed extensive pyroclastic fans similar to those of late Holocene age. Note common prismatically jointed clasts, joint-bounded fragments, and locally preserved breadcrust surface texture. Three samples of prismatically jointed clasts from a lower bed near the south end of the exposure have 63.4–64.3 percent SiO_2 and two samples from higher in the outcrop have 63.8 percent SiO_2.

A plot of K_2O versus silica for clasts from south-flank deposits of the Polallie eruptive period, dome-lava-rich till, and Steel Cliff lava dome (Stops 13 and 18C) shows compositional similarity (fig. 55). Some of the lava dome(s) from which south-flank deposits of Polallie age were derived were likely removed from the summit by a debris avlanche that occurred at or near the start of late Holocene eruptions.

Travel

Continue 0.7 mi to main parking lot at Timberline Lodge; Northwest Forest Pass is not required.

Figure 54. *A*, Photograph of deposits of Polallie eruptive period (h2pc) overlying andesite of south flank (h4sf) in cuts along Timberline Road about 4.6 mi from U.S. 26 and just north of Alpine Campground (Stop 17C). *B*, Sequence of crudely bedded bouldery diamicts with sandy matrix and common, prismatically jointed clasts and joint-bounded fragments. C, Clast with preserved breadcrust surface texture. *D*, Friable sandy matrix of pebbly diamict.

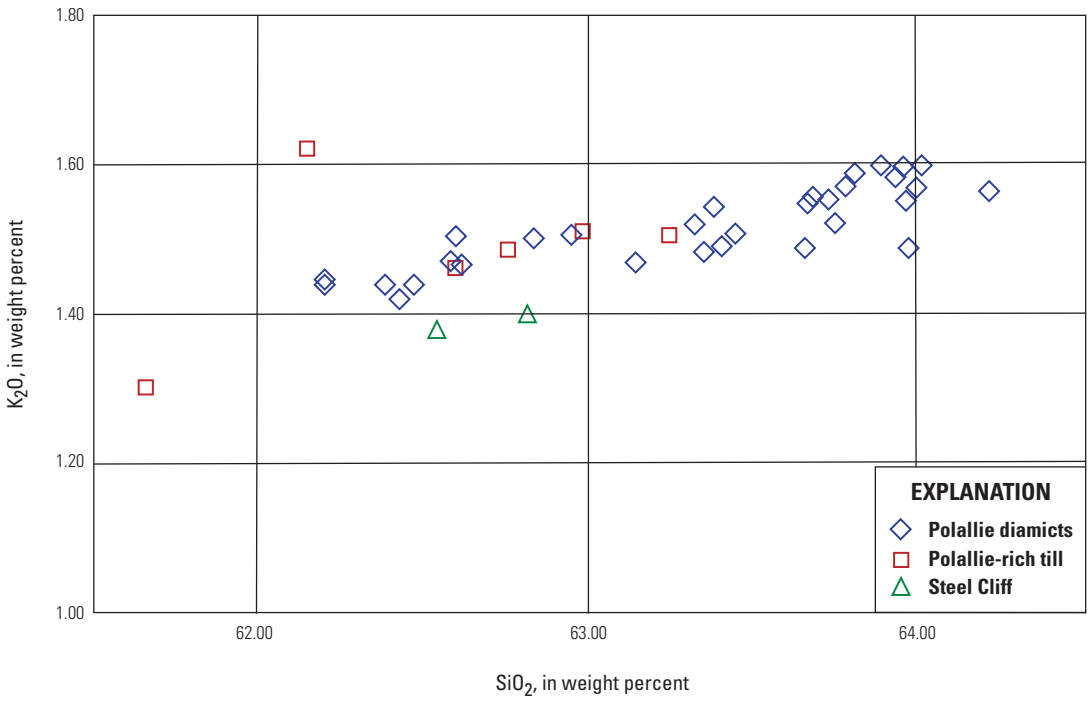

Figure 55. Plot of K_2O versus silica for clasts from deposits of Polallie eruptive period, Steel Cliff lava dome, and prismatically jointed clasts from recessional till rich in Polallie dome lava, all from south flank localities. Chemical similarity of some of the clasts in till and nearby Polallie flow deposits is a reflection of eruption during glacier recession.

Timberline Lodge Area

Timberline Lodge, designated a National Historic Landmark in 1977, was built during the Great Depression under auspices of the Works Progress Administration (WPA), part of the Roosevelt administration's New Deal. Construction began in the spring of 1936 and, remarkably, the largely completed lodge was dedicated by President Franklin Roosevelt on September 28, 1937. By February 1938 the lodge was opened to the public. The work of numerous artists (workers in wood, metal, mosaic, painting, and textile, among others) is displayed throughout the lodge. The nonprofit Friends of Timberline (http://www.friendsoftimberline.org/) have worked tirelessly since 1975 to preserve and replace textiles and artifacts. Numerous other projects have enhanced the lodge and ski area (http://www.timberlinelodge.com/), which is operated by RLK and Company, and managed by the Mount Hood National Forest (http://www.fs.usda.gov/main/mthood/home). Forest Service interpreters provide tours of the lodge and surroundings.

Striking views of the upper south flank and crater abound from the Timberline Lodge area (fig. 56). Around-the-volcano Timberline Trail passes just upslope of the lodge and offers access to several field-trip stops described below. A primitive road (authorized vehicles only) leads to Silcox Hut, located at about 7,000 ft, near the base of the upper ski lift that provides skiing through much of the summer on Palmer "Glacier," which is actually a perennial snowfield. The Magic Mile Lift, whose base is just west of the lodge, offers scenic chairlift rides during the summer to near Silcox Hut. Crater Rock and thermal areas (weak fumaroles) are accessible by hiking from Palmer snowfield. The main climbing route passes east of Crater Rock and up to the summit on steep ice, snow, and rock. Climbing season is chiefly in late winter and spring. The rockfall hazard above Crater Rock is severe in summer; snow avalanches and severe weather are concerns in winter and spring.

Views southward show two major High Cascade composite volcanic centers of Quaternary age—Mount Jefferson (78 km south-southwest) and Three Sisters (145 km south). Numerous regional shield volcanoes form the range between the composite centers.

Trampling of vegetation and creation of new paths by hikers is of great concern here and much has been done to revegetate and protect off-trail areas. Stay on the trails.

The Mount Hood Wilderness Area, which has restrictions on use, size of party (typically 12), and livestock, wraps around the ski area. Signs along trails mark the Wilderness boundary and have registration forms that need to be filled out and carried on pack or clothing.

The Timberline fan extends upslope to the base of Crater Rock at about 3,050 m (10,000 ft); the upper part of the fan is buried by bouldery deposits of Old Maid age and late neoglacial till. Crater Rock (63.4–64.4 percent SiO_2, fig. 56) is a residual plug of the youngest lava dome on the volcano and marks the vent during the late-18th-century Old Maid eruptive period. The vent for eruptions during the Timberline eruptive period about 1.5 ka was likely in the same position. Crater Rock lies in the breached summit crater, which was likely formed by a debris avalanche(s), probably at or near the beginning of the Timberline eruptive period.

Stop 18. Hike East from Timberline Lodge on Timberline Trail to Rim of White River Canyon and Additional Sites

Walk north from Timberline Lodge to the Timberline Trail and hike east; total distance to Stop 18D and back is about 3 km (2 mi) with an altitude change of about 125 m (400 ft). This area is at the eastern margin of the large south-flank pyroclastic fan of Timberline age (fig. 57). Typical reddish-gray pyroclastic-flow and lahar deposits of the Timberline eruptive period (1.5 ka) overlie an erosional unconformity marked by a yellowish-brown buried soil and distinctly grayer deposits of the latest Pleistocene Polallie eruptive period. Seismic station TIMB lies at base of the old concrete water tower in a grove of trees upslope from the trail.

Stop 18A. Thin Deposit of Pyroclastic Density Current of Old Maid Age

Location: 45.3334° N., 121.7070° W.; UTM 10T 601320E, 5020585N; altitude 6,000 ft

A thin, gray, granular deposit is sporadically preserved ahead along the trail. It originated from a low-density pyroclastic-density current (also called a pyroclastic surge) during the Old Maid eruptive period of the late 18th century. Most flow deposits of Old Maid age followed White River canyon (Stop 14) or the western margin of the fan (figs. 7, 57) to the upper Sandy River (Stop 23). But this single surge swept the

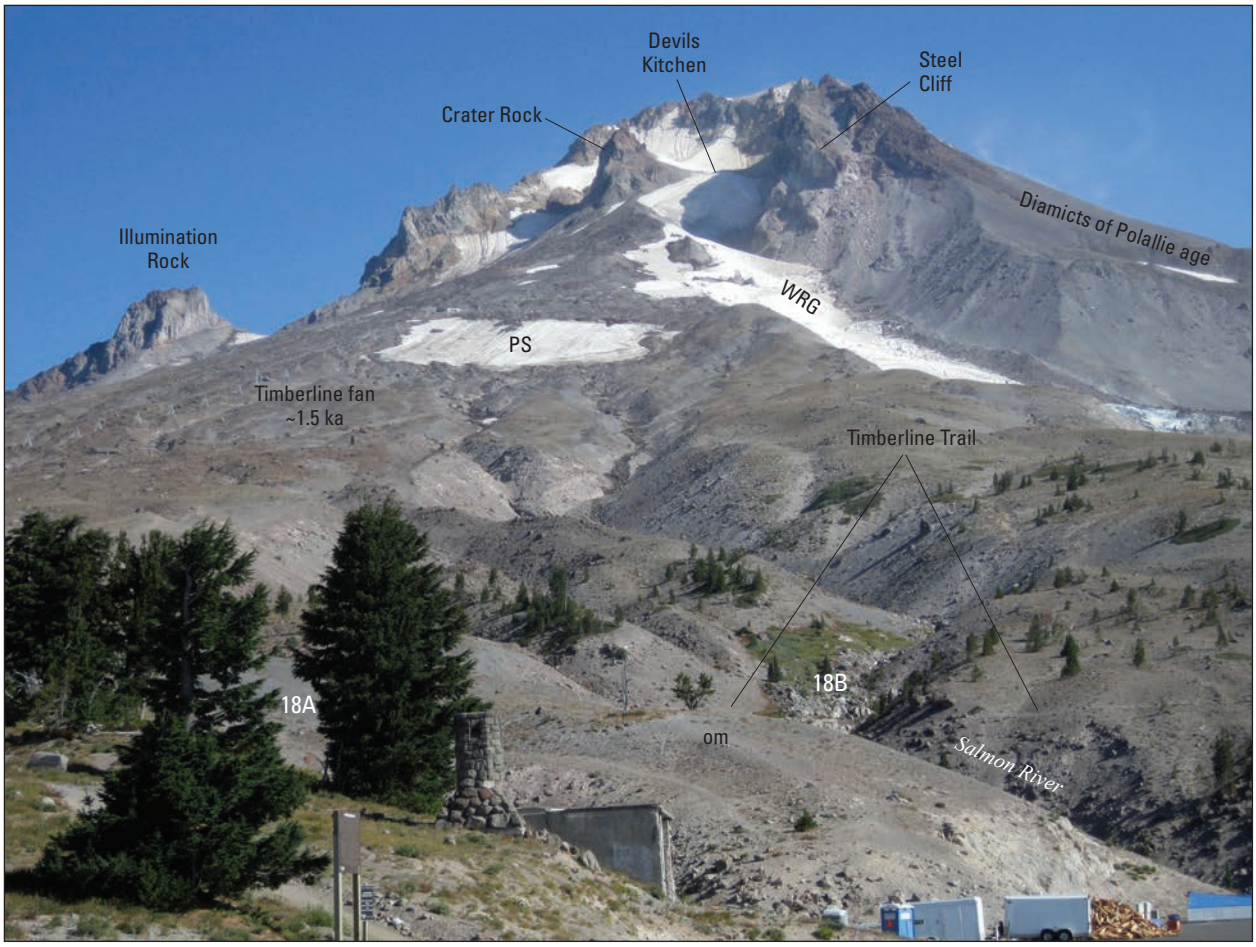

Figure 56. View from north edge of the main Timberline Lodge parking lot. In near distance by trailers is overflow parking area and base of road to Silcox Hut (only open to authorized vehicles). Late Holocene vent is marked by Crater Rock lava dome in breached summit crater; Devils Kitchen is one of several thermal areas with weak fumaroles. Steel Cliff lava dome, cut by east crater wall, is of Polallie age. The south flank Timberline fan consists primarily of pyroclastic-flow and lahar deposits of the late Holocene Timberline eruptive period (~1.5 ka. Timberline Trail (here part of the Pacific Crest National Scenic Trail) heads east and west from Timberline Lodge, which lies to left of view. Two stops are shown along the hike to White River overlook: Stop 18A, where thin deposits of a pyroclastic density current of Old Maid age (om) are discussed, and Stop 18B, at the highest exposure of andesite of south flank. PS, Palmer snowfield; WRG, White River Glacier.

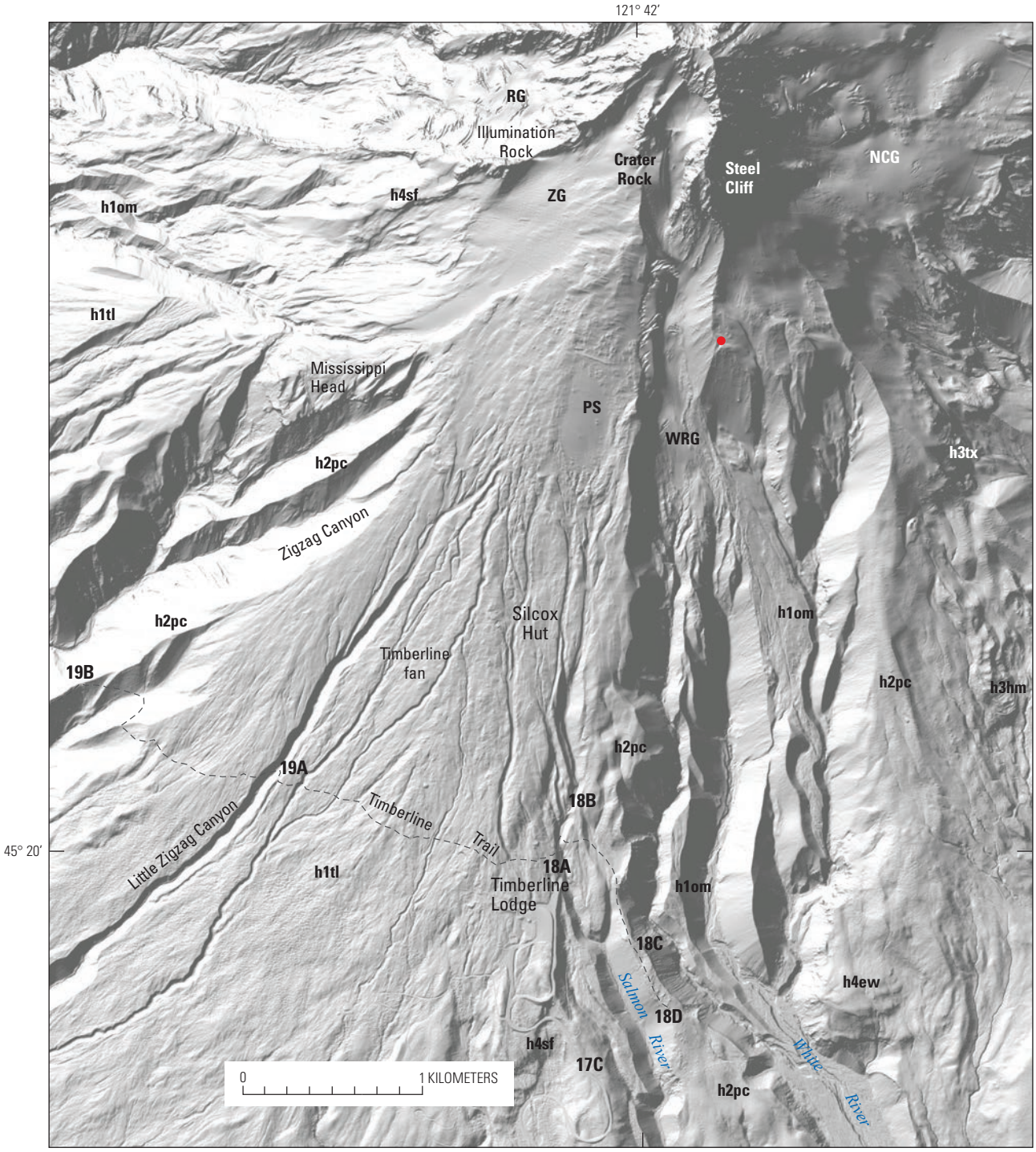

Base from 2010 Oregon Department of Geology and Mineral Industries, Oregon Lidar Consortium, Mount Hood lidar data quadrangle series, hillslope-shaded, bare-earth elevation model, 3 ft interval; Government Camp and Mount Hood South quadrangles

EXPLANATION

10 **Field-trip stop**

Timberline age deposit in upper White River

Trail

Figure 57. Shaded-relief lidar image of area from Timberline Lodge to summit showing key features and location of hiking Stops 18 and 19, as well as Stop 17C. h1om, deposits of Old Maid eruptive period; h1tl, deposits of Timberline eruptive period; h2pc, deposits of Polallie eruptive period; h3tx, 44.5-ka andesite of Texas; h3hm, 70–60-ka andesite of Mount Hood Meadows; h4sf, ~130-ka andesite of south flank; h4ew, 140-ka andesite of east fork White River. PS, Palmer snowfield; ZG, Zigzag Glacier; WRG, White River Glacier; NCG, Newton Clark Glacier; RG, Reid Glacier.

Figure 58. Photograph of dug pit east of Timberline Lodge in ~30-cm-thick, gray, friable deposit of pyroclastic density current of Old Maid age. Deposit overlies thin gray to pink ash-cloud deposits that bury thin soil with black organic horizon and slightly weathered surface of pinkish-gray pyroclastic-flow deposit of Timberline age. The friable deposit contains scattered angular to subangular glassy lapilli and occasional small blocks. Inset shows an outsized clast of dome lava ~25 cm in diameter in a pit farther south. Pen is 13.5-cm long.

headwaters of Salmon River and can be traced at least 1 km farther downstream. Unlike the meter-or-more-thick, cobble- and boulder-rich pyroclastic-flow deposits typical of collapsing lava domes, this deposit is tens of centimeters thick and relatively deficient in coarse clasts (fig. 58). Clasts are commonly angular to subangular and glassy. The deposit lies on pinkish-gray block-and-ash-flow deposits of Timberline age. We infer that it may be related to the extensive pyroclastic-flow deposit in White River (Stop 14). We surmise this surge may have originated as an overriding, less-dense cloud that swept down the Salmon River while the denser pyroclastic flow followed the deep White River valley. Except for this potentially deadly event and ashfall, areas around Timberline Lodge were probably affected little by Old Maid eruptions.

Analyses of clasts from diamicts of the Timberline and Old Maid eruptive periods are quite similar, but Timberline deposits show a larger silica range and about 0.1 percent higher K_2O (fig. 59) for a given silica content. Such a range in K_2O for successive but closely spaced eruptive episodes is reminiscent of the K_2O range in analyses from many map units of older lavas and diamicts, such as the andesite of Mount Hood Meadows (fig. 43) and Polallie deposits (fig. 55).

Paleomagnetic data distinguish Old Maid from Timberline deposits and suggest both had durations of less than a century, while Polallie deposits display a wide range in paleomagnetic data consistent with the eruptive period's long duration (fig. 60). As with chemical data, the small but consistent change in paleomagnetic direction between deposits of Old Maid and Timberline age is reminiscent of similar changes in older lava-flow units that may span a millennium or more.

Travel

The trail ahead traverses the shallow canyon of Salmon River. Stop 18B is about 200 m north of the stream crossing. While hiking off the main trail, avoid trampling vegetation, keep to existing paths or walk along the largely barren stream bottom.

Stop 18B. Andesite of South Flank Underlying Deposits of Pyroclastic Flows and Lahars of Latest Pleistocene and Late Holocene Age

Location: 45.3358° N., 121.7053° W., UTM 10T 601448E, 5020857N; altitude 6,100 ft

Salmon River, which heads as a meltwater stream from the Palmer snowfield (glacier during 19th century), has cut

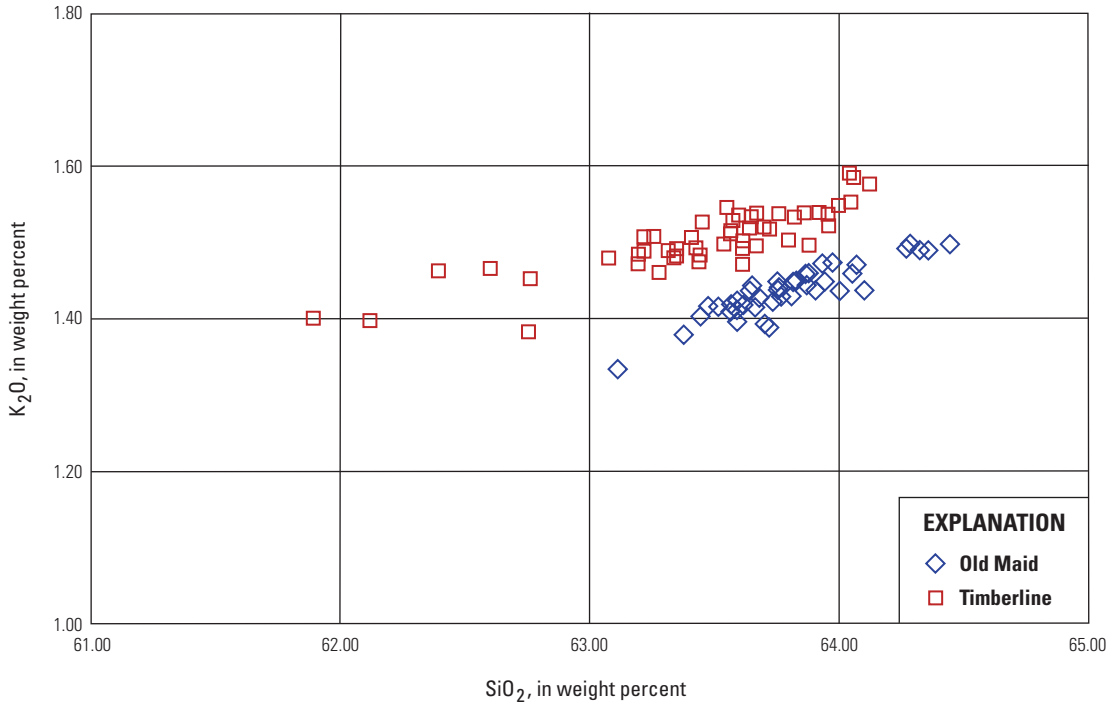

Figure 59. Plot of K_2O versus silica for samples of blocks from deposits of Old Maid and Timberline eruptive periods showing ~0.1 percent higher K_2O in Timberline lava. Additional details of Old Maid analyses are in figure 48.

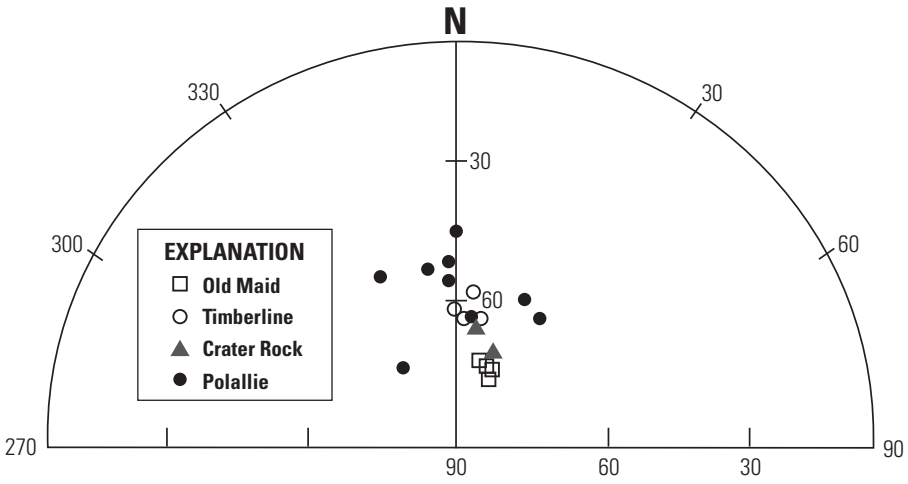

Figure 60. Upper-hemisphere plot of paleomagnetic directions for pyroclastic-flow deposits from Old Maid (late 18th century), Timberline (~1.5 ka), and Polallie (30–15 ka) eruptive periods and the Crater Rock lava dome. Mean direction of Old Maid is D=18.5°, I=70°, and for Timberline, D=5°, I=62°. Polallie directions vary owing to its long duration.

this shallow canyon through the south-flank volcaniclastic fan of latest Quaternary age to expose an underlying lava flow of the andesite of south flank (h4sf: fig. 61). This is the highest exposure of the andesite of south flank in this sector. The lava (K-Ar age of 145±8 ka; $^{40}Ar/^{39}Ar$ age of 132.1±2.1 ka) is part of the sequence of flows of similar age and composition that we have followed from U.S. 26 (figs. 50, 62). The lava is typical Mount Hood andesite. It contains 60.4 percent SiO_2, 1.23 percent K_2O, and 44.5 percent crystals (phenocrysts and microphenocrysts), composed dominantly of plagioclase with lesser amounts of orthopyroxene and minor clinopyroxene. As in most lava from Mount Hood, this flow contains abundant, mostly rounded, fine-grained mafic enclaves.

Illumination Rock (62.9–63.3 percent SiO_2; undated but <130 ka), the prominent tower below and west of the summit, overlies diamicts, which in turn overlie a sequence of lava flows on the southwest flank that are grouped with the andesite of south flank on the basis of similar chemical composition and age (fig. 62).

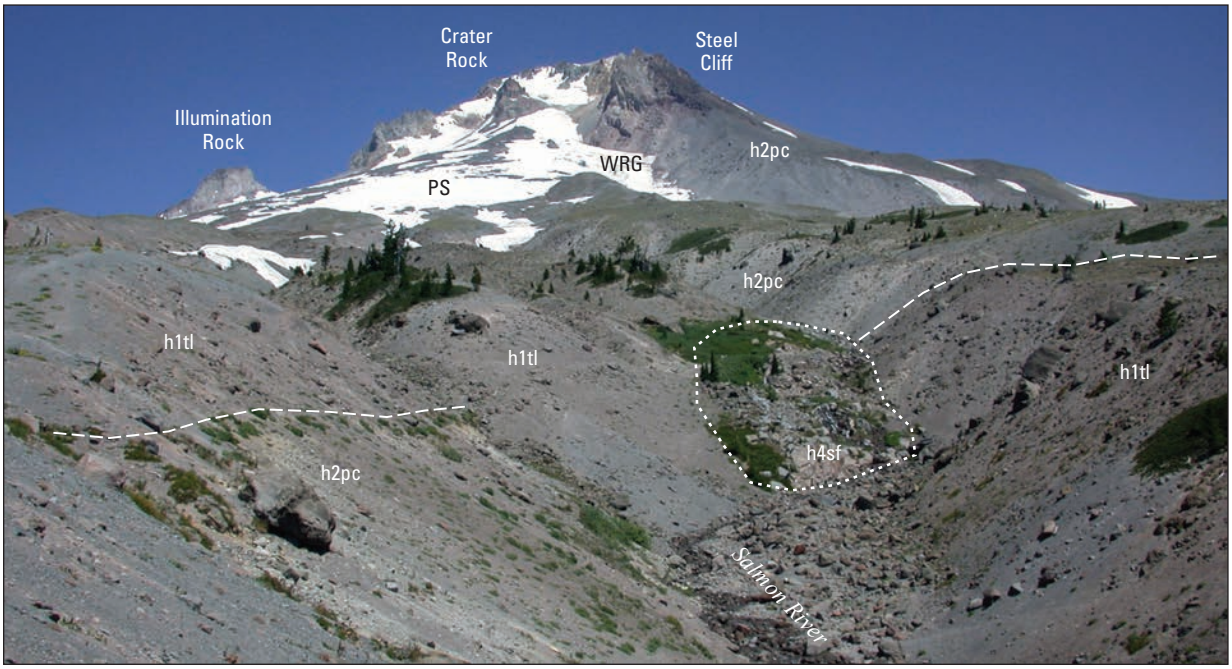

Figure 61. Photograph of Stop 18B along Salmon River above Timberline Trail crossing. This is the highest outcrop of andesite of south flank (h4sf) in this sector; above here it is buried by younger diamicts of Polallie (h2pc) and Timberline (h1tl) eruptive periods. Yellowish soil (dashed line at center left) marks disconformity eroded into a broad fan of Polallie deposits prior to burial by Timberline deposits. This area lies at the east margin of the Timberline fan. $^{40}Ar/^{39}Ar$ age from this site is 132.1±2.1 ka. PS, Palmer snowfield; WRG, White River Glacier.

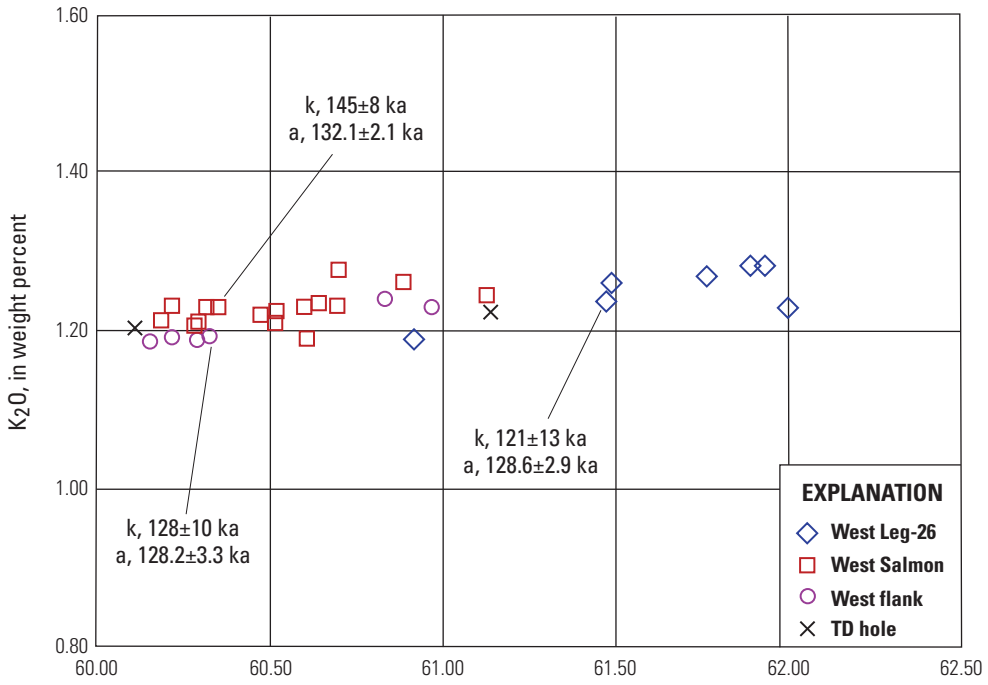

Figure 62. Plot of K_2O versus silica for samples of andesite of south flank arranged by geographic distribution. West Leg-26, low-altitude samples from south flank; West Salmon, samples from upper Timberline Road to Stop18B; West-flank, samples from beneath Illumination Rock westward to Lost Creek; TD hole, samples from 425-m-deep drill hole located about 270 m south of Timberline Lodge (White, 1980). The sample (TDH-1) with 60.1 weight percent SiO_2 is from the first lava flow below about 25 m of diamicts of Timberline and Polallie age; the sample (TDH-3) with 61.1 weight percent SiO_2 is from the third lava flow below the surface diamicts. K-Ar (k; Scott and others, 1997a) and $^{40}Ar/^{39}Ar$ (a; Calvert and D. Ferguson, written commun., 2016) results are given in thousands of years (ka).

Travel

Return to the stream crossing and continue east along Timberline Trail towards White River canyon. The hike ascends reddish diamicts of Timberline age with huge prismatically jointed blocks; ahead the contact with deposits of Polallie age is marked by a change to grayer diamicts in which a yellowish-brown soil is formed, and a change to rolling terrain. The trail descends and reaches the rim of White River canyon and continues through meadows and clumps of mountain hemlock and whitebark pine. Choose an appropriate viewpoint along rim.

Stop 18C. View from Rim of White River Canyon

Location: 45.3300° N., 121.7014° W., UTM 10T 601764E, 5020211N; altitude 5,760 ft

The two forks of White River visible from here are deeply incised in unconsolidated diamicts (fig. 63). The forks head at two snouts of White River Glacier, a steep narrow glacier that is fed chiefly by snowdrift from the broad fan surface west of the glacier. Such augmented accumulation allows the glacier to extend to relatively low altitude for its southern exposure. The glacier is eroding a trench along the eastern margin of the south-flank fan leading up to Crater Rock, which ensures that White River will be one of the principal pathways for pyroclastic flows if lava extrusion begins anew in the Crater Rock area.

An andesite lava flow (h4ww, 60.8–61.2 percent SiO_2) exposed in the informally named west fork White River is about 100 m lower in altitude than the lava flow at Stop 17B and on the basis of chemical composition (higher K_2O) is probably an unrelated flow. Vegetation enhanced by spring seepage marks the contact between permeable diamicts and the lava flow.

The lava flow is deeply buried by gray diamicts of Polallie age, which are well exposed in the cliff below and in terraces farther downstream. The diamicts occur in beds 1 to 3 m thick, are bouldery, poorly sorted, locally graded, and appear to have accumulated relatively rapidly, as there is no sign of weathering or significant erosional disconformities between flow units. Prismatically jointed clasts occur in many beds. Reddish-gray diamicts of Timberline age locally cap the Polallie sequence farther up valley.

The wall of a paleovalley that was cut in Polallie deposits is visible below where a soil that contains rooted snags is buried by diamicts of the Old Maid eruptive period. The lack of charring of the snags is evidence that the initial diamicts that buried the paleovalley were not hot enough to burn vegetation. The snags yield radiocarbon ages of about 200 yr; detailed dendrochronology of trees killed or damaged during the Old Maid eruptive period suggests that eruptions began in 1781 C.E. and lasted until the mid-1790s (see summary in Pierson and others, 2011). The Old Maid deposits in the upper White River valley form two broad surfaces; the terrace below the viewpoint (Mesa terrace) lies between the west and middle forks of White River, and the surface east of the middle fork that terminates at a high ridge formed of deposits of Polallie age. Not visible from here is a canyon of the east fork White River, which lies between the two ridges of Polallie deposits at center right in figure 63.

Diamicts of Timberline age are not conspicuous in upper White River canyon. They occur on the west rim of the upper canyon, but are not found in the reach below us. Lahar, lahar-runout, and alluvium found 20 km downstream record some sort of disturbance of the watershed during Timberline time

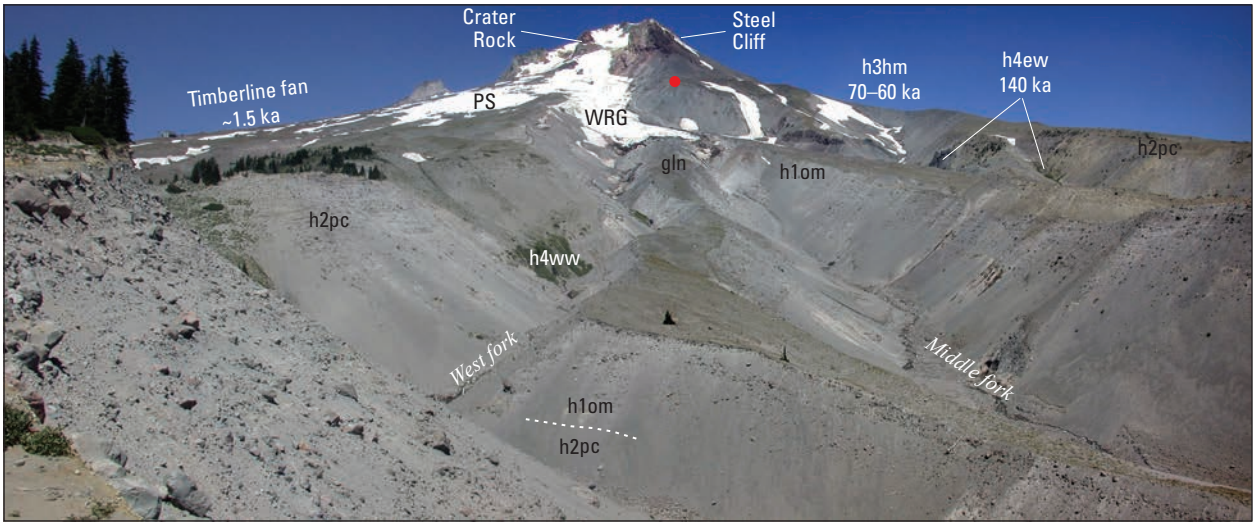

Figure 63. View of upper White River canyon from Stop 18C showing relations between lava flows and younger diamict units. Dotted white line in bottom center marks soil formed on post-Polallie paleovalley wall; tree stumps and logs are locally exposed. A thick fill of diamicts derived from lava-dome growth during Old Maid eruptive period filled the paleovalley. Erosion of fill by three forks of upper White River has created a landscape that produces numerous debris flows, primarily during intense autumn rainstorms and sudden releases of meltwater from White River Glacier. h4ew, andesite of east fork White River; h4ww, andesite of west White River (undated); h3hm, andesite of Mount Hood Meadows; h2pc, diamicts of Polallie eruptive period (30 to ~15-ka); h1om, diamicts of Old Maid eruptive period (late 18th century); gln, neoglacial deposits; WRG, White River Glacier; PS, Palmer snowfield. Red dot marks site of small deposit of Timberline age below Steel Cliff.

Figure 64. View looking downstream from Stop 18C to confluence of three forks of upper White River. The 140-ka andesite of east fork White River (h4ew) lies against high ridge formed by ~170-ka andesite of Switchback Falls (h4sb), both emplaced during glacial periods. Deposits of Polallie eruptive period (h2pc) form high terrace in center right; deposits of Old Maid eruptive period (h1om) form dissected fill. Broad active valley floor attests to frequent debris flows and channel shifts.

(J.J. Major, written commun., 2015), but no proximal deposits are exposed other than high on the east rim below Steel Cliff (red dot, fig. 63). It is likely that a now-eroded divide of Polallie diamicts protected the White River from most of the Timberline pyroclastic flows and lahars. Headward erosion by the White River and Glacier between Timberline and Old Maid eruptive periods breached the divide and exposed the canyon to flows of Old Maid age.

The view of the crater and summit area is much like that from Stop 18B, but from here there is a better perspective of the fan of Polallie diamicts that was derived from the growth and collapse of Steel Cliff and other near summit lava domes. A lava block from the upper fan deposits at Steel Cliff yielded an imprecise K-Ar age of 16±8 ka. Blocks from Polallie deposits are not chemically identical to those of Steel Cliff, but they are on similar trends (fig. 55).

Downstream, andesite lava flows that form the prominent ridge east and north of White River are andesite of east fork White River (h4ew; K-Ar age of 140±11 ka) and ~170-ka andesite of Switchback Falls (h4sb; fig. 64) viewed from Stop 14.

Note the thick deposits of eolian sand derived from dry sloughs of debris off the steep southwest wall of White River canyon. Strong, hot east winds during the summer dry and scour matrix from the diamicts, releasing rockfalls which create more rockfalls that together send up clouds of fine gravel, sand, and silt which are blown onto the ridge top. Presumably this has been a significant process since Old Maid events radically altered the canyon with partial filling and subsequent incision to create steep unstable canyon walls.

Travel

Continue down Timberline Trail about 300–500 m to an area of severe eolian erosion.

Stop 18D. Ash-Cloud Deposits of Timberline Eruptive Period

Location: 45.3260° N., 121.6980° W.; UTM 10T 602038E, 5019767N; altitude 5,560 ft

Numerous blowouts expose the predisturbance surface of thick tephra of Timberline age overlying a soil developed in Polallie deposits (fig. 65*A*). Such tephra, elutriated from moving pyroclastic flows and prevailing westerly winds blowing it eastward, consists of numerous thin beds and laminae. Tephra fallout from small explosive events is a subordinate process at Mount Hood. Tephra of Old Maid age is seldom preserved on this exposed ridge. Where not disrupted by root casts and burrows, the tephra of Timberline age consists of a basal unit composed of thin gray beds (many normally graded) that are slightly coarser grained than an upper pinkish-gray unit. Owing to erosion, the original thickness is difficult to estimate but was probably about 1 m.

Latest Holocene tephra is much better preserved in Elk Meadows (fig. 65*B*), which lies 7 km east-northeast from here and 7 km southeast of the crater. Laminated-tephra deposits of Timberline age are about 50-cm-thick, with a thin interbed of ashy peat just below mid-section. The interbed separates the slightly sandier light-gray basal tephra from the finer, pinkish-gray upper tephra and is evidence of a break in tephra deposition, which allowed peat accumulation. A 73-cm-thick layer of peat separates the Timberline ash from a 7-cm-thick bed of gray ash of Old Maid age, which in turn is overlain by about 15 cm of younger peat. Average rates of peat formation estimated from the thickness of peat between dated horizons (about 0.5 mm/yr) suggest that the 1–2-cm peat within the Timberline sequence formed in roughly four decades. The actual time was probably less owing to the higher inorganic sediment concentration in the interbed compared with that in the peat above and below. In a given exposure, tephra of Old Maid age typically averages about 20 percent of the thickness of tephra of Timberline age. Radiocarbon ages of peat do not provide much precision, but secular-variation paleomagnetic data suggest that the entire Timberline sequence was deposited in less than 100 yr because the paleomagnetic directions of the upper and lower sequences are indistinguishable (D=0°, I=61.2° and D=3.4°, I=62.6°) and consistent with directions from pyroclastic-flow deposits of Timberline age (fig. 60).

Return to Timberline Lodge.

Stop 19. Hike Timberline Trail West from Timberline Lodge to Little Zigzag and Zigzag Canyons

Note: 3.4 km (2 mi) roundtrip to Little Zigzag Canyon (40-m [120-ft] altitude change); 6.6 km (4 mi) roundtrip to rim of Zigzag Canyon (150-m [500-ft] altitude change).

West of Timberline Lodge, Timberline Trail traverses the south flank pyroclastic fan of Timberline age (fig. 57). Its surface is studded with large, prismatically jointed blocks of dense to vesicular dome lava. About 1.7 km west of the lodge, the trail crosses 25-m-deep Little Zigzag Canyon, which exposes a sequence of pyroclastic-flow and lahar deposits of Timberline age that offer relatively easy access (fig. 66*A*).

Stop 19A. Diamicts of Timberline Eruptive Period Exposed in Little Zigzag Canyon

Location: 45.3374° N., 121.7262° W.; UTM 10T 599808E, 5021003N; altitude 5,880 ft

Much of the canyon wall is covered with colluvium, but good outcrops lie on the canyon's west wall about 400 m north of the trail at altitude 6,160 ft (fig. 66*B*). The section consists of typical deposits of the Timberline eruptive period: (upward) lower gray diamict, light-gray ash-cloud deposit (prominent

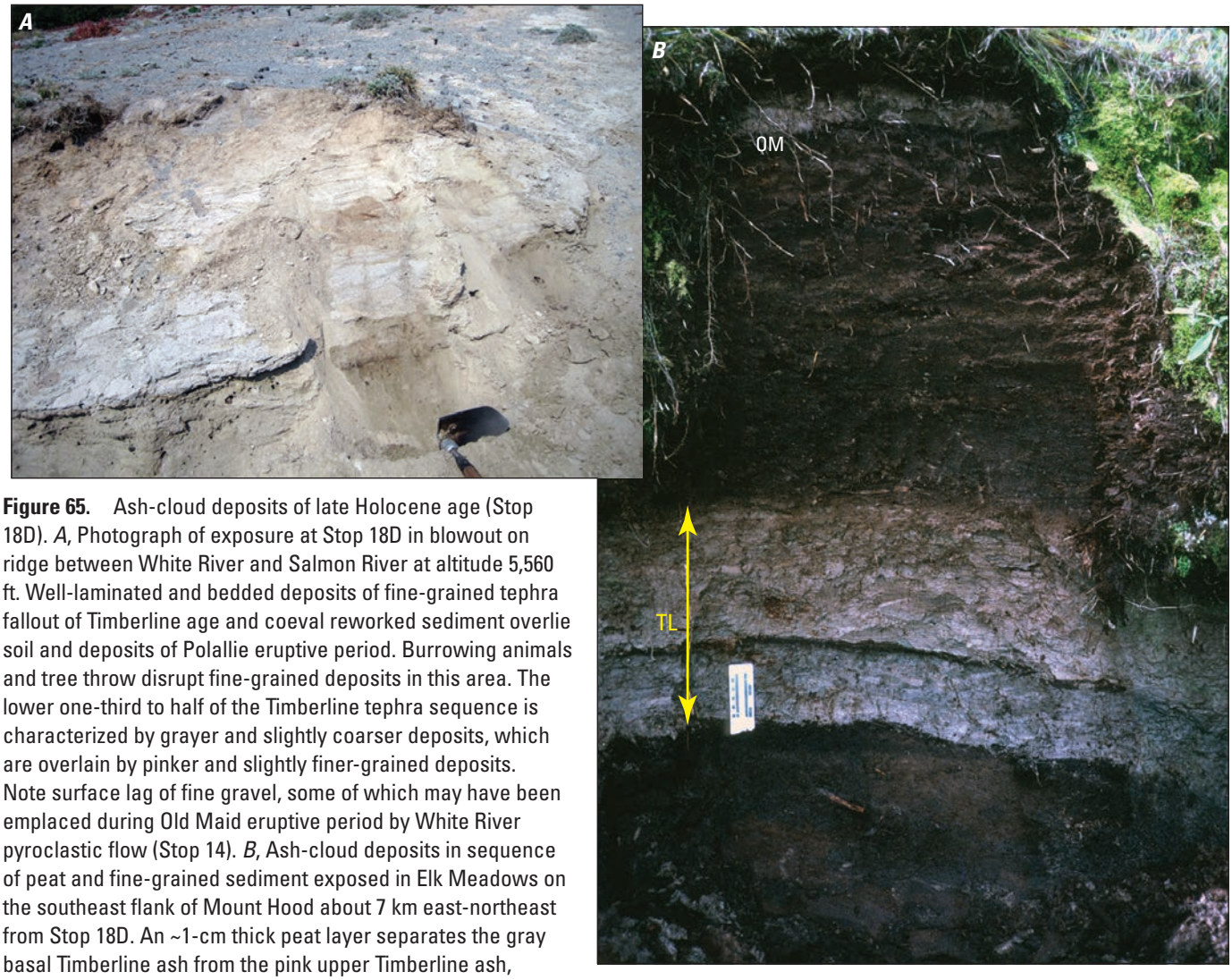

Figure 65. Ash-cloud deposits of late Holocene age (Stop 18D). *A*, Photograph of exposure at Stop 18D in blowout on ridge between White River and Salmon River at altitude 5,560 ft. Well-laminated and bedded deposits of fine-grained tephra fallout of Timberline age and coeval reworked sediment overlie soil and deposits of Polallie eruptive period. Burrowing animals and tree throw disrupt fine-grained deposits in this area. The lower one-third to half of the Timberline tephra sequence is characterized by grayer and slightly coarser deposits, which are overlain by pinker and slightly finer-grained deposits. Note surface lag of fine gravel, some of which may have been emplaced during Old Maid eruptive period by White River pyroclastic flow (Stop 14). *B*, Ash-cloud deposits in sequence of peat and fine-grained sediment exposed in Elk Meadows on the southeast flank of Mount Hood about 7 km east-northeast from Stop 18D. An ~1-cm thick peat layer separates the gray basal Timberline ash from the pink upper Timberline ash, indicating a break in activity during the Timberline eruptive period. Scale is 15 cm total length. A thin bed of ash of Old Maid age lies about 15 cm below ground surface.

Figure 66. Deposits of Timberline eruptive period exposed along Little Zigzag Canyon at Stop 19A. *A*, View from Timberline Trail as it descends east canyon wall. Canyon is about 15–25-m deep. Area of *B* labeled. ZG, Zigzag Glacier. *B*, Exposure of Timberline deposits on west canyon wall about 400 m north of trail crossing; view down canyon. Section consists of (upward from base) lower gray diamict, light-gray ash-cloud deposit, diamict rich in reddish-gray juvenile and hydrothermally stained clasts, and gray diamict at top. Note sitting person for scale just above center of photograph. Tlt, Timberline Trail descending into canyon.

white band), diamict rich in reddish-gray juvenile and hydrothermally stained clasts of older lava, and grayer diamict at surface. Units with juvenile and abundant hydrothermally stained clasts likely reflect incorporation of crater-wall debris into pyroclastic flows, probably facilitated by unstable walls created by debris avalanche(s) early in Timberline time.

The trail crosses Little Zigzag River, traverses the fan surface, descends into a tributary of Zigzag Canyon, and reaches an overlook on the main canyon rim at altitude 5,480 ft.

Stop 19B. View Up Zigzag Canyon to Mississippi Head and Crater

Location: 45.3425° N., 121.7400° W.; UTM 10T 598718E, 5021550N; altitude 5,480 ft

Zigzag Canyon is steep and narrow (fig. 67). Roughly two-thirds of the canyon's depth is incised in unconsolidated diamicts of chiefly Polallie age and a lesser thickness of Timberline age; the lower third is cut in lava flows, but great wedges of colluvium derived from the diamicts prevent detailed mapping of the disconformity between lava flows and diamicts. We infer that the surface of these ~250(?)–210-ka lava flows lay exposed for about 200,000 yr before burial by a broad fan of Polallie diamicts topped by the lava flow of Mississippi Head. Post-Polallie incision initiated canyon cutting at the margin of the Mississippi Head flow and excavation may have encountered and exploited pre-Polallie canyons.

We are puzzled by the role the canyon played during the Timberline eruptive period. Although the upper canyon is rimmed by tens of meters of deposits of Timberline age, we don't find evidence of Timberline deposits in the bottom of the canyon until close to the confluence with Little Zigzag River (Stops 21 and 22). These deposits reached Zigzag Canyon through several tributaries that head on lower reaches of the Timberline fan, including Little Zigzag. We are considering reasons for this pattern, including that Zigzag Canyon was not available to the bulk of pyroclastic flows during the Timberline because it did not extend as far upslope as now, was substantially narrower and shallower, and divides formed by deposits of Polallie age were high enough to keep Timberline flows out of the canyon and directed toward the south and west where they filled post-Polallie topography to create the fan. The Mississippi Head lava flow may also have been instrumental in diversion of flows. Regardless, by post-Timberline time through drainage was established, and no doubt

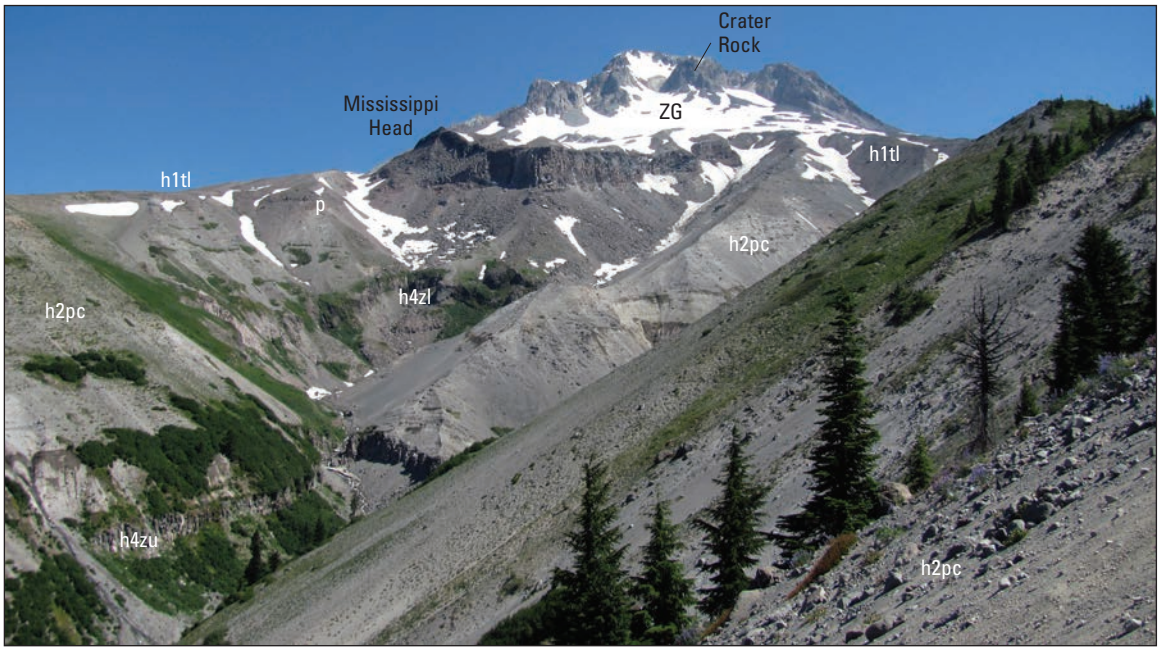

Figure 67. View up 250-m-deep Zigzag Canyon from near Timberline Trail on southeast rim at Stop 19B. A thick sequence of pyroclastic-flow and lahar deposits of Polallie age (h2pc), overlain locally by deposits of pyroclastic fan of Timberline age (h1tl), buries lava flows of the andesite of upper Zigzag Canyon (h4zu; K-Ar age >225±9 ka). We are uncertain if the flow that forms the cliff below Mississippi Head is part of the same unit or is a proximal equivalent of the 210-ka andesite of lower Zigzag Canyon (h4zl; Stop 22). Mississippi Head, the prominent cliff at the canyon head, is formed by a lava flow that caps the Polallie sequence and is probably ~15 ka (attempts to date it have failed), making it the youngest lava flow at Mount Hood. We can trace the lava flow about 1.5 km upslope to where it is buried by younger deposits. Pyroclastic-flow deposits at the top of the Polallie sequence (p) across the snowfield to the left of Mississippi Head have the same chemical composition and secular paleomagnetic direction as the lava flow, so they are probably close to the same age. ZG, Zigzag Glacier. Photograph by T. Berndt, USGS, August 6, 2012.

enhanced, during neoglacial time when expanded glaciers terminated on Mississippi Head and a tongue descended into upper Zigzag Canyon. Rapid canyon incision into diamicts ensued as happened in White River after Old Maid eruptions (Stop 18).

Travel

Return to Timberline Lodge, drive down Timberline Road, and head west on U.S. 26 through Government Camp (fig. 50). The gently sloping lowland formed where the south flank fan impinges against the rugged, eroded terrain of upper Tertiary volcanic rocks provides a hospitable location for roads and settlements. Summit Meadows and Swim Warm Springs offered respite from the rugged conditions on the Oregon Trail. The gentle terrain ends abruptly as U.S. 26 makes a sharp turn at the Mirror Lake Trailhead, about 2.5 mi from Timberline Road (fig. 68). Camp Creek, which drains the west end of the lowland, plunges over Yocum Falls and descends into a deep U-shaped canyon. Trailhead parking is on the south side of U.S. 26, but a safety barrier separates eastbound and westbound lanes. Outcrops across highway are not safely accessible from the trailhead. Parking on the shoulder

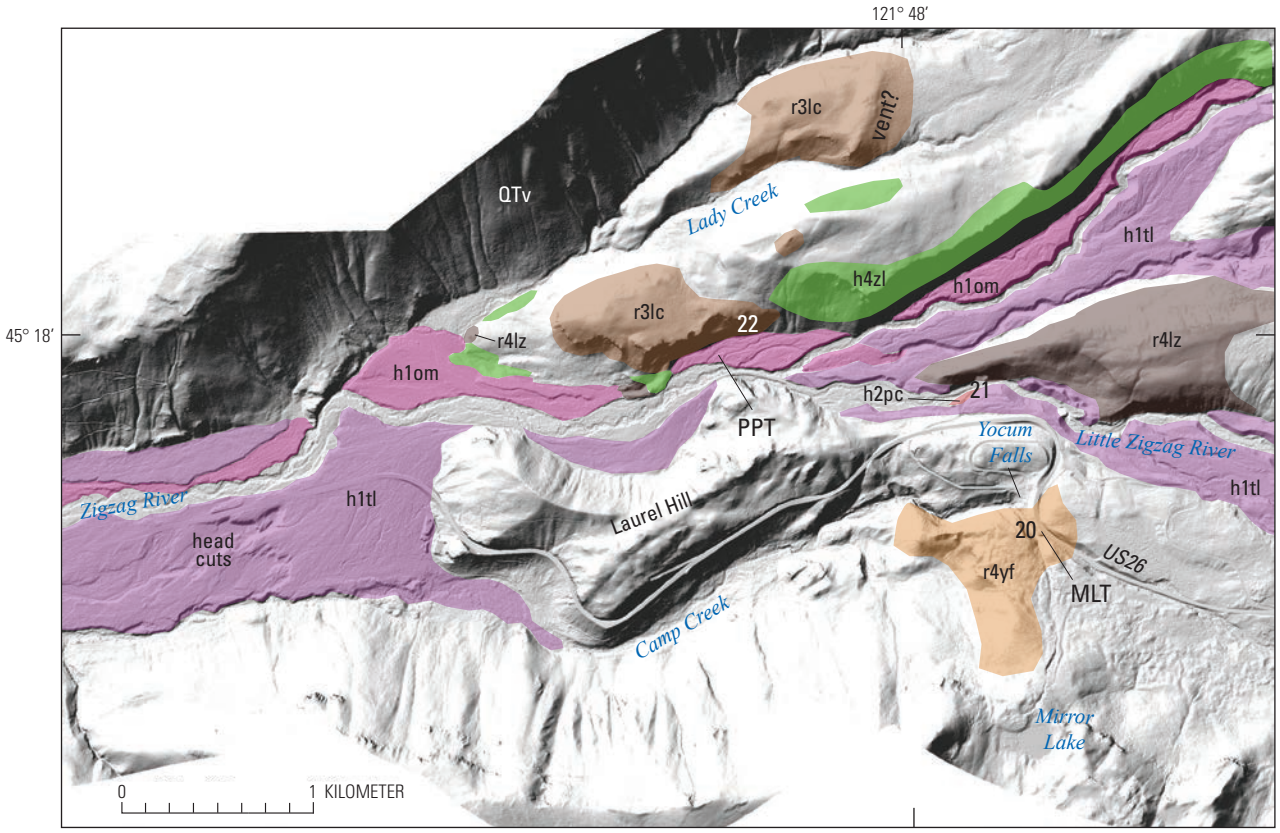

Base from 2010 Oregon Department of Geology and Mineral Industries, Oregon Lidar Consortium, Mount Hood lidar data quadrangle series, hillslope-shaded, bare-earth elevation model, 3 ft interval; Government Camp quadrangle

EXPLANATION

QTv	**Recent**
h1om	**Lahar deposits of Old Maid eruptive period**
h1tl	**Lahar and pyroclastic-flow deposits of Timberline eruptive period**
r3lc	**Andesite of Lady Creek**—71-ka
r4lz	**Basaltic andesite and andesite of Little Zigzag**—160-ka
r4yf	**Andesite of Yocum Falls**—175-ka
h4zl	**Andesite of lower Zigzag Canyon**—210-ka
h2pc	**Deposits of Pollalie eruptive period**
20	**Field-trip stop**

Figure 68. Shaded-relief lidar image of the area around the confluence of Little Zigzag and Zigzag Rivers, showing key units and field trip stops. PPT, Paradise Park Trailhead; MLT, Mirror Lake Trailhead; vent?, possible vent area of andesite of Lady Creek; head cuts, scarps cut by water floods late in Timberline time.

of the westbound lane is possible in places east of the large outcrop of andesite of Yocum Falls. The highway is busy and noisy. Limited outcrops of the andesite are accessible along the Mirror Lake Trail about 1 km from parking lot.

Stop 20. Andesite of Yocum Falls

Location: 45.3071° N., 121.7911° W.; UTM 10T 594776E, 5017560N; altitude 3,440 ft **(Caution: Heavy-traffic area)**

Large outcrops along the inside of the U.S. 26 curve across from Mirror Lake Trailhead expose the andesite of Yocum Falls, which has 57.3–57.5 percent SiO_2 and relatively high K_2O (~1.35 percent) and strontium (850–890 ppm) (figs. 19, 69). The lava contains phenocrysts of plagioclase (11 percent) and orthopyroxene (about 2 percent) with minor clinopyroxene; microphenocrysts have a similar distribution. The lava flow has a K-Ar age 175±12 ka. Wise (1969) mapped it as Mount Hood andesite, but we have traced the lava flow southward for about 1.7 km to near Mirror Lake, which occupies a cirque on the north side of Tom Dick and Harry Mountain. Its vent is not exposed, but we suspect it is near the lake and obscured by glacial erosion and burial by till. Around the U.S. 26 curve, the lava overlies the Miocene Laurel Hill pluton.

Travel

After making a sharp turn just past the trailhead, the highway makes another sharp turn to the west over a ridge and opens views to cliffs of 210-ka andesite of lower Zigzag Canyon on the north side of Zigzag Canyon, and then descends Laurel Hill, the ridge forming the divide between Camp Creek and Little Zigzag River. Most of the ridge is formed of a diorite pluton of Miocene age. Several dikes, conspicuous by their transverse polygonal jointing, cut the pluton. The grade ends on the broad lahar fill of the Zigzag River valley.

Shortly after U.S. 26 straightens, turn right (northeast) onto F.R. 2639. The road is an old alignment of U.S. 26 that dead-ends about 2.3 mi ahead at an old quarry.

Stop 21. Quarry in Basaltic Andesite and Andesite of Little Zigzag River; Timberline Deposits and Contact Between Timberline and Polallie Deposits

Location: 45.3142° N., 121.7950° W.; UTM 10T 594454E, 5018346N; altitude 3,320 ft

Basaltic andesite and andesite of Little Zigzag River (r4lz) is a locally thick (60–100 m) sequence of lava flows with 56.5–60.02 percent SiO_2 and 0.6–1.0 percent K_2O; samples from the quarry yielded an imprecise K-Ar age of 137±24 ka and a $^{40}Ar/^{39}Ar$ age of 162.6±4.8 ka. A sample from a downstream site yielded a $^{40}Ar/^{39}Ar$ age of 157.8±7.4 ka. The lavas range widely in phenocryst content (2–12 percent) of plagioclase > orthopyroxene, but display well-defined trends in variation diagrams (figs. 19, 69). We can trace the unit about 1.8 km upstream and 2.7 km downstream from the quarry (fig. 68). In downstream sites outcrops are close to river level, whereas the unit forms a high divide between Little Zigzag and Zigzag Canyons in its upper reaches. We suspect that the lava flows were emplaced during a time of substantial glacier cover and its age suggests eruption during MIS 6. Flows descending through a canyon melted in the glacier and ponding locally would explain its great thickness and narrow width. Nowhere do we see quenched flow margins, hyaloclastite, or jointing indicative of glacier interaction. However, this area was subject to extensive glacial erosion during more recent glaciations.

A key question is the vent location for this unit. At present we consider the unit a product of a regional volcano, not Mount Hood proper. We can trace this unit no closer than 8 km from the Mount Hood vent, as it is thickly buried by deposits of the south-flank fan. Previous workers have mapped this as Mount Hood lava (Wise, 1968, 1969; Keith and others, 1982), but its locally low phenocryst content and compositional range extending to low silica and potassium contents are more similar to lavas of regional volcanoes (figs. 19, 69).

Outcrops a short distance up the old highway from the pedestrian bridge across Little Zigzag River expose a sequence of pyroclastic-flow and lahar deposits of Timberline age overlying a soil (now buried below thin colluvium but accessible by digging) formed in deposits of the Polallie eruptive period. Outcrops west of the quarry along the north side of F.R. 2639 also expose (poorly) Timberline deposits, among them some of the farthest travelled (12 km) pyroclastic flows of late Holocene age. These used to be well exposed in a small borrow pit across from Kiwanis Camp (Scott and others, 1997a).

Travel

Drive about half way back to U.S. 26 and turn right, cross the bridge, and park at Paradise Park Trailhead. The trailhead is on bouldery deposits of post-Old Maid age.

Stop 22. Andesite of Lower Zigzag Canyon and Andesite of Lady Creek

Location: 45.3146° N., 121.8144° W.; UTM 10T 592931E, 5018369N; altitude 2,810 ft

A short (~0.75 mi) hike up the Paradise Park Trail accesses Mount Hood andesite of lower Zigzag Canyon (h4zl) and the overlying andesite of Lady Creek (r3lc; fig. 68). The

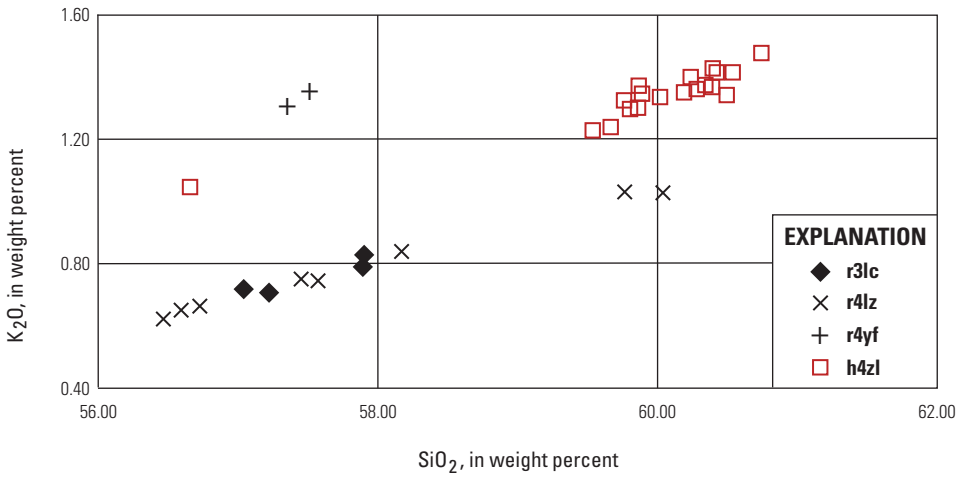

Figure 69. Plot of K_2O versus silica content of units exposed around confluence of Little Zigzag and Zigzag Rivers. Andesite of Lady Creek (r3lc) and basaltic andesite and andesite of Little Zigzag (r4lz) are similar in major-element chemistry, but unit r3lc has lower titanium and strontium and higher zirconium and barium. r4yf, andesite of Yocum Falls; h4zl, andesite of lower Zigzag Canyon.

trail heads east across lahar deposits of Old Maid age, crosses the Wilderness boundary, switchbacks, and then climbs through an extensive forested talus and passes small outcrops of andesite of lower Zigzag Canyon (h4zl; 3 samples, 59.8–60.0 percent SiO_2; ~1.3 percent K_2O; and slightly elevated strontium, ~725 ppm); the rocks yield a K-Ar age of 235±13 ka and a $^{40}Ar/^{39}Ar$ age of 210.5±2.3 ka. Additional chemical analyses from elsewhere in the unit expand the compositional range (fig. 69). The lowest-silica sample is from a small outcrop of quenched and intensely jointed lava on the canyon floor upstream; it may be unrelated to the rest of unit. Two additional K-Ar ages are 213±9 and a puzzling 158±9 ka, which suggests the unit may combine chemically similar lavas of different ages

As the trail nears the top of the north valley wall, outcrops expose strikingly aphanitic andesite of Lady Creek. Four samples have 57.0–57.9 percent SiO_2 and low K_2O, 0.71–0.83 percent (figs. 19, 69). The unit's great thickness (almost 100 m), mesa-like form, locally intense fracturing, and glassy character suggest glacier interaction. Steep cliffs along the south margin of the mesa provide extensive exposures. A north-northeast-striking, poorly exposed, linear ridge about 1.6 km northeast of the mesa may be the vent area (fig. 68). With a phenocryst and microphenocryst content of only a few percent, it is the least crystalline of any product of a Quaternary regional volcano in the Mount Hood region. Ages suggest emplacement during MIS 4 (K-Ar, 51±14 ka; $^{40}Ar/^{39}Ar$, 71.2±6 ka).

Travel

Return to U.S. 26 and head west on the surface of lahar deposits of the Timberline eruptive period. A typical characteristic of the forest growing on thick sequences of granular lahar deposits is their relative openness and mossy ground surface. Such characteristics are caused by an excessively drained substrate that produces seasonally low soil moisture during the region's typically dry summers. Continue to the village of Zigzag and turn north on East Lolo Pass Road (F.R. 18); cross Zigzag and Sandy Rivers. Below we describe several stops on roads and trails that access views of the west flank of Mount Hood.

About 4 mi from U.S. 26, turn right on F.R. 1825 (incorrectly labeled Muddy Fork Road on some online maps), which provides access to the upper Sandy River valley. Drive 0.7 mi to the junction with F.R. 1828. Stay right on F.R. 1825, cross the Sandy River, and pass McNeil Campground. IAVCEI Field Trip #A6 (Pierson and others) has a stop near the campground (also see Pierson and others, 2009) that describes lahar and related deposits of Old Maid age that are well exposed along the south bank of Sandy River. Continue up valley and bear left onto F.R. 1825-100; drive 0.3 mi and turn left on F.R. 1825-024 to trailhead. Directions and other trail information are available at: https://www.fs.usda.gov/recarea/mthood/recreation/hiking/recarea/?recid=53600&actid=50 Trailhead location: 45.3869° N., 121.8308° W.; UTM 10T 591530E, 5026382N; altitude 2,440 ft.

To reach good exposures of lahar deposits of Timberline and Old Maid age requires hiking at least 4–7 mi (7–11 km) round trip, mainly in the Mount Hood Wilderness Area. Hike about 1.3 mi to the Pacific Crest Trail (PCT) including a crossing of Sandy River on a seasonal footbridge. Head east on the PCT, which follows the north bank of Sandy River. Outcrops along the north bank of Sandy River lie a short distance south of trail. One example is given below.

Stop 23. Late Holocene Lahar Deposits Along Upper Sandy River

Location: 45.3854° N., 121.7928° W.; UTM 10T 594509E, 5026259N; altitude 3,050 ft

Good cut-bank exposures of Holocene deposits are ephemeral features, but a typical sequence of units consists of several meters of gray lahar deposits of Old Maid age overlying reddish-gray lahar deposits of Timberline age that extend below channel level. Locally, the two units are separated by a sequence of debris-flow deposits and related alluvium of noneruptive origin composed chiefly of reddish-gray material reworked from Timberline deposits.

This particular reach was severely eroded by high flows in the mid-2000s, creating 14–18-m-high exposures along several hundred meters of the north bank of Sandy River (fig. 70). The upper sequence of gray diamicts is of Old Maid age. The deposits inundated mature forest as evidenced by common rooted snags (Cameron and Pringle, 1991). As snags rot they can create deep cylindrical wells, so be aware as you walk off trail. Deposits are locally rich in charcoal including some large logs, which suggests they may have originated from hot lahars (Crandell, 1980). The base of the Old Maid deposits is marked by a distinct disconformity highlighted by a color change to reddish-gray diamicts. Much of the outcrop below the disconformity is not composed of deposits of Timberline age, but rather deposits derived from erosion of them. A thick fill of Timberline diamicts enters the upper Sandy River through two tributary valleys upstream. Posteruption erosion removed tens of millions of cubic meters from the fill and built a fan of debris-flow and alluvial deposits in this reach. A western red-cedar snag rooted in the lower half of the reddish-gray unit has a 2σ wiggle-match ^{14}C age of 735–830 calendar yr B.P. Other radiocarbon ages show the fan accumulated during the millennium following Timberline eruptions. Lahar deposits of demonstrably Timberline age lie near the base of the outcrop and are mostly covered by colluvium, but they underlie a prominent terrace on the south side of the river, which is best exposed farther upstream below where the PCT crosses the Sandy River.

Figure 70. Photograph of exposure along north bank of upper Sandy River at Stop 23 that shows typical sequence of diamicts of late Holocene age. Upper, gray unit consists of several lahar deposits of late-18th century Old Maid eruptive period; note partly exhumed, in-place buried stump and charred log. Yellow arrow marks disconformity cut in sequence of reddish debris-flow deposits of non-eruptive origin derived from erosion of deposits of Timberline age (1.5-ka). Lahar deposits of the Timberline eruptive period lie at the base of the exposure, partly covered by recent colluvium.

Travel

The following are two stops that provide a view of Mount Hood's west flank and underlying early Pleistocene Sandy Glacier volcano. At the north end of the F.R. 1825 bridge across Sandy River by McNeil Campground, turn either left or right depending on your plan. To the left, F.R. 1825 returns to East Lolo Pass Road as it begins its climb to the pass; to the right F.R. 1828 also leads to East Lolo Pass Road but high on the west side of the pass. The view from Stop 24 is closer, requires no hike, and is lower in altitude (access to Stop 25 can be closed by snow in winter and spring). Both stops can be visited by making a circuit of the three roads. Stop 24 lies along East Lolo Pass Road about 0.8 mi east of its junction with F.R. 1825. East Lolo Pass Road follows a powerline corridor on the north valley wall with views up Sandy River toward Mount Hood. Several narrow turnouts provide places to park for views of Mount Hood's west flank.

Stop 24. West Flank of Mount Hood and Sandy Glacier Volcano

Location: 45.3898° N., 121.8691° W.; UTM 10T 588530E, 5026656N; altitude 2,340 ft

This viewpoint shows the west flank of Mount Hood and the upper Sandy River valley (fig. 71) with its broad flat fill of lahar and other unconsolidated deposits of Old Maid age. Geothermal drilling, about 5 km up valley and around the bend in the lower center of photograph, penetrated 30–80 m of lahar deposits (Priest and others, 1982). At the head of the valley, Wise (1968, 1969) mapped lava flows and diamicts of what he named the Sandy Glacier volcano dipping southeastward under west-dipping Mount Hood products. The rugged valley step below the Sandy Glacier (terminus about 1,900 m altitude) exposes andesitic lava flows and pyroclastic deposits of the upper part of Sandy Glacier volcano, which are compositionally and texturally similar to those of Mount Hood. The lower part of the volcano consists of basalt and basaltic andesite lava flows and tuffs; numerous dikes cut both sequences. A lava flow with reversed-polarity magnetization near the terminus of Sandy Glacier yielded a K-Ar age of 3.2±0.3 Ma (Wise, 1969), but more recent K-Ar dating attempts suggest a younger age—1.14 and 1.35±0.05 Ma (Keith and others, 1985), a weighted mean age of 1.27±0.02 Ma (Sherrod and Scott, 1995), and 1.2±0.015 Ma (Sherrod and Scott, 1995).

This view of Mount Hood shows the contrast between the smooth south slopes formed in a fan of fragmental deposits of Timberline age and the rugged, steep, glacially eroded slopes on the west and north flanks. The headwalls of Sandy and Reid Glaciers expose hydrothermally altered rock, and both

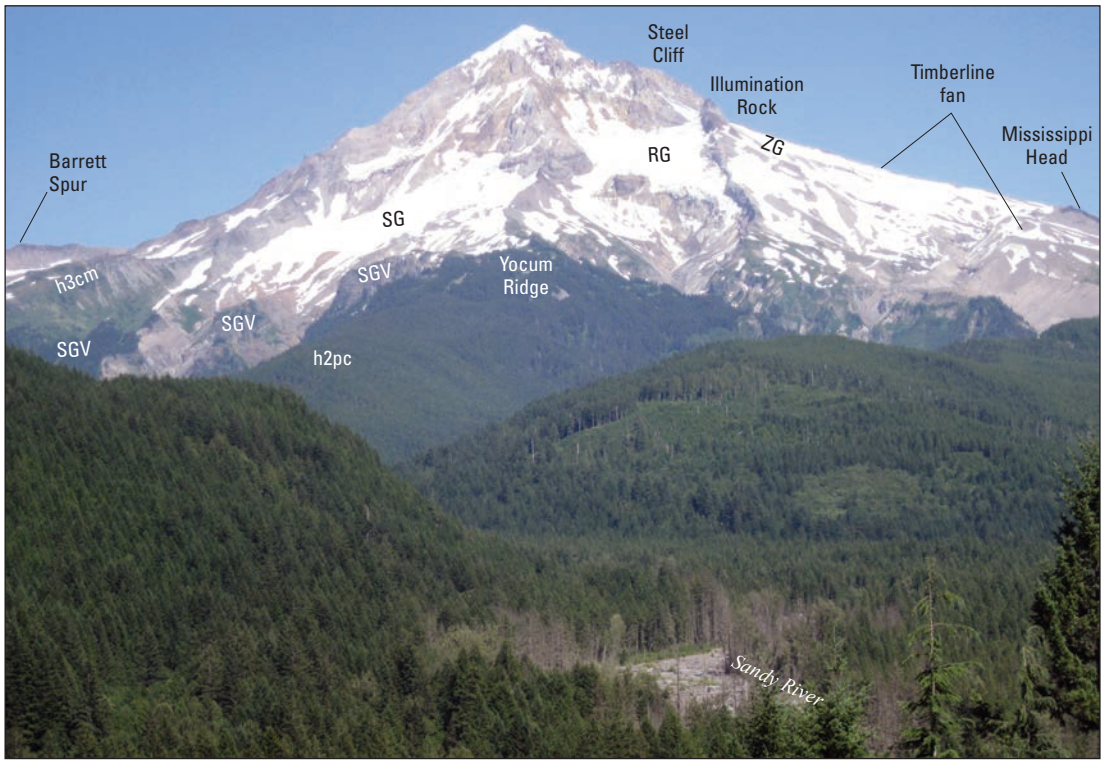

Figure 71. Photograph of west flank of Mount Hood, upper Sandy River valley, and Sandy Glacier volcano (SGV) from East Lolo Pass Road (Stop 24). Yocum Ridge consists of several sequences of Mount Hood lavas that overlie rocks of the 1.2-Ma Sandy Glacier volcano (figs. 31, 72). McNeil Ridge (h3cm) exposes a sequence of ~60-ka lava flows. Note debris near snout of Sandy Glacier (SG) rich in hydrothermally altered material from upper part of cone. RG, Reid Glacier; ZG, Zigzag Glacier; h2pc, deposits of Polallie eruptive period.

areas have been sources of small rock avalanches and debris flows during this century (note rusty-colored debris at snout of Sandy Glacier).

Travel

For a better view of the upper west flank, drive East Lolo Pass Road almost to the crest of Lolo Pass and turn right on F.R. 1828. Drive about 2.5 mi to F.R. 1828-118, turn left and continue to Top Spur Trailhead. An alternative route from McNeil Campground to the trailhead is to go east on F.R. 1828 to F.R. 1828-118 (see https://www.fs.usda.gov/recarea/mthood/recreation/hiking/recarea/?recid=53632&actid=50). Hike Top Spur Trail 0.5 mi to junction with Timberline and Pacific Crest Trails. Take the Timberline Trail around west and south sides of Bald Mountain for a great view up the Muddy Fork of Sandy River.

Stop 25. Basalt of Bald Mountain, and View of West Flank of Mount Hood and Sandy Glacier Volcano

Location: 45.4017° N., 121.7740° W.; UTM 10T 595951E, 5028085N; altitude 4,360 ft

Bald Mountain is a late Pliocene or early Quaternary basalt (50.8–51.2 percent SiO_2) volcano that is geochemically similar to the 2.5-Ma basalt of Tilly Jane (Stop 4) but contains higher MgO and lower FeO. Dense flow interiors are separated by thick breccia. The steep, rugged terrain in the upper reaches of Muddy Fork exposes a ~550-m section of lava flows and fragmental deposits of 1.2-Ma Sandy Glacier volcano (fig.72). Several dikes cut through the section. The area around labeled dike (D) failed as a rock avalanche in 2004. The oldest Mount Hood unit lying on Sandy Glacier volcano is the ~320-ka andesite of Yocum Ridge (h4yr). Other overlying Mount Hood units are the ~140-ka andesite of upper Sandy (h4us) and lavas we correlate to the 224-ka andesite of Dollar Lake (h4dl), which in turn are overlain by the ~60-ka andesite of Cathedral and McNeil Ridges (h3cm). Moraines of late neoglacial age at the snout of Sandy Glacier contain a high proportion of hydrothermally altered debris derived from the summit area.

Travel

Return to U.S. 26 at Zigzag and head west (right) through a broad, 2.4-km-wide valley at the confluence of the Sandy and Salmon Rivers (fig. 73). For the next few miles, the highway is built on a flat surface formed by lahar deposits of Timberline age. Much of the surface is underlain by a lahar deposit at or near the base of the Timberline sequence which has common hydrothermally altered clasts and a slightly yellowish matrix that contains more fines than younger deposits of Timberline age. This lahar deposit is found throughout the lower Sandy valley all the way to the Columbia River. We infer it originated from a debris avalanche that formed the

Figure 72. Photograph of west side of Mount Hood and products of 1.2-Ma Sandy Glacier volcano (fig. 31) from Timberline Trail on south side of Bald Mountain (Stop 25). View up Muddy Fork shows several Hood units: h3cm, ~60-ka andesite of Cathedral and McNeil Point; h4us, ~140-ka andesite of upper Sandy River; h4dl, 266–224-ka andesite of Dollar Lake; and h4yr, ~320-ka andesite of Yocum Ridge. D, dike; SG, Sandy Glacier; RG, Reid Glacier.

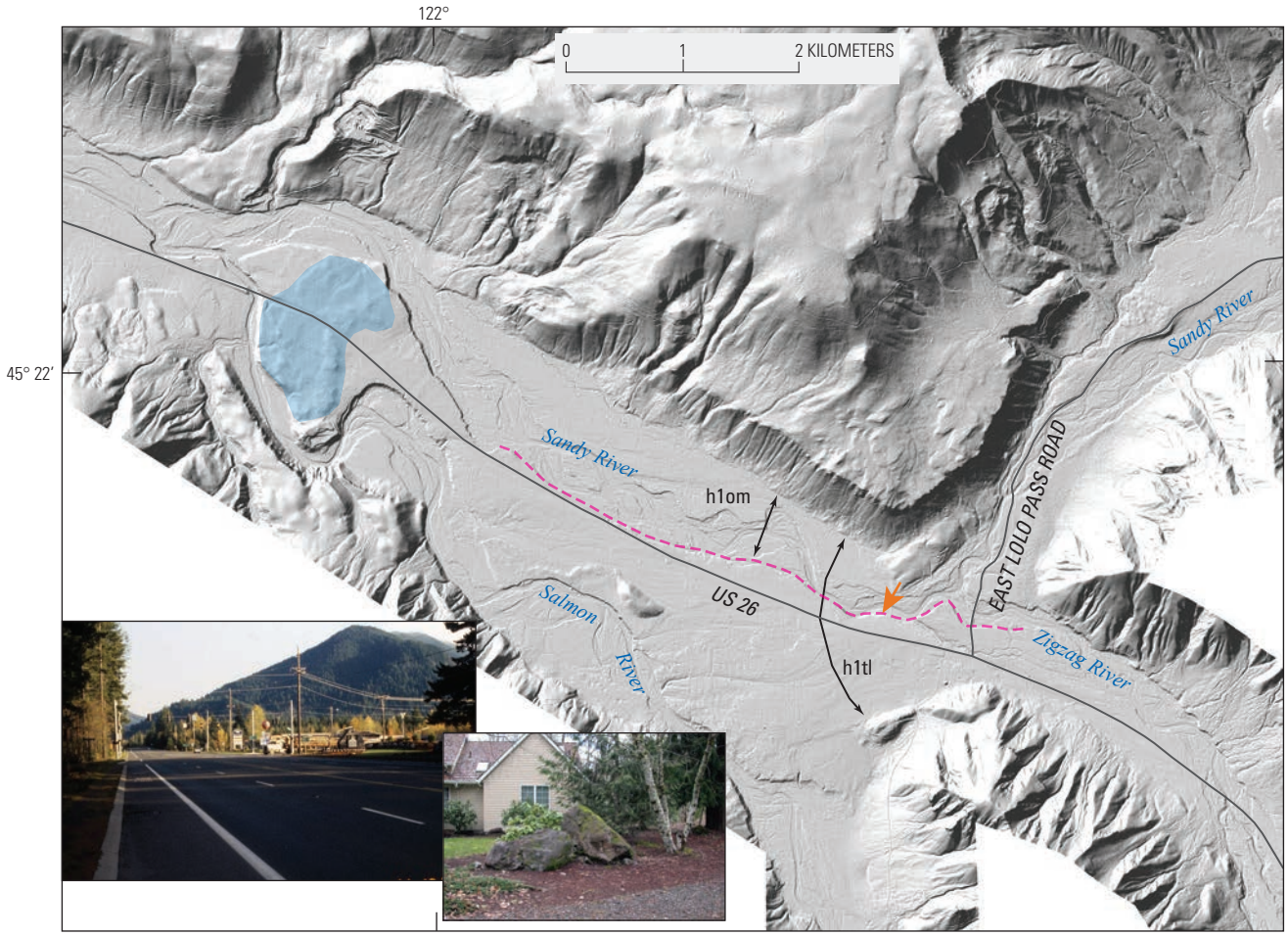

Base from 2010 Oregon Department of Geology and Mineral Industries, Oregon Lidar Consortium, Mount Hood lidar data quadrangle series, hillslope-shaded, bare-earth elevation model, 3 ft interval; Brightwood, Government Camp, Hickman Butte, and Wildcat Mountain quadrangles

EXPLANATION

- End moraine
- Extent of Old Maid eruptive period lahars
- Width of lahar inundation
- Location of section
- Road

Figure 73. Shaded-relief lidar image of Sandy River near its confluence with Zigzag and Salmon Rivers. Lumpy terrain (light blue) east of Sandy-Salmon confluence is end moraine of middle Pleistocene age (MIS 6). Arrows show widths of lahar inundation during Old Maid (h1om) and Timberline (h1tl) eruptive periods; pink dashed line marks southern extent of Old Maid eruptive period lahars against high terrace of Timberline age. Inset photographs show U.S. 26 crossing flat surface of lahar deposits of Timberline age and lahar boulders that are used widely in landscaping.

breached summit crater at or close to the beginning of the Timberline eruptive period and constituted the largest flow of late Holocene time. We will see a distal equivalent of this deposit on the Sandy River delta at Stop 27. Note the large, scattered boulders from the lahar deposit, many of which have been used for landscaping (fig. 73, inset). Exposures into the surface on the south bank of Sandy River in this area are on private land; access requires permission. A typical exposure (orange arrow in fig. 73) consists of basal bouldery gravel (probably outwash) of latest Pleistocene age and lahar and lahar-runout deposits of Polallie age underlying the avalanche-derived lahar of Timberline age. One or more sandy lahar deposits of Timberline age overlie the avalanche lahar in areas near the Sandy River, but these do not bury the entire surface of the avalanche lahar. Apparently later Timberline lahars were largely restricted to the north side of the valley. Thin deposits of Old Maid age are present locally on Timberline deposits at the north edge of the surface, but most was conveyed through a channel eroded into Timberline fill at the north side of the valley.

Gently rolling terrain (light blue polygon in figure 73) just east of the bridge across the Salmon River is formed of subdued moraines of middle Pleistocene age, probably MIS 6. Sloping, largely vegetated roadcuts reveal cobbles and boulders from Mount Hood, but primarily clasts of older volcanic and intrusive rocks. The moraine lies about 15 km (10 mi) downvalley from moraines of the LGM (MIS 2).

For the next 5 mi, the highway traverses poorly exposed lahar and lahar-runout deposits of Polallie age, and alluvial fan and landslide deposits derived from the south valley wall. Sandy River is seldom visible, but it lies north of the highway, flanked locally by terraces formed of lahar deposits of Timberline and Old Maid age. U.S. 26 leaves the floor of the Sandy River valley at Alder Creek and for the next 7 mi rolls through rarely exposed lahar deposits and gravelly alluvium of early and middle Pleistocene age. At the City of Sandy the river makes an abrupt turn northward towards the Columbia River (fig. 1). The one-way west-bound lane of U.S. 26 rejoins the east-bound land at Bluff Road on the west side of Sandy. Turn north (right) on Bluff Road. Stop at Jonsrud Viewpoint Park about 1 mi north of U.S. 26.

Stop 26. Jonsrud Viewpoint Park

Location: 45.4106° N., 122.2722° W.; UTM 10T 556950E, 5028610N; altitude 850 ft

Interpretive signs describe the Oregon Trail. Mount Hood is about 40 km away and displays contrasting smooth, southward sloping debris fan and rugged west and north flanks. The seldom-exposed lower to middle Pleistocene lahar and alluvial deposits covered by thick, deeply weathered loess that we crossed east of the City of Sandy continue westward into the Portland Basin (Evarts and others, 2013), but the Sandy River turns abruptly northward, probably owing to stream capture from a Columbia River tributary perhaps aided by tectonism. As the Sandy River entrenched its canyon, numerous terraces were cut, some mantled by deposits of Mount Hood lahars and related alluvium. The youngest prominent terrace visible from the overlook is the grass-covered area upstream (fig. 74). It lies about 50 m above the current channel and is underlain by lahar and lahar-runout deposits of Polallie age. Last-glacial outwash probably also contributes to fill below the terrace. In contrast, late Holocene lahars of the Timberline and Old Maid eruptive periods were constrained to within about 10–15 m vertically of the channel.

Figure 74. View east from Jonsrud Viewpoint Park of Sandy River as it turns northward toward Columbia River. Grass-covered terrace (below Mount Hood) is about 50 m above the present channel and is underlain by lahar and lahar-runout deposits of Polallie age. Older terraces as much as 120 m above the river channel are underlain by alluvium and Mount Hood lahars probably as much as several hundred thousand years old (Evarts, and others, 2013). Mount Hood lies about 40 km to east. Photograph copyright Lyn Topinka, used with permission.

Travel

Return to U.S. 26 and head west into the Portland Basin on a deeply weathered, dissected, and loess-covered alluvial and lahar piedmont formed by rivers draining the Cascades prior to capture, diversion, and entrenchment of the Sandy River. Around Boring, Oregon, 5 mi west of Sandy, Pleistocene volcanoes of the Boring Volcanic Field appear on both sides of the highway (fig. 8; Evarts and others, 2009).

Continue on U.S. 26 about 5 mi past the Boring exit and turn right at the traffic light onto Palmquist Road. Almost immediately turn left on Kane Drive, which becomes NE 257th Avenue. From Mount Hood Community College northward, the road is built on a huge gravel bar deposited by Missoula floods (Evarts and O'Connor, 2008) that lies about 100 m above the Columbia River. NE 257th Avenue descends the steep north slope of the bar and becomes Graham Road. Continue north on Graham Road under I-84 and past the Comfort Inn. Just past the inn turn right on Harlow Road, which comes to a dead end just north of the I-84 bridge.

Stop 27. Lahar and Lahar-Runout Deposits of Timberline Age on West Bank of Sandy River

Location: 45.5453° N., 122.3851° W.; UTM 10T 548000E, 5043500N; altitude 30 ft

The broad accumulation of sediment at the confluence of the Sandy and Columbia Rivers is informally called the Sandy River delta (fig. 9). The surface to the west of Sandy River is underlain by as much as 9 m of lahar, lahar-runout, and related alluvial deposits of the Timberline eruptive period, including the distal equivalent of the lahar related to the debris avalanche that created the breached crater, as well as interbeds and surficial mantle of overbank Columbia River deposits (Rapp, 2005; Evarts and O'Connor, 2008; Evarts and others, 2013). A few meters of the Timberline deposits are exposed in this cutbank of Sandy River. Deposits of Old Maid age are restricted to the lower eastern and northern part of the delta where they are largely buried by Sandy and Columbia River sediment.

The lahar and lahar-runout deposits exposed at this stop are sand-rich and mostly free of clasts larger than pebbles. A complete sedimentological discussion of deposits is in Pierson and others; IAVCEI Field Trip #A6). This is a good place from which to contemplate the potential effects of future eruptions.

Mount Hood Volcano Hazards

Hazardous volcanic events at Mount Hood consist of pyroclastic flows (primarily block-and-ash flows) derived from lava-dome and lava-flow collapse, ash fallout, lava flows, ballistic projectiles, debris avalanches, and lahars spawned from debris avalanches or from swift melting of snow and ice by pyroclastic flows (figs. 7, 41, 45, 46, 50, 54). Sustained explosive eruptions and pumiceous deposits are absent or rare in Mount Hood's geologic record. Most tephra-fall deposits originated as ash clouds elutriated from pyroclastic flows and consist of fine lapilli-and-sand or sand-and-silt (Stop 18D). Locally, fall deposits consisting of many individual beds are as much as several meters thick, but thicknesses fall off rapidly and deposits are difficult to discern more than a few tens of kilometers from source.

For planning and emergency management purposes, we divide hazardous areas into proximal and distal hazard zones (fig. 75; Scott and others, 1997b). Proximal hazard zones (PA and PB) are defined by the potential extent of flow events that could affect an area within 30 minutes of onset. The boundary for this zone was constructed using the maximum distance pyroclastic flows have traveled (~12 km from the summit) and by estimating the distance large lahars would travel in 30 minutes (Pierson, 1998), which at Mount Hood is about 24 km from summit. During times of heightened volcanic unrest or eruption, it is unlikely that the ~1,000 people within the proximal zone could be evacuated in less than 30 minutes; therefore, this zone is a guide to areas that should be evacuated before a hazardous event occurs. Hazardous phenomena that are largely confined to the proximal zone are pyroclastic flows, lava flows, lava-dome growth and collapse, ballistic projectiles, near-source tephra falls, and debris avalanches.

Distal hazard zones (DA and DB) are defined by the potential extent of lahars that will take more than 30 minutes to reach an area. Boundaries for the distal hazard zone were constructed through integration of mapping past lahar deposits, models of lahar inundation (for example, LAHARZ, Iverson and others, 1998), and expert judgment. For example, we know that lahar deposits generally do not record the highest level of inundation; thus we located the boundaries higher on valley walls where the valley is narrow and flows would deepen or where flows sweep around bends. Time marks along valleys show approximate travel times of large lahars (Pierson, 1998); smaller lahars would travel more slowly and not reach as far downstream. A lahar zone based on the largest (500 million m^3) debris avalanche and related lahar we think possible (Scott and others, 1997b) is not shown on figure 75.

In addition to separating hazard zones into proximal and distal zones, we, following Crandell (1980), qualitatively assign a higher probability of future eruptive events affecting the south side of the volcano (zones PA and DA) than the north (zones PB and DB). During the late Holocene Timberline and Old Maid eruptive periods, the vent was near Crater Rock (figs. 56, 57), the remnant lava dome of the late 18th century Old Maid eruptive period. Crater Rock lies in a steeply sloping, breached crater (the result of a debris avalanche near the start of the Timberline eruptive period) south of, and about 400 m below, the summit ridge. This geometry protected much of the north and east sides of the

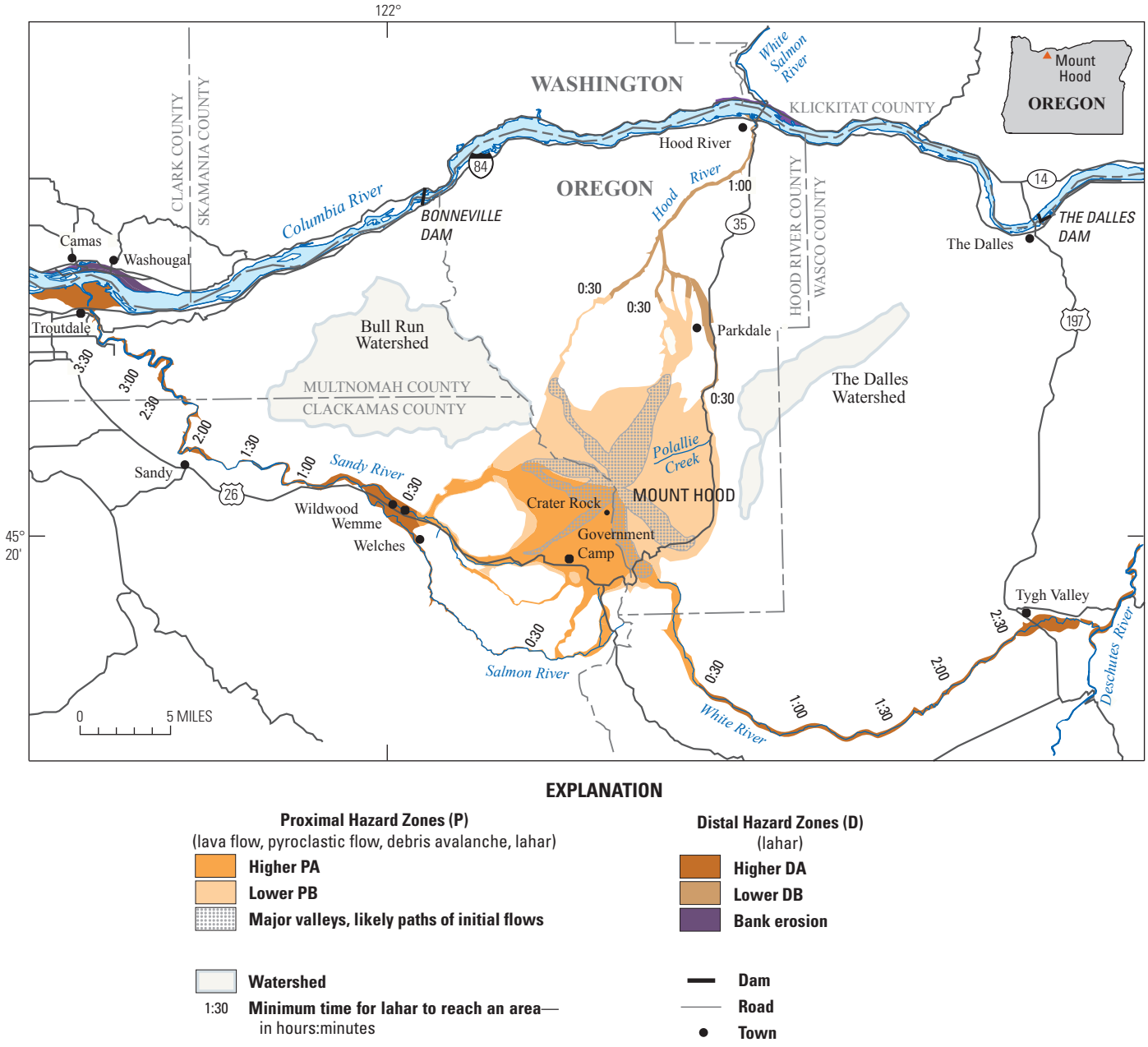

Figure 75. Simplified volcano-hazard map of Mount Hood (derived from Scott and others, 1997b). Areas of higher hazard (PA and DA) correspond to a vent area near present-day Crater Rock, the site of vents of late Holocene age. Areas of lower hazard (PB and DB) would require a vent opening at the summit or on the upper north or east flank. Time marks along river valleys are estimated travel times of large lahars generated on upper flanks.

volcano from pyroclastic flows and large lahars during the past two eruptive periods, although some areas in zone PB were affected by small debris avalanches shed from the summit area and related lahars. The hazard-zonation map also outlines major valleys in zones PA and PB that would be susceptible to initial pyroclastic flows from a growing lava dome. As valleys fill, pyroclastic flows would affect broader areas.

Currently, the Crater Rock area is the only place on the volcano where fumaroles persist. Monitoring over the past several decades show little variation in fumarolic temperature (boiling point) or gas composition (H_2S, CO_2), but both point to the presence of magmatic gases interacting with groundwater. Given the recency of volcanic activity and presence of magmatic degassing, we think the area around Crater Rock is the most likely vent location during the next eruption, making zones PA and DA the most vulnerable to hazardous events. If a vent opens up elsewhere on the upper flank, the lower-probability zones PB and DB would be at risk.

A consequence of increased sedimentation during the past two eruptive periods is the development of a large delta at the mouth of the Sandy River near Troutdale. The delta has narrowed the Columbia River, pushing it against the Washington shore (fig. 9). Future lahars and eruption-induced sedimentation could build the delta farther out into the Columbia River, further narrowing the channel and causing bank erosion and inundation of land in the Camas-Washougal area on the north bank (fig. 75).

Although much of Mount Hood is within National Forest and Wilderness, numerous communities lie within and along the margins of hazard zones. In addition, Mount Hood supports a large transient population of recreationists and visitors year round and a major highway (U.S. 26) into central Oregon passes along its south flank. Bull Run watershed (fig. 75), the major water supply for the Portland metropolitan area, lies typically upwind of the volcano, but is nonetheless vulnerable to ash falls affecting water quality. Many east and westbound flights to Portland International Airport, approximately 75 km west of the volcano, pass within several thousand feet of the summit. The risks associated with future volcanic activity at Mount Hood make it one of most threatening volcanoes in the United States (Ewert and others, 2005). Recent studies have sought to better quantify the exposure of populations and infrastructure in the area (Burns and others, 2011; Mathie and Wood, 2013).

Seismic, deformation, and gas instruments and surveys monitor Mount Hood, which is one of the most seismically active areas in Oregon. The accompanying paper by Thelen and Moran (this volume) discusses the origin of the seismicity and provides a view of background seismicity from which volcanic unrest can be recognized.

References Cited

Bargar, K.E., Keith, T.E.C., and Beeson, M.H., 1993, Hydrothermal alteration in the Mount Hood area, Oregon: U.S. Geological Survey Bulletin 2054, 70 p.

Benito, G., and O'Connor, J.E., 2003, Number and size of last-glacial Missoula floods in the Columbia River valley between the Pasco Basin, Washington, and Portland, Oregon: Geological Society of America Bulletin, v. 115, p. 624638, doi: 10.1130/0016-7606(2003)115<0624:NASOLM>2.0.CO;2.

Burns, W.J., Hughes, K.L.B., Olsen, K.V., McClaughry, J.D., Mickelson, K.A., Coe, D.E., English, J.T., Roberts, J.T., Lyles-Smith, R.R., and Madin, I.P., 2011, Multi-hazard and risk study for the Mount Hood region, Multnomah, Clackamas, and Hood River Counties, Oregon: Oregon Department of Geology and Mineral Industries Open-File Report 0-11-16, 64 p.

Cameron, K.A., and Pringle, P.T., 1986, Post-glacial lahars of the Sandy River basin, Mount Hood, Oregon: Northwest Science, v. 60, no. 4, p. 225–237.

Cameron, K.A., and Pringle, 1987, A detailed chronology of the most recent major eruptive period at Mount Hood, Oregon: Geological Society of America Bulletin, v. 99, p. 845–851.

Cameron, K.A., and Pringle, P.T., 1991, Prehistoric buried forests of Mount Hood: Oregon Geology, v. 53, no. 2, p. 34–43.

Coe, R.S., Singer, B.S., Pringle, M.S., and Zhao, X., 2004, Matuyama-Brunhes reversal and Kamikatsura event on Maui—Paleomagnetic directions, $^{40}A/^{39}Ar$ ages and implications: Earth and Planetary Science Letters, v. 222, p. 667–684, doi: 10.1046/j.epsl.2004.03.003.

Conrey, R.M., Sherrod, D.R., Uto, Kozo, and Uchiumi, Shigeru, 1996, Potassium-argon ages from Mount Hood area of Cascades Range, northern Oregon: Isochron/West, no. 63, p. 10–20.

Crandell, D.R., 1980, Recent eruptive history of Mount Hood, Oregon, and potential hazards from future eruptions: U.S. Geological Survey Bulletin 1492, 81 p.

Cribb, J.W., and Barton, M., 1997, Significance of crustal and source region processes on the evolution of compositionally similar calc-alkaline lavas, Mt. Hood, Oregon: Journal of Volcanology and Geothermal Research, v. 76, p. 229–249.

Darr, C.M., 2006, Magma chamber processes over the past 475,000 years at Mount Hood, Oregon—Insights from crystal zoning and crystal size distribution studies: Corvallis, Oregon State University, M.S. thesis, 141 p.

Evarts, R.C., Conrey, R.M., Fleck, R.J., and Hagstrum, J.T., 2009, The Boring Volcanic Field of the Portland-Vancouver area, Oregon and Washington—Tectonically anomalous forearc volcanism in an urban setting, *in* O'Connor, J.E., Dorsey, R.J., and Madin, I.P., eds., Volcanoes to vineyards—Geologic field trips through the dynamic landscape of the Pacific Northwest: Geological Society of America Field Guide 15, p. 253–270, doi: 10.1130/2009.fld015(13).

Evarts, R.C., and O'Connor, J.E., 2008, Geologic map of the Camas quadrangle, Clark County, Washington, and Multnomah County, Oregon: U.S. Geological Survey Scientific Investigations Map 3017, scale 1:24,000, pamphlet 31 p., accessed January, 2017, at http://pubs.usgs.gov/sim/3017/.

Evarts, R.C., O'Connor, J.E., and Tolan, T.L., 2013, Geologic map of the Washougal quadrangle, Clark County, Washington, and Multnomah County, Oregon: U.S. Geological Survey Scientific Investigations Map 3257, scale 1:24,000, pamphlet 46 p., accessed January, 2017, at http://pubs.usgs.gov/sim/3257/.

Ewert, J.W., Guffanti, Marianne, and Murray, T.L., 2005, An assessment of volcanic threat and monitoring capabilities in the United States: framework for a National Volcano Early Warning System: U.S. Geological Survey Open-File Report 2005–1164, 62 p.

Fleck, R.J., Hagstrum, J.T., Calvert, A.C., Evarts, R.C., and Conrey, R.M., 2014, $^{40}Ar/^{39}Ar$ geochronology, paleomagnetism, and evolution of the Boring Volcanic Field, Oregon and Washington, USA: Geosphere, v. 10, no. 6, p. 1,283–1,324, doi: 10.1130/GES00985.1.

Gallino, G.L., and Pierson, T.C., 1985, Polallie Creek debris flow and subsequent dam-break flood of 1980, East Fork Hood River basin, Oregon: U.S. Geological Survey Water-Supply Paper 2273, 22 p.

Grauer, J., 1975, Mount Hood—A Complete History: Self published, 300 p.

Hammond, P.E., and Korosec, M.A., 1983, Geochemical analyses, age dates, and flow-volume estimates for Quaternary volcanic rocks, southern Cascade Mountains, Washington: Washington Department of Natural Resources, Division of Geology and Earth Resources Open-File Report 83-13, 36 p.

Harris, B.L., 1973, Genesis, mineralogy, and properties of Parkdale Soils, Oregon: Corvallis, Oregon State University, Ph.D. dissertation, 174 p.

Hildreth, Wes, 2007, Quaternary magmatism in the Cascades—Geologic perspectives: U.S. Geological Survey Professional Paper 1744, 125 p.

Iverson, R.M., Schilling, S.P., and Vallance, J.W., 1998, Objective delineation of lahar-inundation hazard zones: Geological Society of America Bulletin, v. 110, no. 8, p. 972–984.

Keith, T.E.C., Beeson, M.H., and Bargar, K.E., 1982, Geologic map of the Mount Hood Wilderness, Clackamas and Hood River Counties, Oregon: U.S. Geological Survey Miscellaneous Field Studies Map MF-1379A, scale 1:62,500.

Keith, T.E.C., Donnelly-Nolan, J.M., Markman, J.L., and Beeson, M.H., 1985, K-Ar ages of rocks in the Mount Hood area, Oregon: Isochron/West, no. 42, p. 12–16.

Kent, A.J.R., Darr, Cristina, Koleszar, A.M., Salisbury, M.J., and Cooper, K.M., 2010, Preferential eruption of andesitic magmas through recharge filtering: Nature Geoscience, v. 3, p. 631–636. doi: 10.1038/NGEO924.

Koleszar, A.M., 2011, Controls on eruption style and magma compositions at Mount Hood, Oregon: Corvallis, Oregon State University, Ph.D. dissertation, 199 p.

Koleszar, A.M., Kent, A.J.R., Wallace, P.J., and Scott, W.E., 2012, Controls on long-term low explosivity at andesitic arc volcanoes—Insights from Mount Hood, Oregon: Journal of Volcanology and Geothermal Research, v. 219–220, p. 1–14, doi:10.1016/j.jvolgeores.2012.01.003

Korosec, M.A., 1987, Geologic map of the Hood River 30- by 60-minute quadrangle, Washington and Oregon: Washington Department of Natural Resources, Division of Geology and Earth Resources Open-File Report 87-6, scale 1:100,000.

Lanphere, M.A., Champion, D.E., Hildreth, Wes, Gardner, C.A., and Scott, W.E., 1997, New evidence on the magnetic reversal time scale from volcanic rocks in the Cascade Range, Washington, Oregon, and California [abs.]: EOS, Transactions of the American Geophysical Union, Fall 1997, F186.

Lilliquist, Karl, and Walker, Karen, 2006, Historical glacier and climate fluctuations at Mount Hood, Oregon: Arctic, Antarctic, and Alpine Research, v. 38, no. 3, p. 399–412.

Lundstrom, S.C., McCafferty, A.E., and Coe, J.A., 1993, Photogrammetric analysis of 1984–89 surface altitude change of the partially debris-covered Eliot Glacier, Mount Hood, Oregon, U.S.A.: Annals of Glaciology, v. 17, p. 167–170.

Madin, I.P., and Ma, L., 2012, The Blue Ridge Fault, a newly discovered Holocene fault near Mount Hood, Oregon [abs.]: Seismological Society of America Annual Meeting Abstracts, v. 83, no. 2, p. 374

Mathie, A., and Wood, N., 2013, Residential and service-population exposure to multiple natural hazards in the Mount Hood region of Clackamas County, Oregon: U.S. Geological Survey Open-File Report 2013–1073, 48 p.

McClaughry, J.D., Wiley, T.J., Conrey, R.M., Jones, C.B., and Lite, K.E., Jr., 2012, Digital geologic map of the Hood River Valley, Hood River and Wasco Counties, Oregon: Oregon Department of Geology and Mineral Industries Open-File Report O-12-03, scale 1:36.000, pamphlet 142 p.

O'Connor, J.E., and Burns, S.F., 2009, Cataclysms and controversy—Aspects of the Columbia River Gorge, *in* O'Connor, J.E., Dorsey, R.J., and Madin, I.P., eds., Volcanoes to vineyards—Geologic field trips through the dynamic landscape of the Pacific Northwest: Geological Society of America Field Guide 15, p. 237–251, doi: 10.1130/2009.fld015(12).

Pierson, T.C., 1998, An empirical method for estimating the travel times for wet volcanic mass flows: Bulletin of Volcanology, v. 60, p. 98–109.

Pierson, T.C., Pringle, P.T., and Cameron, K.A., 2011, Magnitude and timing of downstream channel aggradation and degradation in response to a dome-building eruption at Mount Hood, Oregon: Geological Society of America Bulletin, v. 123, p. 3–20, doi: 10.11 30/B30127.1.

Pierson, T.C., Scott, W.E., Vallance, J.W., and Pringle, P.T., 2009, Eruption-related lahars and sedimentation response downstream of Mount Hood—Field guide to volcaniclastic deposits along the Sandy River, Oregon, *in* O'Connor, J.E., Dorsey, R.J., and Madin, I.P., eds, Volcanoes to vineyards—Geologic field trips through the dynamic landscape of the Pacific Northwest: Geological Society of America Field Guide 15, p. 221–236, doi:10.1130/2009/fld015(11) .

Priest, G.R., Beeson, M.H., Gannett, M.W., and Berri, D.A., 1982, Geology, geochemistry, and geothermal resources of the Old Maid Flat area, Oregon, *in* Priest, G.R., and Vogt, B.F., eds., Geology and geothermal resources of the Mount Hood area, Oregon: Oregon Department of Geology and Mineral Industries Special Paper 14, p. 16–30.

Rapp, E.K., 2005, The Holocene stratigraphy of the Sandy River delta, Oregon: Portland, Portland State University, M.S. thesis, 93 p.

Reid, H.F., 1905, The glaciers of Mt. Hood and Mt. Adams: Mazama, v. 2, p. 194–200.

Scott, W.E., Gardner, C.A., Sherrod, D.A., Tilling, R.I., Lanphere, M.A., and Conrey, R.M., 1997a, Geologic history of Mount Hood volcano, Oregon—A field-trip guidebook: U.S. Geological Survey Open-File Report 97-263, 38 p.

Scott, W.E., Pierson, T.C., Schilling, S.P., Costa, J.E., Gardner, C.A., Vallance, J.W., and Major, J.J., 1997b, Volcano hazards in the Mount Hood region, Oregon: U.S. Geological Survey Open-File Report 97-89, 14 p.

Sherrod, D.R., and Scott, W.E., 1995, Preliminary geologic map of the Mount Hood 30- by 60-minute quadrangle, northern Cascade Range, Oregon: U.S. Geological Survey Open-File Report 95-219, 35 p., scale 1:100,000.

Thouret, J.-C., 2005, The stratigraphy, depositional processes, and environment of the late Pleistocene Polallie-period deposits at Mount Hood volcano, Oregon, USA: Geomorphology, v. 70, p. 12–32, doi:10.1016/j.geomorph.2005.03.008.

Tolan, T.L., and Beeson, M.H., 1984a, Exploring the Neogene history of the Columbia River— Discussion and geologic field trip guide to the Columbia River Gorge, Part I. Discussion: Oregon Geology, v. 46, no. 8, p. 87–97.

Tolan, T.L., and Beeson, M.H., 1984b, Exploring the Neogene history of the Columbia River—Discussion and geologic field trip guide to the Columbia River Gorge, Part II. Road log and comments: Oregon Geology, v. 46, no. 9, p. 103–112.

Vallance, J.W., 1999, Postglacial lahars and potential hazards in the White Salmon River system on the southwest flank of Mount Adams, Washington: U.S. Geological Survey Bulletin 2161, 49 p.

White, Craig, 1980, Geology and geochemistry of Mt. Hood volcano: Oregon Department of Geology and Mineral Industries Special Paper 8, 26 p.

Wise, W.S., 1968, Geology of the Mount Hood volcano, *in* Dole, H.M., ed., Andesite conference guidebook: Oregon Department of Geology and Mineral Industries Bulletin 62, p. 81–98.

Wise, W.S., 1969, Geology and petrology of the Mt. Hood area—A study of High Cascade volcanism: Geological Society of America Bulletin, v. 80, p. 969–1,006.

Woods, M.M., 2004, Compositional and mineralogical relationships between mafic inclusions and host lavas as key to andesite petrogenesis at Mount Hood volcano, Oregon: Portland, Portland State University, M.S. thesis, 170 p.

A Summary of Recent Petrological and Geochemical Studies of Mount Hood, Oregon

By Adam J.R. Kent and Alison Koleszar

A Summary of Recent Petrological and Geochemical Studies of Mount Hood, Oregon

By Adam J.R. Kent[1] and Alison Koleszar[1,2]

Abstract

Mount Hood, Oregon, an archetypal subduction zone stratovolcano, is dominated by extrusive eruptions of lava flows and domes, coupled with a high degree of homogeneity in erupted lava compositions. Over the last ~500,000 years—the age of the current edifice—the volcano has repeatedly erupted crystal-rich andesites and low SiO_2 dacites, with SiO_2 contents largely between 55 and 65 weight percent. Lavas also show similar phenocryst mineralogy, compositions, and textures, and are dominated by plagioclase together with pyroxene, amphibole, and occasional olivine.

The presence of quenched mafic inclusions, bimodal populations of plagioclase and amphibole, mineral zoning, and a range of other evidence also shows that Mount Hood magmas are produced by quasi-binary mixing between relatively mafic (basaltic) and silicic (rhyodacitic-rhyolitic) parental magmas. Mineral zoning shows that magma mixing occurred very late in the petrogenetic history, within weeks to months of eruption. Mount Hood is a volcanic system driven by mafic recharge, where hot mafic magmas ascending from the mantle or lower crust interact with silicic magmas to produce mixed intermediate compositions. Evidence suggests that the silicic parental magma is stored within the shallow crust (3–6 kilometers) beneath the volcano as cool, crystal-rich mush for long periods (>>10 ka) prior to eruptions. Mafic recharge provides both the impetus to erupt and produces the intermediate compositions, resulting in the long-term eruptive output of a homogeneous series of intermediate magmas.

Introduction

Mount Hood dominates the skyline from many parts of western and northern Oregon, and as a result of its proximity to Portland, plays a major role in the State's cultural identity and recreational activities. However, despite the iconic profile, Mount Hood has been understudied with respect to petrological and geochemical aspects of magma production and evolution relative to many other Cascade Range stratovolcanoes. This is partly due to the relatively restricted petrological and geochemical variation evident in erupted Mount Hood magmas—in short the volcano has an undeserved reputation as "boring". Despite this, Mount Hood preserves a rich record of the petrological processes that operate in an archetypal andesite-dominated arc stratovolcano.

In conjunction with a range of collaborators, we have worked to unravel the petrological and geochemical record at Mount Hood. The following summary outlines our conclusions from the past decade of work. Before 2000 there were relatively few studies in the peer-reviewed literature concerning the petrological aspects of Mount Hood (for example, Wise, 1969; Eichelberger, 1978; White, 1980; Cribb and Barton, 1997). Since 2005 we have been involved in a series of papers and graduate theses (Darr, 2006; Kent and others, 2010; Eppich, 2010; Koleszar, 2011; Eppich and others, 2012; Koleszar and others, 2012; Kent, 2013; Cooper and Kent, 2014) exploring the petrology, petrography, geochemistry, geochronology, and other features of Mount Hood lavas. Other studies (for example, Woods, 2004) have also provided additional important data. The composition of the Mount Hood andesite has also been widely used as an experimental standard in studies of intermediate magmas (for example, Eggler and Burnham, 1973; King and others, 2002), although few of these studies aimed to resolve issues specific to this volcano (and as we argue below, Mount Hood andesites are also unlikely to have represented true igneous liquid at any point). Our results focus largely on the youngest two eruptive events (Old Maid, approximately 230 years ago; Timberline, approximately 1,500 years ago), although we have also studied samples of Polallie age (30–12 ka) and some older erupted phases. These results provide insight into the petrogenesis of Mount Hood magmas, the processes that lead to eruption, the conditions and duration of magma storage beneath the volcano, and controls over eruptive style.

The general location of Mount Hood has served as the center of growth for several intermediate composition volcanoes for at least the last 1.4 million years or longer, although the current edifice of Mount Hood was constructed during the last ~500 ka. Growth of the volcano has spanned a number of periods of increased eruption rates followed by quiescence and glacially dominated erosion. The most recent growth phases occurred during the Pollalie eruptive period (30–12 ka), Timberline eruptive period (~1,500 years ago), and Old Maid eruptive period (~230 years ago)(Scott and others, 1997).

[1]College of Earth, Ocean, and Atmospheric Sciences, Oregon State University

[2]Jackson School of Geosciences, The University of Texas at Austin

The compositions of erupted lava samples from Mount Hood are restricted in bulk composition (figs. 1, 2), in that they lie predominantly within the andesite-dacite compositional range, and are also petrographically similar—dominated by plagioclase with lesser mafic minerals (amphibole, orthopyroxene, clinopyroxene, and some olivine) and oxide phases. The overall crystallinity of lava samples is high, typically in the range of 25–40 modal percent (Kent and others, 2010). Mineral and rock textures are typical of intermediate arc magmas with the presence of texturally distinct populations of plagioclase, complex zoning and dissolution features in plagioclase and mafic phases, and opacitic breakdown of amphibole rims. Quenched-texture inclusions (Bacon, 1986) are common in many lavas (for example, Woods, 2004), although the overall abundance varies from sample to sample. Plutonic and cumulate texture inclusions also occur but are relatively rare.

Mount Hood lavas are dominated by andesites, with some low-silica dacites in the mostly recently erupted material. Lavas from flank eruptions are also typically lower in SiO_2 than those from the main edifice (fig. 1); these include the Cloud Cap center, a distinct eruptive center active at ~420 ka formed during the early stages of growth of Mount Hood, and the Parkdale flow, a 7,700 year old flow erupted 12 kilometers (km) north-northeast of the summit.

Chemical, Textural, and Mineralogical Characteristics of Mount Hood Lavas

The bulk composition of Mount Hood lavas (including samples from lava flows, lava domes, and from block and ash flows generated by dome collapse) broadly ranges from andesite to low-silica dacite, with more mafic lavas (mostly basaltic andesites and some basalts) erupted from flank vents (fig. 1). The majority of lavas have SiO_2 contents between 55 and 65 weight percent (figs. 1, 2; Scott and others, 1997; Kent and others, 2010). Chemical variations between lava samples are generally quite simple, with bivariate plots characteristically showing broadly linear arrays (figs. 2, 3), even for elements where it is expected that fractional crystallization would produce strongly curved trends (fig. 3). Quenched-texture inclusions have compositions that range between 55 and 60 weight percent SiO_2 and overlap the more mafic host lava compositions. Rare cumulate-texture inclusions have distinctly more mafic compositions, with SiO_2 contents that extend to less than 50 weight percent (fig. 2).

Lavas from Mount Hood exhibit mineralogical and textural features that are typical for subduction-related intermediate volcanics. Lavas are crystal rich (typically 20–45 modal

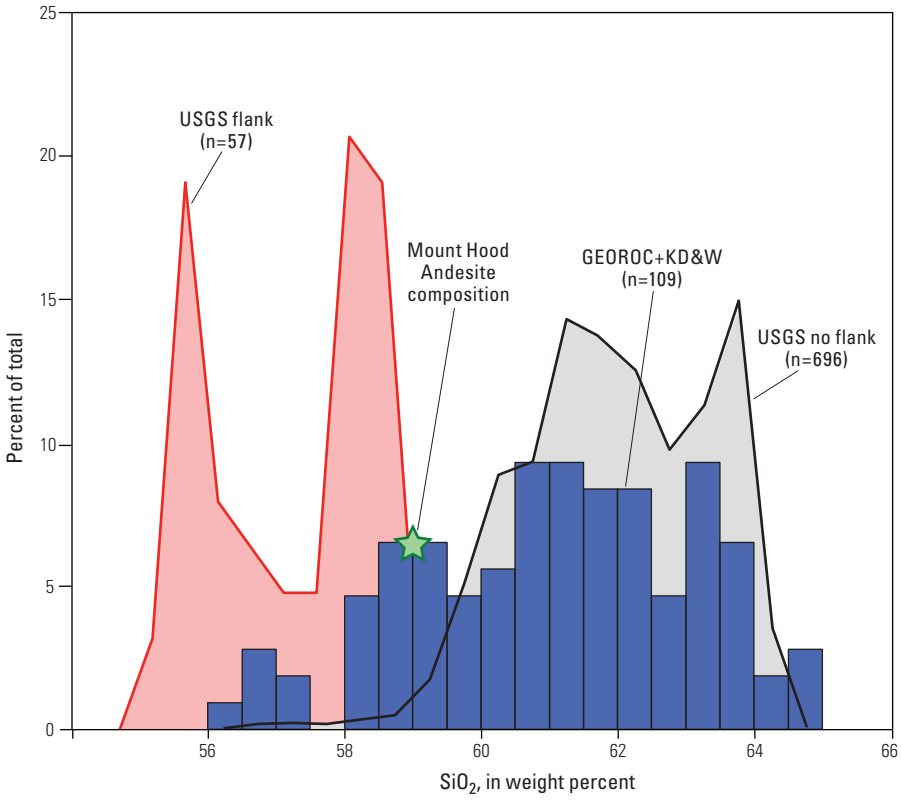

Figure 1. Histogram of SiO_2 content for Mount Hood lavas. Shown here are all U.S. Geological Survey data for Mount Hood and for regional flank vents as well as a smaller dataset (KD&W) from the theses of Koleszar (2011), Darr (2006), and Woods (2004), together with available data from the GEOROC (2016) compilation. The latter contains data for both Mount Hood and regional flank vents such as the Parkdale flow and Cloud Cap vent. The Mount Hood Andesite composition used for experimental studies of andesitic liquids (59.1 weight percent SiO_2; for example, Eggler and Burnham, 1973; King and others, 2002) is also shown (green star).

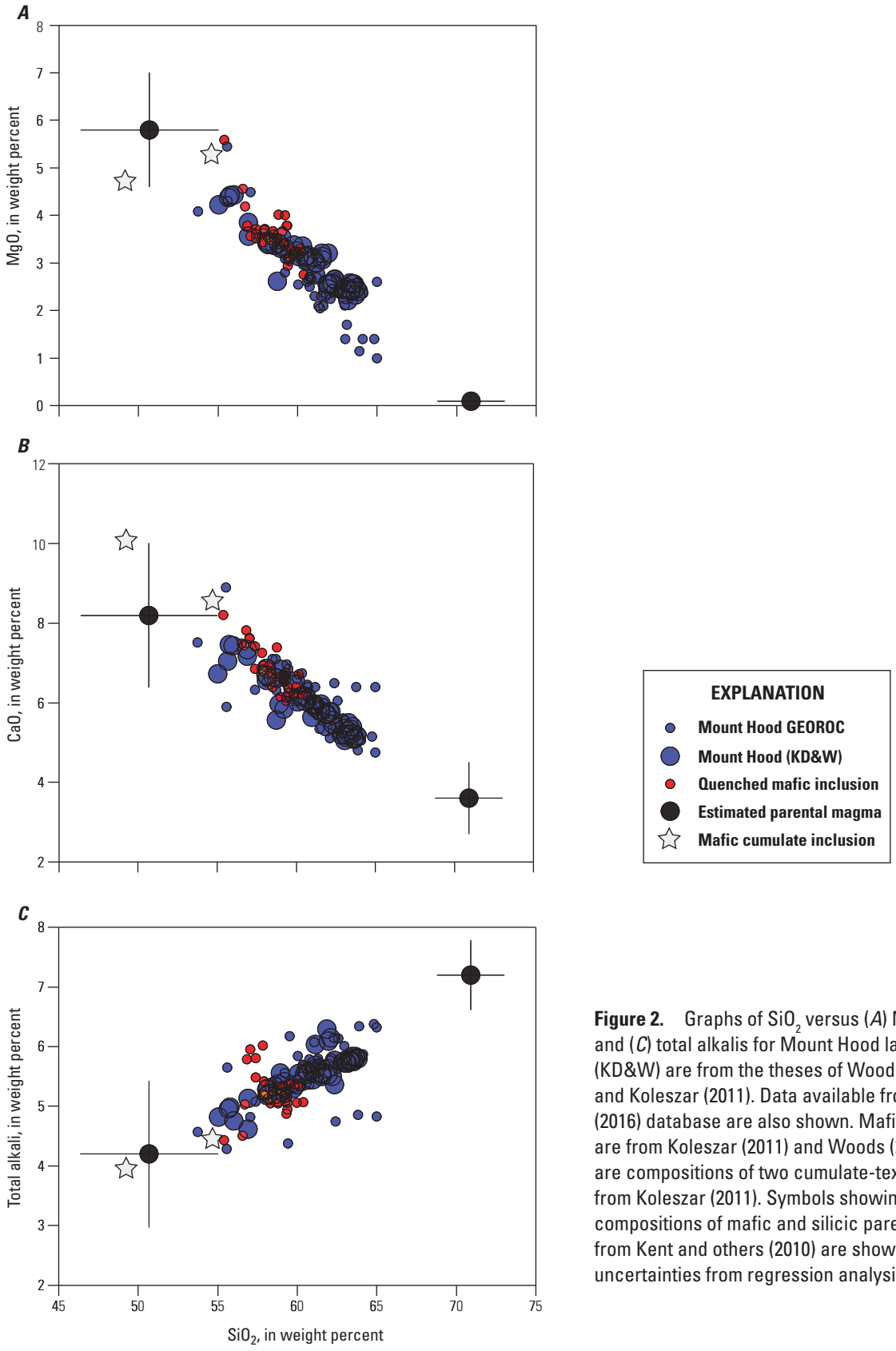

Figure 2. Graphs of SiO_2 versus (*A*) MgO, (*B*) CaO, and (*C*) total alkalis for Mount Hood lavas. Data labeled (KD&W) are from the theses of Woods (2004), Darr (2006), and Koleszar (2011). Data available from the GEOROC (2016) database are also shown. Mafic inclusion data are from Koleszar (2011) and Woods (2004). Also shown are compositions of two cumulate-texture inclusions from Koleszar (2011). Symbols showing the estimated compositions of mafic and silicic parental magmas from Kent and others (2010) are shown with estimated uncertainties from regression analysis.

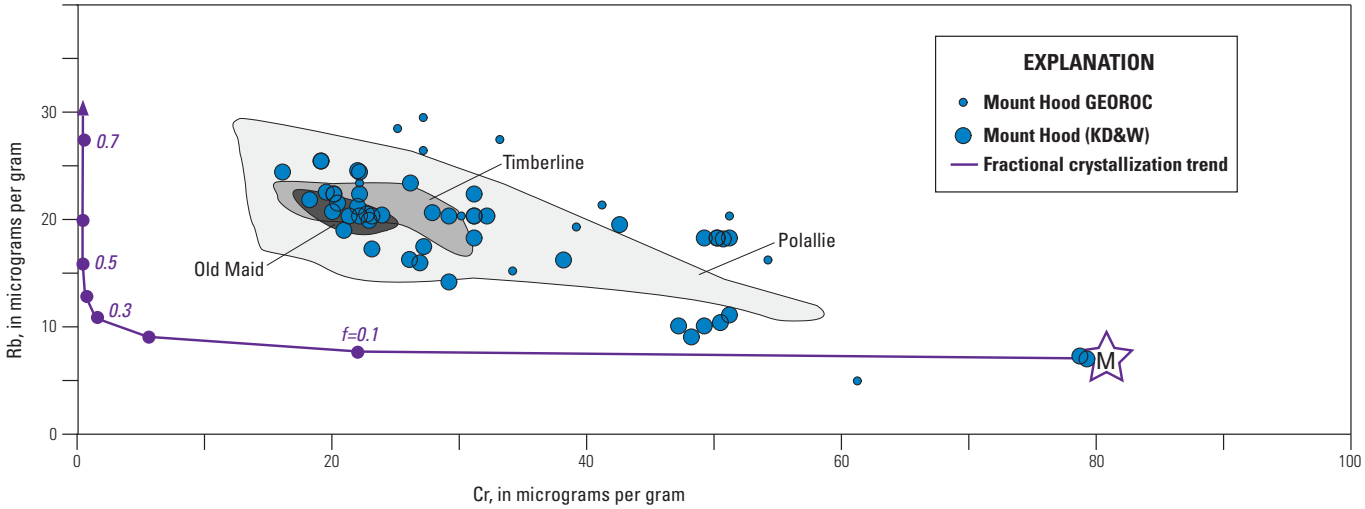

Figure 3. Graph of rubidium versus chromium for Mount Hood lavas from the GEOROC (2016) database and from the theses of Woods (2004), Darr (2006) and Koleszar (2011). Grey fields show the range of values for U.S. Geologic Survey samples for Old Maid, Timberline, and Polallie age samples. Also shown is a calculated fractional crystallization trend of representative mafic melt (M) with an initial composition of 8 micrograms per gram (µg/g) rubidium and 80 µg/g chromium. Calculations used bulk mineral-melt partition coefficients of DRb = 0.01 and DCr = 13, calculated for crystallization of an assemblage consisting of 0.55 (number refers to modal mass fraction) plagioclase, 0.15 orthopyroxene, 0.05 clinopyroxene, 0.20 amphibole, and 0.05 titanomagnetite, using mineral-melt partition coefficients from Rollinson (1993). Crystal fraction values (f) are marked on the fractional crystallization trend.

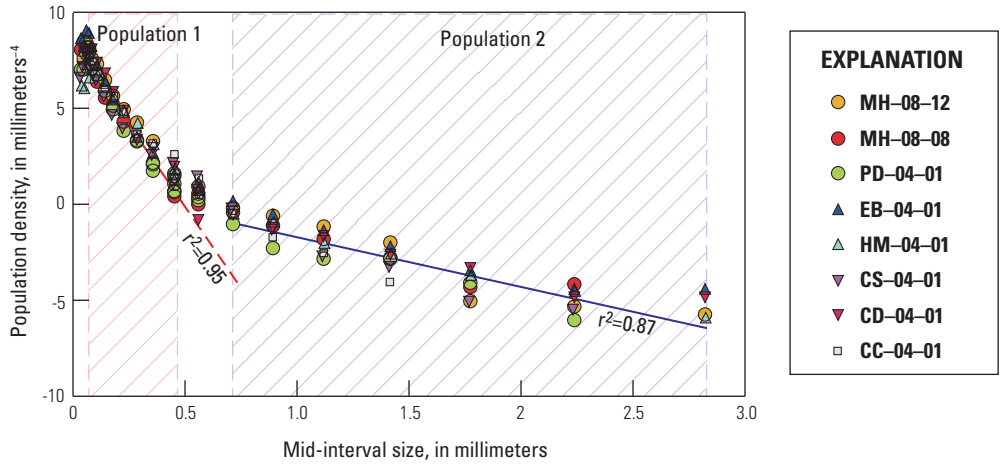

Figure 4. Graph of crystal size distributions for plagioclase from eight lavas from Mount Hood (from Kent and others, 2010). Population 1 and 2 crystals are defined as those with mid-interval sizes between 0.0448–0.448 millimeters and 0.710–2.82 millimeters, respectively. Red and blue lines show least squares best-fit lines to each of these defined populations.

percent crystals) and dominated by plagioclase, which commonly exhibits complex zoning and dissolution textures. The dominant mafic phase in the relatively higher SiO_2 Timberline and Old Maid age samples is amphibole, but orthopyroxene, clinopyroxene, and to a lesser extent, olivine occur as a phenocryst phase in other Mount Hood lavas. Where hornblende is not present, orthopyroxene is typically the dominant mafic phase. Lavas also often include abundant quenched-texture inclusions and less common cumulate- and plutonic-texture inclusion types.

Mount Hood lavas show ubiquitous evidence for texturally and (or) chemically distinct populations of crystals present within individual lava samples; this is most evident in studies of plagioclase. Crystal-size distribution studies (CSD) of plagioclase are remarkably consistent for samples erupted throughout the entire history of the Mount Hood edifice (fig. 4). Almost all CSD are kinked—a classic feature of many intermediate magmas—which suggests that they contain at least two distinct populations of plagioclase that have experienced different nucleation and growth conditions (Marsh, 1998; Higgins, 2006). Kent and others (2010) designated these two groups as population 1 (those with typical crystal sizes between 0.04 and 0.5 millimeters [mm]) and the larger population 2 plagioclase (0.5–3 mm). All samples studied in

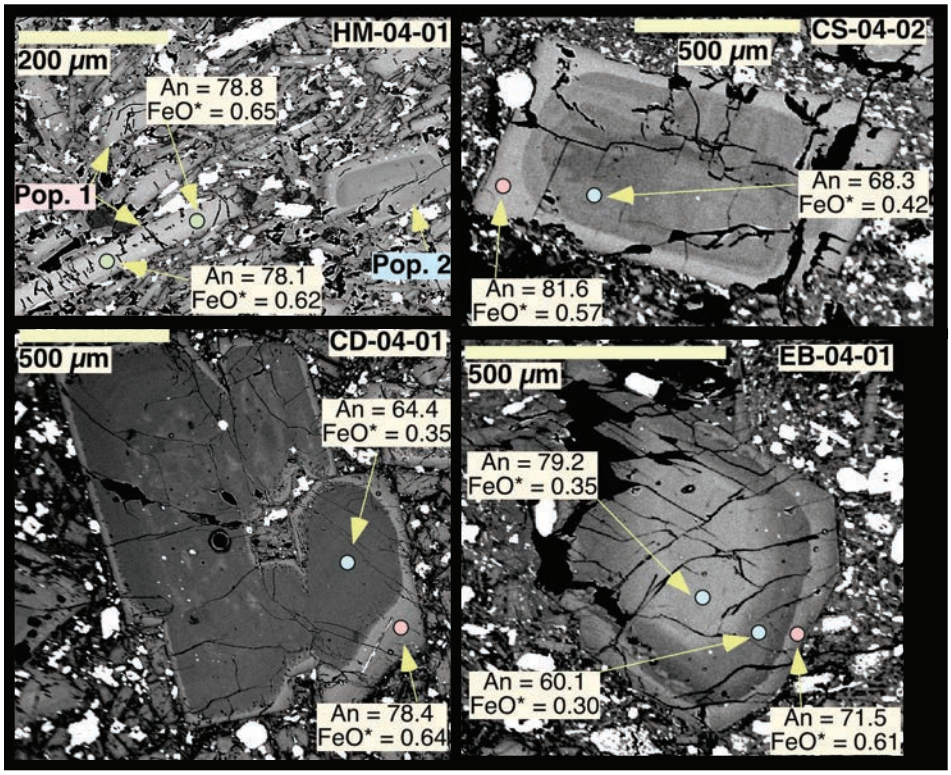

Figure 5. Backscattered electron images of representative plagioclase from Mount Hood lavas (from Kent, 2013). Anorthite and FeO* contents are also shown for selected spot analysis locations.

Kent and others (2010), which range in age from ~425,000 to 230 years old, exhibited near identical CSDs with the exception of a single sample from the more mafic Cloud Cap eruptive center that mostly lacks the larger population 2 crystals (fig. 4).

There are also consistent differences between the population 1 and 2 plagioclase crystals in terms of their crystal form, zoning patterns, and anorthite and trace element contents (figs. 5–8). Population 1 plagioclase crystals are small (typically in the microphenocryst to microlite range, <0.5 mm to <0.1 mm), have acicular form with aspect ratios in excess of 5–10, and often have swallowtail crystal terminations consistent with rapid crystal growth. The crystals are also unzoned or slightly normally zoned with anorthite between ~50–70. Population 1 crystals also have higher concentrations of iron, magnesium, strontium, and titanium, and lower contents of barium and light rare earth elements (LREE; fig. 7). Conversely the larger population 2 plagioclase crystals have blocky or tabular form, often occurring in glomerocrysts, and exhibit complex internal anorthite zoning, with abundant dissolution surfaces and spongy melt-inclusion-rich zones (figs. 5, 8). Overall anorthite contents are more variable (~35–70) than population 1 plagioclase and extend to lower anorthite. Although anorthite varies substantially in the interiors of population 2 plagioclase, they are uniformly low in iron, magnesium, strontium, and titanium, and have low strontium/barium and strontium/LREE relative to population 1 (figs. 5–8). Population 2 crystals also exhibit ubiquitous high-anorthite rims (figs. 6, 8), with anorthite of 50–70. These are typically <50–100 micrometers (μm) thick and, in contrast to the interior of these crystals, have higher iron, magnesium, strontium, and titanium, and higher strontium/barium—similar to that found in population 1 crystals (figs. 5, 8). There is also commonly evidence for crystal resorbtion and dissolution prior to rim growth.

Where amphibole is present, two distinct groups also occur (fig. 9; Koleszar and others, 2012). Amphibole is a mafic phase common in more SiO_2-rich Mount Hood lavas, and occurs in distinct high- and low-aluminum and aluminum/silicon compositions (Koleszar, 2011; Kent, 2013). High-Al_2O_3 amphiboles have Al_2O_3 of ~11–14 weight percent and molar aluminum/silicon of 0.30 to 0.35. Low-Al_2O_3 amphiboles have Al_2O_3 of ~7-10 weight percent and molar aluminum/silicon of 0.16 to 0.25. These two populations also show subtle textural distinctions, with the low Al_2O_3 amphibole ranging to higher aspect ratios, and also show consistent differences in rare earth elements (REE), strontium, zircon, Eu/Eu*, and chlorine (fig. 9; Koleszar and others, 2012). Rare amphibole crystals also show zoning from high to low Al_2O_3 or vice versa (Koleszar, 2011). These differences mirror broader bimodality in amphibole Al_2O_3 and aluminum/silicon ratios that are evident in many subduction zones magmas—particularly intermediate magmas—worldwide (Kent, 2013). The high-aluminum amphiboles are interpreted to derive from hotter and more mafic magmas that recharge shallow silicic magma reservoirs where low-aluminum amphiboles crystallize. As described below, we interpret the low-Al_2O_3 amphiboles to have crystallized from relatively silicic magma at relatively shallow depths (3–6 km).

As noted, lavas from regional flank vents and from the Cloud Cap eruptive center are typically more mafic than summit lavas. Although we have not studied all flank vents in detail, the single Cloud Cap lava for which we have obtained

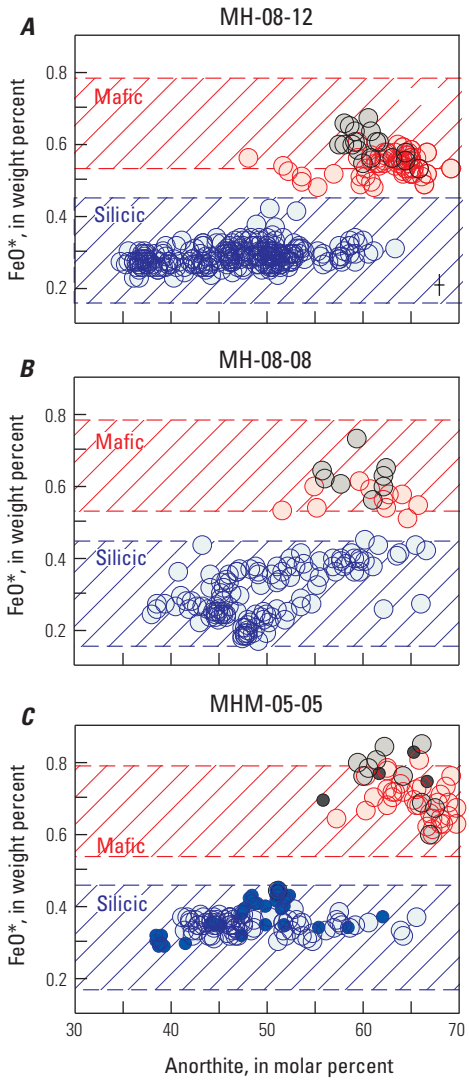

Figure 6. Graphs of anorthite versus FeO* (total Fe as FeO) for population 1 and 2 plagioclase and rims on population 2 crystals for samples (*A*) MH-08-12 (Old Maid), (*B*) MH-08-08 (Timberline), and (*C*) MHM-05-05 (Mount Hood Meadows), modified from Kent and others (2010). The Mount Hood Meadows flow erupted ~55–50 ka. Also shown for MHM-05-05 is data for a quenched-texture inclusion. Red and blue hachured regions represent the expected FeO∗ contents of plagioclase crystallized from silicic and mafic parental endmember magmas using partition coefficients calculated using Lundgaard and Tegner (2004), and with bulk rock FeO/FeO∗ = 0.85. Representative 1 s.d. analytical uncertainties are shown in (*A*).

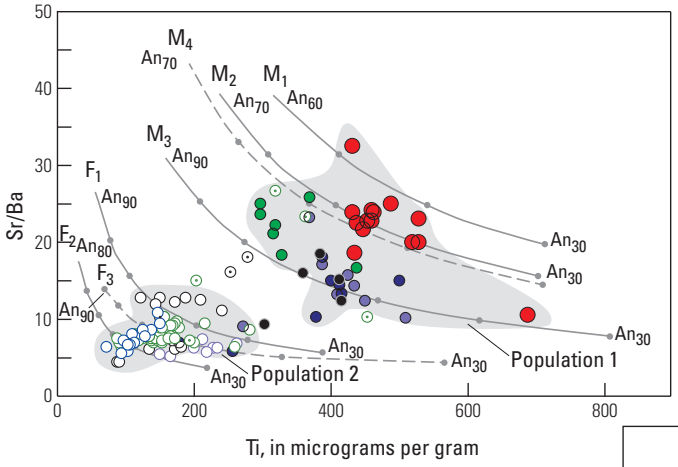

	Model	T°C	Ti µg/g	Sr/Ba
Mafic	M_1	1,000	12,000	2.5
	M_2	1,000	9,000	2.5
	M_3	1,000	6,000	2.0
	M_4	800	9,000	2.5
Felsic	F_1	800	4,200	1.0
	F_2	800	3,000	0.7
	F_3	1,000	4,200	1.0

Figure 7. Graph of representative strontium/barium versus titanium for population 1 and 2 plagioclase crystals, from Kent (2013). Also shown are curves representing equilibrium partitioning between plagioclase and a range of representative mafic and silicic (felsic) parental melt compositions (see inset table). Anorthite contents of equilibrium plagioclase are shown starting at An_{30} (see Kent and others [2010] for sample details). Each point marked along the curves represents an additional 10 molar percent anorthite. Open circle symbols with central dot represent rims to population 2 plagioclase crystals. Analytical uncertainties in both axes are <10 percent. Temperature (T) in degrees Celsius; µg/g, micrograms per gram.

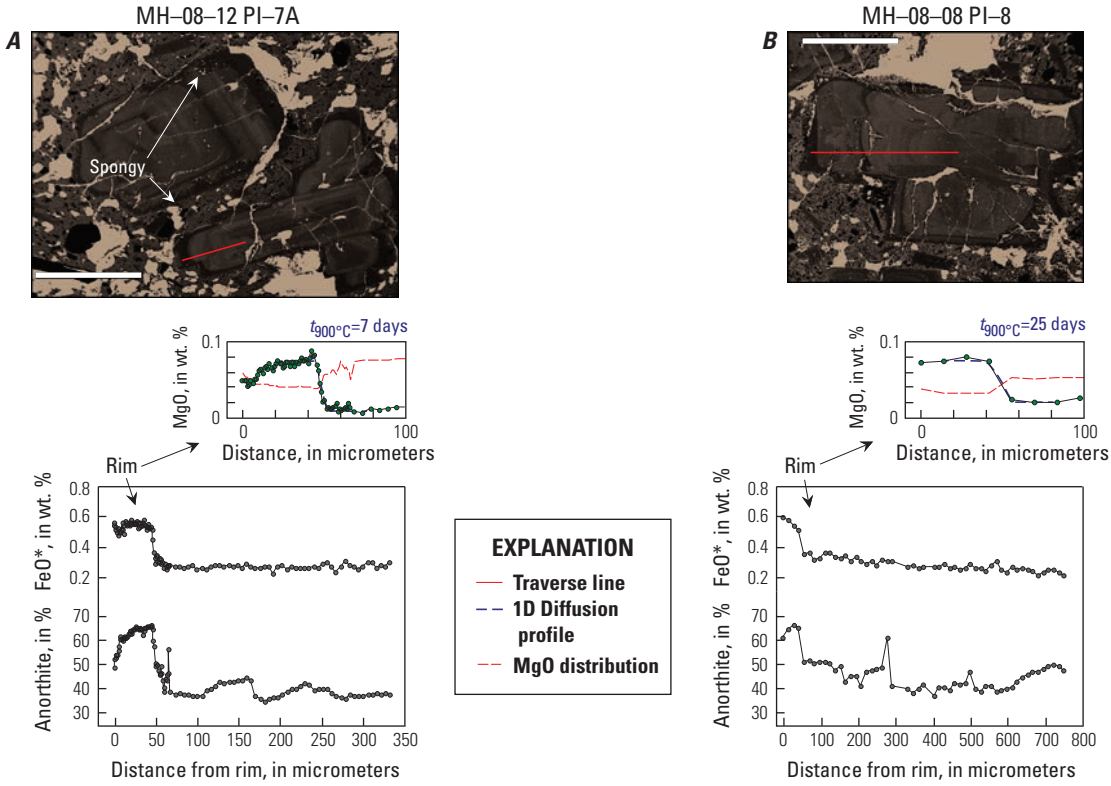

Figure 8. Electron probe measurements of anorthite and FeO* versus distance for selected population 2 plagioclase crystals from (*A*) Old Maid (MH-08-12), and (*B*) Timberline (MH-08-08) age lavas. Also shown are backscattered electron images for each crystal with the line of each traverse in red. White scale bars are 500 micrometers (µm). Insets show MgO zoning in the outermost 100 µm for each crystal, with the calculated equilibrium MgO distributions shown in red (determined following Costa and others, 2003). The blue dashed lines show best-fit 1D diffusion profiles, and the estimated time for an initial step function to decay to the observed distribution is given for 900 °C. At 850 °C the time required is a factor of ~3 longer. Modified from Kent and others (2010). Wt. %, weight percent.

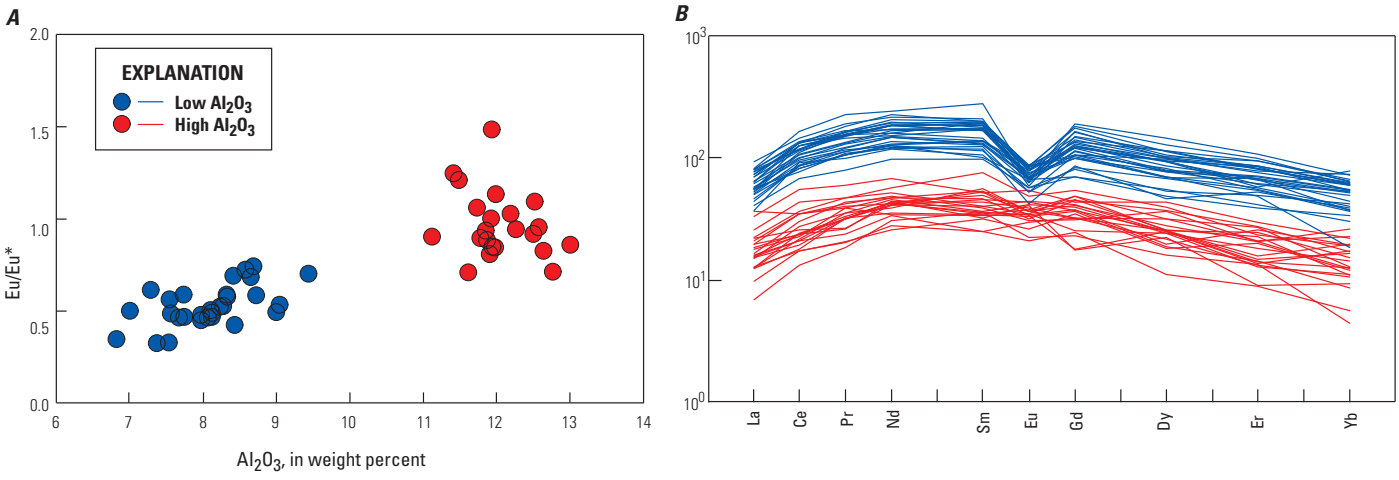

Figure 9. Graph of amphibole compositions from Old Maid, Timberline, and Polallie age lavas from Mount Hood. *A*, Eu/Eu* versus Al_2O_3. *B*, Chondrite normalized rare earth element contents of high and low Al_2O_3 amphiboles. Data from Koleszar (2011).

CSD and mineral chemical data also shows a dearth of larger population 2-type plagioclase, and the plagioclase crystals present in this sample are texturally and compositionally similar to the population 1 plagioclase crystals evident in other samples (see sample CC-04-01 in fig. 7). In contrast, samples of the basaltic andesite Parkdale flank-vent flow, erupted ~12 km north-northeast of the summit, have strongly kinked CSD (fig. 4; sample PD-04-01) that are almost identical to those of other Mount Hood lavas and contain plagioclase populations that closely match population 1 and population 2 plagioclase in terms of both texture and composition (fig. 7). From this we interpret that the magma erupted at Parkdale was probably produced within the same magmatic system as Mount Hood summit lavas, although if so it remains unclear why it erupted at such a distance from the summit.

Petrogenesis of Mount Hood Lavas

The petrologic, textural, field, and geochemical characteristics of Mount Hood lavas are consistent with magma mixing playing a primary role in the petrogenesis of erupted magmas. Evidence for this includes:

- Linear trends on element–element variation diagrams (figs. 2, 3), including elements pairs (for example, rubidium versus chromium) that would be expected to exhibit highly curved trends from fractional crystallization (fig. 3).
- Ubiquitous bimodal amphibole and plagioclase mineral populations as described above (figs. 4–7, 9).
- Zoning patterns in plagioclase that show that the interaction between mafic and silicic magmas occurred at a late stage in the petrogenetic sequence, as shown by ubiquitous iron- and magnesium-rich rims on the larger population 2 plagioclase.
- The common occurrence of quenched-texture inclusions. In most cases the same crystal populations identified in the host lava samples also occur within inclusions, although the population 2 plagioclase and low-Al_2O_3 amphiboles are less common within the inclusions. Quenched-texture inclusions also tend to have more mafic bulk compositions (fig. 2; Woods, 2004; Koleszar, 2011) than the host lavas, though there is overlap between mafic inclusions and lava compositions consistent with a degree of hybridization (for example, Tepley and others, 1999). A less common group of plutonic and cumulate-texture inclusions have the most mafic bulk compositions (fig. 2).

On the basis of this evidence we interpret the vast majority of erupted Mount Hood magmas to have formed through binary mixing between mafic and silicic parental magmas. Mixing between these two parental magmas results in the production of the range of intermediate magma compositions observed in erupted lavas, and produces the range of mineralogical and textural features described above. Mixing may also influence the eruptive style of the volcano.

Magma mixing of this type is a common process in many intermediate arc volcanoes (for example, Anderson, 1976; Eichelberger, 1978; Eichelberger and others, 2006; Kent and others, 2010; Kent, 2013), although the compositions of the parental magmas involved in mixing are often difficult to establish. For Mount Hood, Kent and others (2010) estimated the bulk parental magma compositions involved in mixing by combining quantitative textural and bulk magma compositional data. Specifically there are strong correlations ($P << 0.05$) observed between the abundance of major element oxides (for example, SiO_2, Al_2O_3, TiO_2, MgO, FeO*, K_2O) and the proportion of each type of plagioclase present in the eight lava samples where CSDs are available. Furthermore, higher proportions of population 1 plagioclase correlate with more mafic compositions (lower SiO_2, Al_2O_3, and K_2O, and higher MgO, FeO*, TiO_2, and CaO). Our interpretation is that mixing of mafic and felsic parental magmas produces the juxtaposition of the two different plagioclase populations that we observe, and mixing proportions control both the relative amounts of each type of plagioclase present and the final erupted lava compositions. The observation that these correlations are highly significant also requires that the bulk composition and crystallinity of both parental magmas has remained broadly constant through time—which also has interesting implications for the processes that generate these parental magmas. Note that we do not suggest that the exact same silicic and mafic parental magmas contribute to erupted intermediate lavas, but that mixing to produce the observed range of Mount Hood magmas occurs between parental magmas of consistently similar bulk composition.

We can use the observed correlations between crystallinity and composition to estimate the bulk composition of each parental magma by extending the observed correlations to 100- and 0-percent population 1 plagioclase (Kent and others, 2010; Kent, 2013). These compositions are shown in figure 2 and have SiO_2 contents of 51±4 and 71±2 weight percent SiO_2, and MgO of 5.8±1.2 and 0.10±0.60 weight percent. The uncertainties reflect the uncertainty in the best fit regression. These SiO_2 and MgO contents are consistent with the mafic parental magma being moderately differentiated basaltic or basaltic andesite magma, broadly similar to compositions erupted throughout the Cascade Arc, and the silicic parent being rhyodacitic to rhyolitic in bulk composition.

Contributions from these two parental magma compositions can also explain the observed variability in amphibole and plagioclase populations. The estimated silicic parental magma composition is in equilibrium with the observed iron, magnesium, titanium and strontium/barium of population 2 plagioclase (figs. 6, 7), suggesting that they crystallized from this parental magma. Internal variations in anorthite in population 2 plagioclase crystals, often in conjunction with apparent crystal dissolution surfaces (figs. 5, 8), are not accompanied by variations in iron and magnesium (figs. 6, 8), suggesting no

involvement of mafic magma throughout the growth of population 2 plagioclase. Variations in anorthite probably instead relate to convective self-mixing (Couch and others, 2003) or other variations in pressure and (or) temperature during crystallization, without the addition of material from the mafic parental magma (Ruprecht and Wörner, 2007). Conversely the higher iron, titanium, and strontium/barium contents of the population 1 plagioclase are consistent with the mafic parental magma composition (fig. 6). The smaller sizes, high aspect ratio, simple zoning, and occasional swallowtail crystal terminations show that these crystals grew rapidly and shortly before eruption, and we suggest that they grew rapidly during the latter stages of magma ascent or during cooling associated with recharge and mixing with the silicic parent. The mafic parental magma is also considered to be the source of the high-Al_2O_3 amphibole, which probably grew during magma ascent as well. The silicic parental magma contributes the low-Al_2O_3 amphibole. This interpretation is broadly consistent with SiO_2 contents for melts in equilibrium with these two populations of amphiboles calculated from Ridolfi and others (2010), which suggest equilibrium SiO_2 contents (for coexisting melt, not magma) of ~55 and 75 weight percent for high- and low-Al_2O_3 amphibole, respectively. Differences in Eu/Eu* ratios and REE (fig. 9) between these two groups of amphibole also suggest that high-Al_2O_3 amphiboles grew from a more mafic melt that had experienced little or no plagioclase fractionation, whereas the low-Al_2O_3 amphiboles crystallized from a liquid that had crystallized significant amounts of plagioclase.

Zoning patterns in population 2 plagioclase provide a means to constrain the timing of mixing to produce the compositions of erupted intermediate lavas at Mount Hood. In all of the samples we have studied, which range in age from more than 400,000 to ~220 years old, we observe near-ubiquitous high-anorthite rims on population 2 plagioclase (figs. 3–5). These rims also have elevated iron, magnesium, titanium, strontium/barium, and lower LREE relative the interiors of the crystals. Thus, although the interiors of population 2 plagioclase formed from the silicic parental magma, their rims have grown after mixing with mafic parental melts, resulting in higher An, iron, magnesium, and strontium/barium. Textural indications of plagioclase dissolution prior to growth of high-anorthite rims are also consistent with mixing with a hotter, more mafic magma prior to rim growth. The restriction of high iron and magnesium zones to the exterior of the population 2 plagioclase (figs. 5, 8) indicates that mixing between the mafic and silicic parental magmas is the last major petrological event to affect these crystals, and likely occurred shortly before eruption.

Kent and others (2010) used diffusion modeling of magnesium to further constrain the timescale of eruption following mafic recharge and growth of high-anorthite rims. Assuming that magnesium concentrations initially exhibited a step-function change across the rims from low-magnesium interiors to high-magnesium rims, analytical solutions to the diffusion equation suggest that the observed magnesium distribution represents a maximum time between mafic recharge and cooling upon eruption of ~1–4 weeks for a temperature of 900 °C (fig. 8), which is the estimated temperature of Timberline and Old Maid lavas on eruption (Koleszar and others, 2012). For temperatures of 850 °C (consistent with amphibole temperatures from the felsic parental magma; Koleszar and others, 2012) the calculated timescales are about a factor of three longer. Collectively, these constraints suggest that the time between mafic recharge and eruption are less than a few weeks to a few months, and further support the idea that mixing occurred immediately prior to eruption. Note that this time estimate does not include the time required for population 2 plagioclase to dissolve prior to rim growth, but given that plagioclase dissolution rates are significantly faster than plagioclase growth rates (for example, Ruprecht and others, 2008) this time is likely to be quite short compared to the time of rim growth. These estimates of eruption timescales from plagioclase zoning are also important for understanding future eruption hazards at the volcano, as they provide an estimate for the time that will elapse between mafic recharge at depth (which could be detected by seismic monitoring, gas release, or ground deformation) and eventual eruption. Although these timescales at Mount Hood are quite short, observations and petrologic studies at erupting arc volcanoes suggest short time periods between mafic recharge and eruption are common (for example, Pallister and others, 1992; Nakamura, 1995; Venezky and Rutherford, 1999; Devine and others, 2003).

The Recharge Filtering Model

There are several interesting features of Mount Hood that any petrogenetic model should address. Firstly, there is the compositional homogeneity of the eruptive output of the volcano—with lavas largely restricted to intermediate compositions (over 90 percent of magmas sampled have SiO_2 contents in the range of 56–65 weight percent). The narrow range of lava compositions is even more evident in comparison to other Cascade volcanoes such as Mount St. Helens and Mount Jefferson, the nearest stratovolcano neighbors to the north and south, which have both erupted magmas that are more mafic and more silicic than Mount Hood (Kent and others, 2010; Kent, 2013). Secondly, although it appears that the mafic and silicic parental magma compositions we have defined contribute to almost all lavas at Mount Hood, these parental endmember compositions themselves appear to rarely, if ever, erupt (fig. 2), and almost all lavas fall outside of the estimated compositions of these parental magmas. Thirdly, there is the observation that all Mount Hood lavas that we have studied are the product of magma mixing. Mixing was relatively rapid and efficient, with intimate juxtaposition of crystals from plagioclase populations 1 and 2 and the high- and low-Al_2O_3 amphibole populations. Mixing also appears to be the final event that occurs prior to eruption, occurring within weeks to a few months after magma mixing has occurred. Finally, we see no evidence for mixing events that produce elevated iron and magnesium in the interior of larger plagioclase crystals,

indicating that eruptions only occur following a recharge and mixing event.

These observations can be accounted for by understanding that Mount Hood is a magmatic system that is profoundly influenced by mafic recharge—that is, petrogenesis involves addition of mafic magma to a more silicic magma reservoir to both promote the production of mixed intermediate magmas and to initiate eruptive episodes. Mafic recharge of this type is a commonly observed feature at intermediate arc volcanoes (and many other volcanic systems) and the mechanism by which recharge initiates eruptions has been studied by a range of petrological, numerical, analogue, and other approaches (for example, Sparks and others, 1977; Eichelberger, 1978; Huppert and others, 1982; Gourgaud and others, 1989; Pallister and others, 1992; Murphy and others, 1998, 2000; Eichelberger and others, 2006; Ruprecht and others, 2008).

We suggest that the dependence on mafic recharge to initiate eruptions at Mount Hood also results in the observed compositional homogeneity of eruptive products. Preferential eruption of intermediate magma compositions is an inevitable result of a system where recharge is required to initiate eruptions and also produces intermediate magma compositions. Kent and others (2010) and Kent (2013) termed this interplay "recharge filtering"—namely that the requirement for mafic recharge to initiate eruptions results in production and eruption of intermediate mixed-lava compositions. In contrast the parental magma compositions themselves appear unable to erupt, although they play an important role in petrogenesis of erupted magmas, probably because the silicic parental magma is too viscous (and too cool and crystal-rich; see discussion below) to be mobile, whereas the presence of silicic magma storage zones within the shallow crust represent a density and mechanical barrier for ascending mafic magmas from the deeper crust (Eichelberger and others, 2006; Hildreth, 2007; Karlstrom and others, 2009; Kent and others, 2010; Kent, 2013). The end result is that the eruptive output of the volcano is dominated by mixed intermediate compositions as they are the only magmas able to consistently erupt.

We also note that at Mount Hood, not only do the parental magmas not erupt, but erupted magmas largely represent mixtures produced by approximately subequal proportions of the two parental magmas (50±20 percent; fig. 10*B*). Magmas produced by the addition of 10–20 percent of one parent to the other do not occur in significant proportions (fig. 10*B*). Kent and others (2010) and Kent (2013) suggests that mixing in an approximately 1:1 ratio of mafic to silicic parent produce

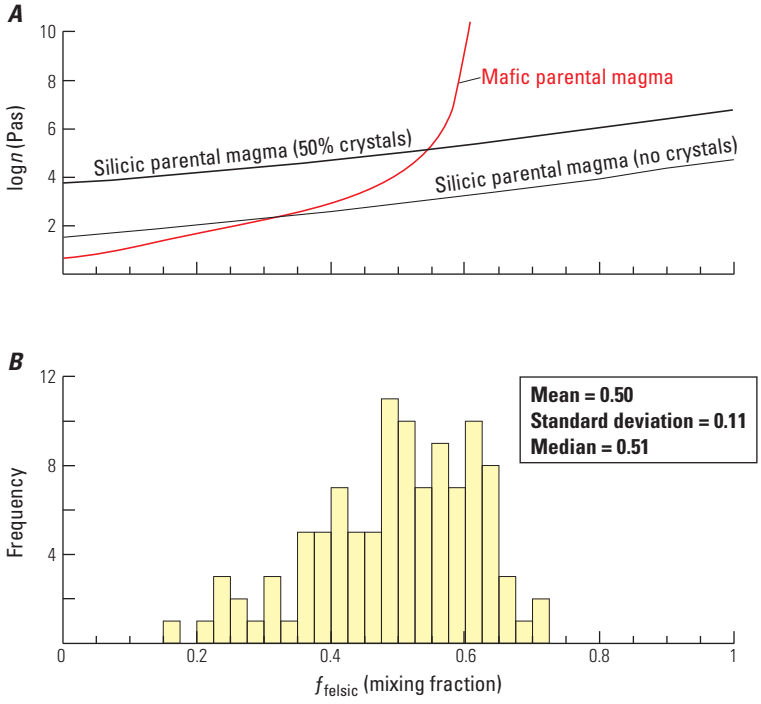

Figure 10. *A*, Graph of calculated viscosity for mixtures of the estimated mafic and silicic parental Mount Hood magma compositions as a function of f_{felsic}, the calculated proportion of silicic parental magma present in mixed magmas. Curves represent the viscosities after thermal equilibration but prior to hybridization, and were calculated following the method outlined in Sparks and Marshall (1986). The approach of Giordano and others (2008) and Marsh (1981) were used to estimate the silicate liquid and magma viscosities and the MELTS algorithm used to estimate the crystallinity of the mafic parent magma during cooling below a liquidus temperature of 1,144 °C. Calculations were performed for 50 percent and 0 percent crystals for the felsic parent composition. *B*, Graph of calculated mixing proportions of felsic parental magma contributing to a set of erupted Mount Hood magma compositions. Mixing fraction was calculated based on SiO_2 contents and the estimated parental magma compositions from Kent and others (2010). For further details see Kent (2013).

magmas within a "goldilocks zone" of magma mobility, with intermediate viscosity and density relative to the two parental magma compositions. However fluid dynamic constraints on efficient mixing may also play a role (Sparks and Marshall, 1986; Kent, 2013). As shown in figure 10, the mode of the distribution of lava compositions (couched in terms of mixing fraction between the parental magma compositions) coincides with a window where thermally equilibrated mafic and silicic parents have approximately similar viscosities. This condition is a requirement for efficient mixing between two liquids and thus likely also plays a role in mobilization of the resultant mixed magma (Sparks and Marshall, 1986).

It is also interesting to consider why Mount Hood appears so strongly controlled by mafic recharge relative to other Cascade and arc volcanoes that erupt a greater array of compositions (Kent, 2013). One possibility is that crustal conditions beneath Mount Hood are less favorable to direct eruption of the parental magmas without recharge than elsewhere along the arc. This may be true, but it is difficult to establish directly. For example, Eichelberger (1978) and Larsen (2016) have argued that compressional environments favor eruption of mixed intermediate magmas because structural conduits for magma ascent are less available. Mount Hood lies in a region of broad crustal compression related to northward rotation of the Oregon coast block and impact with southern Washington (Wells and McCaffrey, 2013). Compression is ongoing, however structures associated with compression in the Mount Hood area are all older than the current Mount Hood edifice, and the structural state of the local crust now appears dominated by intra-arc extension and formation of a half-graben to the east. Kent (2013) also suggested that hydrous mafic magmas are a key to the production of mixed magmas in recharge-driven systems because the higher volatile abundances are more likely to promote the density-driven overturn and subsequent mixing required to produce and erupt mixed intermediate magmas during recharge events (for example, Eichelberger 1980; Ruprecht and others, 2008).

Origin of Parental Magmas

Koleszar (2011) studied the origin of each parental magma type at Mount Hood by using mixing proportions and trace element data to determine the trace element contents of the parental magmas involved in magma mixing. The mafic parental magma composition is consistent with moderate degrees of fractionation (~20 percent) of a typical large-ion lithophile elements (LILE)-enriched Cascade calc-alkaline basaltic magma (for example, barium/zircon ~20, barium/niobium ~25). Following the modeling approach of Reiners and others (2000), Koleszar (2011) estimated that the trace element contents of the mafic parental magma at Mount Hood could be produced by ~15 percent flux melting of a peridotite mantle source by the addition of a few percent of a slab-derived fluid. The origin of the silicic parental magma is less certain but the composition is broadly similar to that expected from 15–20 percent partial melting of amphibolite within the middle to lower crust, which would produce a magma with similar SiO_2 and H_2O contents as the silicic parental magma (63–75 and 3.1–5.2 weight percent), as well as the observed moderate depletion in middle rare earth elements (Conrey and others, 2001; Borg and Clynne, 1998).

Conditions and Duration of Magma Storage at Mount Hood

Constraints on the Duration of Crustal Magma Residence

Application of radiometric dating techniques provides insight into the crustal residence times of magmatic components at Mount Hood. Eppich (2010) and Eppich and others (2012) conducted a uranium-thorium-radium disequilibrium study of samples from the Old Maid and Timberline eruptive periods. Analysis of different plagioclase size fractions in combination with unmixing calculations based on measurements of bulk and mineral chemistry allowed estimates of the age of both population 1 and 2 plagioclase. Population 1 plagioclase have ^{230}Th-^{226}Ra model ages that are relatively imprecise (because even the smallest plagioclase size fractions were dominated by fragments of the larger population 2 plagioclase) but are <<3,000 years, consistent with our interpretation that they form immediately prior to or during mafic recharge and eruption. In contrast ^{230}Th-^{226}Ra model ages for population 2 plagioclase suggest ages older than 4,000–5,000 years. These ages also reflect growth of younger rims immediately prior to eruption, and mass balance models show that the cores of population 2 plagioclase crystals are ≥10,000 years old (due to the ~1,600 year half life of ^{226}Ra, 10,000 years is the upper limit of age resolution for the ^{230}Th-^{226}Ra system). ^{238}U-^{230}Th data from Eppich and others (2012) also provide age information, and because the ~76,000 year half-life of ^{230}Th is significantly longer, can be used to resolve ages as old as 350,000 years. Groundmass–plagioclase isochrons for Old Maid and Timberline samples suggest that the population 2 plagioclase in these lavas have a minimum age of 17,000 years and a mean age of 126,000 years (Eppich and others, 2012; Cooper and Kent, 2014). Once corrections are made for the presence of eruption-age rims, the minimum age of population 2 plagioclase crystals is estimated to be 21,000 years. This shows that the silicic parental magma involved in petrogenesis at Mount Hood has experienced long-term residence (>>10,000 years) within the shallow crust beneath the volcano.

We have also recently obtained ages ^{238}U-^{230}Th for zircons from separated Old Maid and Timberline age lava samples (Klemetti and others, 2015), and these also suggest long term residence of the silicic parental magma. The presence of zircons in Mount Hood lavas also provides additional evidence for

a silicic magma reservoir beneath Mount Hood. Zircon saturation calculations based on the major element composition of Mount Hood melt inclusions (Koleszar and others, 2012) and measured range of zircon contents within melt inclusions of 120–316 micrograms per gram (µg/g; Koleszar, 2011) suggest zircon saturation temperatures of ~740–850 °C, using both the calibrations of Watson and Harrison (1983) and Boehnke and others (2013). Thus the melt component of the silicic parental magma (which is trapped by melt inclusions) is not saturated with zircon at the ~850–900 °C eruption temperatures, and the presence of zircon requires a period of crustal residence at lower temperatures. Measured ^{238}U-^{230}Th zircon model ages range from >350,000 years (the oldest age that the ^{238}U-^{230}Th system can record), to ages that are within uncertainty of the eruption age. The majority of zircon growth appears to have occurred since ~25,000 years ago, approximately since the inception of the Polallie eruptive period.

Depths of Magma Storage and the Structure of the Magmatic System

Our isotopic results and estimates of the composition of parental magma compositions at Mount Hood suggest that erupted magmas contain a significant component of a silicic parental magma that experienced a lengthy period of crustal residence. We infer that this material resides in a shallow crustal magma storage zone beneath the volcano, and that occasional ascent of more mafic magma from deeper within the crust into this zone initiates eruptions. Application of mineral thermometry and barometry, melt inclusion saturation calculations, and constraints from fumarole gases and analysis of recent earthquakes at Mount Hood place constraints on the conditions of shallow magma storage beneath the volcano.

A compilation of depth constraints for magma storage is shown in figure 11. Collectively these estimates are consistent with residence of the silicic parental magmas at depths of ~3–6 km beneath the summit of the volcano. Some pressure estimates from the vapor saturation pressures of melt inclusions are shallower (Koleszar and others, 2012) and may thus represent trapping of melt inclusions or diffusive hydrogen loss during magma ascent rather than during extended residence. In addition some melt inclusions record saturation pressures that are in excess of 500 megapascals (MPa) (although the high CO_2 contents that these pressures reflect were outside the calibration range of the measurement technique and are consequently less accurate), suggesting that some deeper trapping of melt inclusions may also have

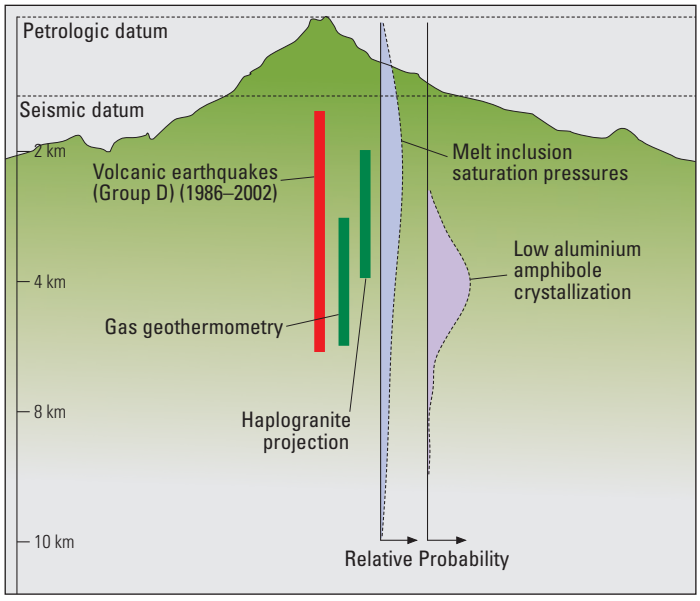

Figure 11. Summary of seismic and petrological constraints on magma storage beneath Mount Hood. Curves show kernel density functions for saturation pressures of melt inclusions (n=38) from Koleszar and others (2012), and for pressures calculated from low-aluminum amphibole compositions using the calibration of Ridolfi and others (2010) (n=35). Melt inclusion pressures were calculated using the approach of Newman and Lowenstern (2002) and do not include melt inclusions with anomalously low H_2O at a given SiO_2—an indication of melt inclusion rupture (Koleszar and others, 2012). Earthquake data are from Jones and Malone (2005) and represent relocated hypocenters with adjusted arrival times. Group D earthquakes are a group of earthquakes that occurred under the summit of Mount Hood from 1986–2002 and interpreted to be generated by volcanic and (or) hydrothermal processes. The depth range of for earthquakes have been also adjusted for differences in the seismic datum and petrologic depth estimates, which refer to depth below the summit. Gas geothermometry based estimates for the depth of magma storage are from Symonds and others (2003) and are based on an empirical gas geothermometer in conjunction with the boiling curve for water. Pressures from the haplogranite projection are based on melt inclusion compositions from Koleszar and others (2012) and follow the method of Blundy and Cashman (2008).

occurred prior to magmas stalling within the shallow crust. Pressure estimates from earthquakes and from the composition of fumarole gases may also, in part, record pressures from the hydrothermal system overlying a magma reservoir. The inferred 3–6 km depth of magma residence is also consistent with a recent global compilation of petrological and geophysical depths of magma storage beneath volcanoes (Chaussard and Amelung, 2014), as well as observations of active and erupting arc volcanoes (for example, Pallister and others, 1992; Nishi and others, 1999; Scandone and others, 2007; Elsworth and others, 2008; Foroozan and others, 2010), and shows that magma storage at these shallow crustal depths is very common beneath arc and other volcanoes. The reasons that ascending magmas stall at such shallow crustal depths remain less well understood (for example, Acocella, 2014) although it may relate to the interplay between ascent rates and changes in viscosity during ongoing ascent, decompression, cooling, and crystallization (for example, Annen and others, 2006).

Temperatures of magma are also constrained by mineral equilibria, and Koleszar and others (2012) applied several different geothermometers to Mount Hood magmas (fig. 12). The results constrain the temperature of crystallization or equilibration of amphibole and plagioclase within the mafic parental magma to temperatures above ~950 °C and within the silicic parental magma to ~850–900 °C (fig. 12). Note that these temperatures are interpreted as those at which these minerals formed, although they do not necessarily represent the temperatures at which long-term silicic magma storage occurred or the temperature at which the mafic magma was intruded. For the mafic magmas, these amphibole-plagioclase temperatures represent minimum temperatures for the recharge magma, as mafic magmas at upper crustal pressures saturate amphibole and temperatures below ~1000 °C and after extended (>50 percent) crystallization (Blatter and others, 2013). Koleszar and others (2012) also determined temperatures of iron-titanium oxide equilibration in the groundmass of erupted magmas from the Old Maid, Timberline, and Polallie eruptive periods. Given the relatively rapid equilibration rate of iron-titanium oxides (for example, Nakamura, 1995) these temperatures are interpreted to reflect the temperatures of eruption, and range between ~900–1040 °C with an average of ~950 °C.

Thermal Conditions of Long-Term Magma Residence

The temperature of long-term magma storage has an important influence on the ability of magma to be mobilized and to eventually erupt at the surface. Magma viscosity is a function of both the viscosity of the silicate liquid fraction and overall crystallinity, and for a given magma composition these are both strongly controlled by temperature (for example, Marsh, 1981; Giordano and others, 2008). Therefore, the thermal history of stored magma has an important influence over the behavior of a given volcanic system. It has long been considered from field observations, thermal considerations, and numerical modeling that magma storage within the crust often involves some residence within a relatively cool, crystal-rich, mushy state in which magmas are too viscous to erupt. Eruption of such crystal-rich magmas requires rejuvenation of this mush by heating to reduce viscosity and promote magma mobility (for example, Bachman and Bergantz, 2008; Huber and others, 2011; Burgisser and Bergantz, 2013), although to date it has not been clear how long magmas are stored as cool

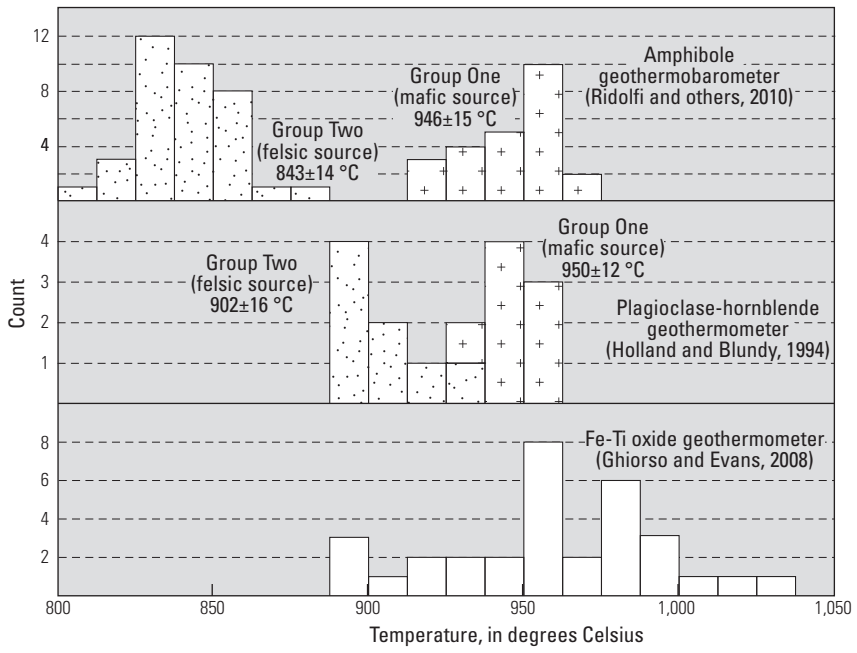

Figure 12. Comparison between pre-eruptive temperatures for Mount Hood magmas calculated using three methods: amphibole compositions (Ridolfi and others, 2010) from the Old Maid, Timberline, and Polallie eruptive periods; plagioclase–hornblende pairs (Holland and Blundy, 1994) from the Old Maid and Timberline eruptive periods; and iron–titanium oxides (Ghiorso and Evans, 2008) from the Old Maid and Timberline eruptive periods. Group 1 amphiboles contain 11–13 weight percent Al_2O_3 and group 2 amphiboles contain 6–9 weight percent Al_2O_3. Figure from Koleszar and others (2012).

and viscous mushes versus a more liquid-rich form which allows ready mobilization and eruption.

Studies at Mount Hood provide a means to quantify this for the silicic parental magma stored within the shallow crust. Although studies of temperature-sensitive mineral equilibria at Mount Hood and elsewhere provide direct constraints on magmatic temperatures (fig. 12), as we noted before, these typically reflect the temperature of mineral formation or equilibration and not the long-term thermal history experienced by magmas. In an alternate approach, Cooper and Kent (2014) combined crystal ages from the uranium-thorium-radium studies with estimates of crystal residence based on the diffusion of strontium in plagioclase and CSDs to investigate this issue. As we noted before, ^{238}U-^{230}Th isochrons constrain the average age of the cores of population 2 plagioclase (which formed from the silicic parental magma) to more than ~21,000 years. However, residence age estimates based on the diffusion of strontium in plagioclase and from CSDs using reasonable crystal growth rate estimates (10^{-8}–10^{-11} centimeters per second) are much shorter—ranging up to a few thousand years at most. The difference between these and the ^{238}U-^{230}Th ages can be reconciled by remembering that crystal growth and diffusion are temperature dependent processes, whereas ^{238}U-^{230}Th ages simply reflect the time since fractionation of the parent-daughter ratio. Magma storage at relatively cool temperatures will result in shorter magma residence time estimates from strontium diffusion and from CSDs. For population 2 plagioclase from Old Maid and Timberline age samples, Cooper and Kent (2014) determined maximum magma residence times of <<2,000 years at 750 °C—a temperature that marks the transition from a rheologically mobile magma to crystal-dominated rheologic solid (Marsh, 1981). As a result, Cooper and Kent (2014) concluded that the silicic parental magma stored beneath Mount Hood has only been in a mobile state, and thus in a condition where it could be erupted, for a small fraction of its total residence (at least <12 percent and probably <1 percent).

The idea of cold storage for magmas within the shallow crust is consistent with our general model that the silicic parental magma at Mount Hood is produced within the lower-middle crust, and ascends and stalls at shallow crustal levels. Amphibole and plagioclase-amphibole temperatures recorded from this magma represent cooling from this mobile stage in the later stages of ascent or after stalling, and do not represent the temperature of long-term magma storage. After emplacement the silicic parental magma cools and is stored as a crystal-rich solid, or perhaps even at subsolidus conditions, prior to being remobilized by later recharge immediately prior to eruption. This scenario of cold storage for the silicic parental magma makes intuitive sense given the relatively small volumes erupted at Mount Hood (typically <<1 km^3; for example Scott and others, 1997) and the inference that magmatic fluxes are relatively low. However ongoing studies of other volcanoes suggest that cold storage of magmas may be relatively common in many arc volcanoes (Cooper and Kent, 2014), even where eruption volumes are much larger than those typical for Mount Hood.

Our results for Mount Hood fit well within an emerging paradigm for intermediate arc volcanoes whereby magma storage is dominated by crystal-rich mush zones within the shallow to middle crust (for example, Cashman and Sparks, 2013; Cooper and Kent, 2014; Edmonds and others, 2016). In this view, magma storage within the crust beneath the volcano occurs in one or more interconnected crystal-rich mush zones, possibly also with smaller melt-rich lenses in some systems. Because convection and inter-crystal diffusion is relatively restricted by the low melt fraction, heterogeneity may develop within and between individual mush horizons (for example, Edmonds and others, 2016). Ascending, hotter, mafic magmas periodically disrupted the crystal-rich mushes to produce the mixed intermediate magmas that erupt (for example, Huber and others, 2011; Burgisser and Bergantz, 2013). Contributions from different mush horizons might introduce additional mineralogical complexity to erupted magmas.

The Volatile Contents of Mount Hood Magmas and a Dearth of Explosive Eruptions

Mount Hood is unusual relative to many other arc stratovolcanoes, including those elsewhere in the Cascades, in that there is little or no evidence for major explosive Plinian activity over at the last ~500,000 years (for example, Scott and others, 1997. Mount Hood eruptions are dominated by summit and flank extrusive activity that forms lava flows or domes, with tephra and pyroclastic flow deposits produced by block and ash flows after dome collapse. Although magma compositions can have an important influence on eruption style, this is unlikely to be the primary control at Mount Hood, as erupted magmas have compositions that overlap those from other Cascade stratovolcanoes, many of which have erupted explosively (Koleszar and others, 2012).

Koleszar and others (2012) studied the lack of major explosive eruptions at Mount Hood in greater detail. Explosive eruptions require that fragmentation occurs during magma ascent, where the proportion of bubbles produced by exsolution and expansion of dissolved vapor species (dominated by H_2O) exceed a critical fraction, typically considered to be ~75 percent (Sparks, 1978), and (or) the expanding melt exceeds a critical strain rate to promote brittle deformation (Cashman and Sparks, 2013). This process is a strong function of the initial magmatic volatile content, together with the viscosity of the ascending magma. Thus, one potential explanation for the low overall explosivity of Mount Hood is that magmatic volatile contents are intrinsically lower in Mount Hood magmas, as has been observed in other volcanoes that erupt explosive and effusive phases (for example, Roggensack and others, 1997). Koleszar and others (2012) measured the volatile

concentrations in plagioclase-, pyroxene- and amphibole-hosted melt inclusions from the Old Maid, Timberline and Polallie eruptive phases. Melt inclusions have H_2O contents of 1.0–5.5 weight percent (fig. 13), CO_2 of 0–~2,500 µg/g, 0.2–0.36 weight percent chlorine, and <200 µg/g sulfur. The large range of H_2O and CO_2 contents in melt inclusions likely reflects pre-eruptive degassing during magma ascent and storage (Koleszar and others, 2012). These values closely overlap melt inclusion volatile contents in other Cascade volcanoes that have erupted explosively, such as Mount St. Helens and Mount Mazama (Bacon and others, 1992; Blundy and others, 2010; Mandeville and others, 2009) and in other intermediate arc volcanoes worldwide (for example, Roman and others, 2006; Humphreys and others, 2009a,b). The maximum content of H_2O—the volatile species most likely to drive magma fragmentation—in Mount Hood magmas is also similar to that observed in many other intermediate arc volcanoes that erupt explosively (for example, Wallace, 2005). From these results Koleszar and others (2012) concluded that it is highly unlikely that the low overall explosivity of Mount Hood eruptions relates solely to intrinsically lower magmatic H_2O content.

In light of this finding, Koleszar and others (2012) argued that the process of magma mixing might have an important influence on the eruptive style of Mount Hood, following the model proposed by Ruprecht and Bachmann (2010) for Volcán Quizapu in Chile. Ruprecht and Bachmann (2010) argued that temperature increases associated with mafic recharge and efficient mixing immediately prior to eruption reduce the likelihood of explosive eruption activity. Increases in magmatic temperatures reduce the viscosity of the magma and allow for more efficient degassing during magma ascent, thus delaying the onset of fragmentation. As we have described for Mount Hood, there is widespread evidence that mafic recharge and magma mixing consistently precede eruption, and Koleszar and others (2012) suggested that this also resulted in increases in magma temperatures, leading to lower melt viscosity and a propensity to erupt effusively.

Mineral geothermometry also supports this scenario. Temperatures of amphibole crystallization in the stored silicic parental magma range from ~850–900 °C (fig. 12; Koleszar and others, 2012), and the temperature of long term storage of this magma was likely <750 °C (Cooper and Kent, 2014). However, iron-titanium oxide temperatures, which are interpreted to record the eruptive temperature of magmas, range from ~900–1050 °C with a median value of ~950 °C (Koleszar and others, 2012). The higher oxide temperatures suggest that reheating of the mixed magma occurred prior to eruption on timescales short enough that only the iron-titanium oxide minerals could re-equilibrate (a few months or less; Nakamura, 1995). Qualitative investigation of this scenario using the CONFLOW model (Mastin and Ghiorso, 2002) shows that this magnitude of reheating (>~100 °C) could lower magma viscosity by at least a factor of 10 and thus significantly delay the onset of magma fragmentation during ascent. In this respect Mount Hood is similar to a number of other intermediate arc volcanoes around the world at which magma mixing is a common process, eruptions are initiated by magma recharge, and the eruptive style is dominated by dome effusion. Examples include Soufriére Hills, Montserrat; Mont Pelée, Martinique; and Mount Unzen, Japan (Kent, 2013).

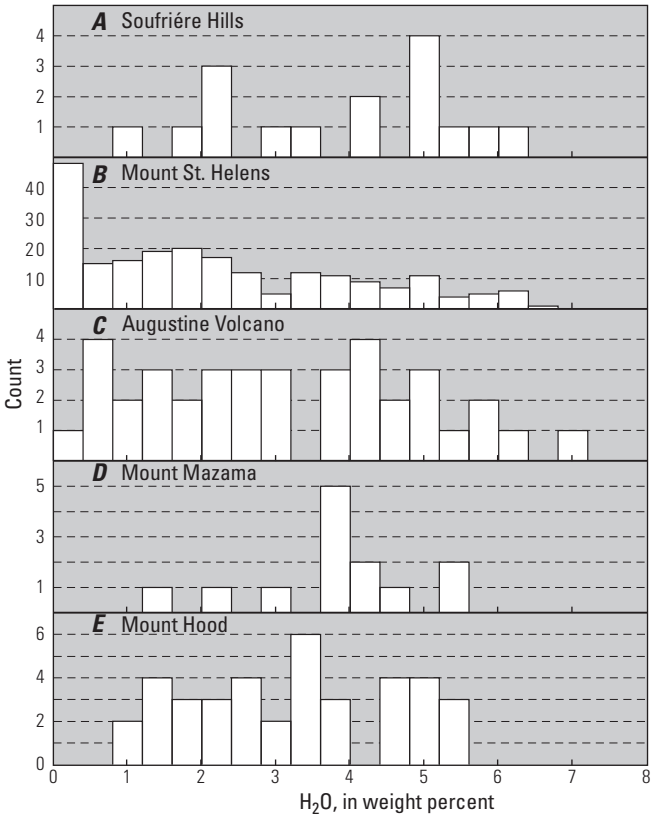

Figure 13. Graph of H_2O contents for melt inclusions from (*A*) Soufriére Hills Volcano (Humphreys and others, 2009a,b), (*B*) Mount St. Helens (Blundy and others, 2010), (*C*) Augustine Volcano (Roman and others, 2006), (*D*) Mount Mazama (Bacon and others, 1992), and (*E*) Mount Hood (Koloeszar and others, 2012). Figure from Koleszar and others (2012).

The Mount Hood Class of Subduction Volcanoes?

A schematic representation of the key processes we have identified as important to petrogenesis and eruption style at Mount Hood is shown in figure 14. These processes are not unique to this volcano however, and in a global context Mount Hood appears to represent a particular class or endmember type of subduction-related stratovolcano (for example Kent, 2013)—a class defined by the following characteristics:

- Restriction of erupted magma compositions largely to intermediate magmas so that andesites and dacites dominate the eruptive output.

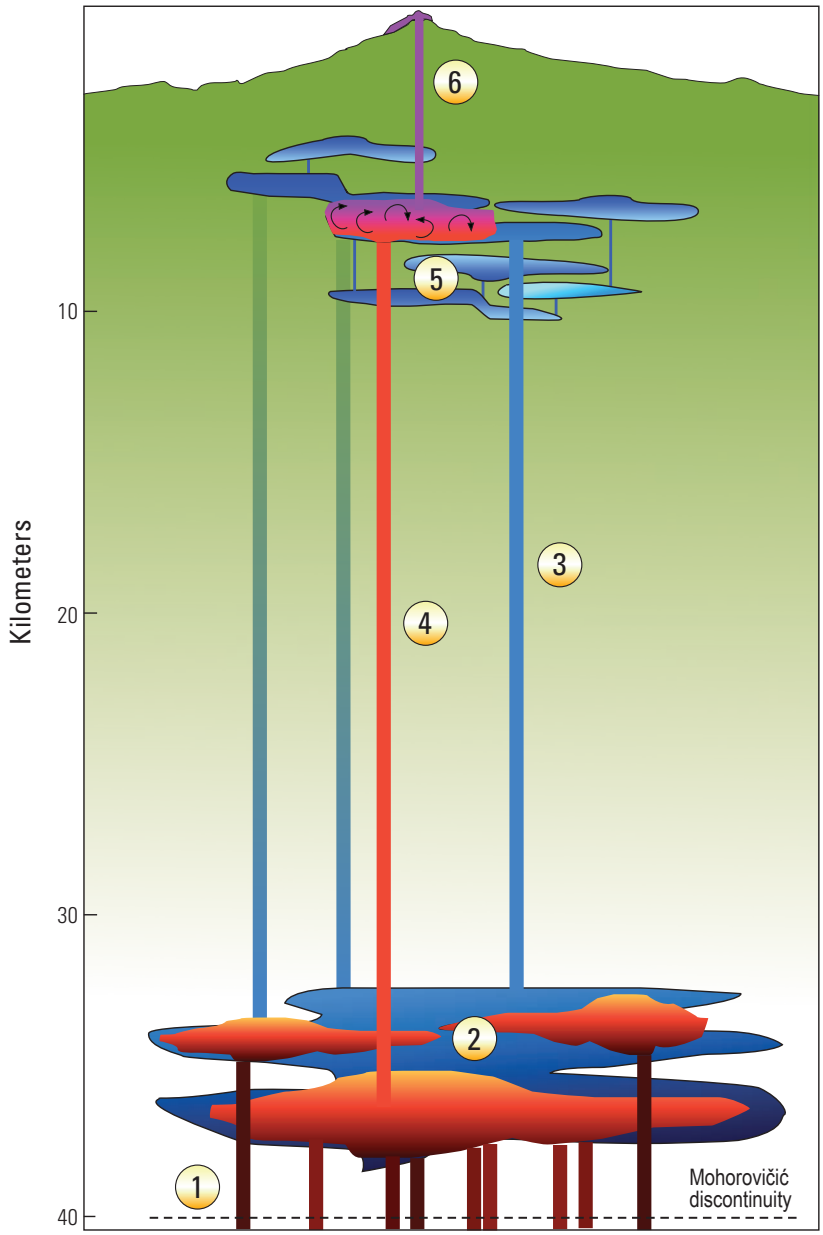

Figure 14. Schematic representation of the Mount Hood magma system. (1) Intrusion of mantle-derived basalts from the mantle wedge feed a MASH (mixing-assimilation-storage-hybridization) zone within the lower to middle crust (Hildreth and Moorbath, 1988). (2) Melting of amphibolite within the MASH zone under high fH_2O conditions—possibly together with hybridization or differentiation of basalts—produces the silicic parental magma composition (Borg and Clynne, 1998; Conrey and others, 2001; Annen and others, 2006). Note that we suggest that MASH processes occur in the lower to middle crust, although the specific depth shown here is not to scale. (3) Silicic parental melts periodically ascend to the shallow crust. This is shown here as dike-controlled transport but could occur conceivably by way of diapirs (for example, Rubin, 1995). The ascending silicic magma stalls at shallow crustal levels, possibly due to viscous stalling (Annen and others, 2006). Silicic magmas reside at shallow crustal levels as cold, crystal-rich mushes, or possibly even subsolidus for tens of thousands of years prior to remobilization. (4) Periodic and relatively rapid ascent of mafic magma. (5) Mafic magmas interact with shallowly stored silicic magmas, mixing occurs to produce intermediate andesites and dacites. (6) Recharge also initiates eruption of the intermediate hybrid magmas. Increased temperature from recharge lowers the viscosity of mixed magmas and delays the onset of fragmentation, promoting effusive eruptions.

- Considerable petrologic and other evidence that individual intermediate magmas are the product of magma mixing. Evidence includes the presence of abundant quenched inclusions, multiple mineral populations and (or) mineral disequilibrium, and bulk chemical trends consistent with magma mixing playing a dominant petrogenetic role.

- Abundant evidence for significant input from both mafic and silicic parental magmas to the erupted intermediate magma compositions. Recent application of detailed in-situ analysis techniques reveals crystals that derive from a mafic parental magma are more abundant than previously considered in many intermediate systems (for example, Browne and others, 2006; Martel and others, 2006; Salisbury and others, 2008; Humphreys and others, 2009b, 2012). Estimates of the composition of the mafic and silicic parent magma vary, but in many cases do not appear to overlap significantly with the range of erupted magma compositions (Kent, 2013).

- Suggestions from mineral zoning studies and other sources that mafic recharge is the dominant process for initiating eruptions, and mixing between the mafic and silicic parental magmas occurs late and immediately prior to eruption (for example, Nakamura, 1995; Venezky and Rutherford, 1999; Devine and others 2003).

- Eruptions dominated by effusive eruption styles, characteristically by formation of lava domes, but with the potential for dome collapse and Peléan style eruptions to produce major pyroclastic deposits.

Examples of volcanoes that appear to fall into this category include Mount Unzen, Soufriére Hills volcano, and Mont Pelée (Kent, 2013). Although details vary, these volcanoes all share many of the basic characteristics of Mount Hood as outlined above. Other potential examples include the Plat Pays complex in the Lesser Antilles; Volcán Aucanchilcha, Chile; and Mount Dutton, Alaska (Miller and others, 1999; Halama and others, 2006; Klemetti and Grunder, 2008; Walker and others, 2012).

For Mount Unzen and Soufriére Hills, recent eruptive activity also means that geophysical, gas, and other observations during eruption may provide additional insight into the process of eruption and the structure of the magma supply and storage system beneath the volcanoes, as well as what might be expected from future eruptions of Mount Hood. Seismic, deformation, gas, phase equilibria, petrologic, and other observations from Mount Unzen and Soufriére Hills suggest a magma plumbing system that is broadly similar to that we have outlined for Mount Hood (fig. 12) with long-term storage of a relatively silicic parental magma within the shallow crust, and initiation of eruptions by more mafic magma ascending from deeper crustal levels (for example, Nakada and others 1995; Aspinall and others, 1998; Barclay and others, 1998; Devine and others, 1998, 2003; Nishi and others, 1999; Scandone and others, 2007; Elsworth and others, 2008; Humphreys and others, 2009a,b, 2012; Christopher and others, 2010; Foroozan and others 2010; Edmonds and others, 2016).

Acknowledgments

The authors wish to thank coauthors on the Mount Hood studies, including Kari Cooper, Cristine Darr, Gary Eppich, Erik Klemetti, and Morgan Salisbury for contributions and discussions. Many thanks also to Willie Scott and Cynthia Gardner for their generous assistance, and to Paul Wallace and Craig White for insightful reviews. This research has been generously supported by National Science Foundation grants 0838421 and 1425491.

References

Acocella, V., 2014, Great challenges in volcanology—How does the volcano factory work?: Frontiers in Earth Science, v. 21, doi:10.3389/feart.2014.00004.

Anderson, A.T., 1976, Magma mixing—Petrological process and volcanological tool: Journal of Volcanology and Geothermal Research, v. 1, p. 3–33.

Annen, C., Blundy, J.D., and Sparks, R.S.J., 2006, The genesis of intermediate and silicic magmas in deep crustal hot zones: Journal of Petrology, v. 47, p. 505–539.

Aspinall, W.P., Miller, A.D., Lynch, L.L., Latchman, J.L., Stewart, R.C., White, R.A., and Power, J.A., 1998, Soufriere Hills eruption, Montserrat, 1995–1997—Volcanic earthquake locations and fault plane solutions: Geophysical Research Letters, v. 25, p. 3397–3400, doi:10.1029/98gl00858.

Bachman, O., and Bergantz, G., 2008, The magma reservoirs that feed supereruptions: Elements, v. 4, p. 17–21, doi: 10.2113/GSELEMENTS.4.1.17.

Bacon, C.R., 1986, Magmatic inclusions in silicic and intermediate volcanic-rocks: Journal of Geophysical Research-Solid Earth and Planets, v. 91, p. 6091–6112, doi:10.1029/Jb091ib06p06091.

Bacon, C.R., Newman, S., and Stolper, E.M., 1992, Water, CO_2, Cl, and F in melt inclusions in phenocrysts from three Holocene explosive eruptions, Crater Lake, Oregon: American Mineralogist, v. 77, p. 1021–1030.

Barclay, J., Rutherford, M.J., Carroll, M.R., Murphy, M.D., Devine, J.D., Gardner, J., and Sparks, R.S.J., 1998, Experimental phase equilibria constraints on pre-eruptive storage conditions of the Soufriere Hills magma: Geophysical Research Letters, v. 25, p. 3437–3440, doi:10.1029/98gl00856.

Blatter, D.L., Sisson, T.W., and Hankins, W.B., 2013, Crystallization of oxidized, moderately hydrous arc basalt at mid- to lower-crustal pressures—Implications for andesite genesis: Contributions to Mineralogy and Petrology, v. 166, p. 861–886, doi: 10.1007/S00410-013-0920-3.

Blundy, J., and Cashman, K., 2008, Petrologic reconstruction of magmatic system variables and processes, *in* Putirka, K.D., Tepley, F.J.I., eds., Minerals, inclusions, and volcanic processes: Reviews in Mineralogy and Geochemistry, Mineralogical Society of America, p. 179–239.

Blundy, J., Cashman, K.V., Rust, A., and Witham, F., 2010, A case for CO_2-rich arc magmas: Earth and Planetary Science Letters, v. 290, p. 289–301.

Boehnke, P., Watson, E.B., Trail, D., Harrison, T.M., and Schmitt, A.K., 2013, Zircon saturation re-revisited: Chemical Geology, v. 351, p. 324–334.

Borg, L.E., and Clynne, M.A., 1998, The petrogenesis of felsic calc-alkaline magmas from the southernmost Cascades, California—Origin by partial melting of basaltic lower crust: Journal of Petrology, v. 39, p. 1197–1222.

Browne, B.L., Eichelberger, J.C., Patino, L.C., Vogel, T.A., Uto, K., and Hoshizumi, H., 2006, Magma mingling as indicated by texture and Sr/Ba ratios of plagioclase phenocrysts from Unzen volcano, SW Japan: Journal of Volcanology and Geothermal Research, v. 154, p. 103–116.

Burgisser, A., and Bergantz, G.W., 2013, A rapid mechanism to remobilize and homogenize highly crystalline magma bodies: Nature, v. 471, p. 212–215.

Cashman, K., and Sparks, R.S.J., 2013, How volcanoes work—A 25 year perspective: Geological Society of America Bulletin, v. 125, p. 664–690, doi: 10.1130/B30720.1.

Chaussard, E., and Amelung, F., 2014, Regional controls on magma ascent and storage in volcanic arcs: Geochemistry Geophysics Geosystems, v. 15, p. 1407–1418, doi:10.1002/2013GC005216.

Christopher, T., Edmonds, M., Humphreys, M.C.S., and Herd, R.A., 2010, Volcanic gas emissions from Soufriere Hills Volcano, Montserrat 1995–2009, with implications for mafic magma supply and degassing: Geophysical Research Letters, v. 37, doi:10.1029/2009gl041325.

Conrey, R.M., Hooper, P.R., Larson, P.B., Chesley, J., and Ruiz, J., 2001, Trace element and isotopic evidence for two types of crustal melting beneath a High Cascade volcanic center, Mt. Jefferson, Oregon: Contributions to Mineralogy and Petrology, v. 141, p. 710–732, doi: 10.1007/s004100100259.

Cooper, K.M., and Kent, A.J.R., 2014, Rapid remobilization of magmatic crystals kept in cold storage: Nature, v. 506, p. 480–483, doi:10.1038/nature12991.

Costa, F., Chakraborty, S., and Dohmen, R., 2003, Diffusion coupling between trace and major elements and a model for calculation of magma residence times using plagioclase: Geochimica Cosmochimica Acta, v. 67, p. 2189–2200.

Couch, S., Sparks, R.S.J., and Carroll, M.R., 2003, Mineral disequilibrium in lavas explained by convective self-mixing in open magma chambers: Nature, v. 411, p. 1037–1039, doi:10.1038/35082540.

Cribb, J.W., and Barton, M., 1997, Significance of crustal and source region processes on the evolution of compositionally similar calc-alkaline lavas, Mt Hood, Oregon: Journal of Volcanology and Geothermal Research, v. 76, p. 229–249.

Darr, C.M., 2006, Magma chamber processes over the past 475,000 years at Mount Hood, Oregon—Insights from crystal zoning and crystal size distribution studies: Corvallis, Oregon State University, M.S. thesis, 154 p.

Devine, J.D., Murphy, M.D., Rutherford, M.J., Barclay, J., Sparks, R.S.J., Carroll, M.R., Young, S.R., and Gardner, J.E., 1998, Petrologic evidence for pre-eruptive pressure-temperature conditions, and recent reheating, of andesitic magma erupting at the Soufriere Hills Volcano, Montserrat, W.I.: Geophysical Research Letters, v. 25, p. 3669–3672, doi 10.1029/98gl01330.

Devine, J.D., Rutherford, M.J., Norton, G.E., and Young, S.R., 2003, Magma storage region processes inferred from geochemistry of Fe-Ti oxides in andesitic magma, Soufriere Hills Volcano, Montserrat, W.I.: Journal of Petrology, v. 44, p. 1375–1400.

Edmonds, M., Kohn, S.C., Hauri, E.H., Humphreys, M.C.S., and Cassidy, M., 2016, Extensive, water-rich magma reservoir beneath southern Montserrat: Lithos, v. 252–253, p. 216–233.

Eggler, D.H., and Burnham, C.W., 1973, Crystallization and fractionation trends in the system andesite-H_2O-CO_2-O_2 at pressures to 10 kb: Geological Society America Bulletin, v. 84, p. 2517–2532.

Eichelberger, J.C., 1978, Andesitic volcanism and crustal evolution: Nature, v. 275, p. 21–27.

Eichelberger, J.C., 1980, Vesiculation of mafic magma during replenishment of silicic magma reservoirs: Nature, v. 288, p. 446–450.

Eichelberger, J.C., Izbekov, P.E., and Browne, B.L., 2006, Bulk chemical trends at arc volcanoes are not liquid lines of descent: Lithos, v. 87, p. 135–154.

Elsworth, D., Mattioli, G., Taron, J., Voight, B., and Herd, R., 2008, Implications of magma transfer between multiple reservoirs on eruption cycling: Science, v. 322, p. 246–248, doi:10.1126/Science.1161297.

Eppich, G.R., 2010, ^{226}Ra-^{230}Th disequilibrium in plagioclase from recent eruptions at Mount Hood volcano, Oregon—Constraints on crystal residence and magma storage timescales: Davis, University of California, M.S. thesis, 149 p.

Eppich, G.R., Cooper, K.M., Kent, A.J.R., and Koleszar, A., 2012, Constraints on crystal storage timescales in mixed magmas—Uranium-series disequilibria in plagioclase from Holocene magmas at Mount Hood, Oregon: Earth and Planetary Science Letters, v. 317, p. 319–330, doi:10.1016/J.Epsl.2011.11.019.

Foroozan, R., Elsworth, D., Voight, B., and Mattioli, G.S., 2010, Dual reservoir structure at Soufriere Hills volcano inferred from continuous GPS observations and heterogeneous elastic modeling: Geophysical Research Letters, v. 37, doi:10.1029/2010gl042511.

Geochemistry of Rocks of the Oceans and Continents (GEOROC), 2016, Cascades: Max Planck Institute for Chemistry, accessed June, 2016, at http://georoc.mpch-mainz.gwdg.de/georoc/.

Ghiorso, M.S., and Evans, B.W., 2008, Thermodynamics of rhombohedral oxide solid solutions and a revision of the Fe–Ti two-oxide geothermometer and oxygen barometer: American Journal of Science, v. 308, p. 957–1039.

Giordano, D., Russell, J.K., and Dingwell, D.B., 2008, Viscosity of magmatic liquids—A Model: Earth and Planetary Science Letters, v. 271, p. 123–134.

Gourgaud, A., Fichaut, M., and Joron, J.-L., 1989, Magmatology of Mt Pelee (Martinique, F.W.I.) .I. Magma mixing and triggering of the 1902 and 1929 Pelean nuees-ardentes: Journal of Volcanology and Geothermal Research, v. 38, p. 143–169.

Halama, R., Boudon, G., Villemant, B., Joron, J.-L., Le Friant, A., and Komorowski, J.-C., 2006, Pre-eruptive crystallization conditions of mafic and silicic magmas at the Plat Pays volcanic complex, Dominica (Lesser Antilles): Journal of Volcanology and Geothermal Research, v. 153, p. 200–220.

Higgins, M.D., 2006, Quantitative textural measurements in igneous and metamorphic petrology: Cambridge, U.K., Cambridge University Press, 265 p.

Hildreth, W., 2007, Quaternary magmatism in the Cascades—Geologic perspectives: U.S. Geological Survey Professional Paper 1744, 125 p.

Hildreth, W., and Moorbath, S., 1988, Crustal contributions to arc magmatism in the Andes of central Chile: Contributions to Mineralogy and Petrology, v. 98, p. 455–489.

Holland, T.J.B., and Blundy, J.D., 1994, Non-ideal interactions in calcic amphiboles and their bearing on amphibole-plagioclase thermometry: Contributions to Mineralogy and Petrology, v. 116, p. 433–447.

Huber, C., Bachmann, O., and Dufek, J., 2011, Thermo-mechanical reactivation of locked crystal mushes—Melting-induced internal fracturing and assimilation processes in magmas: Earth and Planetary Science Letters, v. 304, p. 443–454, doi:10.1016/j.epsl.2011.02.022.

Humphreys, M.C.S., Christopher, T., and Hards, V., 2009b, Microlite transfer by disaggregation of mafic inclusions following magma mixing at Soufriere Hills volcano, Montserrat: Contributions to Mineralogy and Petrology, v. 157, p. 609–624, doi:10.1007/s00410-008-0356-3.

Humphreys, M.C.S., Edmonds, M., Christopher, T., and Hards, V., 2009a, Chlorine variations in the magma of Soufriere Hills Volcano, Montserrat—Insights from Cl in hornblende and melt inclusions: Geochimica et Cosmochimica Acta, v. 73, p. 5693–5708.

Humphreys, M.C.S., Edmonds, M., Plail, M., Barclay, J., Parkes, D., and Christopher, T., 2012, A new method to quantify the real supply of mafic components to a hybrid andesite: Contributions to Mineralogy and Petrology, v. 165, p. 191–215, doi:10.1007/s00410-012-0805-x.

Huppert, H.E., Sparks, R.S.J., and Turner, J.S., 1982, Effects of volatiles on mixing in calc-alkaline magma systems: Nature, v. 297, p. 554–557.

Jones, J., and Malone, S.D., 2005, Mount Hood earthquake activity—Volcanic or tectonic origins?: Bulletin of the Seismological Society of America, v. 95, p. 818–832.

Karlstrom, L., Dufek, J., and Manga, M., 2009, Organization of volcanic plumbing through magmatic lensing by magma chambers and volcanic loads: Journal of Geophysical Research-Solid Earth, v. 114, doi:0.1029/2009jb006339.

Kent, A.J.R., 2013, Preferential eruption of andesitic magmas—Implications for volcanic magma fluxes at convergent margins, *in* Gomez-Tuena, A., Straub, S.M., and Zellmer, G.F., eds., Orogenic andesites and crustal growth: Geological Society, London, Special Publications, v. 385, doi:10.1144/SP385.10.

Kent, A.J.R., Darr, C., Koleszar, A.M., Salisbury, M.J., and Cooper, K.M., 2010, Preferential eruption of andesitic magmas through recharge filtering: Nature Geoscience, v. 3, p. 631–636, doi:10.1038/Ngeo924.

King, P.L., Vennemann, T.W., Holloway, J.R., Hervig, R.L., Lowenstern, J.B., and Forneris, J.F., 2002, Analytical techniques for volatiles—A case study using intermediate (andesitic) glasses: American Mineralogist, v. 87, p. 1077–1089.

Klemetti, E.W., Clynne, M.A., Kent, A.J.R., Bertolett, E.M., and Hernandez, L.D., 2015, The influence of crystal mush on magmatism under arc volcanoes recorded in zircon from the Lassen volcanic center, California and Mount Hood, Oregon [abs.]: American Geophysical Union, Conference Abstract 2015.

Klemetti, E.W., and Grunder, A.L., 2008, Volcanic evolution of Volcan Aucanquilcha—A long-lived dacite volcano in the Central Andes of northern Chile: Bulletin of Volcanology, v. 70, p. 633–650, doi:10.1007/S00445-007-0158-X.

Koleszar, A., 2011, Controls on eruption style and magma compositions at Mount Hood, Oregon: Corvallis, Oregon State University, Ph. D. dissertation, 181 p.

Koleszar, A.M., Kent, A.J.R., Wallace, P.J., and Scott, W.E., 2012, Controls on long-term low explosivity at andesitic arc volcanoes—Insights from Mount Hood, Oregon, Journal of Volcanology and Geothermal Research, v. 219, p. 1–14, Doi:0.1016/J.Jvolgeores.2012.01.003.

Larsen, J.F., 2016, Unraveling the diversity in arc volcanic eruption styles—Examples from the Aleutian volcanic arc, Alaska: Journal of Volcanology and Geothermal Research, v. 327, p. 643–668, http://dx.doi.org/10.1016/j.jvolgeores.2016.09.008

Lundgaard, K.L., and Tegner, C., 2004, Partitioning of ferric and ferrous iron between plagioclase and silicate melt: Contributions to Mineralogy and Petrology, v. 147, p. 470–483.

Mandeville, C.W., Webster, J.D., Tappen, C., Taylor, B.E., and Timbal, A., 2009, Stable isotope and petrologic evidence for open-system degassing during the climactic and preclimactic eruptions of Mt. Mazama, Crater Lake, Oregon: Geochimica et Cosmochimica Acta, v. 73, p. 2978–3012.

Marsh, B.D., 1981, On the crystallinity, probability of occurrence, and rheology of lava and magma: Contributions to Mineralogy and Petrology, v. 78, p. 85–98.

Marsh, B.D., 1998, On the interpretation of crystal size distributions in magmatic systems: Journal of Petrology, v. 39, p. 553–599, doi: 10.1093/petroj/39.4.553.

Martel, C., Ali, A.R., Poussineau, S., Gourgaud, A., and Pichavant, M., 2006, Basalt-inherited microlites in silicic magmas—Evidence from Mount Pelee (Martinique, French West Indies: Geology, 34, p. 905–908.

Mastin, L., and Ghiorso, M.S., 2002, Insights into volcanic conduit flow from an open-source numerical model: Geochemistry Geophysics Geosystems, v. 3, doi:10.1029/2001GC000192.

Miller, T.P., Chertkoff, D.G., Eichelberger, J.C., and Coombs, M.L., 1999, Mount Dutton volcano, Alaska—Aleutian arc analog to Unzen volcano, Japan: Journal of Volcanology and Geothermal Research, v. 89, p. 275–301.

Murphy, M.D., Sparks, R.S.J., Barclay, J., Carroll, M.R., and Brewer, T.S., 2000, Remobilization of andesite magma by intrusion of mafic magma at the Soufriere Hills Volcano, Montserrat, West Indies: Journal of Petrology, v. 41, p. 21–42.

Murphy, M.D., Sparks, R.S.J., Barclay, J., Carroll, M.R., Lejeune, A.M., Brewer, T.S., Macdonald, R., Black, S., and Young, S., 1998, The role of magma mixing in triggering the current eruption at the Soufriere Hills volcano, Montserrat, West Indies: Geophysical Research Letters, v. 25, p. 3433–3436.

Nakada, S., Motomura, Y., and Shimizu, H., 1995, Manner of magma ascent at Unzen Volcano (Japan): Geophysical Research Letters, v. 22, p. 567–570.

Nakamura, M., 1995, Continuous mixing of crystal mush and replenished magma in the ongoing Unzen eruption: Geology, v. 23, p. 807–810.

Newman, S., and Lowenstern, J.B., 2002, VolatileCalc—A silicate melt-H_2O-CO_2 solution model written in Visual Basic for Excel: Computers and Geosciences, v. 28, p. 597–604.

Nishi, K., Ono, H., and Mori, H., 1999, Global positioning system measurements of ground deformation caused by magma intrusion and lava discharge—The 1990–1995 eruption at Unzendake volcano, Kyushu, Japan: Journal of Volcanology and Geothermal Research, 89, p. 23–54.

Pallister, J.S., Hoblitt, R.P., and Reyes, A.G., 1992, A basalt trigger for the 1991 eruptions of Pinatubo Volcano: Nature, v. 356, p. 426–428.

Reiners, P.W., Hammond, P.E., McKenna, J.M., and Duncan, R.A., 2000, Young basalts of the central Washington Cascades, flux melting of the mantle, and trace element signatures of primary arc magmas: Contributions to Mineralogy and Petrology, v. 138, p. 249–264.

Ridolfi, F., Renzulli, A., and Puerini, M., 2010, Stability and chemical equilibrium of amphibole in calc-alkaline magmas—An overview, new thermobarometric formulations and application to subduction-related volcanoes: Contributions to Mineralogy and Petrology, v. 160, p. 45–66, doi:10.1007/S00410-009-0465-7.

Roggensack, K., Hervig, R.L., McKnight, S.B., and Williams, S.N., 1997, Explosive basaltic volcanism from Cerro Negro Volcano—Influence of volatiles on eruptive style: Science, v. 277, p. 1639–1642.

Rollinson, H., 1993, Using geochemical data—Evaluation, presentation, interpretation: New York, Routledge, 352 p.

Roman, D.C., Cashman, K.V., Gardner, C.A., Wallace, P.J., and Donovan, J.J., 2006, Storage and interaction of compositionally heterogeneous magmas from the 1986 eruption of Augustine Volcano, Alaska: Bulletin of Volcanology, v. 68, p. 240–254.

Rubin, A.M., 1995, Getting granite dikes out of the source region: Journal of Geophysical Research-Solid Earth, v. 100, p. 5911–5929.

Ruprecht, P., and Bachmann, O., 2010, Pre-eruptive reheating during magma mixing at Quizapu volcano and the implications for the explosiveness of silicic arc volcanoes: Geology, v. 38, p. 919–922, doi:10.1130/G31110.1.

Ruprecht, P., Bergantz, G.W., and Dufek, J., 2008, Modeling of gas-driven magmatic overturn—Tracking of phenocryst dispersal and gathering during magma mixing: Geochemistry Geophysics Geosystems, v. 9, doi:10.1029/2008GC002022.

Ruprecht, P., and Wörner, G., 2007, Variable regimes in magma systems documented in palgioclase zoning patterns—El Misti stratovolcano and Andahua monogenetic cones: Journal of Volcanology and Geothermal Research, v. 165, p. 142–162, doi:10.1016/J.Jvolgeores.2007.06.002.

Salisbury, M.J., Bohrson, W.A., Clynne, M.A., Ramos, F.C., and Hoskin, P., 2008, Origin of the 1915 Lassen Peak eruption by magma mixing—Evidence for formation of chemically distinct plagioclase populations from crystal size distributions and in situ chemical data: Journal of Petrology, v. 49, p. 1755–1780.

Scandone, R., Cashman, K.V., and Malone, S.D., 2007, Magma supply, magma ascent and the style of volcanic eruptions: Earth and Planetary Science Letters, v. 253, p. 513–529.

Scott, W.E., Gardner, C.A., Pierson, T.C., Schilling, S.P., Costa, J.E., Vallance, J.W., and Major, J.J., 1997, Geologic history of Mount Hood Volcano, Oregon—A Field-Trip Guidebook: U.S. Geological Survey Open-File Report 97-263, 38 p.

Sparks, R.S.J., 1978, The dynamics of bubble formation and growth in magmas—A review and analysis: Journal of Volcanology and Geothermal Research, v. 3, p. 1–37.

Sparks, R.S.J., and Marshall, L.A., 1986, Thermal and mechanical constraints on mixing between mafic and silicic magmas: Journal of Volcanology and Geothermal Research, v. 29, p. 99–124.

Sparks, S.R.J., Sigurdsson, H., and Wilson, L., 1977, Magma mixing-mechanism for triggering acid explosive eruptions: Nature, v. 267, p. 315–318.

Symonds, R.B., Poreda, R.J., Evans, W.C., Janik, C.J., and Ritchie, B.E., 2003, Mantle and crustal sources of carbon, nitrogen, and noble gases in Cascade-Range and Aleutian-Arc volcanic gases: U.S. Geological Survey Open-File Report 03–436, 26 p. [Also available at http://pubs.usgs.gov/of/2003/0436/.]

Tepley, F.J., III, Davidson, J.P., and Clynne, M.A., 1999, Magmatic interactions as recorded in plagioclase phenocrysts of Chaos Crags, Lassen volcanic center, California: Journal of Petrology, v. 40, p. 787–806, doi: 10.1093/petroj/40.5.787.

Venezky, D.Y., and Rutherford, M.J., 1999, Petrology and Fe-Ti oxide reequilibration of the 1991 Mount Unzen mixed magma: Journal of Volcanology and Geothermal Research, v. 89, p. 213–230.

Walker, B.A., Jr., Klemetti, E.W., Grunder, A.L., Dilles, J.H., Tepley, F.J., and Giles, D., 2012, Crystal reaming during the assembly, maturation, and waning of an eleven-million-year crustal magma cycle—Thermobarometry of the Aucanquilcha Volcanic Cluster: Contributions to Mineralogy and Petrology, v. 165, p 663–682, doi: 10.1007/s00410-012-0829-2.

Wallace, P.J., 2005, Volatiles in subduction zone magmas—Concentrations and fluxes based on melt inclusion and volcanic gas data: Journal of Volcanology and Geothermal Research, v. 140, p. 217–240, doi:10.1016/J.Jvolgeores.2004.07.023.

Watson, E.B., and Harrison, T.M., 1983, Zircon saturation revisited—Temperature and composition effects in a variety of crustal magma types: Earth and Planetary Science Letters, v. 64, p. 295–304.

Wells, R.E., and McCaffrey, R., 2013, Steady rotation of the Cascade arc: Geology, v. 41, p. 1027–1030, doi: 10.1130/G34514.1.

White, C., 1980, Geology and geochemistry of Mt. Hood Volcano: Oregon Department of Geology and Mineral Industries Special Paper 8, 26 p.

Wise, W.S., 1969, Geology and petrology of the Mt. Hood area—A study of High Cascade volcanism: Geological Society of America Bulletin, v. 80, p. 969–1,006.

Woods, M.M., 2004, Compositional and mineralogical relationships between mafic inclusions and host lavas as key to andesite petrogenesis at Mount Hood volcano, Oregon: Portland, Portland State University, M.S. thesis, 181 p.

The Mount Hood Fault Zone—Late Quaternary and Holocene Fault Features Newly Mapped with High-resolution Lidar Imagery

By Ian P. Madin, Ashley R. Streig, William J. Burns, and Lina Ma

The Mount Hood Fault Zone—Late Quaternary and Holocene Fault Features Newly Mapped with High-resolution Lidar Imagery

By Ian P. Madin[1], Ashley R. Streig[2], William J. Burns[1], and Lina Ma[1]

Introduction

Although most of the focus of earthquake resilience efforts in Oregon is on the Cascadia Subduction Zone and its potential for M9 earthquakes, local earthquakes on crustal faults remain a potential, but poorly understood, threat to the region. Few active crustal faults have been identified in western Oregon, in part because of the thick forest that covers most of the state west of the crest of the Cascade Range. In recent years, the Oregon Department of Geology and Mineral Industries (DOGAMI) has collected high-resolution (8 points per square meter [m^2]) light detection and ranging (lidar) data over much of western Oregon. The very closely spaced sampling of the data allows enough laser pulses to penetrate the vegetation and reach the ground that nominal 1-m (3 feet) resolution bare-earth digital elevation models (DEMs) can be produced. By analyzing this data with 2D and 3D visualizations, we have identified a series of late Quaternary-Holocene fault scarps and related features that define a large, previously unknown active fault zone at Mount Hood, a stratovolcano in the Oregon High Cascades last active in the Holocene (fig. 1). The fault features are located in an environment of steep terrain, which is actively being shaped by volcanic eruptions, glaciation, landslides, and debris flows. Below the timberline on Mount Hood the area is covered with dense conifer forest in which wind throw commonly perturbs the ground surface to a depth of 1–2 m. The preservation of so many surface rupture features suggests that the features are either very young and have not yet been obscured by the geomorphic activity, or the faults have high slip rates so that features are frequently refreshed.

We have completed limited reconnaissance of the fault features identified in the lidar imagery and excavated two reconnaissance trenches across one of the scarps. This paper describes the limited data available for two of these faults, and suggests options for further research. These faults are still poorly mapped and we know little about their slip rates, earthquake history, and recurrence intervals. Because the system is so extensive, it could conceivably generate large earthquakes, and may pose a significant threat to the surrounding communities and critical infrastructure. It is therefore important to investigate these faults in detail in future studies.

[1]Oregon Department of Geology & Mineral Industries

[2]Portland State University

Mount Hood Fault Zone

The Mount Hood Fault Zone consists of four north-trending normal fault segments and extends ~55 kilometers (km) north from Clear Lake to the Columbia River (figs. 1, 2). South of Mount Hood, the zone roughly defines a 6-km-wide graben bounded on the west by the east-dipping Multorpor Mountain Fault, and on the east by the west-dipping Twin Lakes Fault. North of Mount Hood, the west-dipping Blue Ridge Fault and east-dipping Gate Creek Fault form a north-northwest trending en-echelon zone. None of these faults can be mapped across the volcanic edifice of Mount Hood, which is not surprising given its recent history of eruptions, glaciation, erosion, and debris flows. This paper will describe our current understanding of the Blue Ridge and Twin Lakes Faults.

Blue Ridge Fault Zone

The Blue Ridge Fault Zone is a 12-km-long, 4.5-km-wide area defined by about a dozen scarp segments ranging in length from a few hundred meters to nearly 5 km (figs. 1, 2). All but one segment have west-side-down displacement, and based on their topographic expression are probably west-dipping normal faults. A few short segments were previously mapped, but not recognized as active (Sherrod and Scott, 1995). Several faults in this zone extend up the steep north flank of Mount Hood, reaching elevations of 1,600 m and coming within 5 km of the summit.

The longest segment in the zone is the Blue Ridge Fault, which is defined by a continuous scarp that can be traced approximately 5 km across the top of Blue Ridge, becoming indistinct at either end where it descends into glaciated valleys (figs. 1–3). The scarp cuts and offsets a well-defined lateral moraine (fig. 3) which we correlate with the latest Pleistocene (~20 ka) Evans Creek unit of Sherrod and Scott (1995), indicating relatively recent movement. Numerous scarp profiles extracted from the lidar data show single-event scarps, ranging in height from 1.2 to 2.1 m with surface offset ranging from

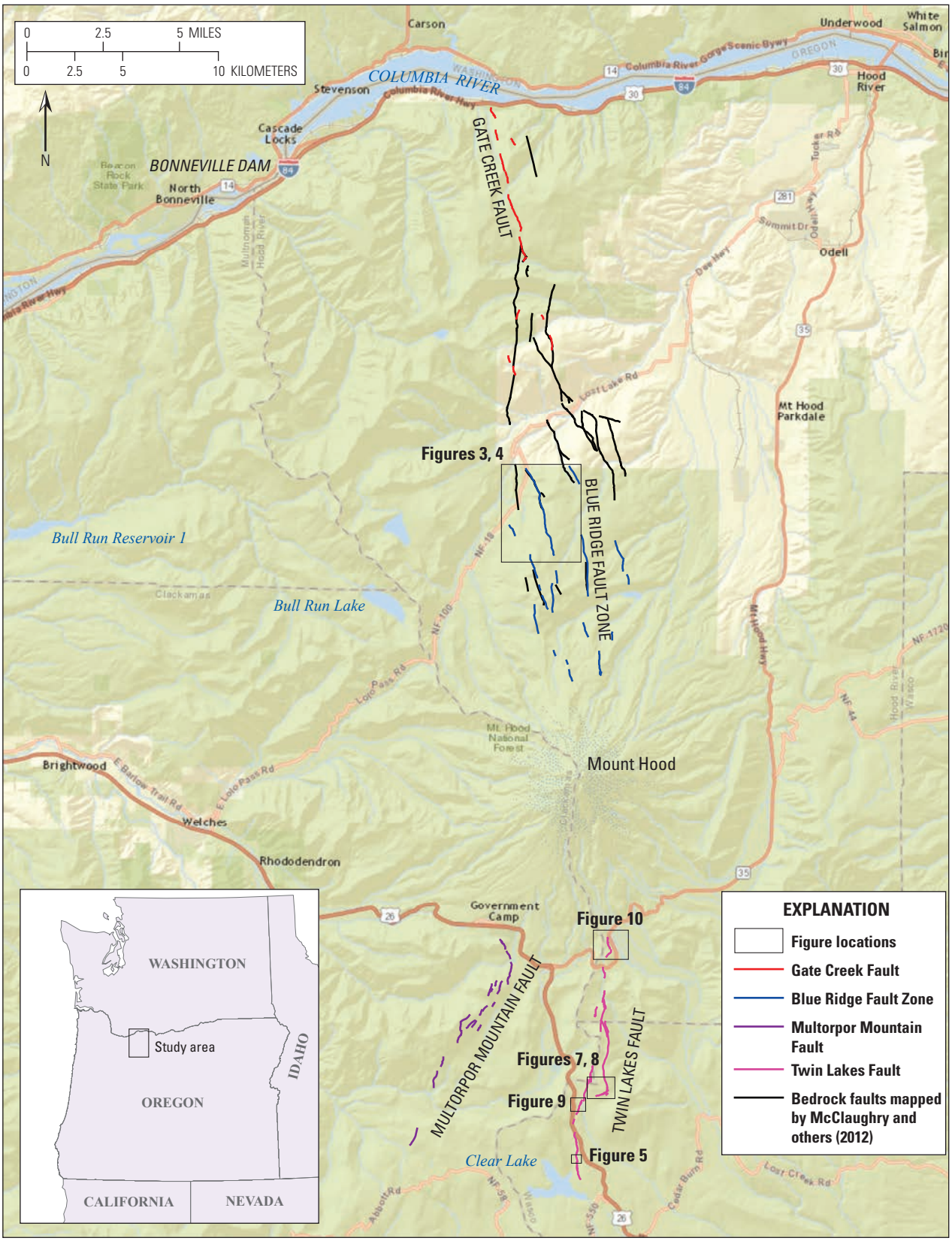

Sources: Esri, HERE, DeLorme, USGS, Intermap, INCREMENT P, NRCan, Esri Japan, METI, Esri China (Hong Kong), Esri Korea, Esri (Thailand), MapmyIndia, NGCC, © OpenStreetMap contributors, and the GIS User Community

Figure 1. Location map of the Mount Hood Fault Zone. Lidar-mapped fault features shown in color, black rectangles show locations of other figures in this paper, and heavy black lines are bedrock faults from recent geologic mapping by McClaughry and others (2012).

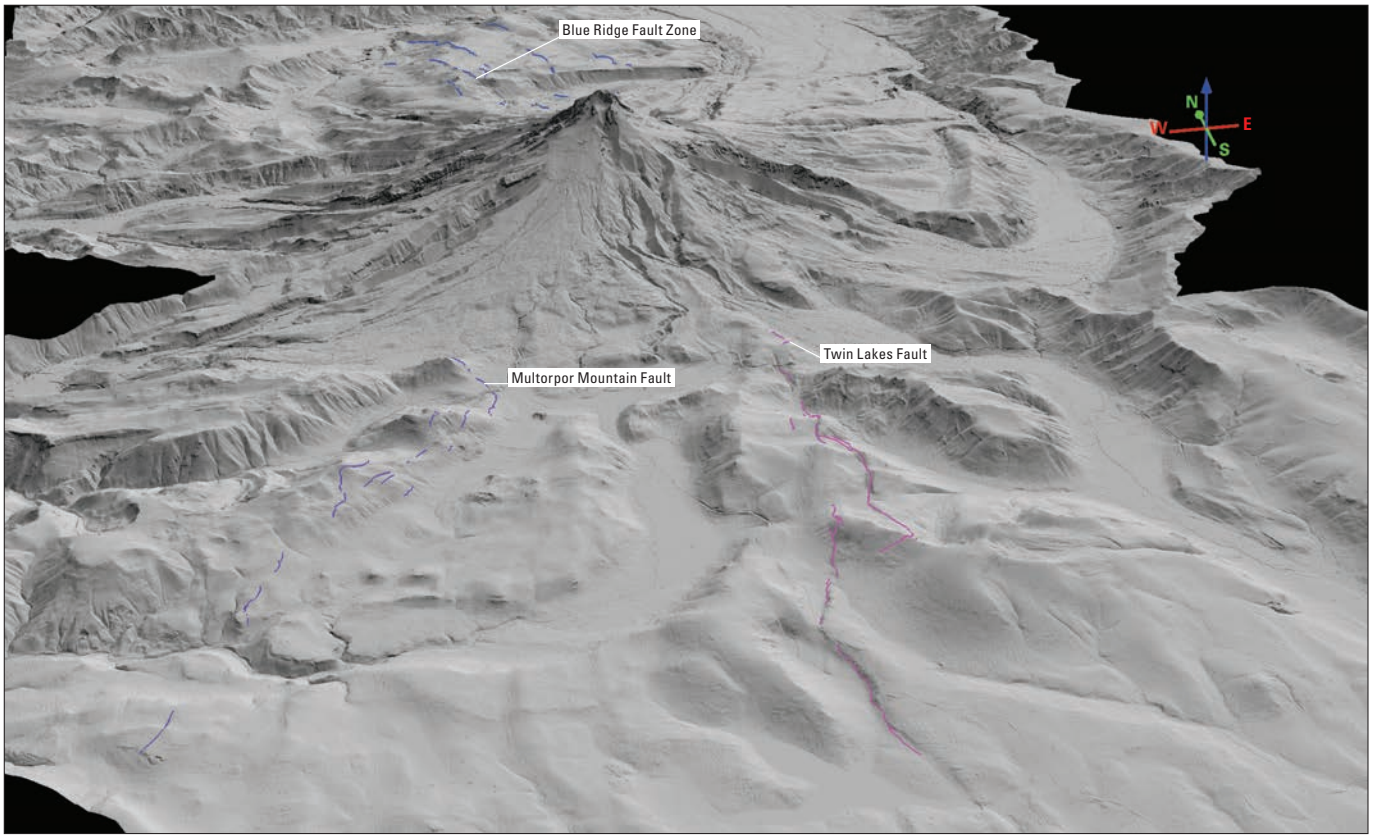

Figure 2. Perspective view of Mount Hood from the south-southwest,, based on nominal 1 meter lidar data. Magenta, Twin Lakes Fault; purple, Multorpor Mountain Fault; blue, Blue Ridge Fault. Scale varies in this perspective view, the Twin Lakes Fault is 12.75 km long.

1.2 to 1.8 m (fig. 3). In 2011, DOGAMI partnered with the Portland Water Bureau (excavation equipment and staff) and U.S. Geological Survey (USGS, trench logging staff and ^{14}C dates) to excavate two exploratory trenches across the Blue Ridge scarp (Madin and Ma, 2012). Both trenches exposed well consolidated till, which was offset by a west-dipping normal fault. A simplified log of trench BR-1 is shown in figure 4; the till (unit A) is offset vertically by 1.8 m and has a fissure 6-m wide at the foot of the scarp. The bottom of the fissure is filled with scarp collapse rubble (unit B) consisting of blocks of till (unit AB) and loose cobbles and boulders of platy lava (fig. 4). A depression in the top surface of the collapse rubble unit is filled with muddy pebble colluvium (unit C). These units, and the till on either side of the fissure are overlain by three additional colluvium layers (units D–F) and the entire sequence is overlain by an organic-rich A horizon (unit G). Detrital charcoal was recovered from all four of the colluvial units, and accelerator mass spectroscopy (AMS) ^{14}C ages were determined for six samples (table 1). The preliminary investigation of trench BR-1 shows evidence for a single earthquake event, which occurred between ~13,540 and 9,835 years before present (B.P.). We interpret the scarp collapse unit (unit B, fig. 4) to be material that slid into the fissure during and for some time immediately after the earthquake, and the muddy pebble colluvium to be material that washed into the fissure during the first significant rainy period after the earthquake (unit C, fig. 4). In this interpretation, the muddy colluvium was deposited within years of the earthquake, and its age approximates the age of the event. The three AMS ^{14}C samples (table 1) from this unit have 2σ calibrated ages of 13,600–13,380 years B.P., 13,640–13,400 years B.P., and 13,710–13,430 years B.P., providing a lower bound age for the event of ~13,540 years B.P. Units D–G are successively younger, unfaulted colluvial units that drape both the faulted till and the fissure-filling units. The oldest of these (unit D) yielded a single detrital charcoal AMS ^{14}C sample (table 1), which has a 2σ calibrated age range of 10,160 to 9,980 years B.P. and 9,970 to 9,700 years B.P., which provides an upper bounding age for the earthquake of ~9,835 years B.P.

Trench BR-2 exposed similar till, vertically offset by 1.5–2 m, but without the fissure. No dateable material was recovered from the colluvium layers that postdated the event. However, together these results suggest that the Blue Ridge Fault is nominally Holocene in age.

Twin Lakes Fault

The Twin Lakes Fault extends north for more than 12 km from Clear Lake to Oregon Route 35, and forms the southeast margin of the Mount Hood Fault Zone. The Twin Lakes Fault consists of two en-echelon west-dipping normal fault

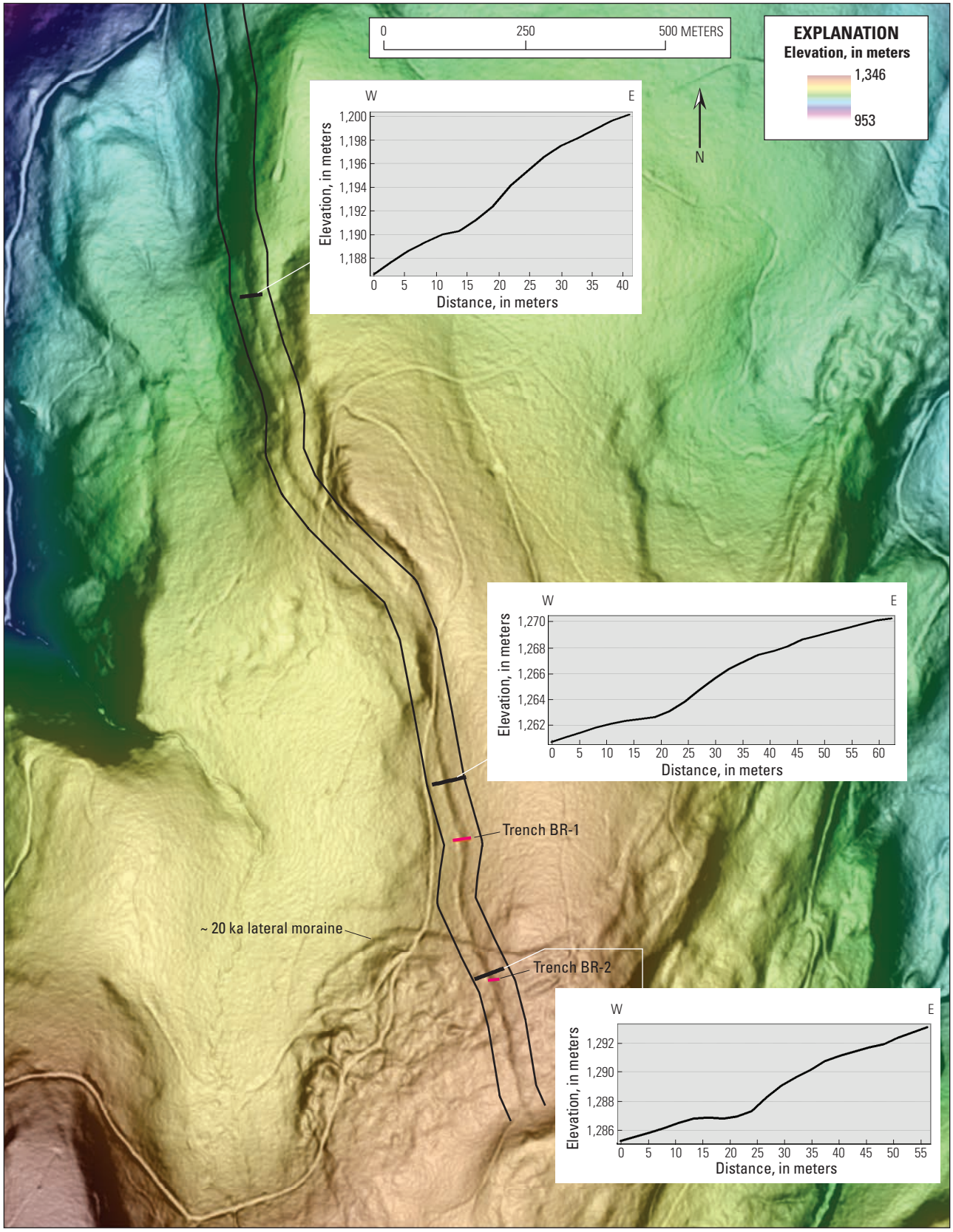

Figure 3. Map of the Blue Ridge Fault. Base map is 1-meter resolution lidar imagery combined with elevation color gradient over slopeshade. Double lines bracket the fault trace, which is expressed as a north-northwest trending, west-facing scarp. The fault offsets an ~20 ka glacial moraine that appears as a sinuous north-facing break in slope. Inset profiles are fault-normal, profile locations are shown by black lines. Red lines, location of 2011 trenches.

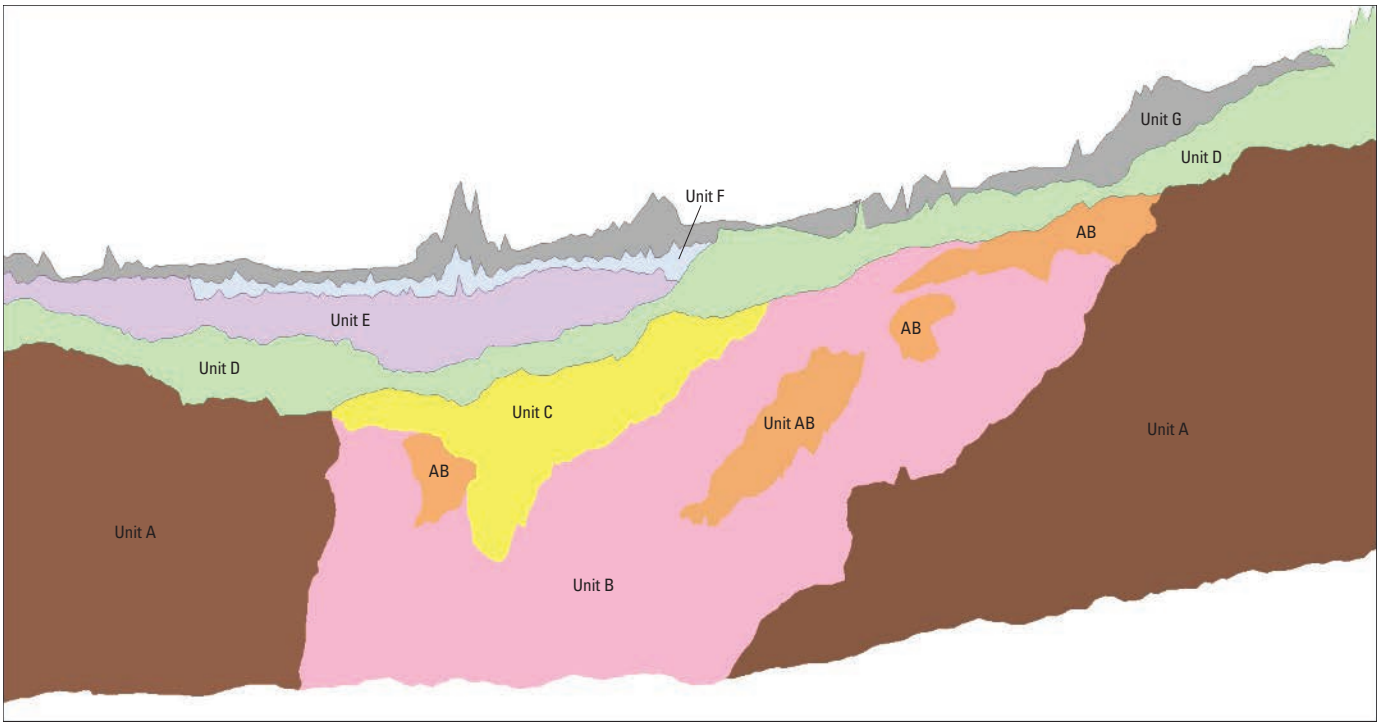

Figure 4. Simplified diagram of the log. Trench walls were sloped at approximately 1:1, and features were mapped in 3D on a 2-centimeter resolution digital elevation model (DEM) developed from a terrestrial lidar scan. This figure is a projection of the trench wall onto a vertical plane oriented east-west. The spiky appearance of units at top is due to inclusion of roots in the DEM. Scale varies due to the projection of a sloping surface, overall the area shown is ~10 meters wide and 2.5 meters high. Unit A is till older than 20 ka, and unit B is scarp-collapse rubble that fills a fissure formed along the fault. Unit AB is composed of blocks of till within the collapse rubble. Unit C is a muddy pebble colluvium that fills a depression in the middle of the fissure. Units D-F are colluvial layers that drape the entire scarp face, and unit G is the modern forest soil A horizon.

Table 1. Accelerator mass spectroscopy radiocarbon age data for samples from trench BR-1 (figs. 3, 4).

[All ages in years before present. Analyses by Beta Analytic]

Sample	Unit	Conventional radiocarbon age	2σ calibrated age
BR1_10/3-8	F	1,330 ± 30	1,300–1,240
			1,200–1,180
BR1_10/3-9	E	2,050 ± 30	2,040–2,020
			2,010–1,920
			1,920–1,900
BR1_10/3-2	D	8,830 ± 40	10,160–9,980
			9,970–9,700
BR1_MC-4	C	11,640 ± 50	13,600–13,380
BR1_MC-8	C	11,670 ± 50	13,640–13,400
BR1_MC-9	C	11,720 ± 50	13,710–13,430

segments, connected by a nearly continuous stepover. The fault impounds Frog Lake and the Twin Lakes along their eastern margins, and extends nearly to the dam at the east end of Clear Lake. The Twin Lakes appear to occupy a 50-m-deep half-graben formed by long-term movement on the fault and perhaps enhanced by glaciation. The fault parallels Oregon Route 35, and many features are easily accessible from the highway.

The southern segment of the fault is a single, fairly continuous scarp, which is well preserved near Clear Lake where the scarp cuts a debris fan originating from a small drainage (fig. 5). Little new fan material has been deposited across the scarp, suggesting that it formed in a fairly recent earthquake. Figure 6 shows the stepover area between the northern and southern segments of the fault where the northern segment forms a bench on an east-facing slope, the western segment forms scarps on west-facing slopes, and the stepover forms a north-facing scarp crossing the ridge east of Frog Lake. A detailed view of the stepover fault crossing the ridge, where it forms a sharp 1.5-m-high scarp in bedrock is shown in figure 7. Exposed bedrock on the scarp at this location is a good candidate for ^{3}He cosmogenic dating.

The northern segment of the Twin Lakes Fault impounds Frog Lake, and the basin around the lake is surrounded by a large fringing meadow that grades into forest (fig. 8). Exploratory hand-auger holes showed that there are at least 2 m of basin-filling sand and pebble gravel under the meadow and the edge of the forest. This is a good target for additional trenches or cores to look for dateable material and stratigraphic and sedimentological evidence of abrupt lake-level changes associated with fault movement raising the outlet level. Currently, the lake has no outlet, but there is a well-developed abandoned channel on the upthrown side of the fault (fig. 8). The abandoned channel floor is approximately 1 m above the current lake level.

At the northern end of the Twin Lakes Fault (figs. 1, 2) lidar data show a clear scarp extending west-northwest for 500 m along the southwest edge of the glaciated canyon of the White River (figs. 1–2, 9). Field observations confirm the presence of a sharp, well-preserved feature about 2-m high that extends along the break in slope at the top of the canyon wall. The scarp is formed in boulder colluvium or till, and forested with mature trees, which suggest that it has been several hundred years since the most recent movement. A small stream on

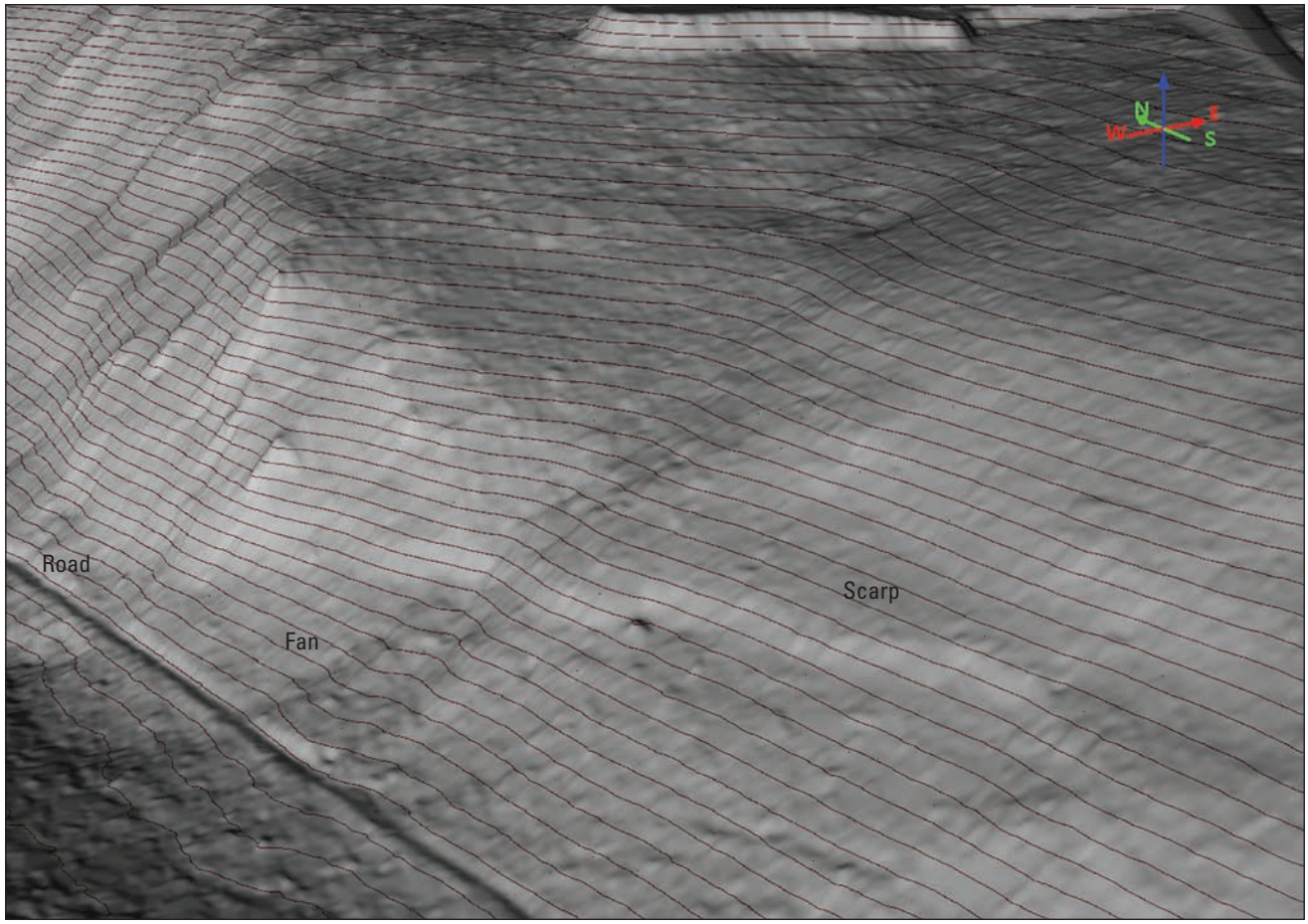

Figure 5. A 3D perspective view of a small, offset fan along the Twin Lakes Fault near Clear Lake. The fan has been beheaded by the scarp and no fan material appears to have been deposited across the scarp since it formed. Contours are at 2 meter intervals, roadway is ~4 meters wide.

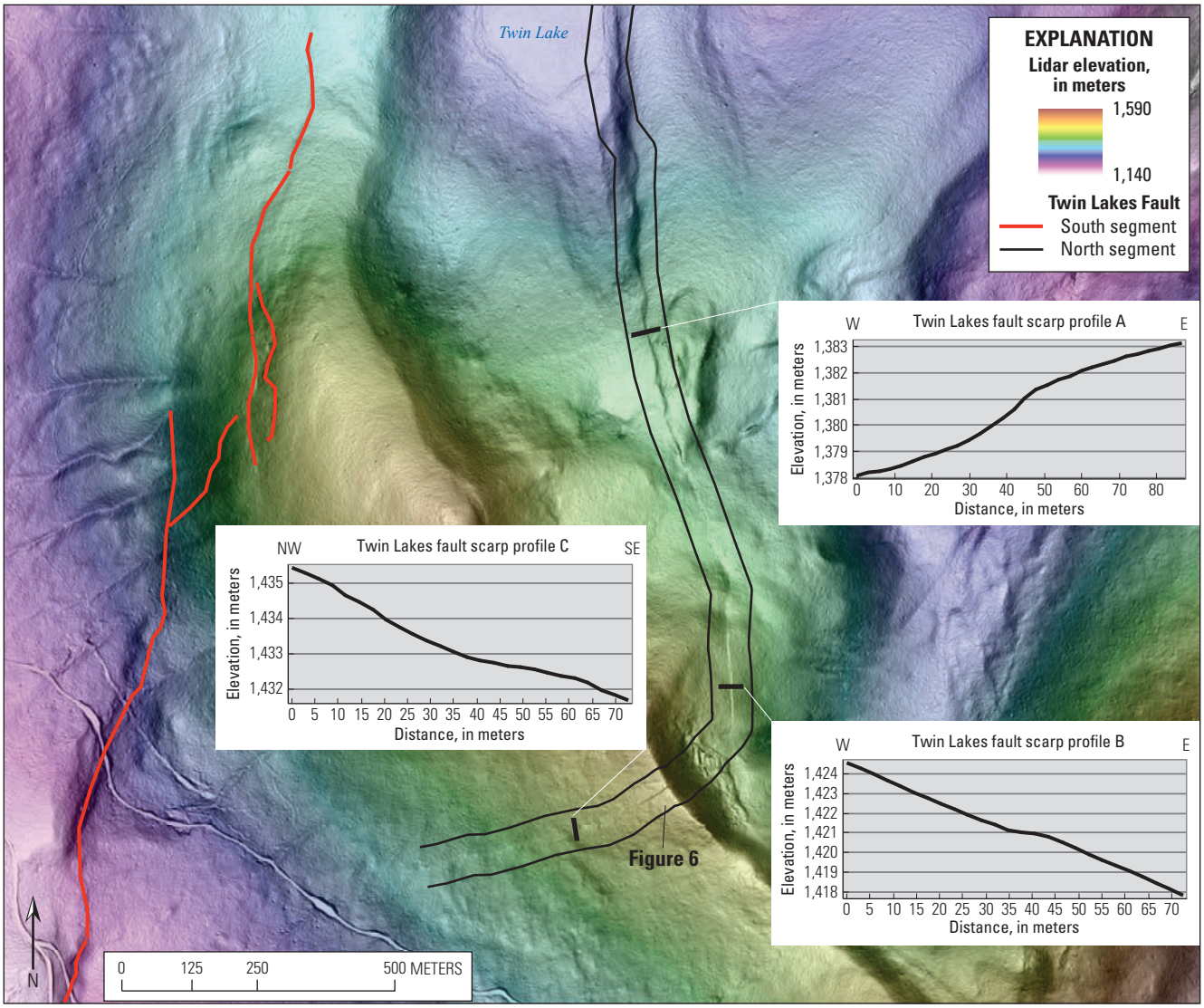

Figure 6. Map of fault features along the stepover zone on the Twin Lakes Fault. The base map is 1-meter lidar slopeshade with an elevation color gradient. Scarp profile locations on are shown by black bars. Profile A shows a west-facing scarp on a west-facing slope. Profile B shows a bench formed by west-side-down motion on an east-facing slope. Profile C shows an uphill-facing scarp where the fault bends to the west at the southern end of the north segment of the fault.

the downthrown side is partly blocked by the scarp, forming a wetland covering a few hundred square meters. Exploratory gouge cores recovered bedded sandy gravel with peat layers, and further coring may provide dateable stratigraphic evidence of fault movement. To the north, the fault descends into the White River canyon where it is buried by the highly active outwash plain of the White River Glacier.

Conclusions

Based on the examination of high-resolution lidar imagery and limited field reconnaissance and trenching, we have defined a major late Quaternary-Holocene age fault zone centered on Mount Hood. The discovery of this active fault system is important for understanding the potential seismic threat for nearby communities. Reconnaissance trenching across the Blue Ridge Fault (figs. 3, 4) identified a single earthquake with approximately 1.8 m of normal slip that occurred between ~13,540 and 9,835 years B.P. (fig. 4, table 1). Holocene-age displacement of 1.8 m suggests that the Mount Hood Fault Zone could produce relatively large crustal earthquakes frequently enough to pose a significant hazard. Although the mode of fault rupture is unknown due to the lack of paleoseismic constraints on past surface-rupturing earthquakes, we can estimate potential earthquake magnitude using empirical scaling laws derived from regressions of observed displacement, rupture length, and moment magnitude for normal fault ruptures from Wells and Coppersmith (1994). Using the measured normal displacement of 1.8 m as both the

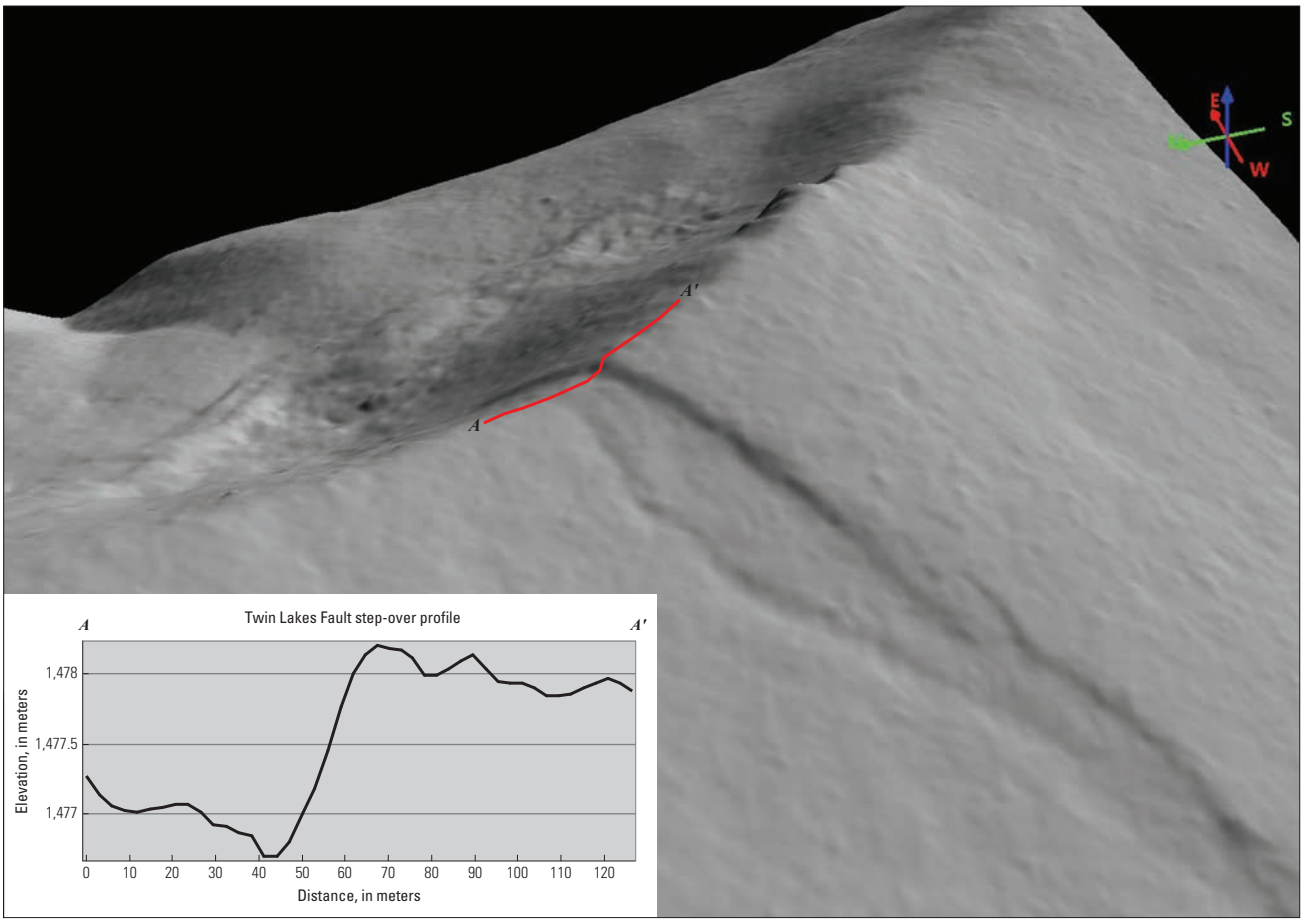

Figure 7. Perspective view of the Twin Lakes Fault stepover on the ridge east of Frog Lake, based on 1-meter lidar topography. Red line corresponds to the inset topographic profile. Scale varies in perspective view.

maximum and average displacement values, we estimate an approximately M6.8 to 6.9 earthquake caused the displacement/created the fault scarp. To evaluate the seismic hazard based on rupture length alone, we consider two end member rupture lengths; a full rupture of the 55-km length fault zone in a single earthquake, and a smaller rupture of 25-km length—just a part of the fault zone. Rupture of the full ~55-km-length of fault traces would result in an earthquake of approximately M7.9 earthquake, and rupture of a 25-km-long segment of the fault zone would result in an earthquake of approximately M7.7 (Wells and Coppersmith, 1994).

Earthquake magnitude estimates for this fault zone are, not surprisingly, poorly constrained, but estimates of earthquake capability, based on observations of average displacement and surface rupture, suggest that this fault zone could produce an earthquake greater than M6.5.

Although distant from major population centers, the fault zone poses a serious seismic threat to the cities of Hood River, Odell, Parkdale, White Salmon, Stevenson, Cascade Locks, Government Camp, and the Villages at Mount Hood. In addition it may pose a threat to critical regional infrastructure including the City of Portland's Bull Run drinking water system, storage reservoirs operated by Portland General Electric, the highway and rail transportation corridors in the Columbia Gorge, and the U.S. Army Corps of Engineers power generation facilities at Bonneville Dam. It is important to understand the spatial and temporal distribution of slip along this fault zone so its impact on regional seismic hazard can be assessed and accommodated in seismic design.

Acknowledgments

We would like to recognize the contributions to this work by Dr. Ray Wells and Elizabeth Barnett of the U.S. Geological Survey (USGS) who helped log and interpret the Blue Ridge Fault trenches. We would also like to thank Dr. Brian Sherrod of the USGS who paid for the accelerator mass spectroscopy ^{14}C dating for the trenches. Mike Marshall helped with the trenching project, and Kaleena Hughes, Dr. Vicki McConnell, Christina Appleby, and Kris Hornsby helped with field reconnaissance visits. This paper benefitted by thorough and thoughtful reviews by Jack Albright and Haley Cabaniss.

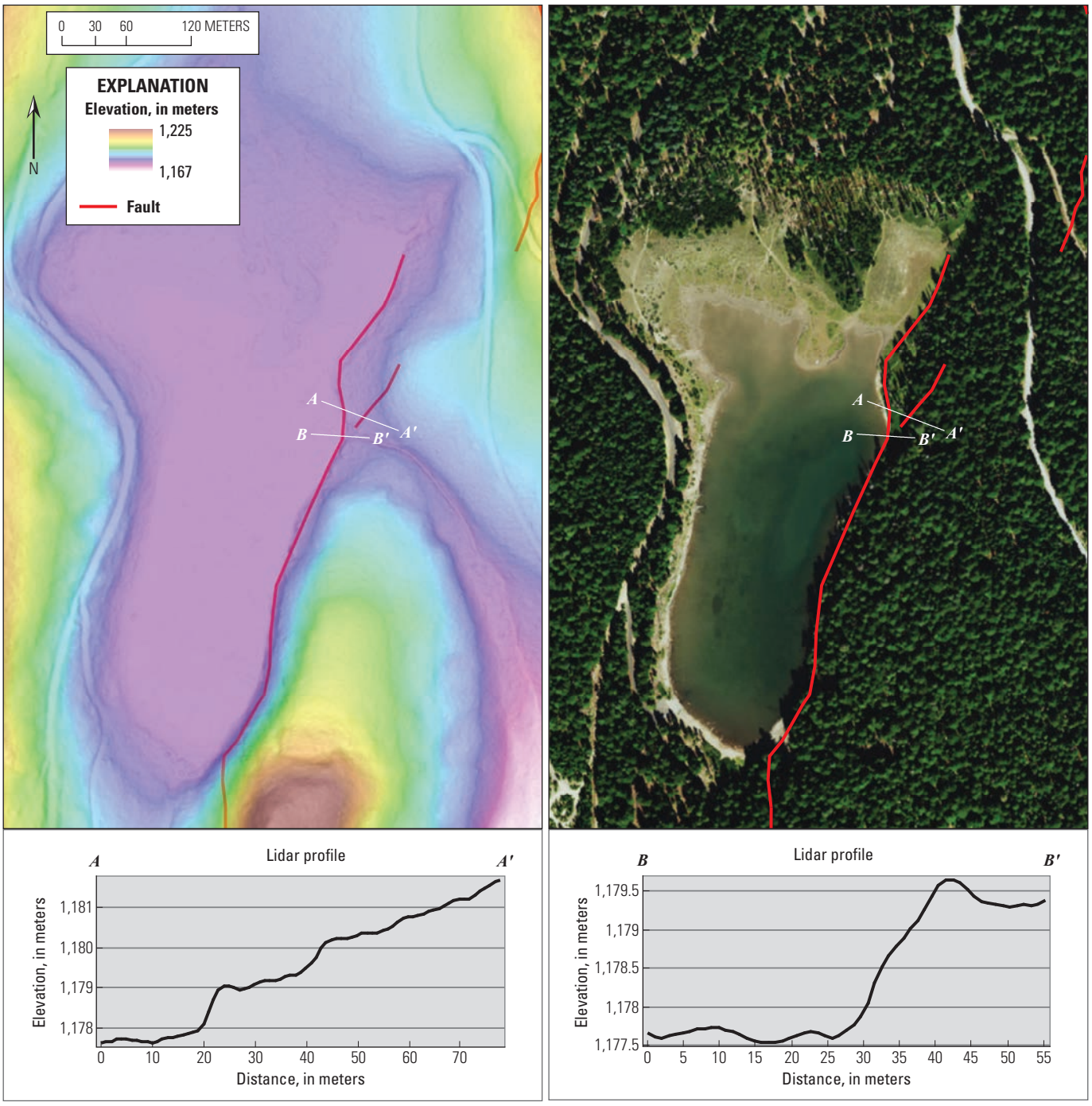

Base from Esri, DigitalGlobe, GeoEye, Earthstar Geographics, CNES/Airbus DS, USDA, USGS, AEX, Getmapping, Aerogrid, IGN, IGP, swisstopo, and the GIS User Community

Figure 8. Map of the Twin Lakes Fault at Frog Lake using (*A*) 1-meter lidar imagery combined with an elevation color gradient and slopeshade, and (*B*) digital orthophotography. The fringing marsh around the lake may have a record of lake level changes associated with past earthquakes. Profile A-A′ shows an offset bench that may be uplifted lake bottom. Profile B-B′ shows the barrier the fault creates at the outlet to the lake.

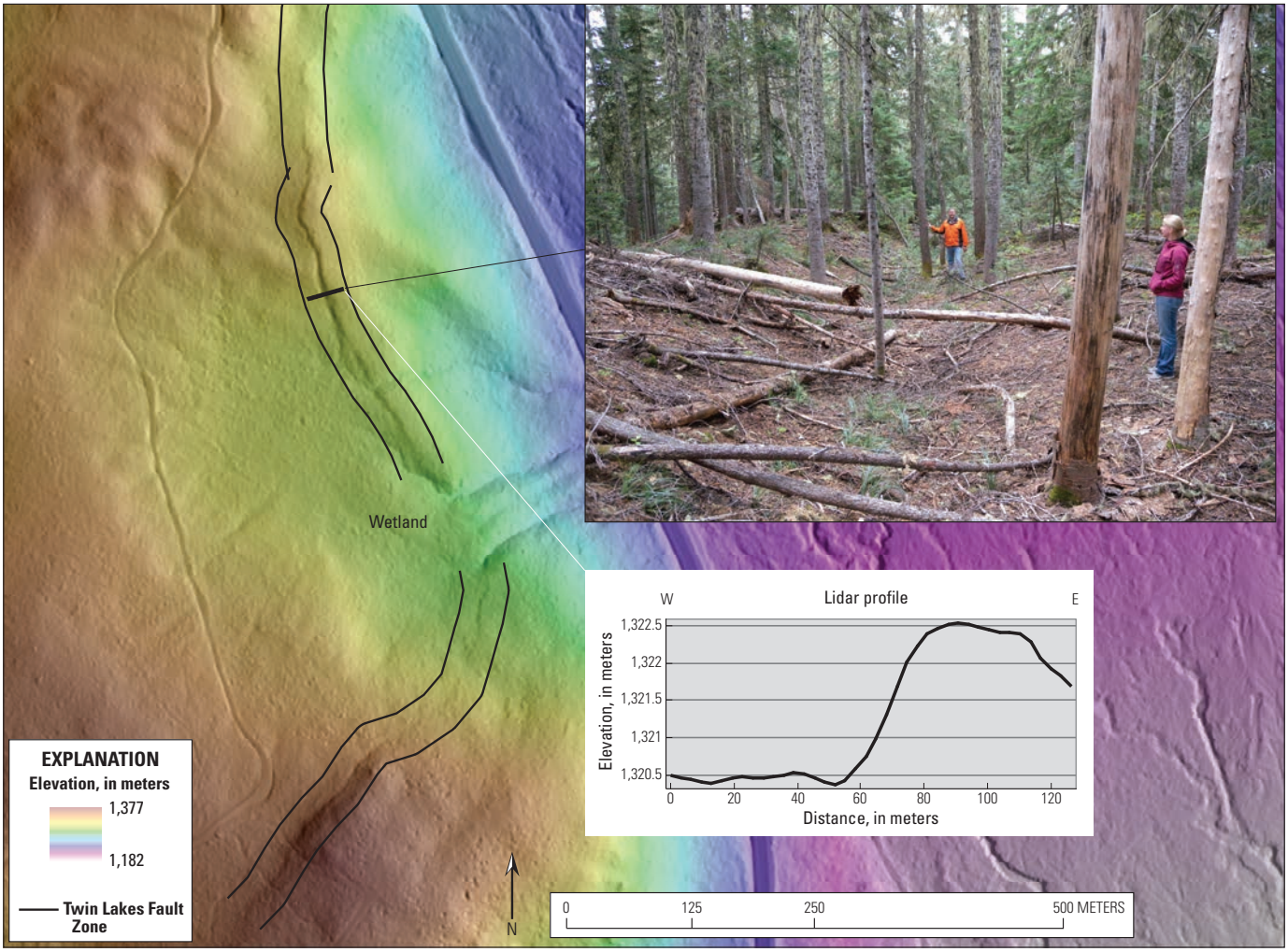

Figure 9. Map of the Twin Lakes Fault near White River. Base map is 1-meter lidar imagery combined with an elevation color gradient and hillshade. Photo at top of figure shows field reconnaissance of scarp relief along the mapped trace. Person on left is in the fault scarp-generated swale, person on right is standing on the west side of the fault.

References

Madin, I.P., and Ma, L., 2012, The Blue Ridge Fault, a newly discovered Holocene fault near Mt. Hood, Oregon: Seismological Research Letters, v. 83, no. 2, p. 374.

McClaughry, J.D., Wiley, T.J., Jones, C.B., and Lite, K.E., 2012, Digital geologic map of the Hood River Valley, Hood River and Wasco Counties, Oregon: Oregon Department of Geology and Mineral Industries Open-File Report O-12-13, 142 p.

Sherrod, D.R., and Scott, W.E., 1995, Preliminary geologic map of the Mount Hood 30- by 60- minute quadrangle, Northern Cascade range, Oregon: U.S. Geological Survey Open-File Report 95-219, 1 plate, 35 p.

Wells, D.L., and Coppersmith, K.J., 1994, New empirical relationships among magnitude, rupture length, rupture width, rupture area and surface displacement: Bulletin of the Seismological Society of America, v. 84, no. 4, p. 974–1002.

Seismicity At and Around Mount Hood, Oregon

By Weston Thelen and Seth C. Moran

Seismicity At and Around Mount Hood, Oregon

By Weston Thelen and Seth C. Moran

Abstract

Mount Hood is one of six volcanoes in the Cascade Range with persistent shallow seismicity (the others are Mount Rainier, Mount St. Helens, South Sister, Newberry Volcano, and Lassen Peak). Seismic monitoring began at Mount Hood in 1980, and improved steadily as stations were gradually added over the following decades to the point that, after installations planned for 2017 are completed, the seismic network will be one of the densest in the Cascades. There are two types of seismicity associated with Mount Hood; earthquakes occurring beneath the summit vent, and those that occur in clusters located 4–7 kilometers (km) west, south, and southeast of the volcano. The largest earthquakes known to have occurred near Mount Hood were an M4.0 in 1974 and an M4.5 in 2002, both located south-southeast of the summit. Detailed analyses of the off-summit earthquake source areas have concluded that the earthquakes most likely occurred along pre-existing normal faults and are broadly consistent with faulting related to Basin and Range extension (Jones and Malone, 2005). The occurrence of tectonic seismicity around Mount Hood is relatively high compared to other areas of the Cascade Range and thus the stresses from the magmatic and (or) hydrothermal system may serve to accelerate activity on the surrounding faults.

Seismic Network

Permanent seismic monitoring by the Pacific Northwest Seismic Network (PNSN) began in 1980, although there were a number of earlier temporary networks deployed as part of studies exploring volcanic activity or assessing geothermal potential in the area (Westhusig, 1973; Green and others, 1979; Rite and Iyer, 1981; Weaver and others, 1982; Williams and others, 1982). As of 2016, the seismic network consists of eight stations within 20 km of the summit that are operated either by the PNSN or the U.S. Geological Survey Cascades Volcano Observatory (fig. 1). Of these, the two closest stations are at Timberline (TIMB, installed 2006) and the top of the Palmer Lift (PALM, installed 2014). Three additional station installations are proposed to the north and east of the summit in the summer of 2017, at which point Mount Hood will have one of the best seismic networks within the Cascade Range volcanoes.

Summit Seismicity

Seismicity under the summit of Mount Hood is typically shallower than 5 km depth, with all earthquakes having magnitudes M<3.5 (fig. 1). The summit area experiences roughly 0 to 6 earthquakes per month, with very occasional swarms that punctuate a steady background activity (fig. 2). All earthquakes are volcano-tectonic in nature, most likely reflecting slip on faults, similar to typical earthquakes in tectonically active areas. Improved locations of well-recorded summit seismicity between 1985 and 2002 by Jones and Malone (2005) suggests earthquakes within the uppermost 2 km occur along a ring fracture, an interpretation consistent with the location of fumarolic vents at the surface (Friedman and others, 1982).

Off-summit Seismicity

Most of the earthquakes in the vicinity of Mount Hood, including many of the largest earthquakes, occur in clusters 4–7 km to the west, south, and southeast of the summit of Mount Hood at depths between 3 and 8 km (fig. 1). Earthquakes in these clusters generally occur in swarms or mainshock-aftershock sequences, with very low seismicity rates between swarms (fig. 2). Though there is ample scatter in the earthquake locations, much of this scatter is likely due to location error, which can be caused by picking errors due to low signal-to-noise P-wave arrivals and (or) by inadequate station coverage. Re-analysis of off-summit seismicity by Jones and Malone (2005) found that many events had similar waveforms, a finding that is consistent with more recent, unpublished analyses. The similarity in waveforms between individual earthquakes indicates that earthquakes are occurring closer together than indicated by catalog locations. Focal mechanisms of earthquakes to the south of the summit are largely normal with strikes that parallel recognized faults in the area (Jones and Malone, 2005); this, coupled with the correlation between earthquake clusters and recognized faults, including the Twin Lakes Fault (south-southeast of Mount Hood) and Multorpor Mountain Fault (south-southwest of Mount Hood) suggests that these off-summit earthquakes are occurring primarily on faults with orientations consistent with tectonic processes in the region. Interestingly, there are very low rates of seismicity to the north of the volcano, despite the

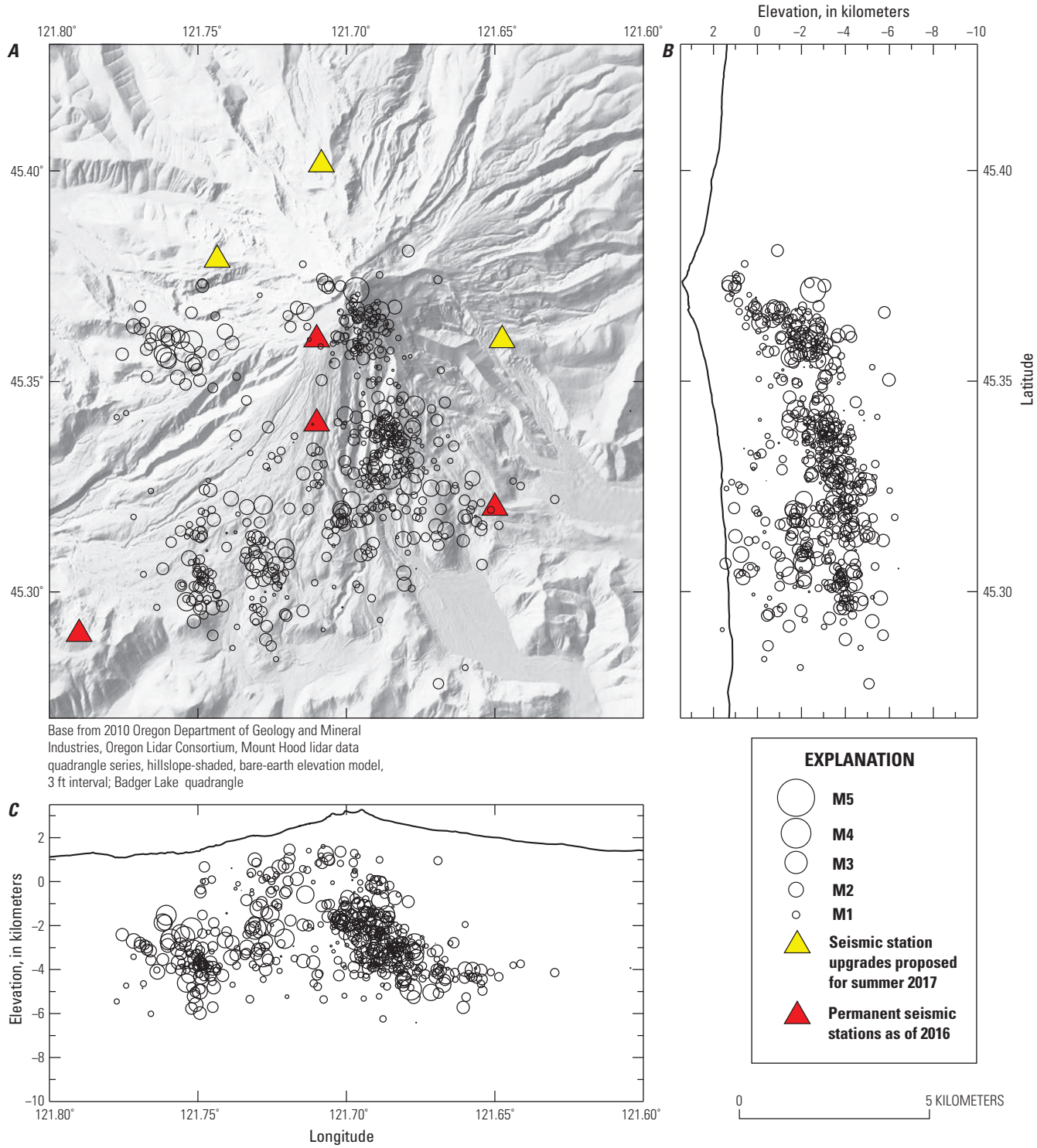

Figure 1. *A*, Map view of earthquakes (circles) near Mount Hood between 1980 and January 1, 2017, from the Pacific Northwest Seismic Network. Only earthquakes with six or more phase picks, a gap between seismic station observations of less than 150 degrees, and a station within 5 kilometers of the epicenter are included. *B*, North-south cross-section view of earthquakes plotted in map view. Black line, local topographic surface. *C*, East-west cross-section view of earthquakes plotted in map view. Black line, local topographic surface.

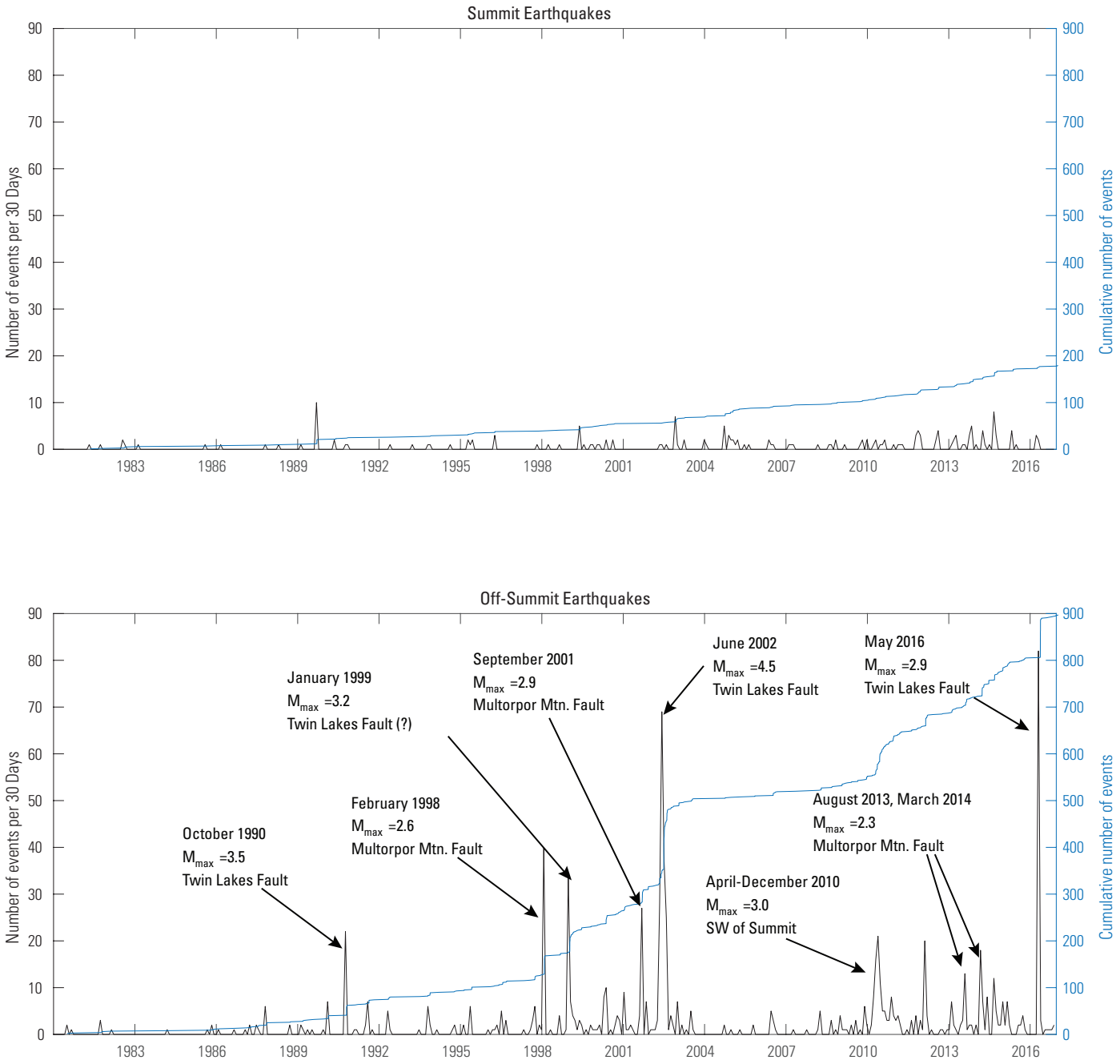

Figure 2. *A*, Time series of earthquake rate using earthquakes within 2.5 kilometers of the summit of Mount Hood (called Summit Earthquakes) between 1980 and January 1, 2017. The blue line is the cumulative number of earthquakes occurring in that region. Only earthquakes with magnitudes above M0.9 are plotted, which is the maximum magnitude of completeness. Both axes are normalized to have the same limits as the off-summit earthquakes below. *B*, Time series of earthquake rates using earthquakes greater than 2.5 kilometers from the summit of Mount Hood (called Off-Summit Earthquakes) between 1980 and January 1, 2017. The blue line is the same as in *A*. Only earthquakes greater than M0.9 are plotted. Swarms of earthquakes are labeled with the closest fault noted and the maximum magnitude of the swarm.

presence of known faults (for example, the Blue Ridge Fault). Although it is possible this could be an artifact of network coverage, seismic networks at Mount Hood have been good enough to reliably detect and locate earthquakes M>1.5 on the north side since the 1990s, therefore the apparent dearth of seismicity on the north side of Mount Hood is likely a true absence of activity.

Conceptual Model

The presence of active fumaroles in the summit area, as well as the relatively regular occurrence rate of summit earthquakes, suggests that the earthquakes are occurring as a manifestation of subsurface hydrothermal circulation. The source of the heat that is driving the hydrothermal system is somewhat enigmatic. Seismic studies (for example, Weaver and others, 1982) and gravity studies (Couch and Gemperle, 1979) failed to find any evidence of a magma chamber, though heat flow measurements (Williams and others, 1982) are suggestive of a magma chamber somewhere in the upper 15 km of the crust. Further, no deep long-period earthquakes have been detected at Mount Hood, which could be interpreted as reflecting little, if any, magma movement within the deep (>15 km) crust. A magma chamber, if one exists in the upper crust, must therefore be either small, crystal rich to the point that there is no geophysical anomaly, or distributed in such a way that it is not detectable by the seismic and gravity methods that have been attempted to date.

Tectonic seismicity rates occurring along faults to the south of Mount Hood are the highest in Oregon and one of the highest in the Cascade Range. The overwhelming dominance of normal faulting is consistent with Basin and Range encroachment, however it doesn't explain the high seismic activity rates. Whether faults with high strain rates facilitate magma extrusion to the surface or whether the volcano is imparting extra stress on those faults causing them to slip is still an unresolved question. At Mount Hood, its possible that stress imparted in the crust from the magma chamber or hydrothermal system is facilitating slip preferentially on the faults to the south. It is also possible that fluids derived either from the hydrothermal system or from deeper magmatic sources are locally raising pore pressures along pre-existing faults that occasionally give rise to seismogenic failures of those faults.

References

Couch, R., and Gemperle, M., 1979, Gravity measurements in the area of Mount Hood, Oregon, *in* Hall, D.A., investigator, and Riccio, J.F., ed., Geothermal resource assessment of Mount Hood: Oregon Department of Geology and Mineral Industries, Open File Report O-78-9, p. 137–189.

Friedman, J.D., Williams, D.L., and Frank, D., 1982, Structural and heat flow implications of infrared anomalies at Mt. Hood, Oregon, 1972–1977: Journal of Geophysical Research, v. 87, no. B4, p. 2793. [Also available at http://doi.org/10.1029/JB087iB04p02793.]

Green, S.M., Weaver, C.S., and Iyer, H.M., 1979, Seismic studies at the Mt. Hood volcano, Northern Cascade Range, Oregon: U.S. Geological Survey Open-File Report 79-1691, 38 p.

Jones, J., and Malone, S.D., 2005, Mount Hood earthquake activity—Volcanic or tectonic origins?: Bulletin of the Seismological Society of America, v. 95, no. 3, p. 818–832.

Rite, A., and Iyer, H.M., 1981, July 1980 Mt. Hood Earthquake Swarm: U.S. Geological Survey Open-File Report 81-43, 21 p.

Weaver, C.S., Green, S.M., and Iyer, H.M., 1982, Seismicity of Mount Hood and structure as determined from teleseismic P wave delay studies: Journal of Geophysical Research, v. 87, no. B4, p. 2782. [Also available at http://doi.org/10.1029/JB087iB04p02782.]

Westhusing, J.K., 1973, Reconnaissance surveys of near-event seismic activity in the volcanoes of the Cascade Range, Oregon: Bulletin Volcanologique, v. 37, no. 2, p. 258–286. [Also available at http://doi.org/10.1007/BF02597134.]

Williams, D.L., Hull, D.A., Ackermann, H.D., and Beeson, M.H., 1982, The Mt. Hood region—Volcanic history, structure, and geothermal energy potential: Journal of Geophysical Research, v. 87, no. B4, p. 2767. [Also available at http://doi.org/10.1029/JB087iB04p02767.]

Menlo Park Publishing Service Center, California
Manuscript approved March 22, 2017
Edited by Katherine Jacques
Design and layout by Vivian Nguyen

ISSN 2328-0328 (online)
https://doi.org/10.3133/sir20175022g